2010

Sorption mechanisms of zinc in different clay minerals and soil systems as influenced by various natural ligands

Mohammed Hashem Stietiya
Louisiana State University and Agricultural and Mechanical College

SORPTION MECHANISMS OF ZINC IN DIFFERENT CLAY MINERALS AND SOIL SYSTEMS AS INFLUENCED BY VARIOUS NATURAL LIGANDS

A Dissertation

Submitted to the Graduate Faculty of the
Louisiana State University and
Agricultural and Mechanical College
in partial fulfillment of the
requirements for the degree of
Doctor of Philosophy

in

The School of Plant, Environmental, and Soil Sciences

By
Mohammed Hashem Stietiya
B.S., Jordan University of Science and Technology, 1997
M.S., University of Jordan, 2000
May 2010

DEDICATION

With great pride I dedicate this dissertation

To my parents, Mr. and Mrs. Stietiya, who provided me with unending and unconditional support throughout my life and continue to do so, lovingly. You have bestowed upon me many gifts, including the love for knowledge.

To my wife, Hiba Bawadi, who stormed my life with love, who gave it new meaning and who continues to bless it with happiness.

To my lovely Zeena and beloved Samir Jr., you are our fountain of joy and the reason for most of our smiles.

ACKNOWLEDGMENTS

I express my sincere appreciation to Dr. Jim Wang for serving as Chairman of my dissertation research. I thank you for your continued guidance and for your technical support throughout this journey. I would also like to thank members of my doctoral committee, Dr. Ronald DeLaune, Dr. Amitava Roy, Dr. Lewis Gaston, and the dean's representative, Dr. Robert Cook. Thank you for your input and valuable insight.

I extend gratitude to all my friends for their continued support: Theophilus Udeigwe, Syam Dodla, Zehua Zhou and Glenn McLellan. Also, my gratitude goes out to Tamer Elbana and Noura Bakr, with whom Hiba and I spent very beautiful days together.

I extend special thanks to my father and mother. Despite being away, you have always encouraged me to do the best I can. Thanks for being the best mom and dad in the world. I also want to thank all of my family members for their support and encouragement.

Very special thanks go to my beloved wife, Mrs. Hiba Bawadi, and my children,
Zeena and Samir. Hiba, dearest, I thank you for your unwavering support, understanding, and allowing me to pursue my dreams. I am so grateful that you kept the family intact during my many days and nights of absence. You are truly a gift from God. Zeena, thank you baby for all your hugs all night long. Samir, your crying in the last month of my Ph.D. journey kept me alert and up to finish this manuscript.

TABLE OF CONTENTS

LIST OF TABLES

LIST OF FIGURES

ABSTRACT

The bioavailability and fate of Zinc (Zn) in soils is influenced by reactions occurring at the water-mineral interface. Understanding Zn interaction with mineral surfaces is essential to the understanding of Zn fate and toxicity. In this study, adsorption experiments investigated the impact of ligands and pH on the adsorption of Zn to mineral surfaces. X-Ray Absorption Fine Structure Spectroscopy (XAFS) was used to elucidate the adsorption mechanisms of Zn to mineral surfaces as impacted by ligands.

Impact of ligands on Zn adsorption was dependent on mineral type and pH of the system. XAFS analysis showed that adsorption mechanisms of Zn were impacted by pH and ligand presence. In the ferrihydrite system, Zn adsorption was enhanced in presence of citrate and phosphate (PO_4), reduced in presence desferrioxamine (DFO-B), and reduced in presence of humic acid (HA) at pH>6.0. XAFS analysis showed that Zn formed strong linkages with high affinity edge sites of ferrihydrite in the control and in presence of enhancing ligands (citrate and PO_4), whereas formed weaker, low affinity linkages in presence of supressing ligands (DFO-B and HA). From an environmental perspective, Zn was more likely to be desorbed from the ferrihydrite surface in the presence HA and DFO-B.

In the kaolinite system, Zn adsorption was reduced in presence of citrate and DFO-B, and increased in presence of HA. Zn formed inner sphere complexes at pH 5.5 in the control and in presence of ligands. At pH 7.5, a Zn-Al layered double hydroxide was formed in the control, that was absent in presence of any ligand, suggesting that ligands suppress the formation of Zn-Al LDH in kaolinite. In the mixed ferrihydrite-gibbsite system, Zn adsorption was enhanced in presence of all ligands, excluding DFO-B. Adsorption mechanisms of Zn to ferrihydrite were unaffected by ligand presence. The impact of organic matter (OM) degradation on heavy metal

distribution in sewage sludge was investigated. Cu, Pb and As were bond with the OM fraction of sludge, whereas Zn was bond to Fe/Mn oxide fraction. OM degradation increased mobility and bioavailability of Zn and Cu, whereas it had less impact on Pb and As.

CHAPTER 1

INTRODUCTION

1.1 Introduction

Zinc (Zn) is an essential element for the growth and development of humans, plants and animals. It is considered one of eight essential trace elements required for crop growth and production and its deficiency in soils may have a profound economic impact in terms of yield loss (Alloway, 2004). Nevertheless, there is concern of Zn being a potential soil contaminant as a result of smelting operations, incinerator emissions, excessive use of fertilizer, runoff from roads and from Zn steeled constructions and use of contaminated sludges (Robson, 1993). The fate and bioavailability of Zn in soils and aquatic systems is influenced by reactions occurring at the water-mineral interface (Nachtegaal and Sparks, 2004). Understanding Zn interaction with mineral surfaces in the soil is therefore essential to the understanding of metal fate and transport, bioavailability and ultimately toxicity. For example, outer-sphere complexes of Zn formed in the soil are considered weak and readily exchangeable, whereas inner sphere complexes are strong and may potentially sequester Zn (Sparks, 2005). The task of elucidating the adsorption mechanisms of Zn requires the use of molecular scale analytical techniques such as X-Ray Absorption Fine Structure Spectroscopy (XAFS) (Trivedi et al., 2003; Sparks, 2005). XAFS spectroscopy is a powerful tool that allows the probing of Zn local coordination environment and the determination of Zn complexes formed with mineral surfaces (Trivedi et al., 2003).

The most important mineral phases involved in the adsorption of heavy metals are phyllosilicates, metal oxides and hydroxides, and metal carbonates and phosphates (Bradl, 2004). A wide range of Zn sorption complexes have been identified with XAFS spectroscopy (Grafe et

al., 2004). Zn was found to form inner sphere complexes with ferrihydrite (Waychunas et al., 2002; Lee and Anderson, 2005), goethite (Trivedi et al., 2001), alumina (Trainor et al., 2000), and gibbsite (Roberts et al., 2003). Outer sphere complexes have been reported to occur in montmorillonite (Schlegel et al., 2001) and ferrhydrite (Trivedi et al., 2001). In addition, formation of precipitate phases such as Zn-Al layered double hydroxide (LDH) has been reported to occur upon adsorption to low surface-area gibbsite (Roberts et al., 2003), alumina powders (Trainor, 2000), and kaolinite (Nachtegaal and Sparks, 2004).

Zn and other metals in the environment are often complexed with ligands of natural or anthropogenic origin such as humic acid, fulvic acid, NTA or EDTA (Bradl, 2004; Davis and Leckie, 1978). Ligands are ubiquitous in the soil environment and impact the partitioning of metals at the water/mineral interface. While adsorption mechanisms of metals such as Ni, Cd, and Cu have been investigated in the presence of low and high molecular weight ligands including citrate and humic acid (Alcacio et al., 2001; Yamaguchi et al., 2002), few studies have documentated the impact of ligands on the mechanisms of Zn adsorption to mineral surfaces.

The other section of this dissertation investigates the relative distribution of heavy metals in sewage sludge (SS) and sewage sludge amended soils as impacted by chemical oxidation of organic matter. One of the major concerns of continued land application of sewage sludge is increased trace metal concentration in soil and uptake by plants. There is controversy within the scientific community over the fate of heavy metals following long term application of biosolids. Some researchers have postulated that the long term application of biosolids would result in the release of heavy metals into the soil due to organic matter mineralization, also known as the "Time Bomb" hypothesis. Other researchers have indicated that the long term application of biosolids would present no hazard, due to the high adsorptive capacity of inorganic phases within

biosolids, also known as the "Protection" hypothesis (McBride, 1995; Frost et al., 2000; Li et al., 2001; McBride, 2003; Bergkvist et al., 2005; Hettiarachichi et al., 2006). In this study, we have focused on exploring the distribution of trace metals in different pools of bioavailability in SS and SS-amended soils at different stages of OM degradation using sequential fractionation.

1.2 Objectives

This dissertation contains research focused on elucidating Zn adsorption mechanisms to various mineral surfaces in the presence of organic and inorganic ligands (citrate, humic acid, siderophore, and phosphate). The general objectives of this study are to (i) investigate Zn adsorption to single mineral systems of ferrihydrite and kaolinite in the presence of citrate, humic acid, siderophore, and phosphate as a function of pH; (ii) to elucidate the mechanisms of Zn adsorption to ferrihydrite and kaolinite in the presence of ligands using X-Ray Absorption Fine Structure Spectroscopy (XAFS); (iii) investigate Zn adsorption in mixed mineral systems of ferrihydrite-gibbsite and goethite-kaolinite in the presence of citrate, humic acid, siderophore, and phosphate as a function of pH; (iv) to elucidate the mechanisms of Zn adsorption in mixed mineral systems; (v) to investigate the relative distribution of Cu, As, Zn and Pb in sewage sludge and sewage sludge amended soils as impacted by chemical oxidation.

1.3 References

Alcacio, T.E., D. Hesterberg, J.W. Chou, J.D. Martin, S. Beauchemin, and D.E. Sayers. 2001. Molecular scale characteristics of Cu(II) bonding in goethite–humate complexes. Geochim. Cosmochim. Ac. 65(9): 1355–1366.

Alloway, B.J. 2004. Zinc in soils and crop nutrition. International Zinc Association Communications. IZA, Brussels, Belgium.

Bergkvist, P., D. Berggren, and N. Jarvis. 2005. Cadmium solubility and sorption in a long-term sludge-amended arable Soil. J. Environ. Qual. 34:1530–1538.

Bradl, H.B., 2004. Adsorption of heavy metal ions of soils and soils constituents. J. Colloid Interf. Sci. 277: 1–18.

Davis, J.A. and J.O. Leckie. 1978. Effect of adsorbed complexing ligands on trace metal uptake by hydrous oxides. Environ. Sci. Technol. 12(12): 1309-1315.

Frost, H.L. and L.H. Ketchum, 2000. Trace metal concentration in durum wheat from application of sewage sludge and commercial fertilizer. Advances in Environmental Research. 4: 347-355.

Gräfe, M., M. Nachtegaal, and D.L. Sparks. 2004. Formation of metal-arsenate precipitates at the goethite-water interface. Environ. Sci. Technol. 38: 6561-6570.

Hettiarachchi, G.M., K.G. Scheckel, J.A. Ryan, S.R. Sutton, and M. Newville. 2006. μ-XANES and μ-XRF investigations of metal binding mechanisms in biosolids. J. Environ. Qual. 35:342–351.

Lee, S. and P.R. Anderson. 2005. EXAFS study of Zn sorption mechanisms on hydrous ferric oxide over extended reaction time. J. Colloid Interface Sci. 286: 82-89.

Li, Z., J.A. Ryan, J.L. Chen, and S.R. Al-Abed. 2001. Adsorption of cadmium on biosolids-amended soils. J. Environ. Qual. 30:903–911.

McBride, M.B. 1995. Toxic metal accumulation from agricultural use of sludge: Are USEPA regulations protective? J. Environ. Qual. 24: 5–18.

McBride, M.B. 2003. Toxic metals in sewage sludge-amended soils: Has promotion of beneficial use discounted the risks? Adv. Environ. Res. 8:5–19.

Nachtegaal, M., and D.L. Sparks. 2004. Effect of iron oxide coatings on zinc sorption mechanisms at the clay-mineral/water interface. Journal of Colloid and Interface Science 276: 13–23.

Roberts, D. R., R. G.Ford and D. L. Sparks. 2003. Kinetics and mechanisms of Zn complexation on metal oxides using EXAFS spectroscopy. J. Colloid Interf. Sci. 263(2): 364-376.

Robson, A.D. 1993. Zinc in Soils and Plants. Vol. 55, Proceedings of the International Symposium on `Zinc in Soils and Plants'. Kluwer Academic publisher, The Netherlands.

Schlegel, M.L., A. Manceau, L. Charlet,and J.L. Hazemann. 2001. Adsorption Mechanisms of Zn on Hectorite as a Function of Time, ph, and Ionic Strength. American Journal of Science 301: 798–830.

Sparks, D.L. 2005.Toxic metals in the environment: the role of surfaces. Elements. 1: 193-197.

Trainor, T.P., G.E. Brown, and G.A. Parks.2000. Adsorption and Precipitation of Aqueous Zn(II) on Alumina Powders. Journal of Colloid and Interface Science 231: 359–372.

Trivedi, P., J.A. Dyer, and D.L. Sparks. 2003. Lead Sorption onto Ferrihydrite. 1. A Macroscopic and Spectroscopic Assessment. Environ. Sci. Technol. 37: 908-914.

Trivedi, P., L. Axe, and T.A. Tyson. 2001. An Analysis of Zinc Sorption to Amorphous versus Crystalline Iron Oxides Using XAS. J. Colloid Interf. Sci. 244: 230–238.

Waychunas, G.A., C.C. Fuller, and J.A. Davis. 2002. Surface complexation and precipitate geometry for aqueous Zn(II) sorption on ferrihydrite I: X-ray absorption extended fine structure spectroscopy analysis. Geochimica et Cosmochimica Acta. 66(7): 1119-1137.

Yamaguchi, N. U., A. C. Scheinost, and D.L. Sparks. 2002. Influence of gibbsite surface area and citrate on Ni sorption mechanisms at pH 7.5. Clays and Clay Minerals 50(6): 784-790.

CHAPTER 2

LITERATURE REVIEW

2.1 Zinc in the Environment

Zinc (Zn) is a bluish-white metal with atomic number 30 and atomic mass of 65.38 a.m.u. It is the first element of group 12 (IIb) in the periodic table with an electron configuration of [Ar] $4s^2 3d^{10}$. Divalent Zn is the only natural oxidation state of this element. Since *d* subshells are complete in the Zn(II) ion, it is considered a post-transition metal. Zn concentration in the Earth's crust is 70 mg kg^{-1}, making it the 25th most abundant element (Robson,1993). Zn has five stable isotopes of 64, 66, 67, 68 and 70 with different abundances of 48.63%, 27.90%, 4.10%, 18.75%, 0.62%, respectively (Juillot et al., 2008). It has a Lewis acidity similar to that of Cu(II) and ionic radius of 1.31Å comparable to that of Mg(II) (Robson, 1993; Barak and Helmke, 1993; Eisler, 1993; Juillot et al., 2008).

Long before it was recognized as an element in the fourteenth century A.D., Zn ores were used to make brass. As early as 200B.C., copper (Cu) and a Zn ore known as calamine [$Zn_4(Si_2O_7)$] were used in brass making. Zn became the 8th known element in the 14th century in India and in the 16th century Zn production had moved to China. Zn was recognized as a separate metal in Europe in the 16th century by German mineralogist George Bauer. Zn was recognized as an essential nutrient for plants and animals in 1869. (Bolt and Bruggenwert, 1976; Eisler, 1993; Porter, 1991).

Commercial ores of Zn include the sulfides sphalerite(ZnS) and wurtzite ((Zn,Fe)S), smithsonite ($ZnCO_3$), hemimorphite ($Zn_4(Si_2O_7)$), zincite (ZnO) and willemite (Zn_2SiO_4) (Eisler, 1993). Most of the Zn produced in the world is used for the production of corrosion resistant coating on other metals. The Zn coating preferentially corrodes to protect the underlying metal.

Zn is also found in many manufactured products such as motor oils, lubricants, tires, fuel oils, batteries, galvanized steel products, cosmetics, and pharmaceuticals. Compounds such as Zn oxide and Zn sulfate are used in coating photocopy paper and in fungicides, respectively (Jones and Burgess, 1984; Eisler, 1993; Mulligan, 2001).

Natural levels of Zn in the soil range from 10-300 mg kg^{-1} with an average of 50 mg kg^{-1} (Bolt and Bruggenwert, 1976; Mulligan et al., 2001). It is estimated that 30% of the world's cultivated soils are deficient in Zn (Suzuki et al., 2006). Nevertheless, anthropogenic sources of Zn contamination in the soil include: mining and smelting of ores, electroplating, fertilizer application, combustion of fossil fuels, road runoff, and municipal waste (Eisler, 1993; Lasat, 2000). Zn is considered one of the most hazardous heavy metals included in the EPA's list of priority pollutants in addition to Cd, Cu, Hg, Pb, and Ni (Lasat, 2000; Mulligan, 2001).

Soils have the ability to retain Zn and control its plant availability in the soil. Solubility of Zn in soils is affected by pH, amount of metal, cation exchange capacity (CEC), organic matter content, and soil mineralogy (Martínez and Motto, 2000). The inorganic interfaces involved in heavy metal adsorption are clays, metals oxides-hydroxides, metal carbonates, and metal phosphates (Bradl, 2004). Adsorption of Zn and other heavy metals to these surfaces and to organic matter regulates their concentration in the soil solution. In the following sections, the adsorption of Zn to mineral surfaces and the factors impacting adsorption are discussed.

2.2 Organic Ligands in the Soil Environment

2.2.1 Low Molecular Weight Organic Ligands

Low molecular weight organic acids (LMWOA) are carbon compounds characterized by the possession of one or more carboxyl groups with a maximum molecular weight of 300 daltons (Jones, 1998; Strobel, 2001). They are formed in the soil from organic matter degradation,

microbial metabolites, and from plant root or fungi exudation (Strobel, 2001; Qin et al., 2004; van Hees et al., 2000). The most common organic acids in the soil include oxalate, acetate, citrate, and formate (van Hees et al., 2005). Low molecular weight organic acids (LMWOA) are common in the soil, where their concentration in the rhizosphere can be higher than a millimolar (Huang et al., 2003). In the soil solution, the concentration of organic acids may be in the micromolar range, usually <50μM (van Hees et al., 2005). Organic acids may be classified as aromatic or aliphatic carboxylic acids (Strobel, 2001; van Hees et al., 2005). Aliphatic acids may be mono-, di-, or tricarboxylic acids such as formate, oxalate and citrate, respectively (Ryan et al., 2001). Aromatic acids may be mono- or di- carboxylic acids such as salicyclic and phthalic, respectively (Martinez et al., 1998). Phenolic and aromatic carboxylic acids that have been found in soils include: gallic, vanillic, benzoic, *p*-hydroxybenzoic, *p*-coumaric, and protocatechuic acid (van Hees et al., 2000).

LMWOA serve several beneficial functions in the soil such as reduction in Al toxicity in acid soils by complexation, increase in availability of K for plant uptake by enhancing the weathering of K containing minerals, and posing the ability to solubilize phosphate precipitates (Jones, 1998; Strobel, 2001). For example, due to their acidic and chelating properties, organic acids increase the solubility of P in soil by increasing the solubility of P-containing compounds and by decreasing P adsorption (Bolan et al., 1994). The dissolution of phosphate rocks occurs according to the following reaction (Ryan et al., 2001):

$$Ca_{10}(PO_4)_6F_2 + 12H^+ \longrightarrow 10Ca^{+2} + 6H_2PO_4^- + F^-$$

Dissolution of phosphate compounds is enhanced by supplying protons and complexing Ca^{+2} ions by LMWOA (Ryan et al., 2001). Organic acids have been shown to enhance the weathering rate of soils by three times (van Hees et al., 2000). On the other hand, their

concentration in the soil is generally small (Jones et al., 2003). LMWOA are also energy sources for micro-organisms and important in C cycling (Martinez et al., 1998). LMWOA can form coordination compounds or complexes with metals. The degree of complexation is dependent on the nature of organic acid (number of carboxylic groups), pH of soil solution, and type of metal and its concentration (Jones, 1998). The number of carboxylic groups and their position determines the stability of ligand: metal complexes (Ryan et al., 2001). Lactate, formate and acetate have only one carboxyl group which results in them having little metal-complexing ability. Malate, oxalate, and malonate have two carboxyl groups and therefore chelate cations more strongly than monocarboxylates. Tricarboxylates such as citrate have high affinity for trivalent metals such as Fe^{+3} and Al^{+3}(Jones, 1998; Ryan et al., 2001).

2.2.2 High Molecular Weight Organic Ligands

Organic matter in the soil may be divided into two classes of compounds: non-humic material and humic substances (Jones and Bryan, 1998). Humic substances are widely distributed in soils, sediments and water bodies, constituting 80% of soil organic matter and 60% of surface-water organic matter (Jones and Bryan, 1998; Alvarez-Puebla et al., 2004). They may be fractioned into humic acid, fulvic acid and humin based on their solubility in acids and alkalis (Essington, 2004; Sparks, 1995). Fulvic acids are soluble at all pH, humic acid is soluble at pH> 2, and humin is insoluble at all pH (Jones and Bryan, 1998).

Humic acids are high molecular weight compounds (1000-500,000 Daltons) with low mobility in the soil, which give them the capacity to immobilize heavy metals (Arias et al., 2002; Buerge-Weirich et al., 2003; Essington, 2004). The most important surface functional groups in humic acid are the carboxylic, carbonyl, and phenolic groups (Bradl, 2004). Carboxyls in humic acid have pKa in the range of 4-6 and phenols in the range from 9-11. On average, 50% of the

total acidity is due to carboxylic groups. They have a greater tendency to ionize at low pH and are therefore most likely to be involved in the adsorption reactions (Lai et al., 2002, Xia et al., 1997).

Fulvic acid is the water-soluble humic material with lower molecular weight (500-2000 Daltons) than humic acid (Ogner and Schnitzer, 1970). Although fulvic acid is known to compose the bulk of dissolved organic carbon fraction in soil, the soil solution contains low molecular weight compounds such as aliphatic and aromatic organic acids (LMWOA), peptides, amino acids, sugars and siderophores. It is estimated that <10% of dissolved organic carbon in soil consists of low molecular weight compounds (van Hees et al., 2005).

2.2.3 Siderophores

Siderophores, meaning "iron-bearers" in Greek, are low molecular weight (500-1000 daltons) metabolites with a high affinity for Fe^{+3} and low affinity for Fe^{+2}. They are produced by living organisms under conditions of Fe limitation for the purpose of mobilizing Fe (Bossier et al., 1988; Crowley et al., 1991; Neilands and Leong, 1986).

Iron is an essential plant nutrient and is required for a variety of metabolic processes in almost all living organisms. Iron deficiency in most soils is not triggered by low total Fe concentrations where soils contain between 1 to 6% total Fe, but by low Fe availability (Powell et al., 1980; Kraemer, 2004). A limiting factor of Fe availability is the low solubility and slow dissolution kinetics of Fe-bearing minerals (Kraemer, 2004). The solubility product of ferric hydroxide is 10^{-38} and the concentration of soluble ferric ion at pH 7 is ~10^{-17} M (Leong, 1986). Siderophores have high stability constants ranging from 10^{25} to 10^{35} and in exceptional cases as high as 10^{51} (Kalinowski et al., 2000). Siderophores bind Fe(III) more effectively than organic acids such as oxalic and citric acids whose formation constants are $10^{7.6}$ and $10^{17.3}$, respectively

(Powell et al., 1980; Kalinowski et al., 2000). Siderophore concentration in a typical soil is ~174 μm and may reach a few millimoles per liter (Kalinowski et al., 2000; Neubauer et al., 2000).

Siderophores are also released during Zn deficiency (Römheld, 1991; Cakmak et al., 1996). Sorghum and wheat plants were found to increase the release of phytosiderophores during Zn deficiency whereas corn did not, which may explain why Zn deficiency is more common in corn than in wheat or sorghum (Hopkins et al., 1998).

Siderophores are produced by bacteria, fungi, and graminaceous plants. Nearly all aerobic and facultative anaerobic bacteria produce siderophores with a few exceptions (Kraemer, 2004; Crowley et al., 1991). Microbes produce a great number and variety of siderophores, whereas few phytosiderophores are produced by Fe-efficient grasses.

Nearly 200 siderophore compounds have been isolated, the majority of which are either hydroxamates or phenolates-catecholates (Kraemer, 2004; Hersman et al., 1995). Fungi generally produce siderophores with hydroxamate Fe(III)-binding groups and bacteria produce siderophores with catecholate Fe(III)-binding groups (Leong, 1986; Neubauer et al., 2002). Mugineic acid is a phytosiderophore with carboxylate, hydroxyl, and amine binding groups (Kraemer, 2004). The functional group in hydroxamates is hydroxamic acid, which is a carbonyl oxygen combined with an amino group. The catecholamides have hydroxyl oxygens on an aromatic ring (Kalinowski et al., 2000).

Despite wide variation among siderophores, they all form thermodynamically stable six-coordinate octahedral complexes with the ferric ion. The hydroxamic functional group can form a five membered chelate ring with Fe^{+3}. Three hydroxamate groups are often found in a single siderophore molecule and form six-coordinate octahedral complexes with Fe(III) through two oxygen atoms (Raymond et al., 1984; Guerinot, 1994; Hersman et al., 1995). The formation of

metal complexes with siderophores is dependent on the protonation state of the hydroxamate functional groups and complexation is favored at high pH (Neubauer et al., 2002).

2.3 Inorganic Ligands in the Environment

Inorganic anions can be classified in terms of their adsorption characteristics into three groups. The first group includes those that have non-specific adsorption characteristics such as NO_3^-, Cl^-, and ClO_4^-. The second group includes ligands that are specifically adsorbed and are completely dissociated acids such as SO_4^{-2} and F^-. The third group includes anions that are specifically adsorbed and that are incompletely dissociated acids such as: PO_4^{-3} and SiO_3^{-2} (Yu et al., 2005). Adsorption of inorganic anions to mineral surfaces has many significant environmental implications. For example, sulfate occurs in high concentrations in acid mine runoff as a result of geochemical recycling of pyrite (Peak et al., 1999). The adsorption of sulfate on variable charge minerals plays an important role in acidification of soils, as H^+ and sulfate are withdrawn from solution thereby buffering pH (Karltun, 1997). Excess P is considered a serious non-point source pollutant that results in eutrophication of waters (Arai and Sparks, 2001). Adsorption of P to mineral surfaces is therefore extremely important from environmental water quality perspective. In addition, phosphate adsorbed to mineral surfaces has been used to reduce the biological availability of Pb in soils (Taylor et al., 2009).

Sulfate adsorption to mineral surfaces may occur via inner or outer sphere complexation. Peak et al. (1999) reported that sulfate formed both inner and outer sphere complexes on goethite at pH below 6, whereas formed only outer sphere complexes above that pH. In the case of inner sphere complexation, the possible sorption geometries may include monodentate, bidentate, or bridging bidentate (Persson and Lövgren, 1996). Phosphate was found to adsorb to ferrihydrite forming bidentate binuclear complexes at pH > 7.5 (Arai and Sparks, 2001). Upon adsorption to

hematite, three different phosphate complexes were formed, the importance of which varied with pH and phosphate surface coverage. The complexes found were monodentate binuclear, monodentate mononuclear, and a non-protonated monodentate mononuclear complex (Elzinga and Sparks, 2007). Kwon and Kubicki (2004) found that phosphate binds to iron oxides in different ways depending on pH: at pH 4-6 a diprotonated bidentate complex is formed; at pH 7.9, a monoprotonated monodentate complex is formed; and at pH 12.9, a deprotonated monodentate complex is formed.

2.4 X-Ray Absorption Fine Structure Spectroscopy

Researchers use direct and indirect methods to elucidate the adsorption mechanisms of Zn and other heavy metals to mineral surfaces (Grafe, 2004). Indirect methods rely on macroscopic data including kinetics, pH envelopes, and adsorption isotherms to provide information pertaining to the mechanism of adsorption (Grafe, 2004). Direct methods used to characterize heavy metal adsorption mechanisms include Fourier Transform Infrared Spectroscopy (FTIR), X-Ray Photoelectron Spectroscopy (XPS), and X-Ray Absorption Fine Structure Spectroscopy (XAFS). With XAFS spectroscopy, samples are bombarded with synchrotron produced, high energy X-rays that are capable of ejecting a core electron to the continuum, as process known as photoionization (Webb, 2001; Parsons et al., 2002). Following photoionization, several processes may occur to the excited atom. First, an outer shell electron may fill the shell vacancy resulting in the emission of fluorescent X-ray photon which is characteristic of the absorbing atom (Webb, 2001). The other major process is referred to as the Auger effect. In this process, the vacancy created by the ejected photoelectron is filled by an electron from a higher shell while the atom simultaneously emits another electron (Webb, 2001). X-ray energies are sufficiently high to eject one or more core electrons from an atom (Penner-

Hahn, 1999). The absorption edge refers to X-ray photon having just enough energy to free a bound electron in the atom. When electrons are in the most tightly bound shell (n=1), the edge is called K-edge (Mishra, 2006). Absorption edges are named according to the electron that is excited (K=1s; L_I=2s; L_{II}, L_{III} = 2p) (Penner-Hahn, 1999).

The XAFS spectrum is divided into two regions: the X-Ray Absorption Near Edge Structure (XANES) region and the Extended X-Ray Absorption Fine Structure (EXAFS) region. The separation of these two regions on the XAFS spectrum is loosely defined (Parsons et al., 2002). In general, the XANES region covers the pre-edge region to ~50eV above the absorption edge and the EXAFS region extends to 1000eV above the absorption edge (Parsons et al., 2002; Vasconcelos, 2006). The XANES region provides information on the chemical state of the absorbing atom, while the EXAFS region provides structural information such as coordination environment and nearest neighbor atoms surrounding the absorbing atom (Parsons et al., 2002; Vasconcelos, 2006). Figure 2.1 shows the XAFS spectrum of ZnO divided into pre-edge, XANES, and EXAFS regions.

2.4.1 Extended X-Ray Absorption Fine Structure Spectroscopy

The excited photoelectron with a wave number *k* is emitted away from the absorbing atom to neighboring atoms and is scattered back to the absorbing atom by electrons of neighboring atoms. The interactions of the scattering and backscattering photoelectron waves creates the EXAFS oscillations (Parsons et al., 2002). Figure 2.2 shows the K-edge EXAFS spectrum of ZnO. The EXAFS spectrum $\chi(k)$ is defined by the following formula:

$$\chi(k) = \frac{\mu(k) - \mu_0(k)}{\mu_0(k)} \qquad (2.1)$$

where μ(k) is the measured absorption coefficient of the sample under study, $\mu_0(k)$ is the atomic absorption coefficient, and k is the photoelectron wave vector emitted in the absorption process. The value of k is related to the binding energy of the photoelectron, or threshold energy (E_0) as:

$$k = [2m(E- E_0)/\hbar^2]^{1/2} \qquad (2.2)$$

Equation 2.1 can also be expressed as:

$$x^{(k)} = \sum \frac{N_j f_j(k) e^{-2k^2\sigma^2 j}}{kR_j^2} \sin\left[2kR_j + \delta_j(k)\right] \qquad (2.3)$$

where N_j is the number of atoms belonging to the jth coordination shell; R_j is the distance to the neighboring atom; f(k) and δ(k) are scattering properties of neighboring atoms (scattering amplitude and phase shift, respectively); and σ^2 (Debye-Waller factor) is the disorder in neighbor distance (Ford et al., 2005).

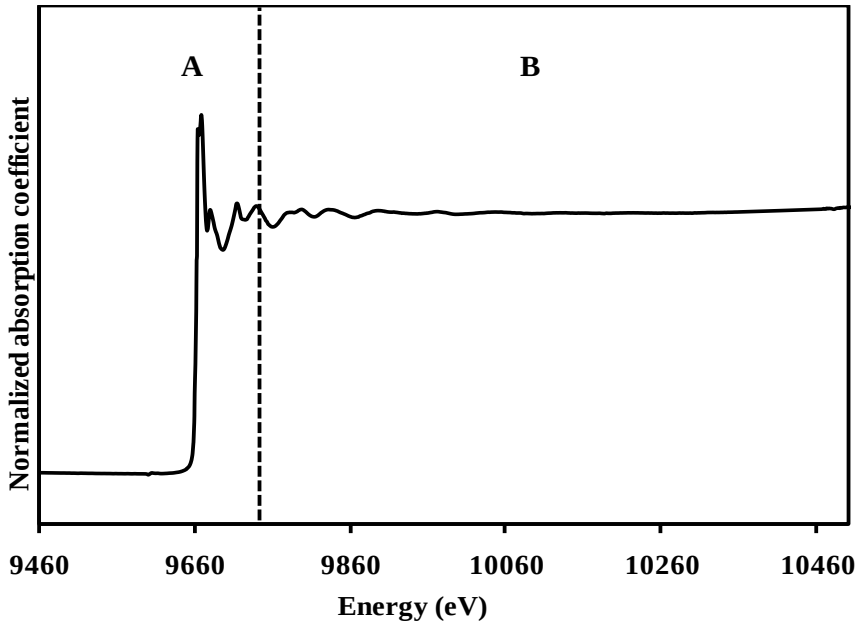

Figure 2.1 X-Ray absorption spectrum of zinc oxide (ZnO) showing the (A) X-Ray Absorption Near Edge Structure (XANES) region, and (B) Extended X-Ray Absorption Fine Structure (EXAFS) region.

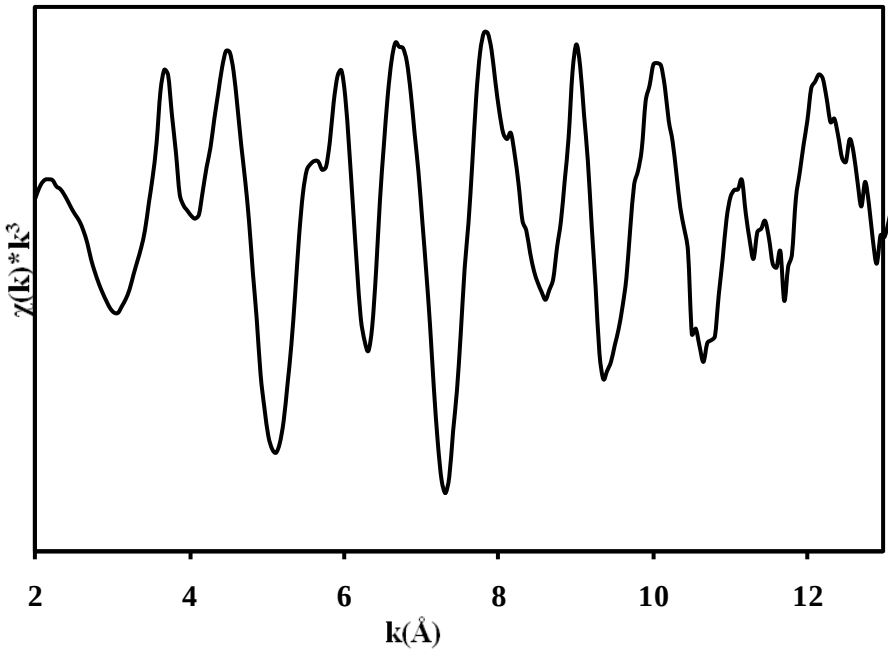

Figure 2.2 The EXAFS $\chi(k)$ function for ZnO.

The use of macroscopic techniques is essential to the understanding of metal adsorption behavior as impacted by ligands. However, microscopic techniques such XAFS spectroscopy are valuable tools that allow us to elucidate the mechanisms of metal adsorption onto various mineral surfaces. EXAFS spectroscopy has been used to characterize adsorption mechanisms of metals to phyllosilicate and oxide mineral surfaces. Grafe et al. (2007) found that Cd was adsorbed to kaolinite predominantly in the form of outer sphere complexes, while Pb formed polymeric complexes bond via edge sharing to the Al octahedra. Similarly, Vasconcelos et al. (2008) confirmed outer sphere complex formation of Cd with the kaolinite surface. Nachtegaal and Sparks (2004) on the other hand found that Zn formed inner sphere complexes with kaolinite at pH 7.0 and outer sphere at pH 5.0. Few studies however have investigated the impact of ligands on the adsorption mechanisms of metals to mineral surfaces, particularly kaolinite. In oxide minerals, Collins et al. (1999) characterized the adsorption mechanisms of Cd sorbed to

goethite in the presence of organic and inorganic ligands. Various studies have investigated the impact of ligands on the formation of surface precipitates. For instance, the impact of citrate on Ni-layered double hydroxide (LDH) formation in gibbsite was investigated by Yamguchi et al. (2002). Similarly, the impact of humic acid on layered double hydroxide (LDH) formation in kaolinite was investigated by Nachtegaal and Sparks (2003).

2.5 Zn Adsorption to Mineral Surfaces

2.5.1 Definition

Adsorption is the two-dimensional accumulation of a dissolved substance (adsorbate) at the solid (adsorbent) and water interface. Surface precipitation is the three-dimensional growth of an adsorbate on the surface of adsorbent, which begins to dominate as the concentration of adsorbate to adsorbent (surface loading) is increased. Absorption is the diffusion of a dissolved substance into the three-dimensional network of adsorbent. As it is very often difficult to identify the retention mechanism (adsorption, precipitation, or absorption) of a dissolved substance, the process is simply referred to as “sorption” (Sparks, 1995; Bradl, 2004; Essington, 2004). Heavy metals adsorb to mineral surfaces by either losing their primary hydration shell upon adsorption forming inner sphere complexes or by retaining their waters of hydration forming outer sphere complexes. Distinguishing between the different forms of complexes is crucial to the understanding of metal mobility and bioavailability. Metals forming inner sphere complexes are immobile and therefore difficult to desorb except at high pH values. However, metals forming outer sphere complexes are easily desorbed because no direct chemical bonds are formed (Sparks, 1995; Brown et al., 1999; Trivedi et al., 2001; Essington, 2004). Inner sphere complexes result in the formation of chemical bonds between the metal and mineral surface functional groups. The complex can be either a monodentate, bidentate or tridentate depending on the

number of chemical bonds formed. Typically, the more bonds formed the more difficult the metal is desorbed (Brown et al., 1999). As with other heavy metals, the nature of complexes formed between Zn and mineral surfaces at the water/mineral interface impacts its bioavailability, toxicity, reactivity and transport in soils and waters (Roberts et al., 2003).

2.5.2 Factors Influencing Zn Adsorption

Properties of the soil solution that impact the adsorption of heavy metals to mineral surfaces include pH, ionic strength, loading rate, counter ions, and competing ions (Harter and Naidu, 2001). The following sections discuss the impact of soil properties impacting Zn adsorption and that are of interest to this study.

2.5.2.1 pH

Minerals containing variable charge surfaces have surface charge that varies with pH to maintain constant potential (Harter and Naidu, 2001). pH is therefore a very important factor that impacts the adsorption of metals to variable charge surfaces. With increase in pH, enhanced adsorption of metals to variable charge surfaces is observed as a result of increase in the availability of sites for adsorption or by changing the concentration of metal species (hydrolysis) (Violante et al., 2003). Metal ions exhibit marked increases in adsorption (0 to 100%) at the pH range in which metal hydrolysis takes place. (James et al., 1975; Crawford et al., 1997; Srivastava et al., 2005). James and Haley (1972) indicated that adsorption is abruptly enhanced by hydrolysis because metal hydrolysis lowers the ionic charge and decreases the ion-solvent interaction, causing the ions to approach closer to the interface, hence resulting in greater coulombic energies. Zn adsorption to birnessite increased from 50 to 100% in the pH range from 4 to 7 (Power et al., 2005). Similar trends were reported for Zn adsorption to gibbsite and silica (Roberts et al., 2003). The effect of pH on Cu and Pb adsorption is more marked than for other

metals such as Cd, Mn, Ni, and Zn due to their greater capacity to form inner sphere complexes at the edge sites. This is due to their ability to hydrolyze, where the hydrolysis constant (pK_h) for Cu, Pb, Zn, Ni and Cd is 7.9, 7.7, 9.0, 9.9, and 10.1, respectively (Malandrino et al., 2006).

pH also impacts the adsorption mechanisms of Zn to various mineral surfaces. Using X-Ray Absorption Fine Structure (XAFS) spectroscopic analysis, Zn was found to form corner sharing monodentate binuclear complexes with ferrihydrite at pH below 6.5. With increase in pH above 6.5, sorption mechanisms were dependent on sorption densities where corner sharing complexes were formed at low densities and Zn polynuclear complexes at high densities (Trivedi et al., 2004).

pH was also found to impact the first shell coordination environment of Zn. EXAFS spectral analysis indicates that Zn may form tetrahedral, octahedral, or a mixture of both forms with first shell oxygen atoms upon adsorption to various mineral surfaces. The coordination form is determined by the first shell Zn-O interatomic radial distance, where values characteristic of tetrahedral and octahedral coordination range from 1.92 to 1.99ºA and 2.02 to 2.12ºA, respectively (Roberts et al., 2003, Waychunas et al., 2002). A transition from one form to the other might occur depending on factors such as pH and sorption density. Zn has a completely filled d shell and therefore it does not lose or gain energy when it changes from octahedral to tetrahedral coordination. Upon changing from octahedral to tetrahedral, 2 water molecules come off and entropy is gained (Nachtegaal and Sparks, 2004). It has been reported that with increase in pH to and above neutral values, Zn adsorbed onto iron oxides and other minerals exhibits a Zn-O first shell coordination transition from octahedral to predominantly tetrahedral (Lee and Anderson, 2005; Roberts et al., 2003; Bochatay and Persson, 2000). In addition, Waychunas et al. (2002) reported that this transition is favored as a result of increase in the oxygen bond

valence sum to ~2.0 as opposed to ~1.83 for octahedral coordination. Bochatay and Persson (2000) indicate that this transition could be a possible explanation for the extensive hydrolysis that Zn(II) exhibits upon adsorption to iron oxides.

2.5.2.2 Ionic Strength

The dependence of metal adsorption on pH and ionic strength can be used to differentiate between cation exchange (outer sphere adsorption) and layer edge adsorption (inner sphere adsorption). At high ionic strength the electrolyte ions (commonly Na^+ ions) compete with the adsorptive ions for the planar sites and adsorption therefore becomes more pH dependent. At low ionic strength, sorption is less pH dependent and adsorption is predominantly outer sphere if pH is low (Strawn and Sparks, 1999; Schlegel et al., 2001). Zn was found to form inner sphere surface complexes on hectorite edges at high ionic strength, and both inner and outer sphere complexes at low ionic strength and pH 6.5 (Schlegel et al., 2001). Similar results were reported for Pb adsorption to montmorillonite (Strawn and Sparks, 1999) and Co adsorption to montmorillonite (Papelis and Hayes, 1996). In the study conducted by Schlegel et al. (2001), Polarized-EXAFS spectroscopic analysis showed that at low ionic strength (0.01M $NaNO_3$), Zn adsorption changed from predominantly outer sphere to predominantly inner sphere with increase in reaction time to 120hrs and at pH 6.5. It was concluded that Zn is initially adsorbed on the planar sites of hectorite and then migrates to layer edges. In oxide minerals, Zn adsorption to ferrihydrite, goethite, and manganite was found to be independent of ionic strength, indicating that inner sphere complexation was the main mechanism of adsorption (Trivedi et al., 2001; 2004; Li et al., 2004).

2.5.2.3 Loading Rate

Surface loading was found to impact the adsorption mechanisms of Zn to mineral surfaces. In a Zn adsorption to ferrihydrite study, bidentate mononuclear complexes dominated at high surface loading and pH values above 5, whereas monodentate mononuclear complexes were dominant at lower surface loading and lower pH values (Dyer et al., 2003; Trivedi et al., 2003). In hematite nanopartices, Zn formed bidentate mononuclear complexes at pH 5.5 and low surface loading (Γ=1.1 μmol/m^2), whereas formed a mixed-metal hydrotalcite like coprecipitate at high loading (Γ=3.38 μmol/m^2) (Ha et al., 2009). In alumina powders, inner sphere bidentate complexes of Zn dominated at low densities and hydrotalcite type precipitates formed at high sorption densities (Trainor et al., 2000). The influence of surface loading on adsorption mechanisms of metals other than Zn has also been investigated. Arsenate adsorption on goethite was found to form different complexes depending on the surface coverage level. At low surface coverage monodentate surface complexes dominated, whereas bidentate mononuclear and bidentate binuclear complexes dominate at high surface coverage with monolayer capacity (O'Reilly et al., 2001). In accordance, Pb sorption studies on ferrihydrite have also shown that bidentate mononuclear surface complexes tend to dominate with increase in surface loading and in pH values above 5 (Trivedi et al., 2003).

2.5.2.4 Effect of Organic Ligands on Heavy Metal Adsorption

The expected adsorption trend of acid anion ligands to variable charge surfaces is increase in adsorption with pH decrease. Citrate adsorption to goethite strongly increased with pH decrease below the PZC of 9.2 (Geelhoed et al., 1998). The maximum adsorption of acid anions tends to occur at pH values close to their pKa values (Martinez et al., 1998).

In the soil solution, protons from organic acids may dissociate to form negatively charged ligands capable of binding heavy metals. Ligands may enhance or inhibit metal adsorption to mineral surfaces depending on factors such as pH, nature of ligand, surface properties of sorbent, and concentration of ligand and heavy metal (Violante et al., 2003; Yamaguchi et al., 2001). In general, ligands play an inhibitory role under conditions in which they compete with the mineral surface for the metal and form soluble complexes that are non adsorbable. On the other hand, ligands may enhance metal adsorption by forming metal-ligand-surface ternary complexes, by increasing the surface electrostatic potential or by formation of metal-ligand precipitates (Davis and Bhatnagar, 1995; Collins et al., 1999). The net impact of an organic ligand on the adsorption of metals is dependent on the relative strength of the surface and solution complexes formed; adsorption is decreased when formation of surface complexes are not able to compete with stable solution complexes (Schwab et al., 2005). For example, citrate was found to enhance Cd adsorption to Al_2O_3 in the pH range from 3.5-7.2 (Boily and Fein, 1996), while it reduced Ni adsorption to gibbsite at neutral pH (Yamaguchi et al., 2002) and reduced Cd^{+2} adsorption onto kaolinite in the pH range from 5.0 to 8.0 (Liao, 2006; Lackovic et al., 2004). The degree to which Cd^{+2} is suppressed is dependent on the citric acid: Cd^{+2} ratio; the higher the ratio the more adsorption is suppressed (Lackovic et al., 2004).

Low molecular weight ligands differ in terms of their impact on heavy metal adsorption to mineral surfaces depending on their ability to complex metals (formation constants with metals). Buerge-Weirich et al. (2003) found that oxalate decreased Cu and Ni adsorption to goethite at pH above 6.0 more than pyromelliate as a result of the former being a stronger complexant. Wu et al. (2003) showed that EDTA had a higher capacity to decrease Pb adsorption to goethite than citric acid as a result of the former being a stronger metal chelator than the latter.

It was concluded that the stronger the chelator, the less Pb is adsorbed to goethite. Violante et al. (2003) indicated that the critical concentration of a low molecular weight organic ligand to prevent the adsorption of heavy metals is dependent on the chelating ability of ligand for a metal, pH, and sorbent surface properties. They also found that the sequence of addition of metal and ligand impacts metal adsorption. When tartrate was added before Pb, more Pb was adsorbed to mixed Fe/Al oxides than when Pb was added before or alone. They hypothesized that the added tartrate anion increased the surface negative charge and hence promoted Pb adsorption.

2.5.2.5 Effect of Siderophores on Zn Adsorption

Siderophores impact the adsorption of Zn and other heavy metals to clay mineral surfaces. Desferrioxamine B, a hydroxamate siderophore that occurs in soil, was found to enhance Zn adsorption to montmorillonite and reduce adsorption to kaolinite over the pH range of 4 – 10. Addtionally, desferrioxamine B showed strong affinity to montmorillonite and low affinity to kaolinite in the same pH range (Neubauer et al., 2000; Hepinstall et al., 2005). In another study, desferrioxamine B adsorption to kaolinite exhibited a cation-like behavior with increase in adsorption above kaolinite's pH_{PZNPC} of 4.9 (Rosenberg and Maurice, 2003). With metals other than Zn, it was found that a variety of siderophores reduced the adsorption of Pb and Cd to kaolinite. Adsorption of Pb decreased above pH 6 and Cd adsorption decreased above pH 8 (Hepinstall et al., 2005).

In iron oxide minerals, Desferrioxamine B reduced the adsorption of Zn to ferrihydrite with the effect being more pronounced as pH increased (Neubauer et al., 2002). This is maybe due to repulsion between the positively charged ferrihydrite surface and the positively charged Zn-desferrioxamine B at neutral pH (Neubauer et al., 2002). Adsorption of desferrioxamine B to goethite was found to be small at pH less than 7(1.5 μm/g) and slightly increased to 2.51 μm/g at

higher pH. This may be explained by the pKa_4 of 8.3 for desferrioxamine B conversion from the cationic form to the neutral species (Kraemer et al., 2002).

2.5.2.6 Effect of Humic and Fulvic Acids on Zn Adsorption

Adsorption of humic acid on mineral surfaces has been shown to increase with pH decrease, as the negatively charged humic acid adsorbs to the positively charged surface sites of minerals in accordance with the anion exchange mechanism between carboxyl groups of humic acid and the inorganic hydroxyl groups of minerals (Murphy and Zachara, 1995). First, surface hydroxyl groups on the mineral surfaces are protonated allowing the formation of outer sphere complexes between humic acid and the mineral surface. Then, a ligand exchange mechanism develops allowing the formation of an inner sphere complex (Petrovic et al., 1999; Liu and Gonzalez, 1999; Murphy and Zachara, 1995; Davis and Bhatnagar, 1995). The sorption of humic acid onto mineral surfaces appears to be dependent on the type of humic acid as adsorption is proportional to the carbon content but inversely proportional to the O/C ratio and hydrophilicity. As an example, marine humic substances are less aromatic in character and less hydrophobic than soil humic substances, which makes humic substances of marine origin less adsorbed (Petrovic et al., 1999).

As humic acid is adsorbed on the oxide surface, humic acid sites of high affinity for metals become available for the formation of ternary complexes (Lai et al., 2002). Carboxylic acid groups of humic acid are ionized at low pH, thus increasing surface charge and the amount of metal adsorbed (Kummert and Stumm, 1980).

Lai et al. (2002) reported enhanced adsorption of Cd to goethite in the presence of humic acid over the pH range from 2-6. Arias et al. (2002) reported enhanced adsorption of Cd and Cu onto kaolinite in the presence of humic acid. However, studies have shown that the role of humic

acid on metal adsorption may deviate from the general consensus. Zuyi et al. (2000) reported that fulvic acid did not impact the adsorption of Zn to Al_2O_3 at pH < 7. They concluded that the effect of humic substances on metal sorption was dependent on the nature of both the oxide and humic substance. Lai et al. (2002) reported that humic acid may bind directly to the iron oxide and block the metal adsorption sites, which may decrease metal adsorption to the mineral surface.

In natural water systems, trace metal ions were reported to have higher affinity for the functional groups of humic substances attached to oxide surfaces than for the oxide surface sites (Davis and Leckie, 1978). Similar results were reported by Vermeer et al. (1999) who showed that metal ions have higher affinity for a mixture of humic acid and iron oxides than for oxides only.

2.6 Formation of Metal Surface Precipitates

When released into the soil, metals such as Zn may adsorb to various soil components such as clay minerals, organic matter, Fe and Mn oxides, and to carbonates. During the process of metal sorption to clay minerals and under ambient soil conditions, metal surface precipitates may also form. In other words, metal sorption onto soil minerals not only results in adsorbed (outer- and inner-sphere complexes) phases but may also result in precipitated phases occurring at the surfaces of phyllosilicate minerals.

These 'precipitate phases' or 'newly forming mineral phases' include layered double hydroxide (LDH), phyllosilicate type and hydroxide type precipitates (Ford et al., 1999, Voegelin et al., 2002; Manceau et al., 2005). Another type of layered Zn phase may form under acidic conditions when Zn enters the Al-hydroxy (Al-OH) interlayers of clay minerals (Voegelin et al., 2005; Scheinost et al., 2002). What all these phases share in common is the incorporation of Zn into octahedral sheets of layered minerals (Voegelin et al., 2005).

The LDHs are composed of positively charged octahedral hydroxide layers with the divalent and trivalent metals mixed in the octahedral sites and anions balancing the positive layer charge and occupy the interlayer region. The general structural formula of a metal-Al layered double hydroxide is $[Me^{+2}_{1-X}Me^{+3}_{X}(OH)_2]^{X+}\cdot(x/n)A^{-n}\cdot mH_2O]$ where Me^{+2} can be Mg(II), Ni(II), Co(II), Zn(II), Mn(II) or Fe(II) and Me^{+3} can be Al(III), Fe(III), and Cr(III). A^{-n} is the interlayer anion such as Cl^-, Br^-, I^-, NO_3^-, OH^-, ClO_4^-, and CO_3^{-2}. (Scheidegger et al., 1998; Ford and Sparks, 2000; Trainer et al., 2000; Scheckel and Sparks, 2001; Nachtegaal and Sparks, 2004). To illustrate, a Zn-Al layered double hydroxide (LDH) has the structural formula $Zn_2Al(OH)_6[CO_3]_{0.5}$ and is composed of sheets of edge sharing octahedra separated by anions between the interlayer spaces (Ford et al., 1999, Voegelin et al., 2002 and Manceau et al., 2005). With time, the Zn LDH gradually becomes more stable with respect to weathering leading to the long term sequestration of Zn. This occurs when anionic species in the interlayer space of LDH is replaced by silica polymers (Manceau et al., 2000; Voegelin et al., 2005). Graphical presentations of LDH, Zn phyllosilicate, and Zn in Al hydroxyl interlayered phyllosilicates can be found in Voegelin et al. (2005) and Scheinost et al. (2002).

Studies on Zn speciation have confirmed the formation of Zn-layered double hydroxide (LDH) and Zn-phyllosilicate phases in contaminated soils. Voegelin et al. (2005) studied the transformation of Zn with time (over a 4 year period) in a field soil artificially contaminated with ZnO. Using the EXAFS signal from varying time periods, it was found that 2 months after contamination the soil spectrum changed dramatically and that only minor spectral features relating to ZnO were present after 4 months. After 9 months, spectral features relating to Zn-LDH and Zn-phyllosilicate could be observed with a small splitting in the peak at $3.5A^{o-1}$ as well

as the shape of spectrum above $7A^{o-1}$. No significant changes in Zn speciation occurred from 9 to 48 months. This study concluded the rapid dissolution of ZnO and the rapid formation of layered precipitates; i.e., Zn-LDH and Zn phyllosilicate. It was shown that half of the total Zn in the soil was sequestered into a precipitate of mostly Zn-LDH type (>75%) and a minor fraction of Zn-phyllosilicate (<25%).

Various metal adsorption studies have shown that there is an initial rapid adsorption reaction that is often followed by a slower sorption reaction. The slower sorption process can be attributed to different mechanisms including formation of surface precipitates, diffusion into micro porous solid phase, and surface diffusion from low to high affinity adsorption sites (Voegelin et al., 2002, Scheidegger et al., 1998).

Lee et al. 2004 showed that Zn sorption onto montmorillonite was initially rapid where 40% of Zn was taken up within the first 20 minutes. 80% of the Zn was taken up after 6 months of exposure time. Results have lead to the conclusion that adsorption to available surface sites takes place during the rapid uptake and that slower uptake could be due to sorption to less reactive sites or formation of surface precipitates. Fourier transformed EXAFS spectra showed that there are two distinct peaks representing the first coordination shell of the zinc atom one at 1.7 Aº and 2.8 Aº. The presence of the second peak indicates the formation of multinuclear surface complexes or surface precipitates. The intensity of the second peak generally increased with increasing reaction time especially after 20 days. A Zn phyllosilicate like precipitate (Zn-Si coprecipitate) formed when samples reacted over 20 days and this formation of surface precipitates could account for the slow sorption reaction. Voegelin et al. (2002) also used XAFS and confirmed that the formation of Zn-LDH other than micropore diffusion, was the reason behind slow metal sorption. Scheidegger et al. (1998) however found that adsorption and Ni-Al

LDH formation can occur simultaneously and within minutes. This was this case for the Ni/pyrophyllite and Ni/Gibbsite systems but cannot be extrapolated to other systems like the Ni/montmorillonite system where a Ni – Al LDH formed after 40 minutes.

The formation of LDH and phyllosilicate phases occur at neutral to alkaline pH. In acidic to neutral environments, it is the fast and reversible cation exchange reactions that dominate the sorption of metals like Zn. With increasing pH values slow sorption reactions and Zn incorporation into neo formed precipitates tend to become more prominent (Nachtegaal and Sparks, 2004; Voegelin et al., 2002).

As mentioned in the beginning of this section that under acidic conditions Zn may form another type of layered phase. The formation of a Zn containing phyllosilicate, layered double hydroxide, or formation of inner sphere sorption complexes are unlikely under strongly acidic conditions. Scheinost et al. (2002) studied Zn speciation in a strongly acidic (pH 3.9) smelter contaminated soil. In the subsoil, it was found that almost 50% of the Zn was incorporated by hydroxyl-Al interlayers of phyllosilicates where Zn-Al hydroxide layers are sandwiched between negatively charged phyllosilicate layers. The XAFS spectra of synthesized Zn hydroxy - interlayered montmorillonite (HIM) was used to match the subsoil spectra.

Release of Al and Si from clay mineral weathering controls metal precipitate formation and transformation (Ford et al., 1999). Voegelin et al. (2005) indicated that the availability of Al and Si favor the formation of Zn-LDH and that their supply is controlled by the dissolution of primary and secondary minerals (Voegelin et al., 2005).This is in agreement with Scheidegger et al. (1998) who found that the dissolution of clay and Al oxide minerals releasing Al into the solution is the rate controlling factor for the formation of Ni-Al LDH. Metal sorption on clay minerals actually promotes the dissolution of Al. Ford et al. (1999) studied surface precipitate

formation during metal sorption to clay minerals. They found that the LDH is meta-stable and transforms to a phyllosilicate with time. It was hypothesized that silica derived from clay mineral weathering replaces the nitrate (or anionic species) in the interlayer space of the LDH transforming it into a phyllosilicate.

It has been indicated that surface precipitates form at solution conditions undersaturated with respect to homogeneous precipitation (Nachtegaal and Sparks, 2004). For example, Zn LDH precipitates are formed at Zn concentrations below the solubility products of the Zn hydroxide (Voegelin et al., 2002). Scheidegger et al. (1998) reported that formation of polynuclear surface phases have been observed at pH values below that of metal hydroxide precipitate formation and at surface loadings below a theoretical monolayer coverage. A Ni Al LDH phase formed at surface loadings as low as 0.7 mmol m^{-2} corresponding to 5% of monolayer coverage.

2.7 Fate of Heavy Metals in Sewage Sludge

Application of sewage sludge is known to improve chemical and physical properties of soils such as pH, bulk density, porosity, and water retention. It is a source for plant nutrients with high organic matter content, low C/N ratio and high N and P content (Adani and Tambone, 2005). In addition to fertility value for arable farming, application of sewage sludge to soils is an economically and environmentally sound alternative to landfill disposal and incineration (Stacey et al., 2001). Nearly half of the sewage sludge produced in the United States is used for land application. Nevertheless, it is a source of heavy metals most commonly Pb, Ni, Cd, Cr, Cu and Zn (Silveira et al., 2003).

Due to the presence of chemically active surfaces in sewage sludge such as Fe/Mn oxides and organic matter, addition of sewage sludge to soil is not simply the addition of trace metals to

soils. Metals added to soils as constituents of biosolids are less phytoavailable than when metal salts alone are added to soils (Hettiarchchi et al., 2003). The phases responsible for the hindering of metal availability in biosolid amended soils remains disputed (Li et al., 2001). While some studies have postulated that it is the organic fraction of biosolids that plays this role of reduced metal phytoavailability, other studies have indicated that the inorganic surfaces added to biosolids during processing are the responsible phases (Hettiarachchi et al., 2006; Li et al., 2001).

This uncertainty has led to a controversy over the consequences of long term application of biosolids. If the organic fraction was the responsible phase for reduced metal bioavailability, then the long term application of biosolids would result in the release of heavy metals into the soil due to organic matter mineralization, also known as the 'Time Bomb Hypothesis'. If on the other hand, it were the inorganic fractions of biosolids (carbonates, phosphates, amorphous Fe and Mn oxides) that were responsible for the reduced availability of metals, then the long term application of biosolids would present no hazard, due to the high adsorptive capacity of these phases. This is known as the 'Protection' hypothesis. As a matter of fact, legislative standards for sludge use in the United States partly depend on this 'Protection' hypothesis. To date, the long term fate of metals from biosolid application is still not understood (Li et al., 2001; Bergkvist and Jarvis, 2004; Bergkvist et al., 2005; Hettiarachchi et al., 2006).

Various studies have investigated trace metal availability in sewage sludge as a result of organic matter degradation. Stacey et al. (2001) found that sewage sludge decomposition results in the release of Zn and Cd to plant available pools. Hettiarachchi et al. (2006) used μ-XANES and μ-XRF to identify Fe and Mn oxides associated with metals before and after the removal of organic carbon from sewage sludge. Their study suggested that even if metals were associated

with the organic fraction of sewage sludge, the degradation of organic matter will not result in substantial increase in metal availability due to complexation with Fe and Mn oxides, thus negating the 'Time Bomb' hypothesis. In a field study, Oliver et al. (2005) investigated Cu availability in soils amended with sewage sludge for 7 years. It was found that organic matter degradation with time did not result in significant increases in Cu availability probably due to retention by inorganic fractions, which also seemed to refute the TB hypothesis. Bergkvist and Jarvis (2004) modeled organic carbon dynamics to predict scenarios under which the fate of Cd would behave as predicted by either the PT or TB hypothesis. It was reported that either of the two scenarios were likely to occur depending on the ratio of sludge adsorption capacity to soil adsorption capacity, proportion of sludge adsorption capacity contributed by inorganic fraction, and Cd sludge loading.

The change in heavy metal adsorption behavior of SS with time may provide indirect evidence to the long term fate of metals in sewage sludge. Antoniadis et al. (2007) found that incubating SS amended soils for around 1year resulted in reduced organic C by 31%, and changed the adsorption behavior of Cd and Zn. Complete removal of OC from SS was found to reduce Cd adsorption in SS but not in sewage sludge amended soils, indicating the importance of both organic C and Fe/Mn oxides in retaining Cd (Hettiarachchi et al., 2003). Metals in biosolids are found in various chemical forms; either in exchangeable form or bound to various inorganic or organic fractions. There is need to investigate the impact of OM degradation on the distribution of metals in sewage sludge, which may in effect provide insight as to the long-term fate of heavy metals in sewage sludge.

2.8 References

Adani, F. and F. Tambone. 2005. Long-term effect of sewage sludge application on soil humic acids. Chemosphere 60: 1214–1221.

Alvarez-Puebla, R.A., C. Valenzuela-Calahorro, and J.J. Garrido. 2004. Cu(II) retention on a humic substance. J. Colloid Interf. Sci. 270 (1): 47–55.

Antoniadis, V., C.D. Tsadilas, and D.J. Ashworth. 2007. Monometal and competitive adsorption of heavy metals by sewage sludge-amended soil. Chemosphere 68: 489–494.

Arai, Y., and D.L. Sparks. 2001. ATR–FTIR Spectroscopic Investigation on Phosphate Adsorption Mechanisms at the Ferrihydrite–Water Interface. J. Colloid Interf. Sci.241: 317–326.

Arias, M., M.T. Barral, and J.C. Mejuto. 2002. Enhancement of copper and cadmium adsorption on kaolin by the presence of humic acids. Chemosphere 48:1081–1088.

Barak, P., and P.A. Helmke. 1993. The chemistry of zinc. In: Robson A.D., ed. Zinc in soil and plants. Dordrecht, the Netherlands: Kluwer Academic Publishers. 1–13.

Bergkvist, P., and N. Jarvis. 2004. Modeling organic carbon dynamics and cadmium fate in long-term sludge-amended soil. J. Environ. Qual. 33:181–191.

Bergkvist, P., D. Berggren, and N. Jarvis. 2005. Cadmium solubility and sorption in a long-term sludge-amended arable Soil. J. Environ. Qual. 34:1530–1538.

Bochatay, L., and P. Persson. 2000. Metal ion coordination at the water-manganite (γ-MnOOH) interface II. An EXAFS study of zinc(II). J. Colloid Interf. Sci. 229: 593-599.

Boily, J.F., and J.B. Fein. 1996. Experimental study of cadmium-citrate co-adsorption onto α-Al_2O_3. Geochim. Cosmochim. Ac. 60(16):2929-2938.

Bolan, N.S., R. Naidu, S. Mahimairaja, and S. Baskaran. 1994. Influence of low-molecular-weight organic acids on the solubilization of phosphates. Biol. Fert. Soils. 18: 311–319.

Bolt, G.H., and M.G.M. Bruggenwert. 1976. Soil chemistry. A. Basic elements, Part 1. Elsevier, Amsterdam, NL.

Bossier, P., M. Höfte, and W. Verstraete. 1988. Ecological significance of siderophores in soil. Adv. Microb. Ecol. 10:358–414.

Bradl, H.B. 2004. Adsorption of heavy metal ions of soils and soils constituents. J. Colloid Interf. Sci. 277: 1–18.

Brown, G.E., A.L. Foster, and J. D. Ostergren. 1999. Mineral surfaces and bioavailability of heavy metals: A molecular-scale perspective. Proc. Natl. Acad. Sci. 96: 3388–3395.

Buerge-Weirich, D., P. Behra, and L. Sigg. 2003. Adsorption of copper, nickel, and cadmium on goethite in the presence of organic ligands. Aquat. Geochem.. 9(2):65-85.

Collins, C.R., K.V. Ragnarsdottir, D.M. Sherman. 1999. Effect of inorganic and organic ligands on the mechanism of cadmium sorption to goethite. Geochim. Cosmochim. Ac. 63(19): 2989-3002.

Crawford, R.J., D.E. Mainwaring, and I.H. Harding. 1997. Adsorption and coprecipitation of heavy metals from ammoniacal solutions using hydrous metal oxides. Colloids Surf. A: Physicochem. Eng. Aspects. 126: 167–79.

Crowley, D.E., Y.C. Wang, C.P.P. Reid, and P.J. Szansiszla. 1991. Mechanism of iron acquisition from siderophores by microorganisms and plants. Plant Soil 130:179–198.

Davis, A.P., and V. Bhatnagar. 1995. Adsorption of cadmium and humic acid onto hematite**.** Chemosphere 30: 243–256.

Davis, J.A. and J.O. Leckie. 1978. Effect of adsorbed complexing ligands on trace metal uptake by hydrous oxides. Environ. Sci. Technol. 12(12): 1309-1315.

Dyer, J.A., P. Trivedi, N.C. Scrivner, and D.L. Sparks. 2003. Lead Sorption onto Ferrihydrite. 2. Surface Complexation Modeling.Environ. Sci. Technol. 37:915-922.

Eisler, R. 1993. Zinc hazards to fish, wildlife, and invertebrate: a synoptic review. In Biological Report 10. Washington, DC: US Department of Interior, Fish and Wildlife Service.

Elzinga, E.J., and D.L. Sparks. 2007. Phosophate adsorption onto hematite: An in situ ATR-FTIR investigation of the effects of pH and loading level on the mode of phosphate surface complexation. J. Colloid Interf. Sci. 308: 53-70.

Essington, M.E. 2004. Soil and water chemistry: An integrative approach. CRC Press, Boca Raton, FL.

Ford, R.G., A.C. Scheinost, K.G. Scheckel, and D.L. Sparks. 1999. The Link between Clay Mineral Weathering and the Stabilization of Ni Surface Precipitates. Environ. Sci. Technol. 33: 3140-3144.

Ford, R.G., and D.L. Sparks. 2000. The nature of Zn precipitates formed in the presence of pyrophyllite. Environ. Sci. Technol. 34: 2479-2483.

Ford, R.G., R.T. Wilkin, K.G. Scheckel, C.J. Paul, F. Beck, P. Clark, and T. Lee. 2005. Field study of the fate of arsenic, lead, and zinc at the ground- water/surface-water interface (91 pp, 6.4M), EPA Report, U.S. Environmental Protection Agency, Cincinnati, OH, EPA/600/R-05/161.

Geelhoed, J.S., T. Hiemstra, and W.H. Vanriemsdijk. 1998. Competitive interaction between phosphate and citrate on goethite. Environ. Sci. Technol. 32: 2119-2123.

Gräfe, M. 2004. Ph.D. Dissertation. 2004. Formation and occurrence of metal-arsenate precipitates in the environment. University of Delaware.

Gräfe, M., B. Singh, and M. Balasubramanian. 2007. Surface speciation of Cd(II) and Pb(II) on kaolinite by XAFS spectroscopy. J. Colloid Interf. Sci. 315: 21-32.

Guerinot, M.L. 1994. Microbial iron transport. Annu. Rev. Microbiol. 48: 743–772.

Ha, J., T.P. Trainor, F. Farges, and G.E. Brown. 2009. Interaction of aqueous Zn(II) with hematite nanoparticles and microparticles. Part 1. EXAFS study of Zn(II) adsorption and precipitation. Langmuir. 25: 5574–5585.

Harter, R.D., and R. Naidu. 2001. An assessment of environmental and solution parameter impact on trace-metal sorption by soils. Soil Sci. Soc. Am. J. 65: 597–612.

Hepinstall, S.E., B.F. Turner, and P.A. Maurice. 2005. Effects of siderophores on Pb and Cd adsorption to kaolinite. Clay Clay Miner. 53(6): 557-563.

Hersman, L., T. Lloyd, and G. Sposito. 1995. Siderophore-promoted dissolution of hematite. Geochim. Cosmochim. Ac. 59 (16): 3327–3330.

Hettiarachchi, G.M., J.A. Ryan, R.L. Chaney, and C.M. LaFleur. 2003. Sorption and desorption of cadmium by different fractions of biosolids-amended soils. J. Environ. Qual. 32:1684–1693.

Hettiarachchi, G.M., K.G. Scheckel, J.A. Ryan, S.R. Sutton, and M. Newville. 2006. μ-XANES and μ-XRF investigations of metal binding mechanisms in biosolids. J. Environ. Qual. 35:342–351.

Hopkins, B.G., D.A. Whitney, R.E. Lamond, and V.D. Jolley. 1998. Phytosiderophore release by sorghum, wheat, and corn under zinc deficiency. J. Plant Nutr. 21:2623–2637.

Huang, Q., Z. Zhao, and W. Chen. 2003. Effects of several low-molecular weight organic acids and phosphate on the adsorption of acid phosphatase by soil colloids and minerals. Chemosphere. 52(3): 571-578.

James, R.O., and T.W. Healy. 1972. Adsorption of hydrolyzable metal ions at the oxide-water interface: III. A thermodynamic model of adsorption. Journal Colloid Interf. Sci. 40(1):65-81.

James, R.O., P.J. Stiglich, and T.L. Healy. 1975. Analysis of models of adsorption of metal ions at oxide/water interfaces**.** Faraday Discuss. Chem. Soc. 59: 142 – 156.

Jones, M. N., and N.D. Bryan. 1998. Colloidal properties of humic substances. Adv. Colloid Interf. 78: 1–48.

Jones, D.L. 1998. Organic acids in the rhizosphere—a critical review. Plant Soil. 205: 25-44.

Jones, D.L., P.G. Dennis, A.G. Owen, and P.A.W. van Hees. 2003. Organic acid behavior in soils—misconceptions and knowledge gaps. Plant Soil. 248: 31–41.

Jones, R., and M.S.E. Burgess. 1984. Zinc and cadmium in soils and plants near electrical transmission (hydro) towers. Environ. Sci. Technol. 18 (10): 731-734.

Juillot, F., C. Maréchal, M. Ponthieu, S. Cacaly, G. Morin, M. Benedetti, J.L. Hazemann, O. Proux, and F. Guyot. 2008. Zn isotopic fractionation caused by sorption on goethite and 2-Lines ferrihydrite. Geochim. Cosmochim. Ac. 72: 4886-4900.

Kalinowski, B.E., L.J. Liermann, S. Givens, and S.L. Brantley. 2000. Rates of bacteria-promoted solubilization of Fe from minerals: A review of problems and approaches. Chem. Geol. 169: 357–370.

Karltun, E. 1997. Modeling SO_4^{-2} surface complexation on variable charge minerals:I. H^+ and SO_4^{-2} exchange under different solution conditions. Eur. J. Soil Sci.48: 483-491.

Kraemer, S.M., J. Xu, K.N. Raymond, and G. Sposito. 2002. Adsorption of Pb(II) and Eu(II) by oxide minerals in the presence of natural and synthetic hydroxamate siderophores. Environ. Sci. Technol. 36: 1287– 1291.

Kraemer, S.M. 2004. Iron oxide dissolution and solubility in the presence of siderophores. Aquat. Sci. 66: 3–18.

Kummert, R., and W. Stumm. 1980. The surface complexation of organic acids on hydrous γ-Al_2O_3. J. Colloid Interf. Sci. 75(2):373-385.

Kwon, K.D., and J.D. Kubicki. 2004. Molecular orbital theory study on surface complex structures of phosphates to iron hydroxides: calculation of vibrational frequencies and adsorption energies. Langmuir. 20: 9249–9254.

Lackovic, K., M.J. Angove, J.D. Wells and B.B. Johnson. 2004. Modeling the adsorption of Cd(II) onto goethite in the presence of citric acid. J. Colloid Interf. Sci. 269(1): 37-45.

Lai, C.H., C.Y. Chen, B.L.Wei and S.H. Yeh. 2002. Cadmium adsorption on goethite-coated sand in the presence of humic acid. Water Res. 36: 4943–4950.

Lasat, M. 2000. Phytoextraction of metals from contaminated soil: a review of plant/soil/ metal interaction and assessment of pertinent agronomic issues. J. Hazardous Substance Research. 2: 5–25.

Lee, S. and P.R. Anderson. 2005. EXAFS study of Zn sorption mechanisms on hydrous ferric oxide over extended reaction time. J. Colloid Interf. Sci. 286: 82-89.

Lee, S., P.R. Anderson, G.B. Bunker, and C. Karanfil. 2004. EXAFS Study of Zn sorption mechanisms on montmorillonite. Environ. Sci. Technol. 38: 5426-5432.

Leong, J. 1986. Siderophores: their biochemistry and possible role in the biocontrol of plant pathogens. Annu. Rev. Phytopathol. 24:187–208.

Li, X., G. Pan, Y. Qin, T. Hu, Z. Wu, and Y. Xie. 2004. EXAFS studies on adsorption-desorption reversibility at manganese oxide-water interfaces II. Reversible adsorption of zinc on δ-MnO_2. J. Colloid interf. Sci. 271: 35-40.

Li, Z., J.A. Ryan, J.L. Chen, and S.R. Al-Abed. 2001. Adsorption of cadmium on biosolids-amended soils. J. Environ. Qual. 30:903–911.

Liao, M. 2006. Effects of organic acids on adsorption of cadmium onto kaolinite, goethite, and bayerite. Pedosphere. 16(2): 185-191.

Liu, A., and R.D. Gonzalez. 1999. Adsorption/desorption in a system consisting of humic acidm heavy metals, and clay minerals. J. Colloid Interf. Sci. 218: 225-232.

Lombnaes, P., A.C. Chang, and B.R. Singh. 2008. Organic ligand, competing cation, and pH effects on dissolution of zinc in soils. Pedosphere. 18(1): 92-101.

Malandrino, M., O. Abollino, A. Giacomino, M. Aceto, and E. Mentasti. 2006. Adsorption of heavy metals on vermiculite: Influence of pH and organic ligands. J. Colloid Interf. Sci. 299: 537–546.

Manceau, A., B. Lanson, M.L. Schlegel, J.C. Harge, M. Musso, L. Eybert-Berard, J.L. Hazemann, D. Chateigner, and G.M. Lamble. 2000. Quantitative Zn Speciation in smelter-contaminated soils by EXAFS spectroscopy. Am. J. Sci.. 300: 289–343.

Manceau, A., C. Tommaseo, S. Rihs, N. Geoffroy, D. Chateigner, M. Schlegel, D. Tisserand, M. Marcus, N. Tamura, and Z. Chen. 2005. Natural speciation of Mn, Ni, and Zn at the micrometer scale in a clayey paddy soil using X-ray fluorescence, absorption, and diffraction. Geochim. Cosmochim. Ac. 69(16): 4007–4034.

Martínez, C.E., and H.L. Motto. 2000. Solubility of lead, zinc, and copper added to mineral soils. Environ. Pollut. 107: 153-158.

Martinez, C.E., A.W. Kleinschmidt, and M.A. Tabatabai. 1998. Sulfate adsorption by variable charge soils: effect of low-molecular-weight organic acids. Biol. Fertil. Soils. 26: 157-163.

Mulligan, C.N., R.N. Yong, and B.F. Gibbs. 2001. Remediation technologies for metal-contaminated soils groundwater: an evaluation. Eng. Geol. 60: 193-207.

Murphy, E.M., and J.M. Zachara. 1995. The role of sorbed humic acid substances on the distribution of organic and inorganic contaminants in groundwater. Geoderma 67: 103-124.

Nachtegaal, M., and D.L. Sparks. 2003. Nickel sequestration in a kaolinite-humic acid complex. Environ. Sci. Technol. 37:529-534.

Nachtegaal, M., and D.L. Sparks. 2004. Effect of iron oxide coatings on zinc sorption mechanisms at the clay-mineral/water interface. J. Colloid Interf. Sci. 276: 13–23.

Neilands, J. B., and S. A. Leong. 1986. Siderophores in relation to plant disease. Annu. Rev. Plant Physiol. 37:187-208.

Neubauer, U., B. Mowack, G. Furrer, and R. Schulin. 2000. Heavy metal sorption of clay minerals affected by the siderophore desferrioxamine B. Environ. Sci. Technol. 34:2749–2755.

Neubauer, U., G. Furrer and R. Schulin, 2002. Heavy metal sorption on soil minerals affected by the siderophore desferrioxamine B: the role of Fe(III) (hydr)oxides and dissolved Fe(III). Europ. J. Soil Sci. 53: 45–55.

Ogner, G., and M. Schnitzer. 1970. Humic substances: fulvic acid-dialkyl phthalate complexes and their role in pollution. Science 170: 317.

Oliver, I.W., A. Hass, G. Merrington, P. Fine, and M.J. McLaughlin. 2005. Copper availability in seven Israeli soils incubated with and without biosolids. J. Environ. Qual. 34: 508-513.

O'Reilly, S.E., D.G. Strawn, and D.L. Sparks. 2001. Residence Time Effects on Arsenate Adsorption/Desorption Mechanisms on Goethite. Soil Sci. Soc. Am. J. 65:67–77.

Papelis, C., and K. F. Hayes 1996. Distinguishing between interlayer and external sorption sites of clay minerals using X-ray absorption spectroscopy. Coll. Surfaces 107: 89–96.

Parsons, J.G., M.V. Aldrich, and J.L. Gardea-Torresdey. 2002. Environmental and biological applications of extended X-ray absorption fine structure (EXAFS) and X-ray absorption near edge structure (XANES) spectroscopies. Appl. Spectrosc. Rev. 37(2): 187–222.

Peak, D., R.G. Ford, and D.L. Sparks. 1999. An *in situ* ATR-FTIR investigation of sulfate bonding mechanisms on goethite. J. Colloid Interf. Sci. 218:289-299.

Penner-Hahn, J.E. 1999. X-ray absorption spectroscopy in coordination chemistry. Coordination Chemistry Reviews. 190-192: 1101-1123.

Persson, P, and L. Lövgren. 1996. Potentiometric and spectroscopic studies of sulfate complexation at the goethite-water interface. Geochim. Cosmochim. Ac. 60(15): 2789-2799.

Petrovic, M., M. Kaštelan-Macan and A.J.M. Horvat.1999. Interactive sorption of metal ions and humic acids onto mineral particles.Water air soil poll. 111: 41–56.

Porter F. 1991. Zinc handbook — properties, processing and use in design. New York: Marcel Dekker, Inc.

Powell, P.E., G.R. Cline, C.P.P Reid, and P.J. Szaniszlo. 1980. Occurrence of hydroxamate siderphore iron chelators in soils. Nature. 287: 833-834.

Power, L.E., Y.Arai, and D.L. Sparks. 2005. Zinc adsorption effects on arsenic oxidation kinetics at the birnessite–water interface. Environ. Sci. Technol. 39:181–187.

Qin, F., X.Q. Shan, and B. Wei. 2004. Effects of low-molecular-weight organic acids and residence time on desorption of Cu, Cd, and Pb from soils. Chemosphere. 57 (4): 253-263.

Raymond, K. N., G. Muller, and B. F. Matzanke. 1984. Complexation of iron by siderophores. A review of their solution and structural chemistry and biological function. Top. Curr. Chem. 123:50–101.

Roberts, D. R., R.G. Ford and D.L. Sparks. 2003. Kinetics and mechanisms of Zn complexation on metal oxides using EXAFS spectroscopy. J Colloid Interf. Sci. 263(2): 364-376.

Robson, A.D. 1993**.** Zinc in Soils and Plants**.** Vol. 55, Proceedings of the International Symposium on Zinc in Soils and Plants'. Kluwer Academic publisher, The Netherlands.

Römheld, V. 1991. The role of phytosiderophores in acquisition of iron and other micronutrients in graminaceous species: An ecological approach. Plant Soil. 130: 127–134.

Rosenberg, D.R., and P.A. Maurice. 2003. Siderophore adsorption to and dissolution of kaolinite at pH 3 to 7 and 22ºC. Geochim. Cosmochim. Ac. 67 (2): 223-229.

Ryan, P.R., E. Delhaize, and D.L. Jones. 2001. Function and mechanism of organic anion exudation from plant roots. Annu. Rev. Plant Physiol. Plant Mol. Biol. 52: 5277-560.

Scheckel, K.G. and D.L. Sparks. 2001. Dissolution Kinetics of Nickel Surface Precipitates on Clay Mineral and Oxide Surfaces. Soil Sci. Soc. Am. J. 65:685–694.

Scheidegger, A.M., D.S. Strawn, G.M. Lamble, and D.L. Sparks. 1998. The kinetics of mixed Ni-Al hydroxide formation on clay and aluminum oxide minerals: A time-resolved XAFS study. Geochim. Cosmochim. Ac. 62(13): 2233–2245.

Scheinost, A.C., R. kretzschmar, and S. pfister, and D.R. Roberts. 2002. Combining Selective Sequential Extractions, X-ray Absorption Spectroscopy, and Principal Component Analysis for Quantitative Zinc Speciation in Soil. Environ. Sci. Technol. 36: 5021-5028.

Schlegel, M.L., A. Manceau, L. Charlet, and J.L. Hazemann. 2001. Adsorption mechanisms of Zn on hectorite as a function of time, pH, and ionic strength. American J. Sci. 301: 798–830.

Schwab, A.P., Y.H. He, and M.K. Banks. 2005. The influence of organic ligands on the retention of lead in soil. Chemosphere. 61: 856–866.

Silveira, M.L.A., L.R.F Alleoni, and L.R.G. Guilherme. 2003. Biosolids and Heavy Metals in Soils. Scientia Agricola. 60(4): 793-806.

Sparks D. L. 1995. Environmental Soil Chemistry. Academic Press.

Srivastava, P., S. Balwant, and M. Angove. 2005. Competitive adsorption behavior of heavy metals on kaolinite. J. Colloid Interf. Sci. 290: 28–38.

Stacey, S., G. Merrington, and M.J. McLaughlin. 2001. The effect of aging biosolids on the availability of cadmium and zinc in soil. Eur. J. Soil Sci. 52: 313-321.

Strawn, D.G.,and D.L. Sparks. 1999. The use of XAFS to distinguish between Inner- and outer-sphere lead adsorption complexes on montmorillonite. J. Colloid Interf. Sci. 216: 257–269.

Strobel, B.W. 2001. Influence of vegetation on low molecular weight carboxylic acids in soil solution-a review. Geoderma. 99: 169–198.

Suzuki, M., M. Takahashi, T. Tsukamoto, S. Watanabe, S. Matsuhashi, J. Yazaki, N. Kishimoto, S. Kikuchi, H. Nakanishi, S. Mori, and N.K. Nishizawa. 2006. Biosynthesis and secretion of mugineic acid family phytosiderophores in zinc-deficient barley. Plant J. 48:85–97.

Taylor, R.W., W.F. Bleam, T.D. Ranatunga, C.P. Schulthess, Z.N. Senwo, and D.R.A. Ranatunga. 2009. X-Ray absorption near edge structure study of lead sorption on phosphate-treated kaolinite. Environ. Sci. Technol. 43: 711-717.

Trainor, T.P., G.E. Brown, and G.A. Parks.2000. Adsorption and Precipitation of Aqueous Zn(II) on Alumina Powders. J. Colloid Interf. Sci. 231: 359–372.

Trivedi, P., J.A. Dyer, and D.L. Sparks. 2003. Lead Sorption onto Ferrihydrite. 1. A Macroscopic and Spectroscopic Assessment. Environ. Sci. Technol. 37: 908-914.

Trivedi, P., J.A. Dyer, D.L. Sparks, and K. Pandya. 2004. Mechanistic and thermodynamic interpretations of zinc sorption onto ferrihydrite. J. Colloid Interf. Sci. 270: 77–85.

Trivedi, P., L. Axe, and T.A. Tyson. 2001. An analysis of Zinc sorption to amorphous versus crystalline iron oxides using XAS. J. Colloid Interf. Sci. 244: 230–238.

van Hees, P.A.W., D.L. Jones, R. Finlay, D.L. Godbold, and U.S. Lundström. 2005. The carbon we do not see – the impact of low molecular weight compounds on carbon dynamics and respiration in forest soils: a review. Soil Biology and Biochemistry 37: 1–13.

van Hees, P.A.W., U.S. Lundström, and R. Giesler. 2000. Low molecular weight organic acids and their Al-complexes in soil solution-composition, distribution and seasonal variation in three podzolized soils. Geoderma. 94: 173-200.

Vasconcelos, I.F., E.A. Haak, P.A. Maurice, and B.A. Bunker. 2008. EXAFS analysis of cadmium(II) adsorption to kaolinite. Chem. Geol. 249: 237-249.

Vermeer, A.W.P., J.K. McCulloch, W.H. Van Riemsdijk, and L.K. Koopal. 1999. Metal ion adsorption to complexes of humic acid and metal oxides: deviations from the additivity rule. Environ. Sci. Technol. 33: 3892-3897.

Violante, A., M.R. Ricciardella, and M. Pigna. 2003. Adsorption of heavy metals on mixed Fe–Al oxides in the absence or presence of organic ligands. Water Air Soil Poll. 145: 289–306.

Voegelin, A., A. Scheinost, K. Buhlmann, K. Barmettler, and R. Kretzschmar. 2002. Slow formation and dissolution of Zn precipitates in soil: A combined column-transport and XAFS study. Environ. Sci. Technol. 36: 3749-3754.

Voegelin, A., S. Pfister, A. Scheinost, M.A. Marcus, and R. Kretzschmar. 2005. Changes in Zinc Speciation in Field Soil after Contamination with Zinc Oxide Environ. Sci. Technol. 39: 6616-6623.

Waychunas, G.A., C.C. Fuller, and J.A. Davis. 2002. Surface complexation and precipitate geometry for aqueous Zn(II) sorption on ferrihydrite I: X-ray absorption extended fine structure spectroscopy analysis. Geochim. Cosmochim. Ac. 66(7): 1119-1137.

Webb, S. 2001. Ph.D. Dissertation. The chemistry of zinc-microbe interactions in the sediments of Lake DePue, IL. Northwestern University.

Wu, Z., Z. Gu, X. Wang, L. Evans, and H. Guo. 2003. Effects of organic acids on adsorption of lead onto montmorillonite, goethite and humic acid. Environ. Pollut. 121: 469–475.

Xia, K., W. Bleam, and P.A. Helmke. 1997. Studies of the nature of Cu^{+2} and Pb^{+2} binding sites in soil humic substances using X-ray absorption spectroscopy. Geochim. Cosmochim. Ac. 61: 2211–2221.

Yamaguchi, N. U., A. C. Scheinost, and D.L. Sparks. 2002. Influence of gibbsite surface area and citrate on Ni sorption mechanisms at pH 7.5. Clay Clay Miner. 50(6): 784-790.

Yamaguchi, N.U., A.C. Scheinost, and D.L. Sparks. 2001. Surface-Induced Nickel Hydroxide Precipitation in the Presence of Citrate and Salicylate Soil Sci. Soc. Am. J. 65:729–736.

Yu, S., Z.L. He, C.Y. Huang, G.C Chen, and D.V. Calvert. 2005. Effect of anions on the capacity and affinity of copper adsorption in two variable charge soils. J. Biogeochemistry.75: 1-18.

Zuyi, T., C. Taiwei, D. Jinzhou, D. XiongXin, and G. Yingjie. 2000. Effect of fulvic acids on sorption of U(VI), Zn, Yb, I and Se(IV) onto oxides of aluminum, iron and silicon. Appl. Geochem. 15: 133-139.

CHAPTER 3

THE EFFECT OF ORGANIC AND INORGANIC LIGANDS ON ZINC ADSORPTION TO FERRIHYDRITE AS A FUNCTION OF pH

3.1 Introduction

Soil contamination with zinc (Zn) may result from various anthropogenic activities such as smelting operations, use of contaminated sludges, incinerator emissions, and from various industries (Voegelin et al., 2008). Although Zn is considered an essential element for the growth of plants, animals, and humans, its presence in elevated concentrations in the soil is detrimental to living organisms (Alloway, 2004). The bioavailability and toxicity of Zn in the soil depend on interactions with mineral surfaces, such as iron oxides (Ponthieu et al., 2006). In soils with a large content of iron oxides, the mobility and bioavailability of Zinc (Zn) is largely controlled by iron oxide minerals (Uygur and Rimmer, 2000; Tivedi et al., 2003). Iron oxides are ubiquitous in soils and sediments occurring as discrete particles or as coatings on the surface of other soil constituents (Trivedi et al., 2003; Violante et al., 2003). Iron oxide mineral surfaces have the ability to specifically adsorb divalent Zn even at low pH where the mineral surface is positively charged (Violante et al., 2003).

Extensive research has been conducted on Zn adsorption to iron oxide mineral surfaces at the macroscopic level. Although pivotal to the understanding of Zn adsorption to iron oxide surfaces, macroscopic methods do not assess the adsorption mechanisms or structure of surface complexes formed. Microscopic techniques such X-Ray Absorption Fine Structure (XAFS) spectroscopy are valuable tools in that regard that allow the probing of the local coordination environment of Zn. EXAFS spectroscopy has shown that Zn adsorbs to ferrihydrite through both outer sphere and inner sphere surface complexation as well as formation of surface precipitates

(Trivedi et al., 2001; Waychunas et al., 2002; Waychunas et al., 2002; Lee and Anderson 2005; Ponthieu et al., 2006).

The structure of Zn sorption complexes formed on the surface of ferrihydrite was found to be a function of various factors including pH, surface loading and presence of ligands. pH is a very important factor that impacts the adsorption of Zn and other metals to oxide mineral surfaces. With increase in pH, enhanced adsorption of Zn to variable charged surfaces is observed as a result of increase in the availability of sites for adsorption or by changing the concentration of metal species (hydrolysis) (Violante et al., 2003). Trivedi et al. (2004) found that Zn formed mononuclear bidentate inner sphere complexes with ferrihydrite at pH values below 6.5. Pb sorption studies on ferrihydrite have shown that bidentate mononuclear complexes dominated with increase in surface loading and pH values above 5. Monodentate mononuclear complexes were dominant at lower surface loading and lower pH values (Dyer et al., 2003 and Trivedi et al., 2003).

EXAFS spectral analysis has also shown that pH may impact the first shell coordination sphere of Zn. Zn may form tetrahedral, octahedral, or a mixture of both forms with first shell oxygen atoms upon adsorption to various mineral surfaces. Zn adsorbed to ferrihydrite was found to form tetrahedral coordination with first shell oxygen atoms at neutral pH (Bochatay and Persson, 2000; Waychunas et al., 2002; Roberts et al., 2003). In addition, Roberts et al. (2003) found that Zn favors octahedral coordination at low pH and tetrahedral coordination at high pH in silica and gibbsite adsorption systems. On the other hand, Pan et al. (2004) conducted Zn adsorption on manganite and found an average Zn-O bond length of 2.0ºA at pH 7.5, indicating that Zn^{+2} adsorbs to manganite in a mixture of tetrahedral and octahedral coordination.

Surface loading has been found to impact the formation of Zn hydroxide-like precipitates upon adsorption to oxide mineral surfaces. At low surface loading, Zn adsorbs to ferrihydrite forming inner sphere complexes. At higher surface loading, Zn surface precipitation or Zn hydroxide-like polymers form in addition to inner sphere complexes (Waychunas et al., 2002; Trivedi et al., 2004; Lee and Anderson, 2005; Ha et al., 2009). The impact of high surface loading on Zn polymerization was also reported to occur in other oxide surfaces. At low sorption densities (0.2-1.1 μmol/m^2), Zn formed inner sphere complexes with alumina and at high densities (1.5-3.3 μmol/m^2) formed a hydrotalcite like precipitate (Trainor et al., 2000). Once Zn is adsorbed to an oxide mineral surface, new adsorption sites for the formation of multinuclear complexes may become available, leading to the formation of a Zn hydroxide-like phase (Bochatay and Persson, 2000).

Although extensive research has been conducted on the adsorption mechanisms of Zn to iron oxide mineral surfaces as a function of pH, ionic strength and surface loading, few studies have elucidated the adsorption mechanisms of Zn in the presence of ligands especially with the use of EXAFS spectroscopy. In the presence of EDTA, Zn adsorbed to goethite by maintaining the ZnEDTA structure, precluding a ligand exchange mechanism (Schlegel et al., 1997). Similar results were reported for Cd adsorption to goethite in the presence of citrate and oxalate (Collins et al., 1999). In the presence of humic acid (HA), Zn adsorbed to goethite by inner sphere complexation (Collins et al., 1999). Additionally, the presence of HA affected the formation of Ni-Al layered double hydroxide (LDH) at the kaolinite surface (Nachtegaal and Sparks, 2003). Regarding HA itself, Zn was found to form inner sphere complexes with HA at low concentrations (300-5000mg/kg) and outer sphere complexes at high concentrations (500g/kg) (Sarret et al., 1997). Xia et al. (1997) confirmed that Zn formed inner sphere complexes with

HA. The objectives of this study are: 1) to assess the impacts of citrate, HA, PO_4, and siderophore desferrioxamine-B (DFO-B) on the adsorption of Zn to ferrihydrite at pH levels ranging from 4.5 to 7.5 and at reaction times of 24 hrs and 1 week, and 2) to assess the impact of ligands on the adsorption mechanisms of Zn at pH 7.5 using XAFS spectroscopy.

3.2 Material and Methods

3.2.1 Ferrihydrite Synthesis and Purification

Ferrihydrite used in this study was synthesized according to the procedure described by Schwertmann and Cornell (2000). Briefly, 40g of $Fe(NO_3)_2$ were dissolved in 500ml deionized water and neutralized with NaOH under N_2 atmosphere. The freshly produced material was washed several times by centrifugation to remove any non precipitated iron, then dialyzed against deionized water to remove excess salt. The electrical conductivity of the water was continuously monitored and water was changed several times a day until salt free. The material was then freeze dried and used for experimentation shortly after. The mineral synthesized was confirmed to be ferrihydrite by XRD. The BET-surface area of the synthesized ferrihydrite was expected to be within 200-320m^2/g (Schwertmann and Cornell, 2000).

3.2.2 Purification of Humic Acid (HA)

Humic acid (HA) used in this study was purchased from Sigma-Aldrich (H16752) and subject to a purification process. HA was purified by acid washing and subsequent removal of ash content according to the International Humic Substance Society method (Swift, 1996). Briefly, HA was acidified to pH 1.5, allowed to stand for 16 hrs, settled by low speed centrifugation and then the supernatant was decanted. HA was resuspended under N_2 gas to pH 7.0 using 1M NaOH and allowed to stand for 24 hrs. The precipitation and subsequent redissolution was repeated four times. To remove the ash content from HA, the precipitate was

suspended in 0.1M HCl/0.3M HF and shaken overnight. The process was repeated once and then HA was dialyzed until free of Cl^- as tested using $AgNO_3$. The material was freeze dried and mixed well prior to use.

3.2.3 Sorption Experiment

Adsorption experiments were conducted in 50ml centrifuge tubes under continuous purging of ultra pure N_2 gas. In the case of citrate and HA, experiments were conducted under red light to prevent the photoreduction of ferrihydrite. Zn adsorption was carried out at 4 pH levels (4.5, 5.5, 6.5, and 7.5) in the absence (control) and presence of citrate, HA, PO_4, and DFO-B for 24 hrs and 1 week, respectively. The solid:solution ratio was 20 g/l and the Zn:ligand molar ratio was 1:1 with each at 1.5 mM. HA was prepared on the basis of total carbon content (determined using TOC analyzer), so that total carbon content was similar to that of citrate. The background electrolyte concentration in the system was 0.01M $NaNO_3$. Specifically, 0.6 g of freshly ground and sieved ferrihydrite were placed in centrifuge tubes followed by the addition of 10 ml of 0.03M $NaNO_3$, and the mixtures were allowed to hydrate for 24 hrs. Then, 7.5 ml of 6.0 mM of a specific ligand (citrate, PO_4, or DFO-B) were added at constant mixing by fixing each tube on a vortex shaker using a customized grip. Following the addition of a ligand, 7.5ml of 6 mM of acidified $Zn(NO_3)_2$ were added under constant shaking. The pH of each mixture was adjusted to its respective value using 0.1M of either HNO_3 or NaOH (previously purged with N_2 gas). Centrifuge tubes containing the mixtures were then sealed and placed on a shaker. The pH was continuously monitored (under N_2 purging) and adjusted so that values exhibited minimal fluctuations ($\leq$ 0.3 pH unit). The solid was separated from the solution by centrifugation and the solution was filtered using 0.45 μM membrane filters. The filtrates were analyzed by ICP-AES for Zn, P, and Fe (released from ferrihydrite by action of organic acids). In addition, dissolved

organic carbon in the filtrate was determined using TOC analyzer (Shimadzu). Amount of Zn and ligand adsorption was calculated by the difference in initial and final concentrations in solution. All adsorption experiments were replicated twice. The solid residue after adsorption was washed once with the background electrolyte solution and stored as a paste at 4ºC until use for XAFS spectroscopy analysis.

3.2.4 EXAFS Data Collection and Analysis

EXAFS data were collected on the Ge (220) double-crystal monochromator beamline at the Center for Advanced Microstructures and Devices in Baton Rouge, Louisiana. The electron beam energy was 1.3 GeV with a maximum beam current of 180 mA. Zn metal foil was used to calibrate the beam energy by setting the first inflection point to 9569eV. The EXAFS spectra for adsorption samples were collected at Zn K-edge in fluorescence mode using a Canberra 13 element ultra low energy germanium diode array detector. Multiple scans were collected to improve the signal to noise ratio. The EXAFS data for reference compounds were collected in transmission mode. These compounds included: 1mM $Zn(NO_3)_2$ at pH 2.0, Zn citrate (Pfaltz and Bauer), ZnO (Mallinckrodt), $Zn_3(PO_4)_2$ (Aldrich), $ZnFe_2O_4$ (Alfa Aesar), $Zn(OH)_2$ (MP Biomedicals), $ZnCO_3$ (Fluka).

Data reduction was conducted using Athena interface to IFEFFIT software. A linear polynomial was fit to the pre-edge region using two points, extrapolated to the post edge region and subtracted. In the post-edge region, a cubic polynomial fit was used to remove the background. Normalization was conducted using a Victoreen polynomial. $\mu(E)$ was normalized to go from 0 to 1 so that it represents the absorption of 1 X-ray.

The threshold energy (E_0) determined from the maximum of the first derivative of $\mu(E)$ was used to convert the energy axis to photoelectron wave vector units ($Å^{-1}$). The resulting data

were weighted by k^3 to compensate for damping of the EXAFS spectrum at higher energies. The *k*-weighted $\chi(k)$ spectra were then Fourier transformed over the wavevector *k* range of 2-10Å^{-1} using a Kaiser-bessel apodization window to produce radial structure functions (RSF) that isolate first and second shell components (Yamaguchi et al., 2003; Nachtegaal and Sparks, 2004).

Ab initio Phase shift and amplitude functions of Zn-O and Zn-Fe scattering paths were extracted using franklinite, Zn-Zn path using zincite, Zn-P path using hopeite, and Zn-C path using smithsonite using FEFF 6.0 code. The peaks of interest were isolated and backtransformed in *k* space using a Kaiser-bessel window. Structural parameters (element identity, coordination number, and radial distance) were determined by a non linear least squares curve fitting approach using Artemis interface to IFEFFIT software. Single shell fits were conducted for the first and second peaks selected at R of 1.0-2.2 and 2.3-3.6Å, respectively. The value of S_0^2 was set to 0.84 and determined by fixing the coordination number for Zn-O in aqueous Zn to 6.

The interference of the iron matrix in our samples made it difficult to collect spectra for adsorption samples at pH 5.5. Researchers are often faced with challenges when dealing with Zn EXAFS spectra in iron oxide samples due to the strong absorption and fluorescence of the iron matrix, which degrades the Zn EXAFS signal. This interference makes it difficult to collect signals at low Zn concentrations (Waychunas et al., 2002). For the collected spectra at pH 7.5, a Fourier filtering of 10Å^{-1} was used. Comparing with other researchers working with Zn adsorption to iron oxides, it is noticeable that the noise level of our EXAFS spectra is similar to that of Nachtegaal and Sparks (2004), who used a Fourier filtering range of 1.7-11 Å^{-1} and a smoothing parameter of 4 to suppress artifacts. Similarly, Trivedi et al. (2001) used a Fourier filtering range of 2.3 to 9.2 Å^{-1} for Zn adsorption onto hydrous ferric oxide due to the high noise level at higher k.

3.3 Results and Discussion

3.3.1 Macroscopic Zn Adsorption

3.3.1.1 Citrate

Figure 3.1 shows adsorption in the control and presence of citrate for 24 hrs and 1 week. Citrate enhanced Zn adsorption as evident by the shift in adsorption edges to lower pH values for both reaction times. The largest impact was at pH 5.5, where citrate enhanced Zn adsorption from 23 to 50% for the 24 hr and from 40 to 77% for 1 week reaction times. Zn adsorption increased with time both in the absence (control) and presence of citrate at pH values below 7.5. The largest difference in adsorption between the 24 hr and 1 week reaction times was at pH 5.5, where Zn adsorption increased from 23 to 40% in the absence of citrate and from 50 to 77% in the presence of citrate. The continuation of Zn adsorption with time was consistent with the trend of metal adsorption onto iron oxides, in which rapid initial adsorption to high affinity sites is followed by a slow continuous one. Trivedi et al. (2004) reported that the slow sorption could be due to the migration of Zn ions into the micropores of ferrihydrite via interparticle diffusion. Clover et al. (2002) reported that the slow sorption was likely caused by Zn precipitate formation or change in type of surface complex.

The enhanced adsorption of Zn was also accompanied by citrate removal from the solution. Throughout the pH range studied, up to 94% of citrate was adsorbed. Schwab et al. (2005) reported that a portion of citrate could be biodegraded by microbial activity. However, this was unlikely in this study because caution was taken to ensure minimal loss of citrate by refrigeration and by conducting analysis in the shortest time possible. On the other hand, the expected trend of adsorption for low molecular weight acid anions is generally a decrease in adsorption with pH increase. Geelhoed et al. (1998) showed a strong citrate adsorption to

goethite at pH 3.0 but decreased significantly as pH increased to 9.2. In this study, it was likely that due to the high concentration of ferrihydrite in the system, and hence abundance of surface sites, there was only minor change in citrate adsorption between pH 4.5 and 7.5. The high affinity of citrate for ferrihydrite therefore resulted in enhanced Zn adsorption. This enhancement could be due to decrease in the positive electrostatic potential of the surface following citrate adsorption, or by formation of a ternary complex (Haas and Horowitz, 1986; Collins et al., 2003; Collins et al., 1999).

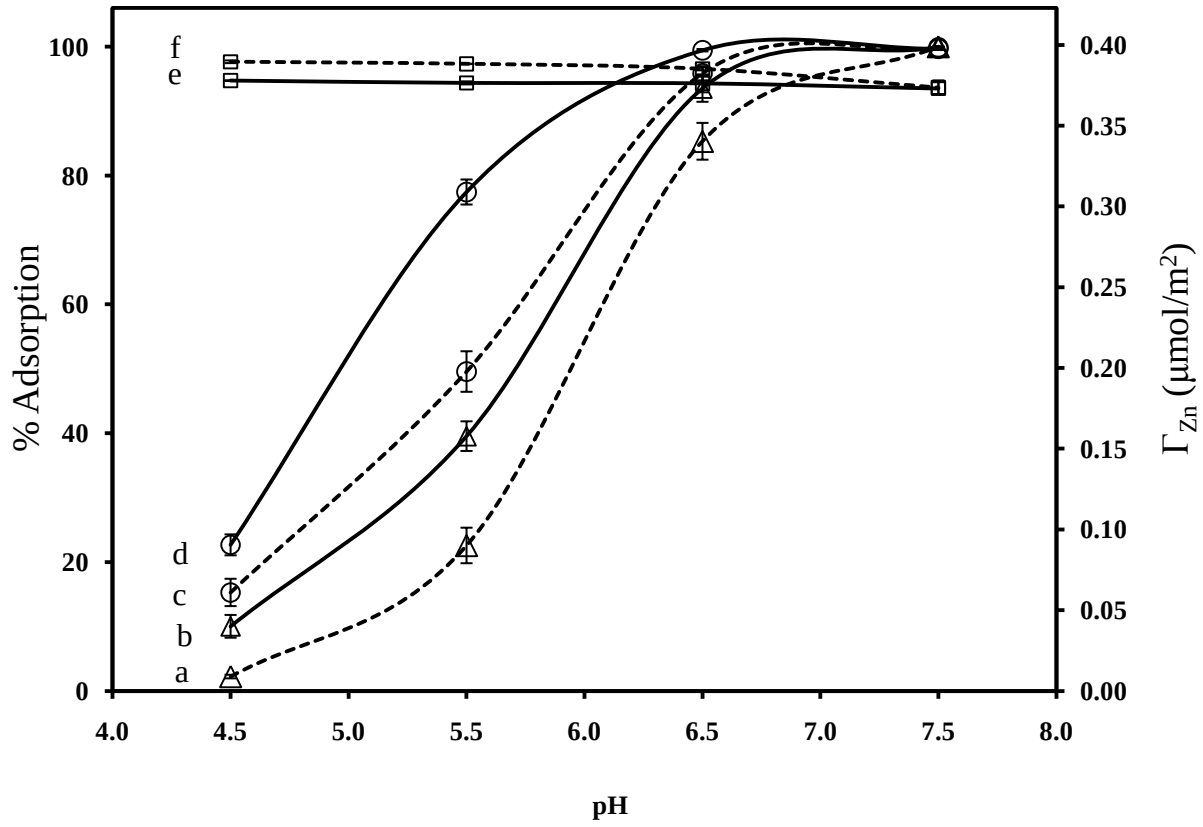

Figure 3.1 Zn adsorption to ferrihydrite as a function of pH and adsorption time in the absence (control) and presence of citrate. Lines a,c: Zn adsorption for 24 hrs in absence and presence of citrate, respectively. Lines b, d: Zn adsorption for 1 week in absence and presence of citrate, respectively. Lines e, f: citrate adsorption for 24 hrs and 1 week, respectively.

Enhanced Zn adsorption due to strong adsorption of citrate to ferrihydrite was different from that of Ni adsorption to gibbsite, in which citrate showed a suppressive effect at pH 7.5 (Yamaguchi et al., 2001). Boily and Fein (1996) reported that the adsorption enhancement of metals by citrate was likely dependent on the amount of citrate that can adsorb to the surface. If the surface sites were saturated with adsorbed citrate, excess solution citrate could begin to compete with the surface for the metal, thus reducing metal adsorption (Boily and Fein, 1996). Our study suggested that the strong adsorption of citrate to ferrihydrite plays a major role in promoting further Zn adsorption.

3.3.1.2 Humic Acid (HA)

Figure 3.2 shows adsorption data in the absence and presence of HA for 24 hrs and 1 week. The effect of HA on Zn adsorption was dependent on pH, where Zn adsorption was enhanced at pH values below ~6.0 and reduced at higher pH. For both time periods, Zn adsorption decreased by only ~10% at pH 7.5 and similarly increased by ~10% at pH 5.5. Comparing Zn adsorption between the 24 hr and 1 week reaction times indicated that more Zn was adsorbed after 1 week in both the absence and presence of HA (Figure 3.2; lines a and c, b and d).

Figure 3.2 (lines e and f) shows that HA adsorption to ferrihydrite decreased with pH increase, consistent with the electrostatic interaction mechanism. As the surface of ferrihydrite becomes more positively charged with pH decrease, deprotonated, negatively charged HA is adsorbed to the positively charged surface sites ($\equiv Fe(OH)^{2+}$). After HA is adsorbed to the oxide surface, HA sites of high affinity for Zn become available for the formation of ternary complexes (Kummert and Stumm, 1980; Lai et al., 2002). Reduced Zn adsorption at pH > 6.0 may be due to competition between HA and the surface of ferrihydrite for Zn, promoting the formation of HA

and Zn complexes that are non-adsorbable (Davis and Bhatnagar, 1995; Boily and Fein 1996). The impact of HA on Zn adsorption was consistent with previous research reported for other metals. Davis and Bhatnagar (1995) reported enhanced adsorption of Cd to hematite in the presence of HA in the pH range 5 to 8. Ho and Miller (1985) reported enhanced adsorption of uranium on hematite in the presence of HA at low pH and reduced adsorption at high pH due to a 'surface blocking effect'.

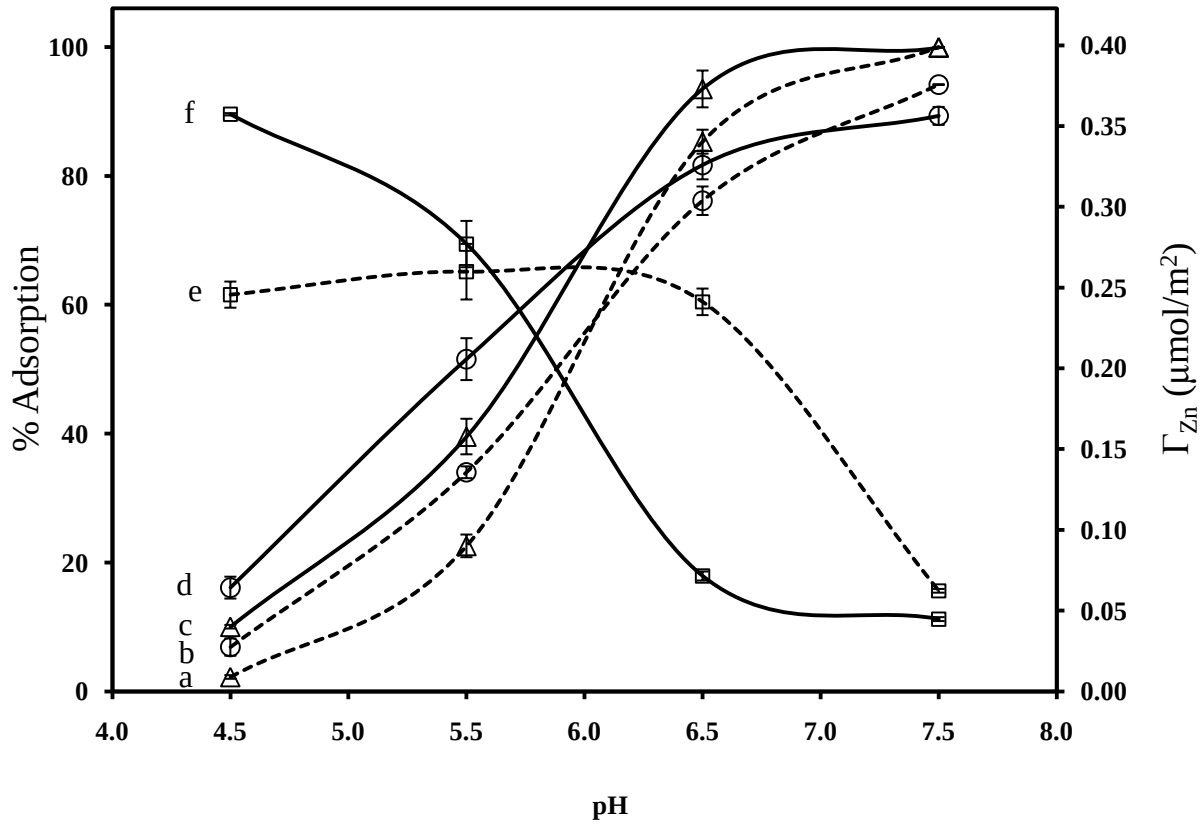

Figure 3.2 Zn adsorption to ferrihydrite as a function of pH and adsorption time in the absence (control) and presence of HA. Lines a,b: Zn adsorption for 24 hrs in absence and presence of HA, respectively. Lines c, d: Zn adsorption for 1 week in absence and presence of HA, respectively. Lines e, f: HA adsorption for 24 hrs and 1 week, respectively.

This study showed that despite large adsorption of HA to the ferrihydrite surface, especially in the 1 week adsorption time, Zn adsorption to ferrihydrite was only slightly

enhanced. Additionally, the presence of substantial quantities of soluble HA at pH 7.5 only slightly reduced the amounts of Zn adsorbed.

3.3.1.3 Phosphate (PO_4)

Figure 3.3 shows adsorption in the absence and presence of the inorganic PO_4 ligand. Zn adsorption was enhanced by the presence of PO_4 as evident by the shift in adsorption edges to lower pH values at 24 hrs and 1week. As in the case of HA, the impact of PO_4 on Zn adsorption was not drastic. The maximum increase was at pH 5.5, where Zn adsorption increased by only ~12% at 24 hrs and 1 week. As adsorption time increased, the amount of Zn adsorbed increased in both the absence and presence of PO_4 at pH below 7.5 (Figure 3.3, lines b and d). Wang and Xing (2004) found that Cd adsorption to goethite was also enhanced by PO_4 for time periods ranging from 15 minutes to 4 weeks. Diaz-Barrientos et al. (1990) indicated that the specific adsorption of PO_4 could cause an increase in negative charge of the inner Helmholtz plane of the mineral surface and therefore have a positive effect on metal cation adsorption. On the other hand, Li et al. (2006) found that PO_4 reduced Cd and Cu adsorption to hematite. They postulated that treating the mineral with PO_4 reduced the inner sphere sorption sites for the metals and therefore decreased metal adsorption.

In this study, the high affinity of PO_4 for ferrihydrite was evident by complete adsorption at all pH levels and in both sorption times. Modeling the data using Visual Minteq (Gustafsson, 2004) based on the diffuse layer model (DLM) confirmed the complete adsorption of PO_4 at all pH levels (data not shown). All PO_4 was in the adsorbed form of $\equiv FePO_4^{-2}$ species that dominated the pH range studied. The high affinity of PO_4 for iron oxides and the low pH dependency of its adsorption edge have also been reported by others (Venema et al., 1997). Our results suggest that despite strong adsorption of PO_4, Zn adsorption enhancement was much less

than in the case of citrate, which also showed strong adsorption to ferrihydrite. These results were illustrated in Figure 1.1 and Figure1.3.

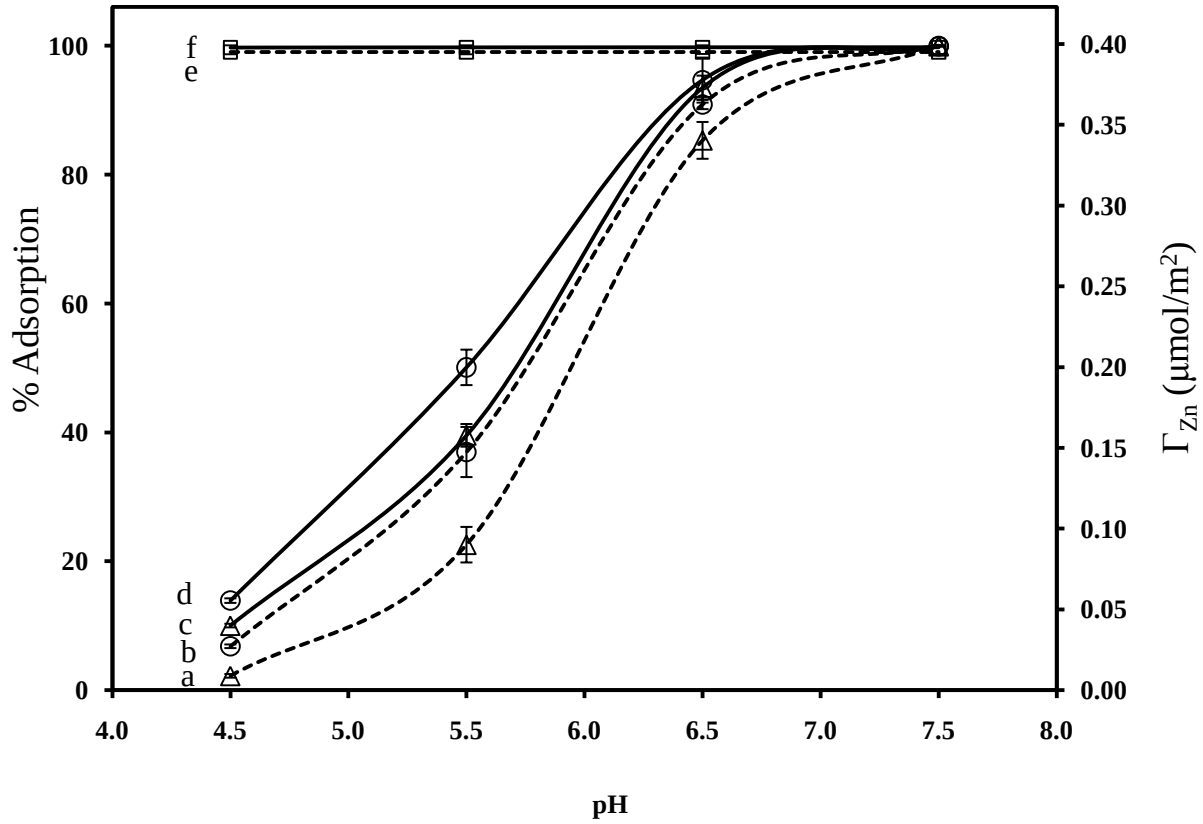

Figure 3.3 Zn adsorption to ferrihydrite as a function of pH and adsorption time in the absence (control) and presence of PO_4. Lines a,b: Zn adsorption for 24 hrs in absence and presence of PO_4, respectively. Lines c, d: Zn adsorption for 1 week in absence and presence of PO_4, respectively. Lines e, f: PO_4 adsorption for 24 hrs and 1 week, respectively.

3.3.1.4 Siderophore (DFO-B)

Figure 3.4 shows adsorption in the absence and presence of DFO-B. Siderophore DFO-B suppressed Zn adsorption at both 24 hrs and 1 week, but especially for the former (lines a and c, b and d). The magnitude of decrease in Zn adsorption ranged from 2 to 45% with pH increase up to 7.5 as compared to the control. Zn and DFO-B could form a positively charged solution complex at neutral pH (Neubauer et al., 2002). This could prevent Zn from adsorption to the

positively charged ferrihydrite surface at pH<9.2 (PZC of ferrihydrite). Our results were in agreement with Neubauer et al. (2002) who showed that siderophore DFO-B reduced the adsorption of Zn to ferrihydrite, with the effect being more pronounced with pH increase up to 7.5. With the increase in sorption time to 1week, much more Zn was adsorbed especially at pH 7.5 suggesting a stronger kinetic effect on Zn adsorption at neutral or slightly alkaline pH (Figure 3.4, lines b and d).

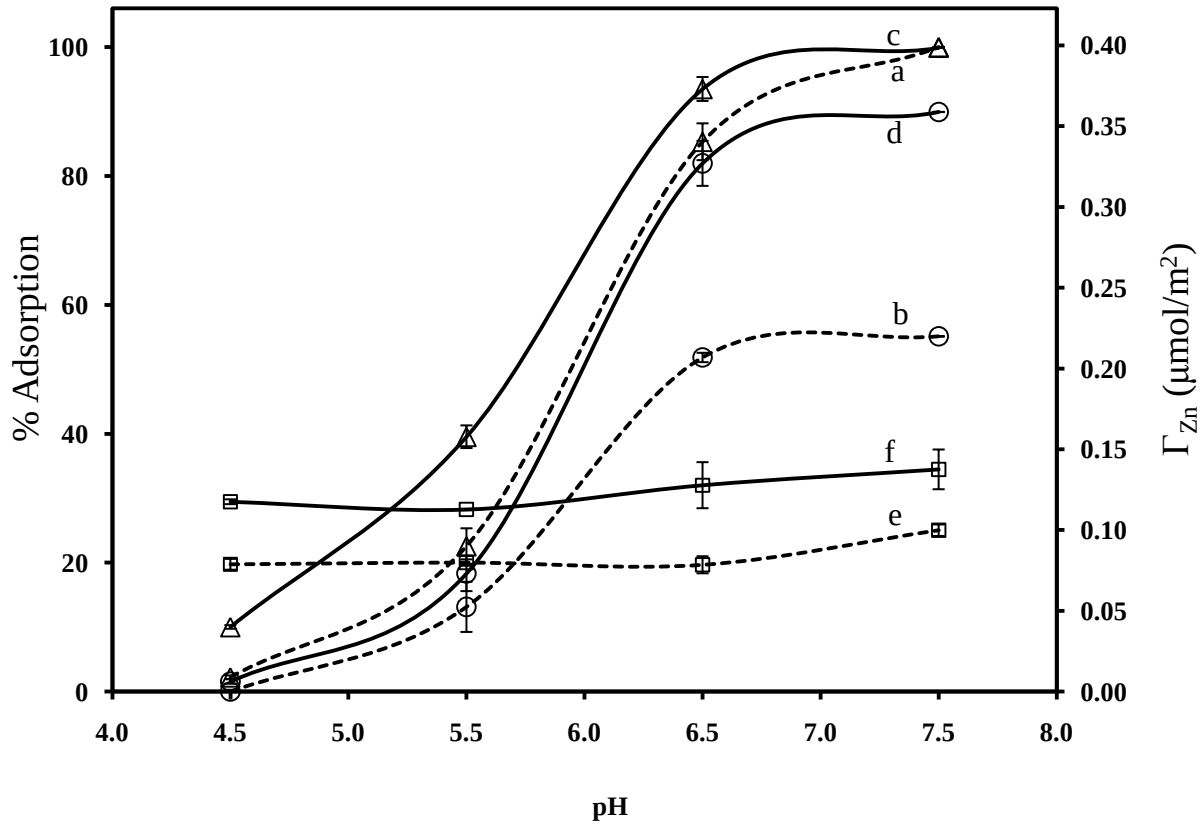

Figure 3.4 Zn adsorption to ferrihydrite as a function of pH and adsorption time in the absence (control) and presence of DFO-B. Lines a,b: Zn adsorption for 24 hrs in absence and presence of DFO-B, respectively. Lines c, d: Zn adsorption for 1 week in absence and presence of DFO-B, respectively. Lines e, f: DFO-B adsorption for 24 hrs and 1 week, respectively.

However, we did detect the release of Fe ions into solution; 8 mgL^{-1} and 35 mgL^{-1} at 24 hrs and 1 week, respectively; indicating the dissolution of ferrihydrite promoted by DFO-B. There was little variation in DFO-B adsorption among the different pH levels. The release of Fe with time from iron oxide surfaces in the presence of DFO-B was also noted by others (Hersman et al., 1995; Neubauer et al., 2002).

3.3.2 X – Ray Absorption Fine Structure Spectroscopy

The normalized k^3-weighted EXAFS spectra, the corresponding Fourier transformed Radial Structural Functions (uncorrected for phase shifts), and fitted inverse Fourier transforms for model and sorption samples are shown in Figures 3.5 and 3.6, respectively. Results of the EXAFS data analysis for both model and sorption samples are shown in Tables 3.1 and 3.2. Fits considered only single scattering from first and second coordination shells.

The k^3-weighted χ spectra of sorption samples and Zn mineral compounds differ from that of aqueous Zn (Figure 3.5b and 3.6a). As expected, the latter exhibits a drastic diminishing of signal with $k(A^{\circ -1})$ due to its single coordination sphere (Nachtegaal and Sparks, 2004). The absence of diminishing amplitude in the model compounds and sorption samples reveals structural information and indicates the presence of heavy second neighbor scattering atoms (Figures 3.5b and 3.6a). This is also evident by the presence of a second shell in their respective Fourier transformed Radial Structural Functions-RSF (Figures 3.5c and 3.6b). For most of the samples, peaks beyond the second shell can also be observed in the RSF due to multiple scattering paths (Roberts et al., 2003).

The shift in χ spectra to higher k values indicates lower first shell coordination number, where tetrahedral Zn compounds such as zincite and franklinite are shifted to higher k values compared with octahedral compounds such as aqueous Zn (Figure 3.5b) (Roberts et al., 2003).

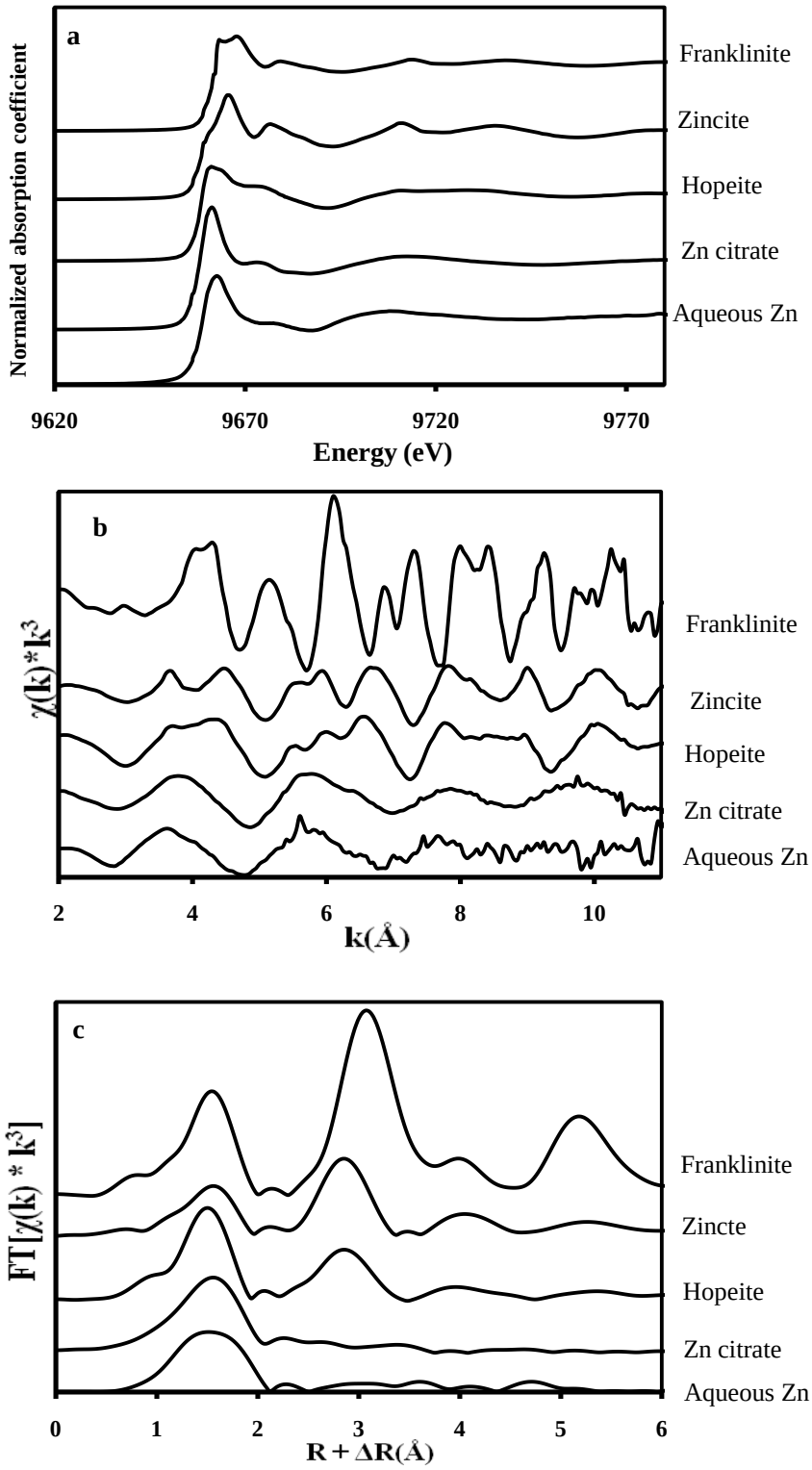

Figure 3.5 Zn K-edge XANES spectra (a), k^3-weighted $\chi(k)$spectra (b), and their respective RSFs (c) for Zn compounds.

In comparison with aqueous Zn, sorption samples indicate mainly tetrahedral first shell coordination as can be seen by comparing the χ spectra (Figure 3.5b and 3.6a). In comparison with the other sorption samples, the PO_4 sample was slightly shifted towards lower *k* values indicating a higher first shell coordination number than the other samples (Figure 3.6a). The position of the first peak of the RSF in the tetrahedrally coordinated samples (control and siderophore) is shifted to lower radial distances compared with the octahedrally coordinated samples such as PO_4 (Figure 3.6b).

3.3.2.1 First Shell Coordination

EXAFS fitting results for the Zn model compounds presented in Table 3.1 show that Zn was in octahedral coordination with first shell oxygen atoms in aqueous Zn and in Zn citrate as evident by the Zn-O interatomic distance of 2.07Å. Additionally, Zn was in tetrahedral coordination in the case of franklinite, zincite, and hopeite, evident by the Zn-O interatomic distance of 1.96Å. Results from EXAFS spectral fitting for the sorption samples indicate that in the absence of ligands (control), Zn adsorbed to ferrihydrite forming tetrahedral coordination with first shell O atoms, as evident by the Zn-O interatomic distance of 1.94Å and coordination number of 4.36 (Table 3.2). Characteristic Zn-O interatomic distances for first shell tetrahedral coordination range from 1.92 to 1.99 Å (Roberts et al., 2003). Although Zn may form either tetrahedral or octahedral coordination with first shell oxygen atoms (Nachtegaal and Sparks, 2004), the formation of Zn-O tetrahedra as opposed to octahedra in the control in this study was in agreement with previous research. It was shown that with increase in pH to and above neutral values, Zn adsorbed onto iron oxides and other minerals exhibited a Zn-O first shell coordination transition from octahedral to predominantly tetrahedral (Lee and Anderson, 2005; Roberts et al.,, 2003; Bochatay and Persson, 2000).

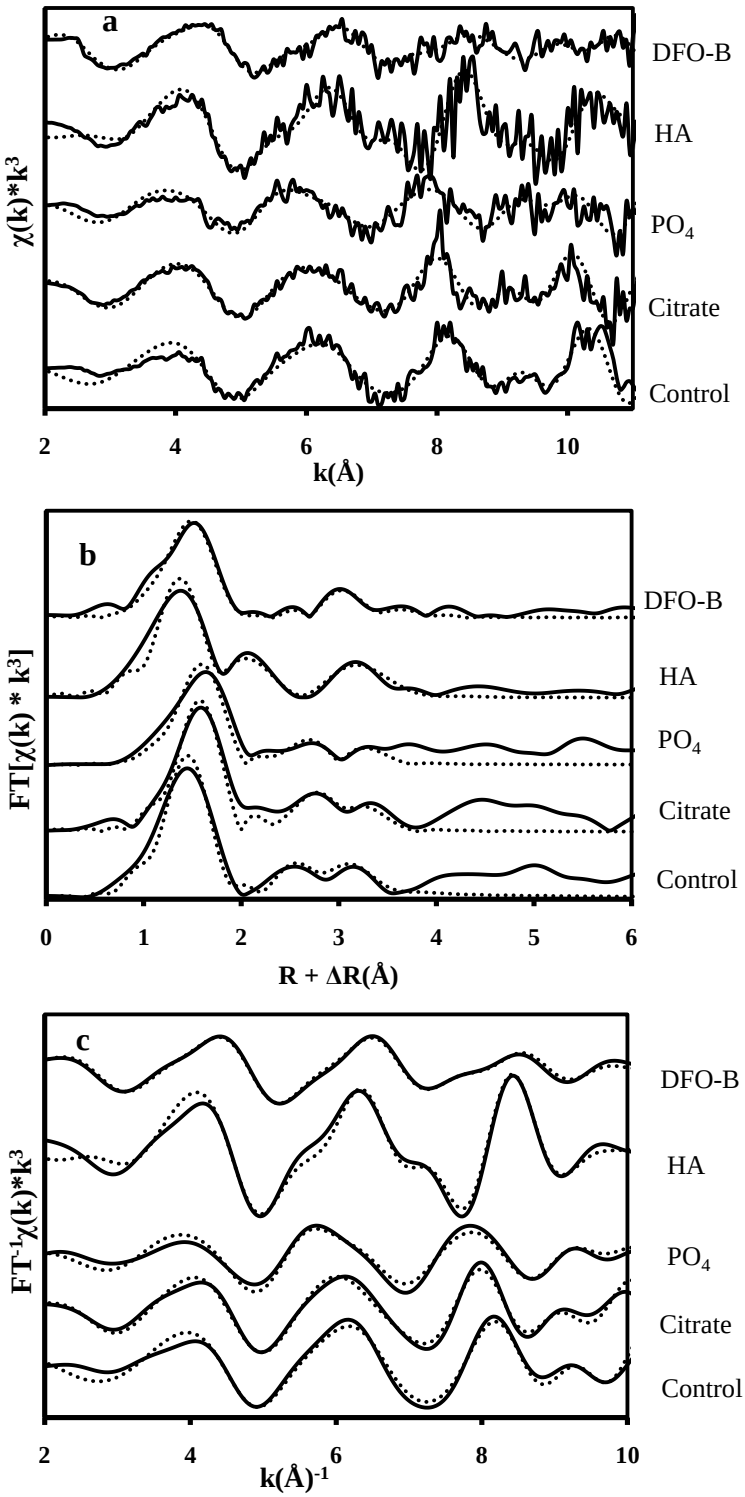

Figure 3.6 k^3-weighted $\chi(k)$ of Zn adsorbed to ferrihydrite at pH 7.5 for 24 hrs (a), their respective Fourier transforms (b), and inverse Fourier transforms (c). The solid lines represent the raw spectra and the dotted lines represent best fits.

In addition, Waychunas et al. (2002) reported that this transition is favored as a result of increase in the oxygen bond valence sum to ~2.0 as opposed to ~1.83 for octahedral coordination. Bochatay and Persson (2000) indicated that this transition could be a possible explanation for the extensive hydrolysis that Zn(II) exhibits upon adsorption to iron oxides.

Table 3.1 Structural parameters for Zn model compounds derived from EXAFS spectral data analysis

Compound	Shell	N	R(Å)	σ^2(Å^2)
Aqueous Zn	Zn-O	5.77	2.07	0.012
Zn citrate	Zn-O	5.96	2.07	0.01
ZnO	Zn-O	3.27	1.95	0.008
	Zn-Zn	12.41	3.23	0.012
$Zn_3(PO_4)_2$	Zn-O	4.09	1.96	0.006
	Zn-P	2.32	3.11	0.003
	Zn-Zn	4.96	3.26	0.008
Franklinite	Zn-O	4.19	1.96	0.005
	Zn-Fe	12.67	3.51	0.006

N = coordination number, R = radial distance (Å), σ^2 = Debye-Waller factor (Å^{-2}). The uncertainties in N are estimated to be 30%. Variations in R are estimated to be 0.03 for all shells.

First shell fitting results for Zn adsorption in presence of HA and DFO-B indicate a tetrahedral coordination similar to that in the control (Table 3.2). On the other hand, the Zn-O radial distances observed in the presence of citrate or PO_4 indicate a different type of first shell coordination environment. The radial distance for Zn adsorption in presence of PO_4 suggests an octahedral coordination where characteristic values range from 2.02 to 2.12 Å (Roberts et al., 2003; Waychunas et al., 2002). For octahedrally coordinated aqueous Zn(II), our fitting results indicate ~6 oxygen atoms at an interatomic radial distance of 2.07Å.

In the case of citrate, the Zn-O radial distance of 2.0 Å was shorter than would be expected for an octahedral coordination. This may be suggestive of a combination of tetrahedral and octahedral coordination spheres. Pan et al. (2004) reported that Zn(II) adsorbs to manganite in a mixture of tetrahedral and octahedral coordination at an average radial distance of 2.0Å. Another possibility for the increase in Zn-O distance is the formation of ternary B complex (discussed below).

Table 3.2 Structural parameters for Zn adsorption to ferrihydrite for 24 hrs derived from EXAFS spectral data analysis

Compound	Shell	N	R(Å)	σ^2(Å^2)
Control	Zn-O	4.36	1.94	0.002
	Zn-Fe	2.81	3.14	0.003
	Zn-Fe	2.80	3.38	0.003
Citrate	Zn-O	4.85	2.00	0.003
	Zn-Fe	3.79	3.23	0.006
	Zn-Fe	4.72	3.48	0.012
PO_4	Zn-O	5.32	2.04	0.003
	Zn-Fe	3.19	3.21	0.003
	Zn-Fe	3.20	3.43	0.003
HA	Zn-O	5.23	1.89	0.002
	Zn-C	5.54	2.78	0.003
	Zn-Fe	2.71	3.48	0.003
DFO-B	Zn-O	3.90	1.93	0.006
	Zn-Fe	6.41	3.40	0.02

N = coordination number, R = radial distance (Å), σ^2 = Debye-Waller factor (Å^{-2}).The uncertainties in N are estimated to be 30%. Variations in R are estimated to be 0.03 for all shells.

3.3.2.2 Second Shell Coordination

Figure 3.6b shows that the RSFs for the control, citrate and PO_4 sorption samples displayed second and third shells, whereas the HA and DFO-B samples displayed a single second shell. The higher shells for the control were at 2.5Å and 3.14Å (uncorrected for phase shift). For the citrate and PO_4 sorption samples, higher shells were at slightly longer radial distances of 2.75Å and 3.33Å (uncorrected for phase shift). The second shell for the HA and DFO-B samples was at 3.12Å and 3.0Å, respectively.

- **Control**

In analyzing the higher shells of Zn adsorption by an Fe containing mineral, it was important to recognize that Zn and Fe have similar phase shift and amplitude functions, which makes it difficult to identify if the second shell backscattering atom is Zn or Fe, both of those atoms, or one of each (O'Day et al., 1998). Zn backscattering contribution to the higher shell would imply the formation of Zn polynuclear complexes (polymerization). Although the formation of Zn polynuclear complexes has been found to occur in systems undersaturated with respect to hydroxide precipitation (Bochatay and Persson, 2000; Trainor et al., 2000; Waychunas et al., 2002), its occurrence at the low surface coverage of this study (Γ=0.4 μmol/m^2) was not expected. Zn polymerization on the surface of manganite and alumina was found to start at surface coverage of 1.1μmol/m^2 at neutral pH (Bochatay and Persson, 2000; Trainor et al., 2000). Waychunas et al. (2002) also reported that Zn adsorption to ferrihydrite at low sorption densities involves inner sphere complexation whereas Zn polymerization is enhanced at higher sorption densities. In addition, Ha et al. (2009) also ruled out Zn polymerization in hematite at surface loading as high as 2.3μmol/m^2 and smaller. We therefore assume that the higher shell backscattering atoms are Fe, not Zn.

The higher shell features for the control sample revealed two Zn-Fe interatomic distances at 3.14 and 3.38Å (Table 3.2). To identify the sorption geometries implied by these radial distances, a spatial geometry method described by several researchers (Spadini et al., 1994; Li et al., 2004; Pan et al., 2004; Breban, 2007) was used to assess the theoretical Zn-Fe distance for the different possible sorption geometries. The Fe-O-Zn bond angle for corner-sharing monodentate (vertex), corner-sharing bidentate (corner), and edge sharing bidentate (edge) linkages are 180°, 130°, and 90°, respectively (Figure 3.7a). Based on the fitted Zn-O radial distance of 1.94Å (Table 3.2) and Fe-O distance of 2.01Å for ferrihydrite (Xu et al., 2006; Julliot et al., 2008), the theoretical Zn-Fe distances for vertex, corner, and edge sharing linkages are 3.97Å, 3.60Å, and 2.81Å, respectively.

The Zn-Fe radial distance of 3.14Å would be too short for corner sharing. Therefore, we propose edge sharing bidentate linkage between ZnO_4 and FeO_6 for the sorption geometry which is shown in Figure 3.7b. This is in agreement with that of Ha et al. (2009) who reported that a Zn-Fe radial distance of 3.10-3.12 Å was consistent with $ZnO_{4,6}$ polyhedra sharing edges with FeO_6 octahedra of hematite in a bidentate, edge shared fashion. Pan et al. (2004) also reported that a Zn-Mn radial distance of 3.07Å was consistent with edge sharing linkage between $ZnO_{4,6}$ polyhedra and MnO_6 octahedra of manganite.

The third shell Zn-Fe radial distance obtained in the control sample was 3.38 Å. The Fe-O-Zn bond angle (Θ) that would result from Zn-O distance of 1.94Å and Zn-Fe distance of 3.38Å would be ~120° according to the following equation (Breban, 2007):

$$\Theta=\cos^{-1}[(R(Zn\text{-}Fe)^2-R(Zn\text{-}O)^2-R(Fe\text{-}O)^2)/(2*R(Zn\text{-}O)*R(Fe\text{-}O))]$$

The monodentate mononuclear (vertex) linkage may have a Fe-O-Zn bond angle ranging from 180° to 120° (Trainor et al., 2000). However, the ZnO_4 tetrahedra would have to tilt 60° to

give a Zn-Fe distance of 3.38Å. Although such sorption geometry cannot be ruled out, it is less likely due to steric constraints (Trainor et al., 2000). The sorption geometry for the third shell was more likely to be corner sharing linkage, with the ZnO_4 tetrahedra sharing two apical oxygens of FeO_6 octahedra (Figure 3.7a). According to c O'Day et al. (2009), corner-sharing linkages of ZnO_4 tetrahedra with FeO_6 octahedera of ferrihydrite may have Zn-Fe radial distances ranging from 3.30-352Å.

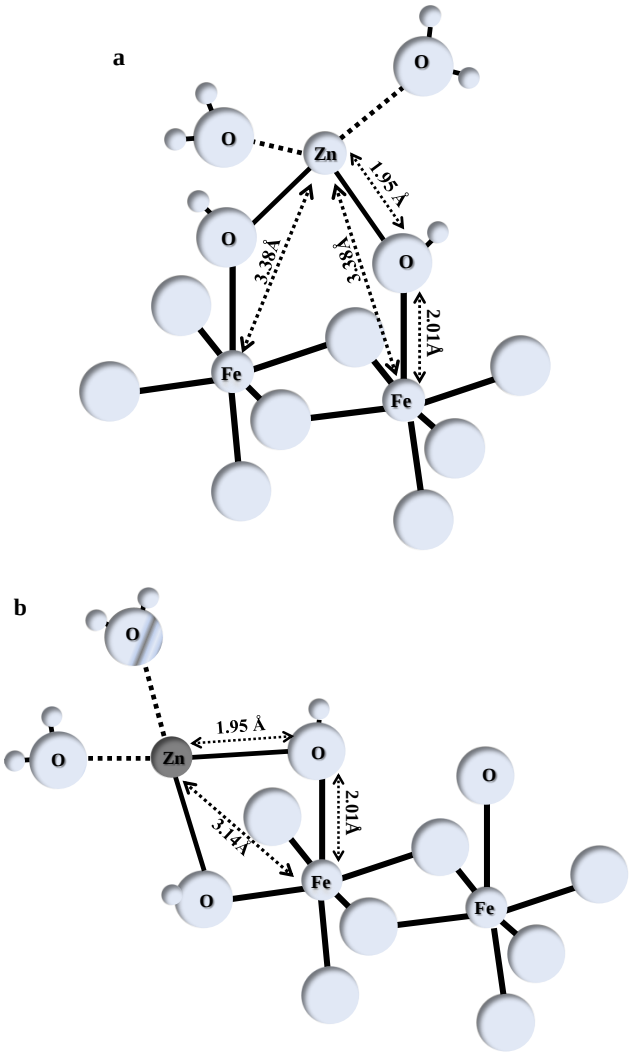

Figure 3.7 Schematic illustrations of possible binding structures of Zn tetrahedra complexed with ferrihydrite (a) corner-sharing bidentate, (b) edge-sharing bidentate. The length of the various bonds represent Zn adsorption in absence of ligands (control).

- **Citrate**

The higher shell features for the Zn sorption sample in the presence of citrate revealed two Zn-Fe interatomic distances at 3.23 and 3.48Å (Table 3.2), which are slightly longer than Zn-Fe distances of the control. The former radial distance was consistent with ZnO_4 sharing edges (bidentate mononuclear) with FeO_6 octahedra (Ponthieu et al., 2006; Juillot et al., 2008). The latter radial distance was consistent with ZnO_4 tetrahedra forming corner sharing linkage with FeO_6 octahedra of ferrihydrite (bidentate mononuclear) (Waychunas et al., 2000; Ponthieu et al., 2006; Juillot et al., 2008).

The presence of Fe at these radial distances would eliminate the possibility of a Zn-citrate-ferrihydrite type A ternary complex formation as O and C atoms would be expected to contribute to second shell backscattering within that radial distance (Yamaguchi et al., 2001). However, formation of a citrate-Zn-ferrihydrite ternary B complex is plausible within these radial distances. In a type B ternary complex, a ligand exchange reaction is expected to occur so that water is replaced by weaker field carboxylic ligands resulting in more water molecules coordinating to a metal; hence longer first shell Me-O radial distances (Alcacio et al., 2001; Yamaguchi et al., 2001). In this study, the longer Zn-O first shell radial distance of 2.0Å in the presence of citrate as compared to 1.94Å in the control may indicate the presence of ternary B complex. Yamaguchi et al. (2002) examined the possibility of ternary B complex formation in Ni adsorbed to gibbsite in the presence of citrate, and found no microscopic evidence as the Ni-O radial distances remained unchanged in presence of citrate. On the other hand, Alcacio et al. (2001) observed an increase in Cu-O radial distance samples of Cu sorbed to humate-goethite and concluded a type B complex formation.

Researchers have proposed that citrate may enhance metal adsorption through the formation of metal-citrate precipitate at the surface of minerals. Collins et al. (1999) showed that Cd^{+2} forms precipitates with oxalate and citrate on the goethite surface as evident by similarities in EXAFS spectral fitting of adsorbed samples with that of Zn oxalate and citrate model compounds. Schlegel et al. (1997) showed that ZnEDTA adsorption to goethite does not involve a ligand exchange mechanism but instead the structure of ZnEDTA was preserved during adsorption to goethite. The absence of C contribution in the second shell and spectral differences between the Zn citrate reference compound and that of the adsorbed samples ruled out the possibility of a Zn citrate precipitate formation on the surface of ferrihydrite.

- **Phosphate (PO_4)**

The higher shell features for the PO_4 sample revealed two Zn-Fe interatomic distances at 3.21 and 3.43Å (Table 3.2) similar to those of the citrate sample, indicating both edge and corner sharing linkages (Figure 3.8). The difference between this sample and that of the control or citrate samples was the first shell coordination sphere, which was octahedral in the PO_4 sample.

The formation of a Zn-PO_4 precipitate in the presence of PO_4 was ruled out due to absence of P backscattering contribution in the higher shell. XANES spectra provide further evidence for absence of a Zn-PO_4 precipitate. Figure 3.9 displays near edge spectra for two mineral systems from a previous study that were saturated with respect to hopeite. The near edge spectra for the two saturated samples display shoulders at 9673 and 9679eV and that of hopeite displays a shoulder at 9673eV (Figure 3.5a). The XANES spectrum for the PO_4 sample which was similar to that of the control indicated the absence of shoulders after the absorption edge. As discussed previously, Visual MINTEQ simulation using initial Zn, PO_4, and ferrihydrite concentrations also indicated no $Zn_3(PO_4)_2$ precipitation (data not shown).

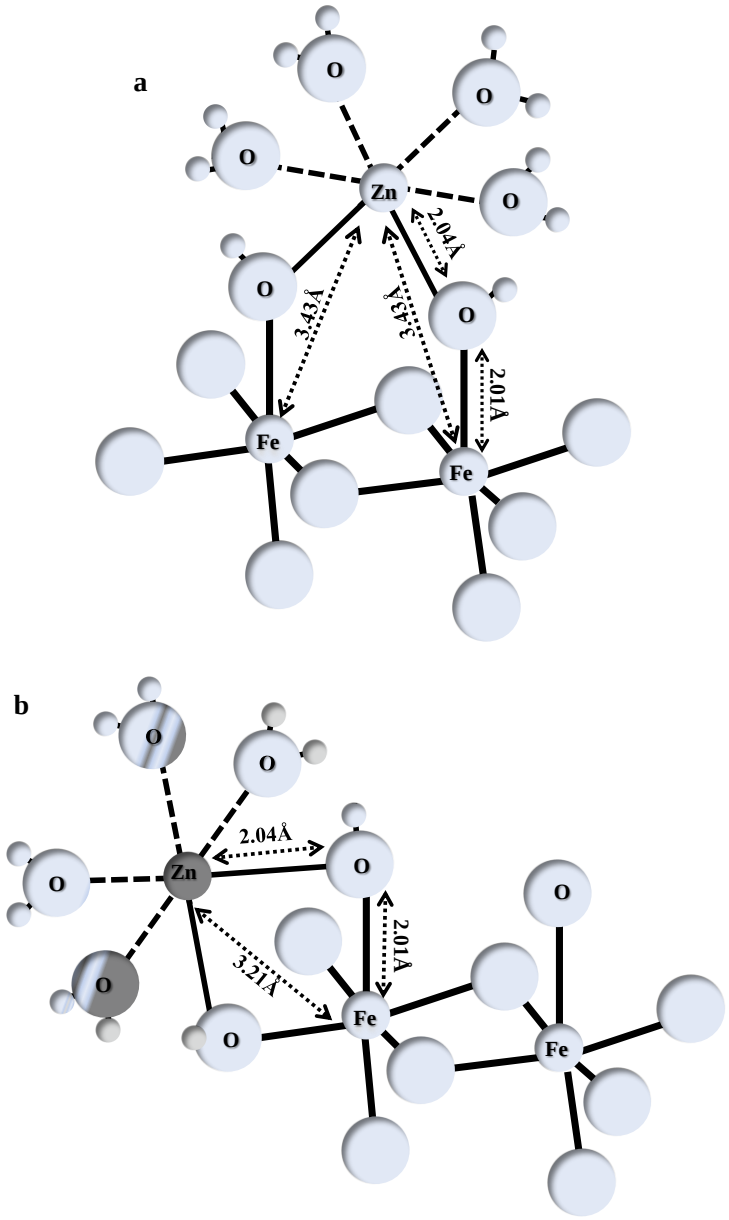

Figure 3.8 Schematic illustrations of possible binding structures of Zn octahedra complexed with ferrihydrite (a) corner-sharing bidentate, (b) edge-sharing bidentate. The length of the various bonds represent Zn adsorption in presence of PO_4.

Collins et al. (1999) reported an enhanced Cd adsorption onto goethite by PO_4 and proposed that enhanced adsorption of Cd was due solely to electrostatic interaction, where PO_4 adsorption to goethite had reduced the overall positive charge, enhancing Cd adsorption. On the other hand, Li et al. (2006) reported that PO_4 decreased the adsorption of Cu and Cd to hematite

because its occupancy of inner sphere sorption sites on the mineral surface reduced the number of sites available for the metals. They concluded that if Cu and Cd were adsorbed as outer sphere complexes, their adsorption would be enhanced by PO_4 and suppressed if their form of adsorption was inner sphere. Our study showed that PO_4 enhanced Zn adsorption at low pH and showed no impact at higher pH. From the EXAFS data we have available, inner sphere complexes were formed at pH 7.5 in the presence of PO_4.

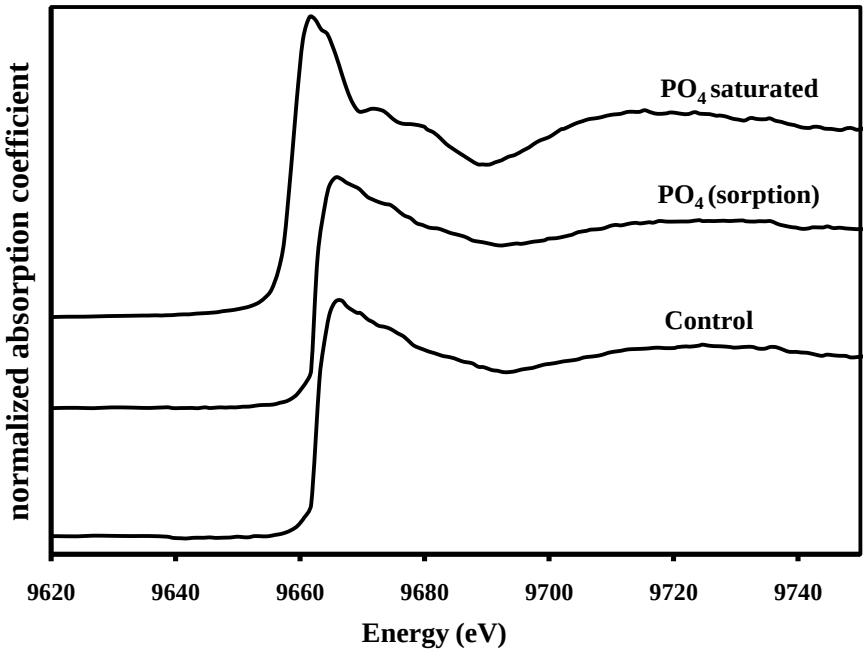

Figure 3.9 XANES spectra for Zn sorption in control and in presence of PO_4 with and without saturation.

- **Humic Acid (HA)**

The second shell for the HA sample revealed Fe atoms at Zn-Fe interatomic distance of 3.48 Å, consistent with ZnO_4 tetrahedra forming corner sharing linkages with ferrihydrite. Inclusion of C atoms resulted in improved goodness of fit, despite that the lightness of C atoms would produce a weak peak in the RSF (Collins et al., 1999). The presence of C atoms at 2.78Å indicated that Zn formed inner sphere complexes with HA. Previous research reported that Zn

adsorbed to HA formed inner sphere complexes at low HA concentration and formed outer sphere complexes only at very high HA concentrations (Sarret et al., 1997; Xia et al., 1997). Results of this study could suggest that in addition to forming inner sphere complexes with ferrihydrite, a small portion of Zn (<10% added Zn) may have precipitated with HA on the surface of ferrihydrite. Although inclusion of C atoms in the fitting results may indicate the formation of a ternary complex, this would be less likely to occur as ternary complexes dominate at low pH where substantially more HA is adsorbed (Figure 3.2).The results presented here are in agreement with Collins et al. (1999) who found that Cd bound to goethite in the presence of HA produced a second shell fit of 1.1 Fe atoms at 3.8 Å and 3 C atoms at 2.7 Å. They concluded the possibility of a cadmium-humate precipitate or a ternary complex formation.

The results also showed that Zn formed corner sharing linkages with ferrihydrite in the presence of HA as compared to both corner sharing and edge sharing linkages in the absence of HA (control).

- **Siderophore (DFO-B)**

The second shell for the DFO-B sample revealed Fe atoms at Zn-Fe interatomic distance of 3.40Å (Table 3.2), implying a ZnO_4-FeO_6 corner sharing linkage as with HA. The Debye Waller factor for second shell was high (0.02), indicating large thermal or static disorder in this shell. DFO-B has been shown to cause the dissolution of ferrhiydrite (Hersman et al., 1995), which might have contributed to the large disorder. The Debye Waller factor is strongly correlated with coordination number of Zn which would explain the large Fe coordination number produced from the fitting results (Trainor et al., 2000).

This study showed that despite DFO-B promoted the dissolution of ferrihydrite, and strongly suppressed Zn adsorption at pH 7.5, Zn remained strongly adsorbed to the mineral

surface by forming inner sphere complexes. This may indicate the high affinity of Zn for specific adsorption to the ferrihydrite surface. In addition, Zn sorption geometry in the presence of DFO-B was different than that of the control in which both corner sharing and edge sharing linkages were detected.

3.4 Summary and Conclusion

Differences existed among the ligands in terms of their impact on Zn adsorption. While citrate and PO_4 enhanced adsorption at pH below 7.5, DFO-B resulted in suppressed adsorption and the impact of HA was a function of pH. Zn adsorption generally increased as equilibrium time increased from 24 hrs to 1 week in the absence and presence of ligands possibly due to diffusion within the ferrihydrite lattice. Citrate and PO_4 also showed very strong adsorption at all pH levels. HA adsorption followed the anion exchange mechanism in which adsorption decreased with pH increase. The overall impact of HA and PO_4 on the adsorption of Zn was relatively small compared to citrate. Despite complete adsorption of PO_4 at all pH levels, it only enhanced Zn adsorption by a maximum of 10%. On the other hand, despite ~85% of HA remained in solution at pH 7.5, only ~10% reduction in Zn adsorption was observed. DFO-B resulted in the dissolution of ferrihydrite at all pH levels as evident by the release of Fe into solution. A large portion of DFO-B remained in solution and its removal was not impacted by pH. In the presence of DFO-B, Zn adsorption was suppressed, particularly for the shorter 24 hour reaction time and at high pH as compared to the longer reaction time of 1 week. DFO-B had less of a suppressive impact on Zn adsorption with increase in reaction time to 1 week.

EXAFS data analysis revealed that differences existed among the ligands in terms of Zn-O first shell coordination. Zn formed tetrahedral coordination with first shell oxygens in the control, HA and DFO-B sorption samples. The coordination environment was different in the

presence of citrate and PO_4, where an increase in Zn-O radial distance was evident. The radial distance and respective coordination number in the case of PO_4 indicate an octahedral coordination of the first shell. The Zn-O radial distance in the case of citrate was slightly higher than would expected be for tetrahedral coordination. The possible increase in distance may be due to the formation of ternary B complex.

EXAFS data fitting of the second shell revealed the formation of inner sphere complexes between Zn and the ferrihydrite surface. Two types of linkages were present in the control, citrate, and PO_4 sorption samples whereas only one type was in the HA and DFO-B samples. $ZnO_{4,6}$ polyhedra formed corner (bidentate binuclear) and edge (bidentate mononuclear) sharing linkages with FeO_6 of ferrihydrite in the control, citrate, and PO_4 sorption samples. In the HA and DFO-B samples, only corner sharing (bidentate binuclear) linkages were evident. Zn has been found to form more than one type of linkage with oxide mineral surfaces. Pan et al. (2004) found that $ZnO_{4,6}$ formed both corner and edge sharing linkages with manganite (γ-MnOOH) at pH 7.5. Zn was also found to form both edge and corner sharing linkages with goethite as evident by Zn-Fe radial distances of 3.0 and 3.20Å, respectively (Schlegel et al.,1997; Juillot et al., 2008). Other metals such as Pb was found to form a mixture of bidentate and monodentate complexes with ferrihydrite at pH 4.5 (Trivedi et al., 2003). Edge sharing linkages are stronger and more energetically favorable than corner sharing linkages. Therefore, Zn adsorption via edge linkages are less likely to be desorbed from mineral surfaces than corner linkages (Pan et al., 2004; Li et al., 2004).

3.5 References

Alcacio, T.E., D. Hesterberg, J.W. Chou, J.D. Martin, S. Beauchemin, and D.E. Sayers. 2001. Molecular scale characteristics of Cu(II) bonding in goethite–humate complexes. Geochim. Cosmochim. Ac. 65(9): 1355–1366.

Alloway, B.J. 2004. Zinc in soils and crop nutrition. International Zinc Association Communications. IZA, Brussels, Belgium.

Bochatay, L., and P. Persson. 2000. Metal ion coordination at the water-manganite (γ-MnOOH) interface II. An EXAFS study of zinc(II). J. Colloid Interf. Sci. 229: 593-599.

Boily, J.F., and J.B. Fein. 1996. Experimental study of cadmium-citrate co-adsorption onto α-Al_2O_3. Geochim. Cosmochim. Ac. 60(16):2929-2938.

Breban, D.C. PhD Dissertation. 2007. Provenance and characterization of aquatic actinide colloids: interaction of actinides with aluminosilicate and humate colloids. Ruprecht-Karls-Universität.

Collins, C.R., K.V. Ragnarsdottir, and D.M. Sherman. 1999. Effect of inorganic and organic ligands on the mechanism of cadmium sorption to goethite. Geochim. Cosmochim. Ac. 63(19): 2989-3002.

Collins, R.N., G. Merrington, M.J. Mclaughlin, and J.L. Morel. 2003. Organic ligand and pH effects on isotopically exchangeable cadmium in polluted soils. Soil Sci. Soc. Am. J. 67: 112–121.

Davis, A.P. and V. Bhatnagar. 1995. Adsorption of cadmium and humic acid onto hematite**,** Chemosphere 30: 243–256.

Delolme, C., C. Hebrard-Labit, L. Spadini, and J.P. Gaudet. 2004. Experimental study and modeling of the transfer of zinc in a low reactive sand column in the presence of acetate. J. Contam. Hydrol. 70:205-224.

Diaz-Barrientos, E., L. Madrid, M.C. Contreras, and E. Morillo. 1990. Simultaneous adsorption of zinc and phosphate on synthetic lepidocrocite. Aust. J. Soil. Res. 28: 549-557.

Dyer, J., and D. Sparks. 2003. Lead Sorption onto Ferrihydrite. 1. A Macroscopic and Spectroscopic Assessment. Environ. Sci. Technol. 37: 908-914.

Geelhoed, J.S., T. Hiemstra, and W.H. Vanriemsdijk. 1998. Competitive interaction between phosphate and citrate on goethite. Environ. Sci. Technol. 32: 2119-2123.

Glover II, L.J., M.J. Eick, and P.V. Brady. 2002. Desorption kinetics of cadmium^{+2} and lead^{+2} from goethite: influence of time and organic acids. Soil Sci. Soc. Am. J. 66: 797–804.

Gustafsson, J. P. 2004. Visual Minteq (2.30). U.S. Environmental Protection Agency.

Ha, J., T.P. Trainor, F. Farges, and G.E. Brown. 2009. Interaction of aqueous Zn(II) with hematite nanoparticles and microparticles. Part 1. EXAFS study of Zn(II) adsorption and precipitation. Langmuir. 25: 5574–5585.

Haas, C.N. and N.D.Horowitz. 1986. Adsorption of cadmium to kaolinite in the presence of organic material. Water Air Soil Poll. 27: 131–140.

Hersman, L., T. Lloyd and G. Sposito 1995. Siderophore-promoted dissolution of hematite. Geochimica at Cosmochimica Acta. 59: 3327-3330.

HO, C.H., and N.H. Miller. 1985. Effect of humic acid on uranium uptake by hematite particles. J. Colloid Interf. Sci. 106(2): 281- 288.

Juillot, F., C. Maréchal, M. Ponthieu, S. Cacaly, G. Morin, M. Benedetti, J.L. Hazemann, O. Proux, and F. Guyot. 2008. Zn isotopic fractionation caused by sorption on goethite and 2-Lines ferrihydrite. Geochim. Cosmochim. Ac. 72: 4886-4900.

Kummert, R. and W. Stumm. 1980. The surface complexation of organic acids on hydrous γ-Al_2O_3. J. Colloid Interf. Sci. 75(2):373-385.

Lai, C.H., C.Y. Chen, B.L.Wei and S.H. Yeh. 2002. Cadmium adsorption on goethite-coated sand in the presence of humic acid. Water Res. 36: 4943–4950.

Lee, S. and P.R. Anderson. 2005. EXAFS study of Zn sorption mechanisms on hydrous ferric oxide over extended reaction time. J. Colloid Interf. Sci. 286: 82-89.

Li, W., S. Zhang, W. Jiang, and X. Shan. 2006. Effect of phosphate on the adsorption of Cu and Cd on natural hematite. Chemosphere. 63: 1235-1241.

Li, X., G. Pan, Y. Qin, T. Hu, Z. Wu, and Y. Xie. 2004. EXAFS studies on adsorption-desorption reversibility at manganese oxide-water interfaces II. Reversible adsorption of zinc on δ-MnO_2. J. Colloid Interf. Sci. 271: 35-40.

Nachtegaal, M., and D.L. Sparks. 2003. Nickel sequestration in a kaolinite-humic acid complex. Environ. Sci. Technol. 37: 529-534.

Nachtegaal, M., and D.L. Sparks. 2004. Effect of iron oxide coatings on zinc sorption mechanisms at the clay-mineral/water interface. J. Colloid Interf. Sci. 276: 13–23.

Neubauer,U., G. Furrer, and R. Schulin. 2002. Heavy metal sorption on soil minerals affected by the siderohpore desferrioxamine B: the role of Fe(III) (hydr)oxides and dissolved Fe(III). Eur. J. Soil Sci 53: 44-55.

O'Day, P.A., S.A. Carroll, and G.A. Waychunas. 1998. Rock- water interactions controlling zinc, cadmium, and lead concentrations in surface waters and sediments, U.S. tri-state mining district. 1. Molecular identification using X-ray absorption spectroscopy. Environ. Sci. Technol. 32(7): 943-955.

Pan, G., Y. Qin, X. Li, T. Hu, Z. Wu and Y. Xie. 2004. EXAFS studies on adsorption-desorption reversibility at manganese oxides-water interfaces I. Irreversible adsorption of Zn onto manganite (γ-MnOOH). J. Colloid Interf. Sci. 271: 28-34.

Ponthieu, M., F. Juillot, T. Hiemstra, W.H. van Riemsdijk, and M.F. Benedetti. 2006. Metal ion binding to iron oxides. Geochim. Cosmochim. Ac. 70: 2679-2698.

Roberts, D. R., R. G.Ford and D. L. Sparks. 2003. Kinetics and mechanisms of Zn complexation on metal oxides using EXAFS spectroscopy. J. Colloid Interf. Sci. 263(2): 364-376.

Sarret, G., A. Manceau, J.L. Hazemann, and A. Gomez. 1997. EXAFS study of the nature of zinc complexation sites in humic substances as a function of Zn concentration. J. Phys. IV France 7: C799-802.

Schlegel, M.L., A. Manceau, and L.Charlet. 1997. EXAFS study of Zn and ZnEDTA sorption at the goethite (α-FeOOH)/water interface.J. Phys IV Fr. 7C-3:823-824.

Schwab, A.P., Y. He, and M.K. Banks. 2005. The influence of organic ligands on the retention of lead in soil. Chemosphere 61: 856–866.

Schwertmann, U., R.M. Cornell. 2000. Iron Oxides in the Laboratory. Wiley-VCH, Weinheim.

Spadini, L., A. Manceau, P.W. Schindler, and L. Charlet. 1994. Structure and stability of Cd^{+2} surface complexes on ferric oxides. 1. Results from EXAFS spectroscopy. J. Colloid Interf. Sci. 168: 73-86.

Swift, R.S. 1996. Organic matter characterization. Chapter 35. *In* D.L. Sparks (ed.) Methods of soil analysis. Part 3. SSSA Book Ser. 5. SSSA, Madison, WI.

Trainor, T.P., G.E. Brown, and G.A. Parks. 2000. Adsorption and precipitation of aqueous Zn(II) on alumina powders. J. Colloid Interf. Sci. 231: 359-373.

Trived, P., J.A. Dyer, and D.L. Sparks. 2003. Lead sorption onto ferrihydrite. 1. A macroscopic and spectroscopic assessment. Environ. Sci. Technol. 37: 908-914.

Trivedi, P., J.A. Dyer, D.L. Sparks, and K. Pandya. 2004. Mechanistic and Thermodynamic interpretations of zinc sorption onto ferrihydrite. J. Colloid Interf. Sci. 270: 77-85.

Trivedi, P., L. Axe, and T.A. Tyson. 2001. An Analysis of Zinc Sorption to Amorphous versus Crystalline Iron Oxides Using XAS. J. Colloid Interf. Sci. 244: 230–238.

Uygur, V., and D.L. Rimmer. 2000. Reactions of zinc with iron oxide coated calcite surfaces at alkaline pH. Eur. J. Soil Sci. 51: 511-516.

Venema,P., T. Hiemstra, and W.H. Van Riemsdijk. 1997. Interaction of Cadmium with Phosphate on Goethite. J. Colloid Interf. Sci. 192: 94–103.

Violante, A., M.R. Ricciardella, and M. Pigna. 2003. Adsorption of heavy metals on mixed Fe–Al oxides in the absence or presence of organic ligands. Water Air Soil Poll. 145: 289–306.

Voegelin, A., G. Tokpa, O. Jacquat, K. Barmettler, and R. Kretzschmar. 2008. Zinc fractionation in contaminated soils by sequential and single extractions: Influence of soil properties and zinc content. J. Environ. Qual. 37: 1190-1200.

Wang, K. and B. Xing. 2004. Mutual effects of cadmium and phosphate on their adsorption and desorption by goethite. Environ. Pollut. 127:13–20.

Waychunas, G.A., C.C. Fuller, and J.A. Davis. 2002. Surface complexation and precipitate geometry for aqueous Zn(II) sorption on ferrihydrite I: X-ray absorption extended fine structure spectroscopy analysis. Geochim. Cosmochim. Ac. 66(7): 1119-1137.

Yamaguchi, N. U., A. C. Scheinost, and D.L. Sparks. 2002. Influence of gibbsite surface area and citrate on Ni sorption mechanisms at pH 7.5. Caly Clay Miner. 50(6): 784-790.

Yamaguchi, N.U., A.C. Scheinost, and D.L. Sparks. 2001. Surface-Induced Nickel Hydroxide Precipitation in the Presence of Citrate and Salicylate Soil Sci. Soc. Am. J. 65:729–736.

Xia, K., W. Bleam, and P.A. Helmke. 1997. Studies of the nature of binding sites of first row transition elements bound to aquatic and soil humic substances using X-ray absorption spectroscopy. Geochim. Cosmochim. Ac. 61(11): 2223-2235.

CHAPTER 4

MACROSCOPIC AND XAFS SPECTROSCOPIC INVESTIGATION OF ZINC ADSORPTION TO KAOLINITE IN THE PRESENCE OF LIGANDS AS A FUNCTION OF pH

4.1 Introduction

Zinc (Zn), an essential element for plant nutrition and microbial growth, can be potentially toxic in soils at elevated levels as a result of contamination from smelting activities, deposition of incinerator emissions, excessive use of fertilizer, runoff from roads and steeled constructions as well as use of contaminated sludges (Robson, 1993; Alloway, 2004). Its fate and bioavailability in soils and aquatic systems is influenced by sorption processes occurring at the water-mineral interface (Roberts et al., 2003). Understanding this process and its influencing factors has both environmental and agricultural significance (Sparks, 2003).

Various factors including pH, ionic strength as well as clay mineralogy have been shown to affect Zn adsorption (McBride, 1989). Increasing pH generally enhances Zn adsorption by soil minerals. At low pH, Zn is considered to be held in an exchangeable form at basal planes of clay minerals, whereas at higher pH Zn could be absorbed by edge sites of clay minerals (McBride, 1994). The pH-dependent nature of metal adsorption has been interpreted at the atomic scale by the formation of inner-sphere complexes (Sparks, 2003). Increasing ionic strength decreases Zn adsorption to the basal planes of clay minerals. However, the decreases depend on solution pH (Schlegel et al., 2001). In general, the change in ionic strength has more impact on Zn adsorption by clay minerals or soils at low pH than at high pH (Shuman, 1986; Schlegel et al., 2001). In addition, lability of adsorbed Zn has been shown to be influenced by different cationic environments (Wang and Harrell, 2005).

The presence of various natural organic and inorganic ligands could also affect heavy metal adsorption by soil minerals (Farrah and Pickering, 1976; Collins et al., 2003). The most

common ligands are high molecular weight humic substances which are ubiquitous in terrestrial and aquatic environments. Strong inner-sphere complexes between heavy metals including Zn and carboxyls of humic acids have been reported (Xia et al., 1997). On the other hand, various living organisms within the soil such as plants, fungi and bacteria excrete low molecular weight ligands such as citrate and oxalate. Citrate from root exudates was found to enhance the solubility of various metals, therefore mobility and bioavailability of these metals in soils (Mench et al., 1991; Yamguchi et al., 2001).

Low molecular weight organic acids have been considered as model ligands to describe the metal binding characteristics of soil organic matter (Buerge-Weirich et al., 2003). However, previous studies suggested that these varying molecular weight ligands may exhibit different impacts on metal sorption in ternary systems that contain metals, mineral surfaces, and ligands (Zachara et al., 1994; Yamaguchi et al., 2001; Nachtegaal and Sparks, 2003). Furthermore, microbial produced siderophores and phytosiderophores are able to dissolve iron oxides and chelate Fe (III) in iron deficient soils. They also chelate various divalent heavy metals and affect their solubility (Neubauer, 2000; Kraemer, 2004). Besides these natural organic ligands, inorganic phosphates especially orthophosphate are also of considerable agricultural and environmental significance. Phosphate fertilizers are routinely applied in soils to increase yield. Such application has been shown to cause different Zn sorption characteristics in acid and calcareous soils (Agbenin, 1998; Wang and Harrell, 2005).

On the other hand, these organic and inorganic ligands are known to interact with soil minerals differently, especially under different pH conditions (Edzwald et al., 1976; Oades, 1988; Lackovic et al., 2003; Siebner-Freibach, 2004). These interactions would likely have different influences on metal sorption by different soil minerals, which have not been fully

investigated. Understanding the specific role of these ligands on Zn interaction with specific soil minerals is of utmost importance for remediation and risk assessment of metals in soils.

Much of previous research employed macroscopic techniques based on sorption isotherms to characterize metal retention in different soil and clay mineral systems. However, recent advancement employing microscopic techniques such as extended X-ray absorption fine structure (EXAFS) spectroscopy has made it possible to elucidate the mechanisms of metal adsorption onto various mineral surfaces based on its coordination chemistry at the local atomic environment (Sparks, 2003). Based on EXAFS spectroscopy, it was shown that Cd adsorption to kaolinite was predominantly in the form of outer sphere complexes, while Pb formed polymeric complexes that were bond via edge sharing to the Al octahedra (Gräfe et al., 2007; Vasconcelos et al., 2008). On the other hand, Zn sorbed to kaolinite was found to form inner-sphere sorption complexes at pH 5.0 and formed a surface-precipitate phase resembling Zn-Al layered double hydroxide (LDH) at pH 7.0 (Nachtegaal and Sparks, 2004).

Similar mixed metal-Al LDH formations have been found for Ni and other metals sorbed by clay minerals, Al oxides, and whole soils (Roberts et al., 1999; Scheinost and Sparks, 2000; Nachtegaal and Sparks, 2003; Voegelin and Kretzschmar, 2005). Under neutral and slightly alkaline conditions, metal- Al LDH such as Ni-Al LDH has been found to form within short reactions times (minutes to days) in different clay mineral and whole soil systems with most occurring in < 24 hrs, although it generally takes longer as solution pH is decreased (Scheidegger et al., 1998; Roberts et al., 1999). On the other hand, the formation of Zn surface precipitate phases was shown to be thermodynamically favored at the kaolinite surface and was not affected by the coating of an iron oxide over-time (Nachtegaal and Sparks, 2004). For Zn sorption with very high loadings or aging over time, a Zn phyllosilicate-like phase has also been

observed at the interface of 1:1 and 2:1 clay minerals (Ford and Sparks, 2000; Lee et al., 2004). Nonetheless, the formation of LDH has been considered as a precursor to Zn fixation in soils abundant in aluminosilicate minerals (Ford and Sparks, 2000). This mechanism of Zn sequestration has not been, however, extensively evaluated in the presence of different natural organic and inorganic ligands that are known to intimately react with soil minerals (Voegelin et al., 2005). Limited research on Ni sorption, however, suggested that the incorporation of Ni into a mixed metal Ni-Al LDH was influenced by the presence of small molecule organic acids and humic acids at the gibbsite and kaolinite surfaces (Yamaguchi et al., 2002; Nachtegaal and Sparks, 2003).

This study was conducted to assess the impact of citrate, humic acid (HA), siderophore DFO-B and phosphate (PO_4) on the sorption of Zn to kaolinite at pH levels ranging from 4.5 to 7.5 and to elucidate the underlying Zn sorption mechanisms to kaolinite in the presence of these ligands using XAFS spectroscopy.

4.2 Material and Methods

4.2.1 Kaolinite Preparation and Purification

Kaolinite used in this study was the low defect Georgia kaolinite (KGa-1b) obtained from the Clay Minerals Society. The <2μm fraction was obtained by the sedimentation method according to Stokes law. To ensure dispersion of kaolinite, it was prepared in 10^{-4}M $NaHCO_3$ with pH adjusted to 9.0 (Freibach and Chen, 2004). A purification process followed in which carbonates, iron oxides, and organic matter were removed. Carbonate removal was conducted using the method of Jackson (1956) in which kaolinite was heated in sodium acetate (pH 5.0) at 95ºC for 30 minutes. Kaolinite was then washed via centrifugation with 1M NaCl solution. Iron removal was conducted using the citrate-bicarbonate-dithionite method described by Aguilera

and Jackson (1953). Afterwards, kaolinite was washed 4 times via centrifugation with a solution of 0.025M HCl and 0.5M NaCl (Ammann, 2003). Organic matter was removed by heating in 3% H_2O_2 at 50ºC for 1 hour, then heating at 70ºC to destroy remaining H_2O_2 (Schlegel et al., 1999). Kaolinite was then washed 5 times with 1M NaCl and washed again with deionized water to remove excess salt (Nachtegaal and Sparks, 2003; Janssen et al., 1997).

Kaolinite was dialyzed against double deionized water until no Cl^- remained as tested by $AgNO_3$. Dialysis bags were pretreated by boiling in a 2% $NaHCO_3$ and 1 mM EDTA solution and washed with deionized water to remove contaminating minerals and polysaccharides (Morillo et al., 2006). The purified kaolinite was then freeze dried, ground and sieved prior to use. The 5 point N_2-BET surface area for kaolinite in this study was found to be 16.39 m^2/g. The reported point zero charge (PZC) and CEC for KGa-1b are 6.0 and 1.83 meq/100g, respectively (Křepelová, 2007).

PO_4, citrate, and DFO-B ligands were prepared from sodium dihydrogen phosphate, trisodium citrate dihydrate, and desferrioxamine mesylate salts, respectively. HA was obtained from Sigma-Aldrich (H16752) and was purified by acid washing and subsequent removal of ash content according to the International Humic Substance Society method (Swift, 1996). Briefly, HA was acidified to pH 1.5, allowed to stand for 16 hours, settled by low speed centrifugation and then the supernatant was decanted. HA was resuspended under N_2 gas to pH 7.0 using 1M NaOH and allowed to stand for 24 hours. The precipitation and subsequent redissolution was repeated four times. To remove the ash content from HA, the precipitate was suspended in 0.1M HCl/0.3M HF and shaken overnight. The process was repeated once and then HA was dialyzed until free of Cl^- as tested using $AgNO_3$. The material was freeze dried and mixed well prior to use.

4.2.2 Sorption Experiment

Adsorption experiments were conducted in 50ml centrifuge tubes under continuous purging of ultra pure N_2 gas. The experimental setup included 4 pH levels (4.5, 5.5, 6.5, and 7.5), five ligand treatments (citrate, PO_4, HA, DFO-B, and $NaNO_3$-control) and replicated twice. The kaolinite concentration was 20 g/L and the metal:ligand ratio constituted a 1:1 molar ratio of 1.5 mM. HA was prepared on the basis of total carbon content (determined using TOC analyzer), so that total carbon content was similar to that of citrate. The background electrolyte concentration of 0.01M $NaNO_3$ dominated the ionic strength of the adsorption suspension.

The purified kaolinite was first allowed to hydrate for 24 hours in $NaNO_3$.The ligand solution of citrate, PO_4, HA or DFO-B was then added to their respective tubes and allowed to react with kaolinite for 10 minutes. Zn was then added dropwise from an acidified solution under constant stirring of suspension. The pH was adjusted to its respective value using 0.1M of either HNO_3 or NaOH (pre-purged with N_2). The final volume was completed and the reaction time was 24 hours. The pH was continuously monitored (under N_2 purging) and adjusted so that values exhibited minimal fluctuations. The solid was separated from the solution by centrifugation and the solution was filtered using 0.45 μM filters. Soluble concentrations of Zn, P, Si and Al were determined using ICP-AES (Spectro). Concentrations of dissolved organic carbon in the system were determined using TOC analyzer (Shimadzu). The amounts of Zn and ligand adsorbed were determined by the difference in initial and final concentrations in solution. The solid portion was stored as a paste at 4ºC until use for XAFS spectroscopy analysis.

4.2.3 EXAFS Data Collection and Analysis

EXAFS data were collected on the Ge (220) double-crystal monochromator beamline at the Center for Advanced Microstructures and Devices (CAMD) in Baton Rouge, Louisiana. The

electron beam energy was 1.3 GeV with a maximum beam current of 180mA. Zn metal foil was used to calibrate the beam energy by setting the first inflection point to 9569eV. The EXAFS spectra for adsorption samples were collected at Zn K-edge in fluorescence mode using a Canberra 13 element ultra low energy germanium diode array detector. Multiple scans were collected to improve the signal to noise ratio. The EXAFS data for reference compounds were collected in transmission mode. These compounds included: 1mM $Zn(NO_3)_2$ at pH 2.0, Zn citrate, ZnO, Zn-Al LDH, and $Zn_3(PO_4)_2$.

Data reduction was conducted using Athena interface to IFEFFIT software. The scans were aligned, merged and deglitched. Standard procedures were used to extract the EXAFS spectra (Ressler et al., 2000; Fay et al., 1992). The threshold energy (E_0) was determined from the maximum of the first derivative of $\mu(E)$ and was used to convert the energy axis to photoelectron wave vector units ($Å^{-1}$). The resulting data were weighted by k^3 to compensate for damping of the EXAFS spectrum at higher energies. The *k*-weighted $\chi(k)$ spectra were then Fourier transformed over the wave vector *k* range of 2-10$Å^{-1}$ using a Kaiser-bessel apodization window to produce radial structure functions (RSF) that isolate first and second shell components (Yamaguchi et al., 2003; Nachtegaal and Sparks, 2004). Ab initio phase shift and amplitude functions of Zn-O, Zn-Al, Zn-P and Zn-Zn scattering paths were extracted using Zn-Al LDH, hopeite ($Zn_3(PO_4)_2 \cdot 4H_2O$), and zincite (ZnO) using FEFF 6.0 code. The peaks of interest were isolated and backtransformed in *k* space using a Kaiser-bessel window. Structural parameters (element identity, coordination number, and radial distance) were determined by a non linear least squares curve fitting approach using Artemis interface to IFEFFIT software. The two major peaks in the Fourier transforms at R of 1.0-3.2Å were isolated and backtransformed. Single shell fits were conducted for the first and second peaks selected, respectively. The value

of S_0^2 was set to 0.84 and determined by fixing the coordination number for Zn-O in aqueous Zn to 6 (Roberts et al., 2003; Alcacio et al., 2001; Scheinost et al., 2002).

4.3 Results

4.3.1 Macroscopic Zn Adsorption

Figure 4.1a-d shows the percentage of Zn and ligand adsorbed to kaolinite as a function of pH. In the control ($NaNO_3$ background), Zn adsorption increased abruptly with increasing pH from 6.0 to 7.5. Zn adsorption reached 95% of added Zn at pH 7.5. Increasing pH increases the negative charges of the kaolinite surface, which is generally expected to facilitate the adsorption of the positively charged Zn ion. On the other hand, the sharp rise in adsorption corresponded to the pH range that first hydrolysis of Zn begins to takes place (James et al., 1975; Srivastava et al., 2005). The formation of hydroxo complexes in this pH range has been suggested to increase the likelihood of specific adsorption of metals (Arias et al., 2002).

The four ligands showed different influences on Zn adsorption to kaolinite. These ligands themselves also had different interactions with kaolinite. Among the three organic ligands, HA had the greatest enhancement on Zn adsorption by kaolinite as compared to the control (with purely NO_3^- background) throughout the pH range between pH 4.5 and 7.5 (Figure 4.1). Zn adsorption ranged from 23% at pH 4.5 to 96% at pH 7.5. The enhanced adsorption of Zn to kaolinite in presence of HA is consistent with the general impact of HA on metal adsorption to alluminosilicate mineral surfaces (Liu and Gonzalez, 1999). Previous studies showed that HA increased Cu and Cd adsorption capacity of kaolinite at low pH, generally < 6.5 (Arias et al., 2002; Hizal and Apak, 2006), whereas the presence of fulvic acid can enhance Cu and Pb adsorption at pH 4 to 8 (Heidmann et al., 2005).

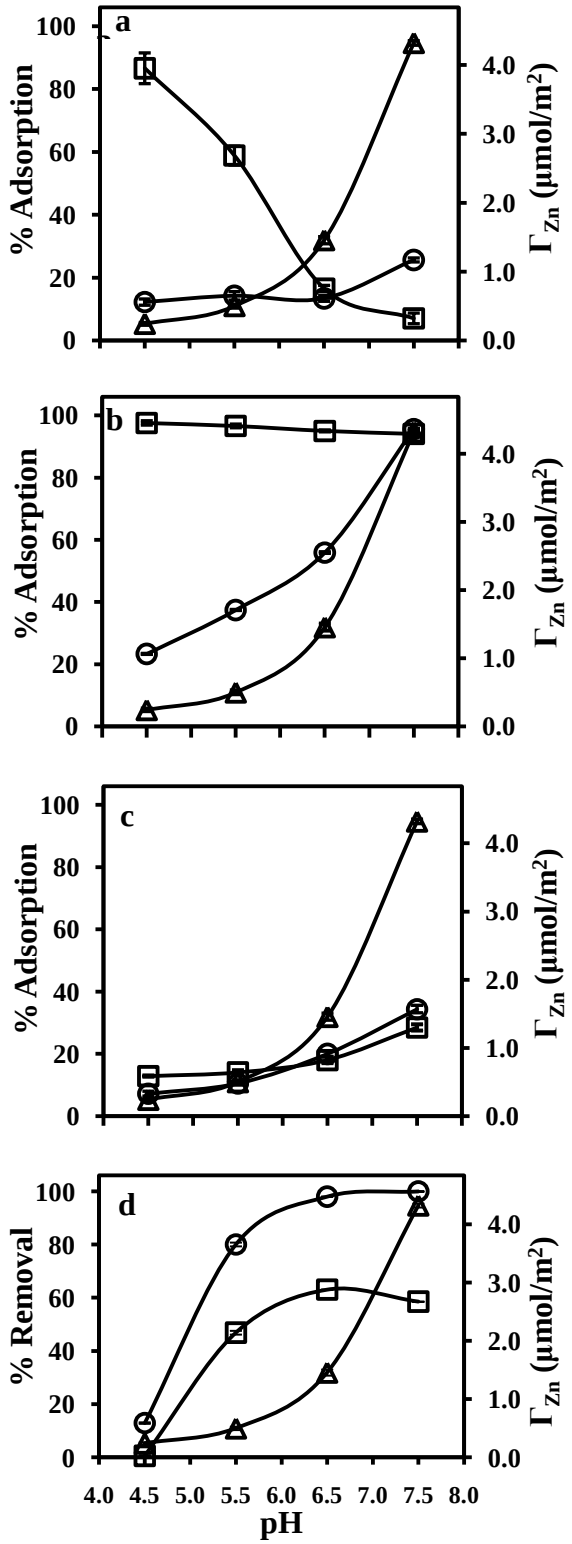

Figure 4.1 Zn adsorption in the presence of citrate (a), HA (b), DFO-B (c), PO_4 (d) as a function of pH.(⊖) Zn adsorption in the control, (⊟) Zn adsorption in presence of ligand, (⊿) adsorption of ligand.

In this study, almost all (96-98%) of added HA was sorbed and there was only a slight decrease (4 %) in sorption as pH increased from 4.5 to 7.5, suggesting very strong interaction of HA with kaolinite and/or Zn in the experimental system. Adsorption of HA onto kaolinite surfaces has been shown to decrease as pH increases, following the anion exchange or electrostatic interaction mechanism (Liu and Gonzalez, 1999; Murphy and Zachara, 1995), even though substantial quantities of HA could be still adsorbed to kaolinite at neutral and high pH values (Hizal and Apak, 2006).

Citrate, on the other hand, slightly enhanced Zn adsorption between pH 4.5 and 5.5 but greatly suppressed adsorption at pH >7.5 as compared with the control (Figure 4.1a). With the presence of citrate, overall Zn sorption was generally low, with 12-26% of added Zn in the pH range of 4.5-7.5. The suppressive effect of citrate on metal sorption to kaolinite has also been reported for Cd^{+2} in the pH range from 5.0 to 8.0 (Lackovic et al., 2004; Liao, 2006). According to Lackovic et al. (2004), the degree to which Cd^{+2} was suppressed was dependent on the citric acid: Cd^{+2} ratio; the higher the ratio the more adsorption was suppressed. The drastic suppression of Zn sorption at pH greater than 6 found in this study as a result of citrate presence could also indicate a high citrate to Zn^{+2} ratio in solution. On the other hand, the suppression clearly corresponded to the sharp drop in sorption of citrate from as much as 87% at pH 4.5 to 7% as pH increased to 7.5. The decrease in citrate sorption was likely due to the repulsive effect between kaolinite and citrate as both become more negatively charged at higher pH (Lackovic et al., 2004). Citrate along with other small organic acids such as oxalate and salicylate have often been used to model the impact of organic matter on metal reactions in soil (Buerge-Weirich et al., 2003). Our study clearly indicated that citrate and HA had different interaction with and/or influence on Zn sorption by kaolinite in the pH range of 4.5 to 7.5.

Siderophore DFO-B had little impact on Zn adsorption between pH 4.5 and 5.5 but, like citrate, also significantly suppressed Zn adsorption when suspension pH was >5.5 as compared to the control. With the presence of DFO-B, overall Zn adsorption was also low, ranging from 7-35% of added Zn in the studied pH range. Our data on the impact of DFO-B on Zn sorption to kaolinite was in agreement with Neubauer et al. (2000) who showed that DFO-B hindered the adsorption of Cu, Zn and Cd to kaolinite in the pH range from 4 to 10, with observable amounts adsorbed at pH above 6. In addition, they reported that DFO-B adsorption was minimal at pH < 6 and increased slightly (up to 5%) at higher pH. In this study, DFO-B sorption was about 12% at pH 4.5 and increased to 48% at pH7.5. Sorption of DFO-B to kaolinite followed the behavior of cation adsorption as pK_a's were ≥ 8.3 for its hydroxamate and amine groups (Hernlem et al., 1996). The cation-like DFO-B could compete with Zn and therefore suppress Zn adsorption onto kaolinite. The low sorption of DFO-B was likely due to generally low charge capacity of kaolinite as compared with other clay minerals such as montmorillonite (Seibner-Freibach et al., 2004; Hepinstall et al., 2005).

The presence of inorganic PO_4 increased Zn adsorption throughout the pH range but especially at pH 5.5, where a 69% increase in Zn removal from solution had occurred in comparison with the control (Figure 4.1 d). PO_4 adsorption also increased with pH increase with an adsorption maximum of 63% of added P at pH 6.5. The trend of PO_4 sorption in this study was consistent with those previously reported for kaolinite with no Zn addition (Edzwald et al., 1976; Bar-Yosef et al., 1988), suggesting that Zn did not influence P interaction with kaolinite surface. Different phyllosilicates, including kaolinite, and oxide minerals have been pretreated with phosphate to enhance the adsorption of Pb and Cd (Wang and Xing, 2002; Adebowale et

al., 2006; Taylor et al., 2009). Our result suggested that the enhancement of Zn sorption by a phosphate-modified kaolinite is most effective at pH 5.5-6.5 than at pH out of this range.

4.3.2 EXAFS Analysis of Zn Model Compounds

Figure 4.2 shows the K-edge XANES spectra, the normalized k^3-weighted EXAFS spectra, and the corresponding Fourier transformed Radial Structural Functions (RSF) (uncorrected for phase shifts) for Zn model compounds. Data analysis obtained from fitting the backtransformed χ spectra are shown in Table 4.1. The RSF for $Zn^{+2}_{(aq)}$ displays a single coordination shell with Zn in octahedral coordination with oxygen atoms, representing an outer sphere complex (Figure 4.2c) (Lee et al., 2004).

The second shell for the Zn-Al LDH model compound was best fit with Zn and Al atoms at radial distances of 3.06 and 3.05Å, respectively (Figure 4.2c; Table 4.1). The Zn-Al and Zn-Zn radial distances for Zn-Al LDH range from 3.05-3.08Å as indicated by XRD (Roberts et al., 2003). Reported Zn-Zn/Al radial distances determined by EXAFS data analysis range from 3.06-3.1Å. Ford and Sparks (2000) reported Zn-Al and Zn-Zn radial distances of 3.06Å and 3.08Å, respectively. Fitting results for Zn citrate, ZnO and $Zn_3(PO_4)_2$ were comparable with previous research (Trainor et al., 2000; Robert et al., 2003; Lee et al., 2004).

4.3.3 EXAFS Analysis of Sorption Samples at pH 5.5

Figure 4.3 (a-c) shows the normalized k^3-weighted EXAFS spectra, the corresponding Fourier transformed Radial Structural Functions (RSF) (uncorrected for phase shifts), and Fourier back transformed spectra for sorption samples in the absence (control) and presence of different ligands at pH 5.5. Data analysis obtained from fitting the backtransformed χ spectra are shown in Table 4.2.

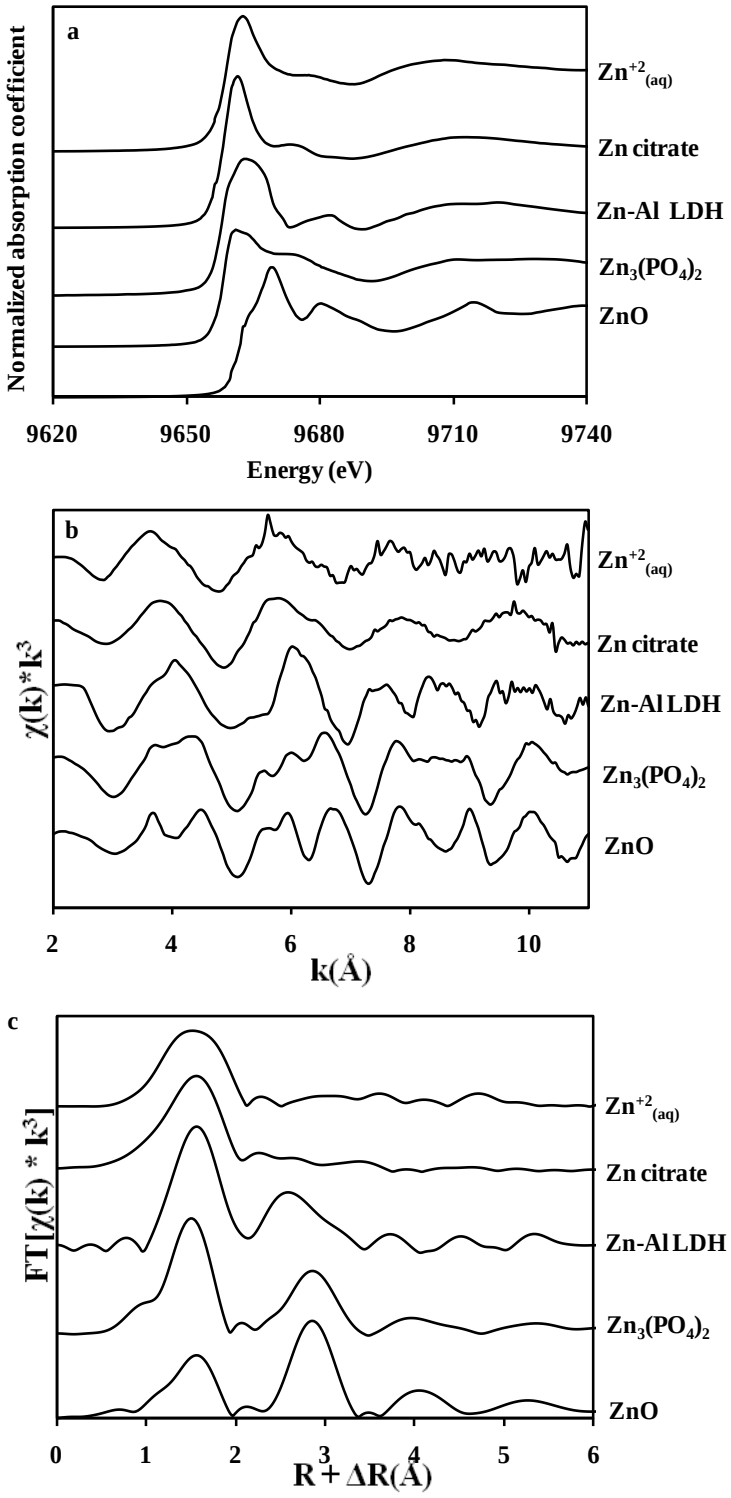

Figure 4.2 Zn K-edge XANES spectra for selected Zn model compounds (a), k^3-weighted $\chi(k)$spectra (b), and their respective RSFs (c).

Table 4.1 Structural parameters for Zn reference compounds derived from EXAFS spectral data analysis

Compound	Shell	N	R(Å)	σ^2(Å^2)
$Zn^{+2}_{(aq)}$	Zn-O	5.77	2.07	0.012
Zn citrate	Zn-O	5.96	2.04	0.010
	Zn-C	4.21	2.79	0.008
Zn-LDH	Zn-O	6.63	2.03	0.010
	Zn-Zn	4.63	3.06	0.012
	Zn-Al	2.18	3.05	0.012
$Zn_3(PO_4)_2$	Zn-O	4.09	1.96	0.006
	Zn-P	2.32	3.11	0.003
	Zn-Zn	4.96	3.26	0.008
ZnO	Zn-O	3.27	1.95	0.008
	Zn-Zn	12.41	3.23	0.012

N = coordination number, R = radial distance (Å), σ^2 = Debye-Waller factor (Å^{-2}).The uncertainties in N are estimated to be 30%. Variations in R are estimated to be 0.03 for all shells.

EXAFS data analysis indicated that Zn formed octahedral coordination with first shell oxygen atoms in the control as evident by the Zn-O radial distance of 2.03Å and coordination number of 5.88 (Table 4.2). In the presence of PO_4, Zn was found to form tetrahedral first shell coordination as evident by the Zn-O radial distance of 1.94Å and coordination number of 3.94. Characteristic Zn-O radial distances for tetrahedral and octahedral coordination range from 1.92 to 1.99Å and from 2.02 to 2.12Å, respectively (Roberts et al., 2003). For the remainder of Zn sorption samples (with citrate, HA, or DFO-B), the Zn-O radial distance was 1.99Å with coordination numbers greater than 5. The Debye-Waller factor values of the first shell were high for these samples indicating highly disordered oxygen atoms (Table 4.2).

The Zn-O radial distance of 1.99Å for the citrate, HA, and DFO-B samples suggested that the first shell Zn-O in these samples was on the borderline of tetrahedral coordination and may

hint to the formation of a mixture of Zn-O tetrahedral and octahedral coordination spheres. Pan et al. (2004) reported that Zn was adsorbed to manganite in a mixture of tetrahedral and octahedral coordination at an average radial distance of 2.0Å. The formation of a mixture of coordination spheres may be further supported by inspecting diagnostic spectral features. The XANES spectra for the sorption samples at pH 5.5 displayed in Figure 4.4(a) exhibit a large drop in absorption after the K-edge in all samples except in the case of PO_4, supporting a lower Zn-O first shell coordination number for this sample. This conclusion is on the basis that the XANES spectra for Zn compounds with octahedral first neighbor shells are characterized by a large drop in absorption after the K-edge that is absent in compounds of tetrahedral first neighbor structures (Waychunas et al., 2003). This can be observed by comparing octahedral compounds such as $Zn^{+2}_{(aq)}$ and Zn-LDH with tetrahedral ZnO and $Zn_3(PO_4)_2$ in Figure 4.2(a).

Table 4.2 Structural parameters for Zn sorbed on kaolinite in the presence and absence of ligands derived from EXAFS spectral data analysis

Ligand	pH 5.5				pH 7.5			
	Shell	N	R(Å)	σ^2(Å^2)	Shell	N	R(Å)	σ^2(Å^2)
Control	Zn-O	5.88	2.03	0.011	Zn-O	5.33	2.01	0.008
	Zn-Al	0.74	3.06	0.003	Zn-Al	1.76	3.09	0.003
					Zn-Zn	4.83	3.08	0.012
Citrate	Zn-O	5.29	1.99	0.017	Zn-O	4.6	1.91	0.012
	Zn-Al	1.05	3.11	0.009				
HA	Zn-O	5.60	1.99	0.014	Zn-O	5.83	2.02	0.001
	Zn-Al	0.66	3.11	0.001	Zn-Al	2.23	3.10	0.002
DFO-B	Zn-O	5.29	1.99	0.008	Zn-O	3.44	1.91	0.003
	Zn-Al	0.91	3.10	0.006	Zn-Al	0.87	3.11	0.003
PO_4	Zn-O	3.94	1.94	0.009	Zn-O	4.04	1.95	0.003
	Zn-P	0.53	3.15	0.001	Zn-P	1.60	3.16	0.001

N = coordination number, R = radial distance (Å), σ^2 = Debye-Waller factor (Å^{-2}).The uncertainties in N are estimated to be 30%. Variations in R are estimated to be 0.03 for all shells.

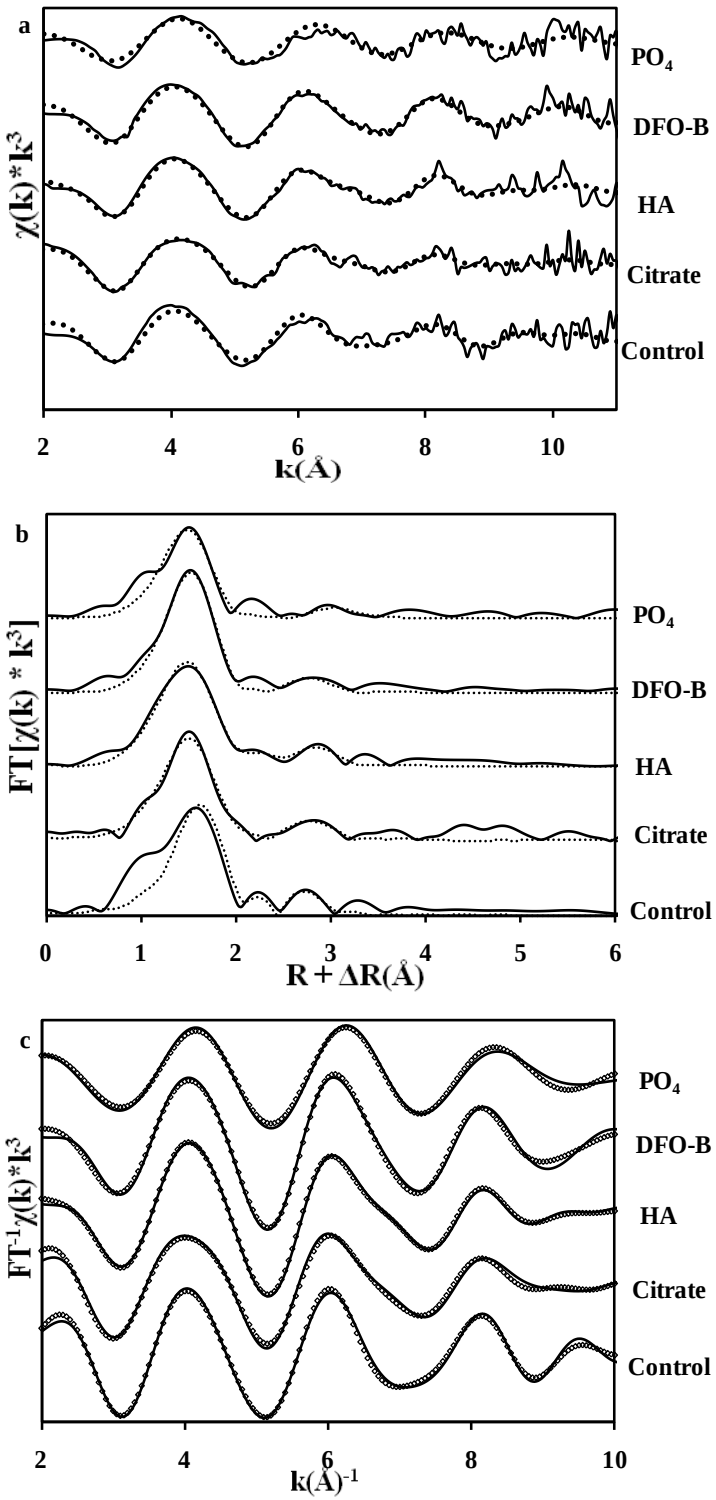

Figure 4.3 The k^3-weighted $\chi(k)$ spectra of Zn sorbed to kaolinite in absence (control) and presence of different ligands at pH 5.5 (a), their respective Fourier transforms (b), and inverse Fourier transforms (c). The solid lines represent the raw spectra and the dotted lines represent best fits.

The drop in absorption for the citrate, HA, and DFO-B samples are characteristic of octahedral first neighbor coordination. In addition, the Zn sorption sample in the presence of PO_4 exhibited a slight shift to higher $k(A^{\circ -1})$ values in comparison with the remainder of samples (Figure 4.3a). Zn compounds with tetrahedral first neighbor shells have been shown to have their χ spectra shifted to higher $k(A^{\circ -1})$ values as compared with octahedral compounds (Roberts et al., 2003; Nachtegaal and Sparks, 2004). The fact that the χ spectra for citrate and DFO-B samples are positioned between the control and the PO_4 samples, indicate that they are likely mixtures of octahedral and tetrahedral Zn-O coordination.

The RSFs displayed in Figure 4.3b reveal the presence of a second coordination shell for all sorption samples at pH 5.5. The second shell position of the control sample was at slightly shorter radial distance than that of citrate, HA, or DFO-B. EXAFS data analysis of the second shell revealed that Zn formed inner sphere surface complexes at pH 5.5 with the kaolinite aluminol groups in all sorption samples excluding PO_4 (Table 4.2). Fitting results indicated the presence of Al atoms at Zn-Al radial distance of 3.06Å for the control and at 3.1Å for the citrate, HA, and DFO-B samples (Table 4.2).

Based on the Al-O bond length of 1.93Å in kaolinite (Vasconcelos et al., 2008) and on the EXAFS fitted Zn-O radial distances, it is possible to determine the likely linkages (corner-sharing monodentate, corner-sharing bidentate, or edge sharing bidentate) formed in the sorption samples. The typical Zn-O distance is 1.95Å in ZnO_4 tetrahedra and 2.10Å in ZnO_6 octahedra (Pan et al., 2004). Using the aforementioned values, a trigonometric function was used to calculate the theoretical Zn-Al radial distance for the various possible linkages (Pan et al., 2004). For corner-sharing monodentate linkages where the Al-O-Zn bond angle is 180°, the theoretical

Zn-Al radial distance would be 3.88Å for tetrahedral ZnO_4 structures and 4.03Å for octahedral structures (Spadini et al., 1994; Pan et al., 2004).

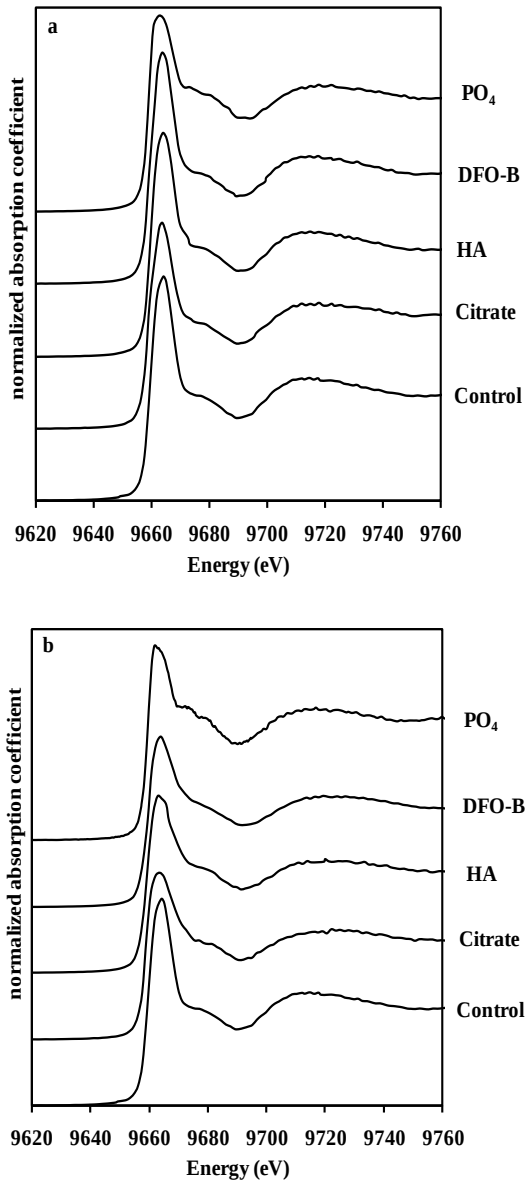

Figure 4.4 Zn K-edge XANES spectra for Zn sorption samples in the absence (control) and presence of ligands at pH 5.5 (a) and pH 7.5 (b).

For corner-sharing bidentate linkage with Al-O-Zn bond angle of 130°, Zn-Al distance would be 3.52Å for tetrahedral and 3.65Å for octahedral structures. For edge sharing bidentate

linkage with Al-O-Zn bond angle of 90°, Zn-Al distance would be 2.74Å for tetrahedral and 2.85Å for octahedral structures (Trainor et al., 2000). The Zn-Al radial distances for the sorption samples shown in Table 4.2 would be too short for corner-sharing monodentate complexes due to steric constraints which may allow us to rule out this sorption geometry. For the control sample, the Zn-Al distance of 3.06Å is also shorter than what would be expected for corner-sharing bidentate. Therefore, edge-sharing bidentate linkage with kaolinite would be most likely. A schematic illustration of the sorption geometry is shown in Figure 4.5. Roberts et al. (2003) found that ZnO_6 octahedra formed edge-sharing bidentate linkages with gibbsite with Zn-Al distance of 3.02Å. Trainor et al. (2000) reported that Zn-Al radial distance for edge-sharing bidentate linkage with α-Al_2O_3 ranged from 2.53-3.03Å.

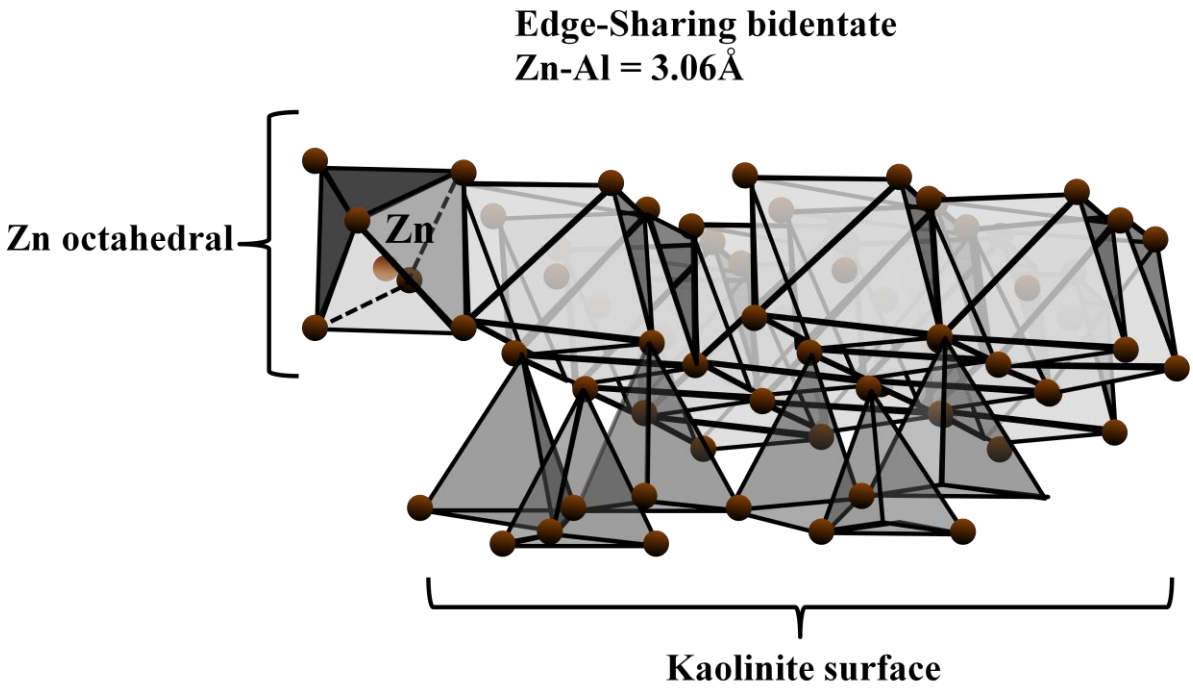

Figure 4.5 Schematic illustration of possible binding structure of Zn octahedra complexed with kaolinite. The Zn-Al radial distance of 3.06Å represents adsorption in the absence of ligands (control) at pH 5.5.

For Zn sorption samples with citrate, HA, or DFO-B at pH 5.5, a longer Zn-Al radial distance of 3.10-3.11Å was found. This distance is longer than suggested for edge-sharing bidentate linkages. However, assuming corner-sharing bidentate linkage would mean that the Al-O-Zn angle would have to be small (~105°) resulting in short O-O distances and strong repulsion (Bochatay and Persson, 2000). Therefore, it is more likely that edge-sharing bidentate linkage is the sorption geometry in these sorption samples (Figure 4.6). The coordination number for these samples are ~1 Al atoms, consistent with edge-sharing bidentate linkage. Nachtegaal and Sparks (2004) also reported a Zn-Al distance of 3.11Å and suggested that ZnO_6 octahedra formed a bidentate complex, although not mentioning edge-sharing, with the aluminol edge sites of kaolinite. On the other hand, Bochatay and Persson (2000) interpreted a Zn-Mn radial distance of 3.08Å to be $ZnO_{4,6}$ polyhedra forming edge-sharing linkages with manganite.

For Zn sorption sample in the presence of PO_4, spectral features indicated the formation of a Zn-PO_4 precipitate. This can be observed in its XANES spectrum where a shoulder was present at 9672eV (Figure 4.4a), similar to that of the $Zn_3(PO_4)_2$ reference sample in Figure 4.2a. The Fourier transform for the sorption sample with PO_4 presence revealed a peak at 2.8Å (uncorrected for phase shift) that was best fit with 0.53 P atoms at a radial distance of 3.15 Å (Figure 4.3b and Table 4.2)

4.3.4 EXAFS Analysis of Sorption Samples at pH 7.5

Figure 4.6 (a-c) displays the k^3-weighted EXAFS spectra, corresponding Radial Structural Functions (uncorrected for phase shifts), and Fourier back transformed spectra for sorption samples in the absence (control) and presence of different ligands at pH 7.5. Data analysis obtained from fitting the backtransformed χ spectra are shown in Table 2.2. EXAFS data analysis of the first shell indicated that Zn formed octahedral coordination with first shell oxygen

atoms in the control and HA sorption samples, whereas formed tetrahedral coordination in the citrate, DFO-B, and PO_4 samples (Table 4.2). As discussed previously, these variations in first neighbor coordination shell are also reflected in the XANES and χ spectra of sorption samples. Only the control and HA samples exhibited a large drop in absorption after the K-edge (Figure 4.4b) and their χ spectra were shifted to lower $k(A^{\circ -1})$ values relative to the remainder of samples (Figure 4.6a), both of which are an indication of higher first neighbor coordination number.

The presence of a second shell was evident in the RSFs for all sorption samples at pH 7.5 except for citrate (Figure 4.6b). EXAFS data analysis of the second shell showed that Zn formed inner sphere complexes with the aluminol functional groups of kaolinite in the HA and DFO-B sorption samples as evident by Al backscattering contribution to the second shell (Table 4.2). The second shell for the PO_4 sorption sample was due to P backscattering indicating the formation of a Zn-PO_4 precipitate as opposed to inner sphere complexation.

For the control sample, the second shell was best fit with 1.76Al atoms at a Zn-Al radial distance of 3.09Å and 4.83 Zn atoms at a Zn-Zn radial distance of 3.08Å, consistent with the formation of Zn-Al LDH. Formation of Zn-Al LDH was found to form in kaolinite (Nachtegaal and Sparks, 2004), low surface-area gibbsite (Roberts et al., 2003), pyrophyllite (Ford and Sparks, 2000), and montmorillonite (Lee et al., 2004) at neutral pH. The octahedral coordination of the first shell and the short Zn-Zn radial distance of 3.08Å rules out the possibility of Zn hydroxide precipitate formation. The Zn-Zn radial distance of tetrahedral Zn hydroxide phases such as γ-$Zn(OH)_2$ and ε-$Zn(OH)_2$ range from 3.30-3.36Å and from 3.40-3.46 Å, respectively (Lee and Anderson, 2005). The distance of tetrahedral zincite is 3.23 Å (Bochatay and Persson, 2000; Roberts et al., 2003; Lee and Anderson, 2005). Formation of Zn carbonate precipitates

such as hydrozincite and Zn carbonate may also be ruled out due to exclusion of CO_2 from the adsorption system.

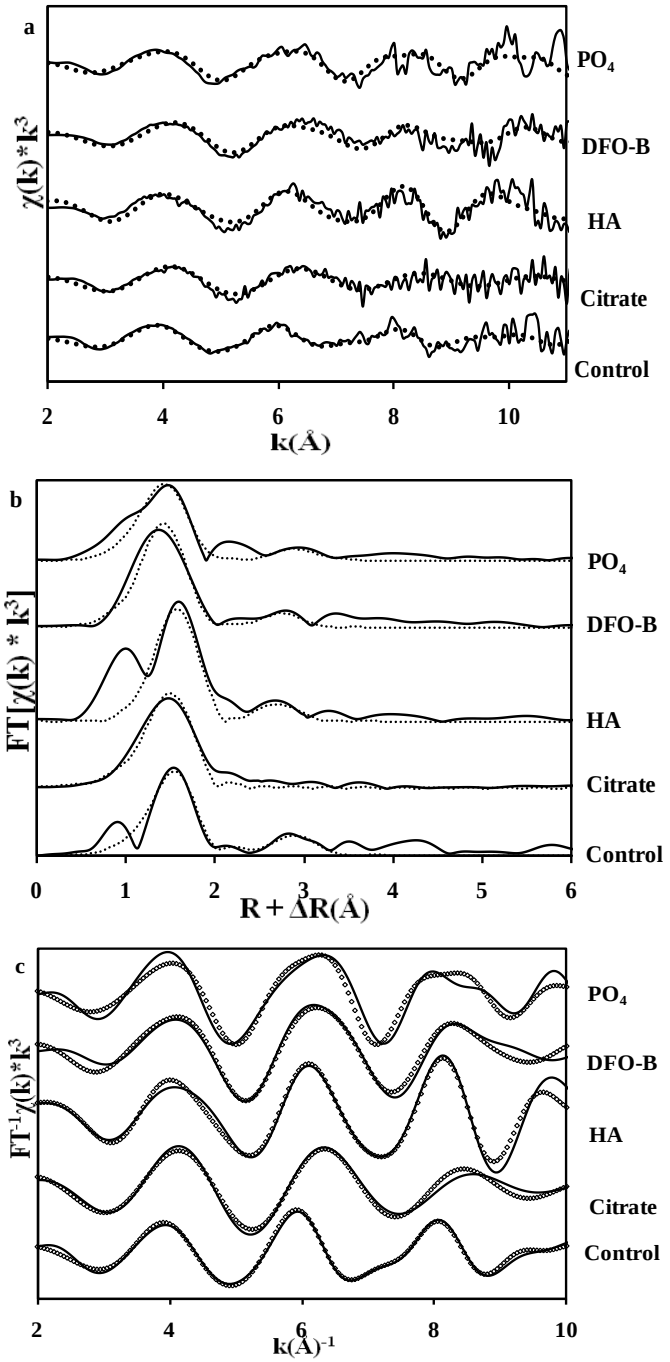

Figure 4.6 The k^3-weighted $\chi(k)$ spectra of Zn sorbed to kaolinite in the absence (control) and presence of ligands at pH 7.5 (a), their respective Fourier transforms (b), and inverse Fourier transforms (c). The solid lines represent the raw spectra and the dotted lines represent best fits.

For the citrate sample, the lack of a second shell in the RSF (Figure 4.6b) and fitted structure parameters (Table 2.2) indicate that Zn formed a single tetrahedral first neighbor coordination shell and adsorbed to kaolinite surface through an outer sphere complexation. At pH 7.5, as much as 93% of citrate was in the soluble form (Figure 4.1a). Past research reported that metals may also form precipitates with organic ligands on oxide surfaces. Based on EXAFS spectral fitting, Cd^{+2} was shown to form precipitates with oxalate and citrate on the goethite surface (Collins et al., 1999). ZnEDTA was also shown to preserve its structure upon adsorption to goethite; a ligand exchange mechanism was absent (Schlegel et al., 1997). In this study, linear combination fitting of the citrate sample at pH 7.5 indicated that 80% of the χ spectrum was Zn citrate, when aqueous Zn^{+2} and Zn citrate were used as fitting standards (data not shown).

The second shells for the HA and DFO-B samples were best fit with 2.23Al atoms at 3.10Å and with 0.87Al atoms at 3.11 Å, respectively. As discussed previously for the sorption samples at pH 5.5, these radial distances suggest that $ZnO_{4,6}$ polyhedra formed edge-sharing bidentate linkages with aluminol surface groups of kaolinite (Figure 4.5). The second shell for the PO_4 sorption sample was best fit with 1.6 P atoms at radial distance of 3.16 Å indicating the formation of a Zn-PO_4 precipitate as opposed to the formation of inner sphere complexes with kaolinite. Spectral features of the PO_4 sample provide further evidence for precipitate formation. In the XANES spectrum shown in figure 4.4b, a shoulder is present at 9672eV similar to that of the $Zn_3(PO_4)_2$ model compound displayed in figure 4.2a. Additionally, similarities in oscillations in χ spectra for the PO_4 sample and that of $Zn_3(PO_4)_2$ are evident.

4.4 Discussion

Macroscopic data indicated that Zn adsorption to kaolinite was impacted by the presence of ligands. The presence of citrate and DFO-B slightly increased Zn adsorption at pH $\leq$ 5.5 but

greatly decreased Zn adsorption at pH > 5.5 as compared to that in the control (NO_3^- background). On the other hand, HA was shown to enhance Zn adsorption in much of the pH range below 7.5. Despite that overall Zn was adsorbed in smaller quantities at pH 5.5 (Figure 4.1a-d), EXAFS data analysis showed that Zn formed inner sphere complexes with the aluminol surface groups of kaolinite in the control, citrate, HA, and DFO-B sorption samples. Formation of inner sphere complexes with kaolinite at low pH is in agreement with previous research. Zn was found to form inner sphere complexes with kaolinite at pH 5.0 and at low surface loadings of 0.89 μmol/m^2 (Nachtegaal and Sparks, 2004). Also, inner sphere complexation of Zn with gibbsite at pH 6 and surface loading of 0.31 μmol/m^2 has been reported (Roberts et al., 2003). Zn surface loading at pH 5.5 in this study was ~0.6 μmol/m^2 for the control and DFO-B, 0.8 μmol/m^2 for the citrate sample and 2.0 μmol/m^2 in the case of HA (Figure 4.1a-d). Our study suggests that the presence of citrate, HA and DFO-B did not change the sorption mechanism as an inner-sphere surface complexation at pH 5.5. It did, however, show a change in the first shell Zn-O coordination from primarily octahedral to a likely mixture of octahedral and tetrahedral, as evident by shorter radial distance and lower coordination numbers (Table 4.2).

At pH 7.5, Zn was incorporated into a LDH precipitate phase in the control sample whereas it remained as inner sphere complexes in the presence of HA and DFO-B. On the other hand in the presence of citrate, Zn was found to be absorbed through the formation of outer sphere complexation with kaolinite surface, which was likely due to the influence of largely soluble citrate.

Zn-Al LDH formation at pH 7.5 in the control sample, changing from inner sphere surface complexion at pH 5.5, corresponded to a high surface loading of 4.3 μmol/m^2 (Figure 4.1 and Table 4.2). This result of changing sorption mechanism upon higher surface loading was

consistent with others reported in the literature. Zn was shown to form inner sphere surface complexation at a surface loading of 1.5 μmol/m^2 at pH 5 but changed to Zn-Al LDH at surface loading of 2.8 μmol/m^2 at pH 7 (Nachtegaal and Sparks, 2004). Zn was also found to form inner sphere complexes with alumina powders at low sorption densities of 0.2-1.1 μmol/m^2 and a LDH like phase at densities ranging from 1.3-3.5 μmol/m^2 (Trainor et al., 2000). Similarly, Zn formed LDH phase upon adsorption to low surface area gibbsite with surface loading of 3.76 μmol/m^2 (Roberts et al., 2003). Our study supports the notion that the formation of Zn-Al LDH likely serve as a major mechanism of Zn sequestration especially at relatively high surface loadings, which often coincides with neutral or slightly high alkaline pH.

EXAFS analysis showed that the presence of the three organic ligands at pH 7.5 inhibited the formation of a Zn-Al LDH phase. The impact of complexing ligands on the formation of LDH phases has been reported for metals other than Zn. Citrate was found to prevent the formation of a Ni-Al LDH while maintaining inner sphere complex formation upon adsorption to gibbsite (Yamaguchi et al., 2002). In the presence of HA coating on the surface of kaolinite, Ni-Al LDH was found to form in the presence of 1% HA coating and suppressed at 5% coating (Nachtegaal and Sparks, 2003). Clearly the results from this study indicated that the presence of organic ligands also likely prevents Zn from forming Zn-Al LDH at neutral pH in kaolinite system even under relatively high surface loadings.

The fitting results showed that at pH 5.5, Zn formed edge-sharing bidentate linkages with the aluminol surface groups of kaolinite in the control, citrate, HA, and DFO-B sorption samples (Table 4.2). The same sorption geometry was also found at pH 7.5 for HA and DFO-B. In addition, the fitting results in Table 4.2 suggested that it was unlikely that a ternary A complex (with ligand in between mineral surface and metal) had formed in the presence of citrate, HA, or

DFO-B due to the short Zn-Al radial distances of 3.10-3.11Å. In order for this to happen, a much larger radial distance of Zn-Al would have to be observed. This result is significant due to the fact that in this study all ligands were added before Zn and in the case of HA it greatly enhanced Zn sorption. Both of these would likely suggest the formation of a type A surface complexation. In fact, the formation of a type A ternary surface complex upon metal sorption has been often suggested in past studies (Alcacio et al., 2001). Our results provide the evidence discrediting this case. As indicated by Yamaguchi et al. (2001) in a study of Ni adsorption to gibbsite in the presence of citrate, Ni would be surrounded with O and C atoms within 3.5Å in a ternary A complex. An alternative explanation of enhanced Zn sorption in the case of HA (Figure 4.1b) could be the reduced positive charge at kaolinite surface upon HA sorption, which then stimulates the Zn specific sorption by kaolinite aluminol group. Collins et al. (1999) reported that the adsorption of organic anions to a mineral surface reduces its positive surface charge, resulting in a more attractive surface for cation adsorption.

Type B ternary surface complex with metal in the between the mineral surface and ligands is another mechanism of surface complexation in a ternary system. In a type B ternary complex, a ligand exchange reaction is expected to occur so that water is replaced by weaker field carboxylic ligands resulting in more water molecules coordinating to Zn; hence longer Zn-O radial distances (Alcacio et al., 2001; Yamaguchi et al., 2001). The Zn-O radial distances in the presence of ligands at pH 5.5 did not exhibit increases, thus no evidence for the formation of ternary B complexes are provided in this study.

Enhanced removal of Zn from solution in the presence of inorganic PO_4 was throughout the pH range studied. Both XANES and EXAFS analysis of Zn sorption sample in the presence of PO_4 at pH 5.5 and 7.5 indicated the formation of a Zn-PO_4 precipitate. This experimental

system contained 3.1 mmol/L of kaolinite surface sites as compared to 1.5 mmol/L of Zn and PO_4. Using MINTEQ (Gustafsson, 2004), it was found that roughly 84% of added Zn would be absorbed by kaolinite with only 15% of added Zn precipitated as uniform $Zn_3(PO_4)_2$ at pH 7.5. EXAFS spectroscopic evidence presented in Figure 4.6 and Table 4.2, however, suggested that $ZnPO_4$ precipitation likely dominated the Zn sorption in a kaolinite system at the neutral pH.

4.5 Conclusion

Macroscopic investigation showed that Zn adsorption to kaolinite was suppressed in the presence of citrate and DFO-B at pH higher than 5.5 and enhanced in the presence of HA, particularly at pH 4.5 and 6.5. The removal of Zn from solution in the presence of PO_4 was due to the formation of a Zn-PO_4 precipitate at pH 5.5 and 7.5. Microscopic data analysis indicated that $ZnO_{4,6}$ polyhedra formed inner sphere edge-sharing bidentate linkages with the aluminol surfaces groups of kaolinite at pH 5.5 in the control and presence of citrate, HA, and DFO-B. The same linkages were found at pH 7.5 in the presence of HA and DFO-B. At this pH, Zn in the presence of citrate was absorbed by outer sphere complexation. The formation of Zn-Al LDH occurred at pH 7.5 and in the absence of ligands. Overall the impact of ligands on the sorption mechanisms of Zn to kaolinite is most significant at high pH.

4.6 References

Adebowale, K.O., I.E. Unuabonah, and B.I. Olu-Owolabi. 2006. The effect of some operating variables on the adsorption of lead and cadmium ions on kaolinite ckay. J Hazard Mater. B134: 130-139.

Agbenin, J.O. 1998. Phosphate-induced zinc retention in a tropical semi-arid soil. Eur. J. Soil Sci. 49: 693-700.

Aguilera, N.H., and M.L. Jackson. 1953. Iron oxide removal from soils and clays. Soil Sci. Soc. Amer. Proc. 17: 359-364.

Alcacio, T.E., D. Hesterberg, J.W. Chou, J.D. Martin, S. Beauchemin, and D.E. Sayers. 2001. Molecular scale characteristics of Cu(II) bonding in goethite–humate complexes. Geochim. Cosmochim. Ac. 65(9): 1355–1366.

Alloway, B.J. 2004. Zinc in soils and crop nutrition. International Zinc Association Communications. IZA, Brussels, Belgium.

Ammann, L. 2003. Cation exchange and adsorption on clays and clay minerals. Ph.D. thesis. Christian-Albrechts-Universität, Kiel, Germany.

Arias, M., M.T. Barral and J.C. Mejuto. 2002. Enhancement of copper and cadmium adsorption on kaolin by the presence of humic acids. Chemosphere 48:1081–1088.

Bar-Yosef, B., U. Kafkafi, R. Rosenberg, and G. Sposito. 1988. Phosphorus adsorption by kaolinite and montmorillonite: effect of time, ionic strength, and pH. Soil Sci. Soc. Am. J. 52: 1580-1585.

Bochatay, L. and P. Persson. 2000. Metal ion coordination at the water-manganite (γ-MnOOH) interface II. An EXAFS study of zinc(II). J. Colloid Interf. Sci. 229: 593-599.

Buerge-Weirich, D., P. Behra, and L. Sigg. 2003. Adsorption of copper, nickel, and cadmium on goethite in the presence of organic ligands. Aquatic Geochemistry. 9(2): 65-85.

Collins, C.R., K.V. Ragnarsdottir, and D.M. Sherman. 1999. Effect of inorganic and organic ligands on the mechanism of cadmium sorption to goethite. Geochim. Cosmochim. Ac. 63(19): 2989-3002.

Collins, R.N., G. Merrington, M.J. Mclaughlin, and J.L. Morel. 2003. Organic ligand and pH effects on isotopically exchangeable cadmium in polluted soils. Soil Sci. Soc. Am. J. 67: 112–121.

Edzwald, J.K., D.C. Toensing and M. C.Y. Leung. 1976. Phosphate Adsorption Reactions with Clay Minerals. Environ. Sci. Technol. 10:485-490.

Farrah, H., and W.F. Pickering. 1976. The sorption of copper species by clays: II. Illite and montmorillonite. Aust. J. Chem. 29: 1177-1184.

Fay, M.L., A. Proctor, D.P. Hoffman, M. Houalla and D. Hercules. 1992. Determination of the Mo Surface Environment of Mo/TiO_2 Catalysts by EXAFS, XANES and PCA. Mikrochim. Acta. 109: 281 – 293.

Ford, R.G., and D.L. Sparks. 2000. The nature of Zn precipitates formed in the presence of pyrophyllite. Environ. Sci. Technol. 34:2479-2483.

Gräfe, M., B. Singh, and M. Balasubramanian. 2007. Surface speciation of Cd(II) and Pb(II) on kaolinite by XAFS spectroscopy. J. Colloid Interf. Sci. 315: 21-32.

Gustafsson, J. P. 2004. Visual Minteq (2.30). U.S. Environmental Protection Agency.

Heidmann, I., I. Christl, and R. Kretzschmar. 2005. Sorption of Cu and Pb to kaolinite-fulvic acid colloids: assessment of sorbent interactions. Geochim Cosmochim Ac. 69(7): 1675-1686.

Hepinstall, S.E., B.F. Turner, and P.A. Maurice. 2005. Effects of siderophores on Pb and Cd adsorption to kaolinite. Clay Clay Miner. 53(6): 557-563.

Hernlem, B.J., L.M. Vane, and G.D. Sayles. 1996. Stability constants for complexes of the siderophore desferrioxamine B with selected heavy metal cations. Inorg. Chim. Acta 244:179–184.

Hizal, J. and R. Apak. 2006. Modeling of copper(II) and lead(II) adsorption on kaolinite-based clay minerals individually and in the presence of humic acid. J. Colloid Interf. Sci. 295:1-13.

Jackson, M.L. 1956. Soil chemical analysis, advanced course. In Soil Survey Laboratory Methods Manual. Soil Survey Investigation Report No.42, Version 4.0, November 2004. Washington, DC.

James, R.O., P.J. Stiglich, and T.L. Healy. 1975. Analysis of models of adsorption of metal ions at oxide/water interfaces. Faraday Discuss. Chem. Soc. 59**:** 142 – 156.

Janssen, R.P.T., M.G.M. Bruggenwert, and W.H. van Riemsdijk, 1997. Interactions between citrate and montmorillonite–Al hydroxide polymer systems. Eur. J. Soil Sci. 48: 463–472.

Kraemer, S.M. 2004. Iron oxide dissolution and solubility in the presence of siderophores. Aquat. Sci. 66: 3–18.

Křepelová, A. 2007. Influence of Humic Acid on the Sorption of Uranium(VI) and Americium(III) onto Kaolinite. Ph.D. thesis. Technischen Universität Dresden.

Lackovic, K., B.B. Johnson, M.J. Angove, and J.D. Wells. 2003. Modeling the adsorption of citric acid onto muloorina illite and related clay minerals. J. Colloid Interf. Sci. 267: 49-59.

Lackovic, K., M.J. Angove, J.D. Wells and B.B. Johnson. 2004. Modeling the adsorption of Cd(II) onto goethite in the presence of citric acid. J. Colloid Interf. Sci. 269(1): 37-45.

Ladeira, A.C.Q., V.S.T. Ciminelli, H.A. Duarte, M.C.M. Alves, and A.Y. Ramos. 2001. Mechanism of anion retention from EXAFS and density functional calculations: Arsenic (V) adsorbed on gibbsite. Geochim. Cosmochim. Ac. 65 (8): 1211-1217.

Lee, S. and P.R. Anderson. 2005. EXAFS study of Zn sorption mechanisms on hydrous ferric oxide over extended reaction time. J. Colloid Interf. Sci. 286: 82-89.

Lee, S., P.R. Anderson, G.B. Bunker, and C. Karanfil. 2004. EXAFS Study of Zn Sorption Mechanisms on Montmorillonite. Environ. Sci. Technol. 38: 5426-5432.

Liao, M. 2006. Effects of Organic Acids on Adsorption of Cadmium onto Kaolinite, Goethite, and Bayerite. Pedosphere. 16(2): 185-191.

Liu, A. and R.D. Gonzalez. 1999. Adsorption/desorption in a system consisting of humic acid, heavy metals, and clay minerals. J. Colloid and Interf. Sci. 218: 225-232.

McBride, M.B. 1989. Surface chemistry of soil minerals. In: Dixon, J.B., S.B. Weeds, editors. Minerals in soil environments, 2nd ed., Madison, WI: Soil Sci. Soc. Am. P 35-88.

McBride, M.B. 1994. Environmental chemistry of soils. New York: Oxford Uni. Pr.

Mench, M., and E. Martin, 1991. Mobilization of cadmium and other metals from two soils by root exudates of Zea may. L., Nicotiana tabbacum L., and Nicatiana rustica L. Plant Soil. 137: 187–196.

Murphy, E.M. and J.M. Zachara. 1995. The role of sorbed humic acid substances on the distribution of organic and inorganic contaminants in groundwater. Geoderma 67: 103-124.

Nachtegaal, M., and D.L. Sparks. 2003. Nickel sequestration in a kaolinite-humic acid complex. Environ. Sci. Technol. 37:529-534.

Nachtegaal, M., and D.L. Sparks. 2004. Effect of iron oxide coatings on zinc sorption mechanisms at the clay-mineral/water interface. J. Colloid Interf. Sci. 276: 13–23.

Neubauer, U., B. Nowack, G. Furrer, and R. Schulin. 2000. Heavy metal sorption on clay minerals affected by the siderophore desferrioxamine B. Environ. Sci. Technol. 34: 2749-2755.

Oades, J.M. 1988. The retention of organic matter in soils. Biogeochemistry. 5: 35-70.

Pan, G., Y. Qin, X. Li, T. Hu, Z. Wu and Y. Xie. 2004. EXAFS studies on adsorption-desorption reversibility at manganese oxides-water interfaces I. Irreversible adsorption of Zn onto manganite (γ-MnOOH). J. Colloid Interf. Sci. 271: 28-34.

Ressler, T., J. Wong, J. Roos and I.L. Smith. 2000. Quantitative Speciation of Mn Bearing Particulates Emitted from Autos Burining (Methylcyclpentadienyl) manganese Tricarbonyl-Added Gasolines Using XANES Spectroscopy. Environ. Sci. Technol. 34: 950 – 958.

Roberts D.R., A.M.Scheidegger, and D.L. Sparks.1999. Kinetics of mixed Ni-Al precipitate formation on a soil clay fraction. Env. Sci.Tech. 33: 3749–3754.

Roberts, D.R., R.G. Ford and D.L. Sparks. 2003. Kinetics and mechanisms of Zn complexation on metal oxides using EXAFS spectroscopy. J Colloid Interf. Sci. 263(2): 364-376.

Robson, A.D. 1993. Zinc in Soils and Plants, Dordrecht, Kluwer Academic Publishers.

Scheidegger, A.M., D.G.Strawn, G.M. Lamble, and D.L. Sparks. 1998. The kinetics of mixed Ni-Al hydroxide formation on clay and aluminum oxide minerals: A time-resolved XAFS study. Geochimica et Cosmochimica Acta 62:2233-2245.

Scheinost A.C. and D.L.Sparks. 2000. Formation of layered single and double metal hydroxide precipitates at the mineral/ water interface:A multiple-scattering XAFS analysis. J. Colloid Interf. Sci. 223: 167–178.

Scheinost, A.C., R. Kretzschmar, and S. Pfister, and D.R. Roberts. 2002. Combining Selective Sequential Extractions, X-ray Absorption Spectroscopy, and Principal Component Analysis for Quantitative Zinc Speciation in Soil. Environ. Sci. Technol. 36: 5021-5028.

Schlegel, M.L. A. Manceau, D. Chateigner, and L. Charlet. 1999. Sorption of Metal Ions on Clay Minerals I. Polarized EXAFS Evidence for the Adsorption of Co on the Edges of Hectorite Particles. J. Colloid Interf. Sci. 215:140-158.

Schlegel, M.L., A. Manceau, and L.Charlet. 1997. EXAFS study of Zn and ZnEDTA sorption at the goethite (α-FeOOH)/water interface.J. Phys IV Fr. 7C-3:823-824.

Schlegel, M.L. A. Manceau, L. Charlet, and J. Hazemann. 2001. Adsorption mechanisms of Zn on hectorite as a fuction of time, pH, and ionic strength. American Journal of Science 301:798-830.

Seibner-Freibach, H.S., Y. Hadar, and Y. Chen. 2004. Interaction of Iron Chelating Agents with Clay Minerals. Soil Sci. Soc. Am. J. 68:470–480.

Shuman, L.M. 1986. Effect of liming on the distribution of manganese, copper, iron, and zinc among soil fractions. Soil Sci. Soc. Am. J. 50:1236–1240.

Spadini, L., A. Manceau, P.W. Schlinder, and L. Charlet. 1994. Structure and stability of Cd^{+2} surface complexes on ferric oxides. J. Colloid Interf. Sci. 168: 73-86.

Sparks, D. L. 2003. Environmental Soil Chemistry; Academic Press: London.

Srivastava, P., S. Balwant, and M. Angove. 2005. Competitive adsorption behavior of heavy metals on kaolinite. J. Colloid Interf. Sci. 290: 28–38.

Swift, R.S. 1996. Organic matter characterization. Chapter 35. *In* D.L. Sparks (ed.) Methods of soil analysis. Part 3. SSSA Book Ser. 5. SSSA, Madison, WI.

Taylor, R.W., W.F. Bleam, T.D. Ranatunga, C.P. Schulthess, Z.N. Senwo, and D.R.A. Ranatunga. 2009. X-ray Absorption Near Edge Structure Study of Lead Sorption on Phosphate-Treated Kaolinite. Environ. Sci. Technol. 43 (3): 711-717.

Trainor, T.P., G.E. Brown, and G.A. Parks. 2000. Adsorption and precipitation of aqueous Zn(II) on alumina powders. J. Colloid Interf. Sci. 231: 359-373.

Vasconcelos, I.F., E.A. Haak, P.A. Maurice, and B.A. Bunker. 2008. EXAFS analysis of cadmium(II) adsorption to kaolinite. Chem. Geol. 249: 237-249.

Voegelin, A., and R. Kretzschmar. 2005. Formation and dissolution of single and mixed Zn and Ni precipitates in soil: Evidence from column experiments and extended X-ray absorption fine structure spectroscopy. Environ. Sci. Technol. 39: 5311-5318.

Voegelin, A., S. Pfister, A.C. Scheinost, M.A. Marcus, and R. Kretzschmar. 2005. Changes in zinc speciation in field soil after contamination with zinc oxide. Environ. Sci. Technol. 39: 6616–6623.

Wang, J.J., and D.L. Harrell. 2005. Effect of ammonium and sodium cations and phosphate, nitrate, and chloride anions on zinc sorption and lability in selected acid and calcareous soils. Soil Sci. Soc. Am. J. 69:1036–1046.

Wang, K., and B. Xing. 2002. Adsorption and desorption of cadmium by goethite pretreated with phosphate. Chemosphere 48: 665–670.

Waychunas G.A., C.C.Fuller, J.A. Davis, and J.J. Rehr.2003. Surface complexation and precipitate geometry for aqueous Zn(II) sorption on ferrihydrite: II. XANES analysis and simulation. Geochim. Cosmochim. Ac. 67 (5), 1031–1043.

Xia, K., W. Bleam, and P.A. Helmke. 1997. Studies of the nature of binding sites of first row transition elements bound to aquatic and soil humic substances using X-ray absorption spectroscopy. Geochim. et Cosmochim. Ac. 61(11): 2223-2235.

Yamaguchi, N. U., A. C. Scheinost, and D.L Sparks. 2002. Influence of gibbsite surface area and citrate on Ni sorption mechanisms at pH 7.5. Clay Clay Miner. 50(6): 784-790.

Yamaguchi, N.U., A.C. Scheinost, and D.L. Sparks. 2001. Surface-Induced Nickel Hydroxide Precipitation in the Presence of Citrate and Salicylate Soil Sci. Soc. Am. J. 65:729–736 (2001).

Zachara, J.M., Smith, SC. and Resch, CT., 1994. Influence of humic substances on Co'+ sorption by a subsurface mineral separate and its mineralogic components. Geochim. Cosmochim. Acta, 58: 553-566.

CHAPTER 5

ZINC ADSORPTION TO A MIXED FERRIHYDRITE AND LOW SURFACE AREA GIBBSITE SYSTEM IN THE PRESENCE AND ABSENCE OF LIGANDS AS A FUNCTION OF pH: A MACROSCOPIC AND XAFS MICROSCOPIC APPROACH

5.1 Introduction

Heavy metal complexation with mineral surfaces occurring at the water/mineral interface impacts the availability, reactivity and transport of heavy metals in soils and waters. Metals in the environment are usually complexed with ligands of natural or anthropogenic origin such as humic acid, fulvic acid, NTA or EDTA (Davis and Leckie, 1978; Bradl, 2004). The presence of ligands impacts the partitioning of metals at the water/mineral interface, playing a key role in controlling mobility and bioavailability of heavy metals. The most important mineral phases involved in the adsorption of heavy metals are phyllosilicates, metal oxides and hydroxides, carbonates, and phosphates (Bradl, 2004). Fe and Al oxides are ubiquitous in the environment occurring as discreet particles or as coatings on other minerals. They have high affinity for metals and selectively adsorb metals at pH levels in which they are positively charged (Violante et al., 2003).

Zinc (Zn) is an essential element for the growth of plants, animal and humans. Yet, elevated concentrations in the environment as a result of smelting activities, use of contaminated sludges, and deposition from incinerator emissions may be detrimental. Due to its environmental significance, Zn adsorption to various mineral surfaces has received considerable attention. Microscopic techniques such as X-Ray Absorption Fine Structure spectroscopy (XAFS) have been employed to elucidate the adsorption mechanisms of Zn to various Fe and Al oxide surfaces. Trivedi et al. (2001) found that Zn adsorbed to ferrihydrite via outer sphere complexation, whereas adsorbed to goethite via inner sphere bidentate complexation at pH ranging from 6-8. Other researchers confirmed inner sphere complex formation with ferrihydrite

at neutral pH (Waychunas et al., 2002; Lee and Anderson, 2005). Zn was found to form inner sphere complexes with Al oxide minerals such as Al_2O_3 (Trainor et al., 2000; 2001) and gibbsite (Roberts et al., 2003). Studies have also shown that Zn polymerization or precipitate formation may occur with increase in Zn surface loadings. At high surface loadings of Zn, precipitate formation was identified upon adsorption to ferrihydrite (Waychunas et al., 2002; Lee and Anderson, 2005). In alumina, high loadings resulted in a mixed metal Zn-Al hydroxide coprecipitate formation (Trainor et al., 2000). In low surface area gibbsite, Zn formed a Zn-Al layered double hydroxide (LDH), whereas formed inner sphere complexes in high surface area gibbsite at the same surface loadings (Roberts et al., 2003).

Macroscopic investigation of Zn adsorption to oxide mineral surfaces as impacted by the presence of ligands has been previously investigated. The presence of citric acid during the formation of iron oxides was found to increase the adsorption of Zn (Xue and Huang, 1995). Siderophores, natural exudates from plants and microorganisms were also shown to impact the adsorption of Zn to oxide mineral surfaces. Neuabauer et al. (2002) found that siderophore DFO-B suppressed the adsorption of Zn to iron oxides over a wide pH range due to repulsion between the positively charged surface and the positively charged $ZnLH_2^+$ complex. Diaz-Barrientoz et al. (1990) reported that increasing concentrations of phosphate resulted in strong increases of Zn adsorption to iron oxide. Vermeer et al. (1999) reported that metal ion adsorption is increased in a humic acid – iron oxide mixture than to the isolated iron oxide. Studies have used XAFS to elucidate the adsorption mechanisms of metals to oxide mineral surfaces in the presence of ligands. While metals such as Cd have been investigated in that regard, few studies have investigated the impact of ligands on the adsorption mechanisms of Zn. Schlegel et al. (1997) reported that Zn was adsorbed to goethite in the form of ZnEDTA, precluding a ligand exchange

mechanism. Other researchers have investigated Zn adsorption mechanisms to humic acid and found Zn to form inner sphere complexes with humic acid (Xia et al., 1997). Sarret et al. (1997) found that Zn formed inner sphere complexes with humic acid at low Zn concentration (300-5000 mg/kg), whereas formed outer sphere complexes at high concentrations (550g/kg) (Sarret et al., 1997). We have not found any reports that have investigated the impact of humic acid on the adsorption mechanisms of Zn to oxide mineral surfaces. There are several reports however that have investigated the impact of ligands on the adsorption of metals such as Cd and Ni. Yamaguchi et al. (2002) investigated the impact of citrate on Ni adsorption to gibbsite and found that Ni formed inner sphere complexes with high surface area gibbsite, whereas formed a Ni-Al LDH in the low area gibbsite. Collins et al. (1999) investigated the impact of ligands on Cd adsorption to goethite and reported the formation of inner sphere complexes in the presence of sulfate, phosphate and humic acid. On the other hand, Cd formed precipitates with citrate and oxalate. There is need to investigate the impact of ligands on the adsorption of Zn to oxide mineral surfaces.

The objectives of this study are to: 1) determine the impact of citrate, phosphate (PO_4), humic acid (HA), and siderophore desferrioxamine-B (DFO-B) on Zn adsorption to mixed ferrihydrite-gibbsite and single gibbsite mineral systems at different pH, and 2) elucidate the adsorption mechanisms of Zn to mineral surfaces in the mixed ferrihydrite-gibbsite and single gibbsite mineral systems in the presence of ligands at pH 7.5.

5.2 Materials and Methods

5.2.1 Ferrihydrite and Gibbsite Preparation

Ferrihydrite was synthesized according to the procedure described by Schwertmann and Cornell (2000) and under flow of N_2 gas. The freshly produced ferrihydrite was then centrifuged

several times to remove any non-precipitated iron. It was then dialyzed against water to remove electrolytes. The electrical conductivity of the water was continuously monitored, and water was changed several times a day. The produced material was then freeze dried and used for experimentation shortly after.

X-Ray Diffraction patterns indicated that the mineral synthesized was ferrihydrite. The BET-surface area of the produced material was 188 m^2/gm. Gibbsite was purchased from Ward's Scientific with a reported surface area of 25 m^2/g (Scheckel et al., 2000), with no further purification conducted on this mineral. PO_4, citrate, and DFO-B ligands were prepared from sodium dihydrogen phosphate, trisodium citrate dihydrate, and desferrioxamine mesylate salts, respectively. HA was obtained from Sigma-Aldrich (H16752) and was purified by acid washing and subsequent removal of ash content according to the International Humic Substance Society method (Swift, 1996).

Briefly, HA was acidified to pH 1.5, allowed to stand for 16 hours, settled by low speed centrifugation and then the supernatant was decanted. HA was resuspended under N_2 gas to pH 7.0 using 1M NaOH and allowed to stand for 24 hours. The precipitation and subsequent redissolution were repeated four times. To remove the ash content from HA, the precipitate was suspended in 0.1M HCl/0.3M HF and shaken overnight. The process was repeated once and then HA was dialyzed until free of Cl^- as tested using $AgNO_3$. The material was freeze dried and mixed well prior to use.

5.2.2 Adsorption Experiment

Adsorption experiments were conducted in 50 ml centrifuge tubes under N_2 atmosphere. The experimental setup included 4 pH levels (4.5, 5.5, 6.5, and 7.5), five ligand treatments (citrate, phosphate (PO_4), humic acid (HA), siderophore (DFO-B), and $NaNO_3$-control) and two

replications. The mixed mineral system was composed of ferrihydrite and gibbsite in a 1:1 weight ratio and total solid/liquid ratio of 20g/l. The single mineral system was composed of gibbsite in a solid/liquid ratio of 20g/l. The metal:ligand ratio constituted a 1:1 molar ratio of 1.5 mM in both mineral systems. HA was prepared on the basis of total carbon content (determined using TOC analyzer), so that total carbon content was similar to that of citrate. The background electrolyte concentration in the system was 0.01M $NaNO_3$.

The experiment was conducted as follows: minerals were first allowed to hydrate for 24 hours in background electrolyte solution. The ligand solution of citrate, PO_4, HA or DFO-B was then added to their respective tubes and allowed to react with kaolinite for 10 minutes. Zn was then added dropwise from an acidified solution under constant stirring of suspension. The pH was adjusted to its respective value using 0.1M of either HNO_3 or NaOH (pre-purged with N_2). The final volume was completed and the reaction time was 24 hours. The pH was continuously monitored (under N_2 purging) and adjusted so that values exhibited minimal fluctuations. The solid was separated from the solution by centrifugation and the solution was filtered using 0.4 μM filters. Soluble concentrations of Zn, P, Si and Al were determined using ICP-AES (Spectro).

Concentrations of dissolved organic carbon in the system were determined using TOC analyzer (Shimadzu). The amounts of Zn and ligand adsorbed were calculated by the difference in initial and final concentrations in solution. The solid portion was stored as a paste at 4ºC until use for XAFS spectroscopy analysis.

5.2.3 EXAFS Data Collection and Analysis

EXAFS data were collected on the Ge (220) double-crystal monochromator beamline at the Center for Advanced Microstructures and Devices in Baton Rouge, Louisiana. The electron

beam energy was 1.3 GeV with a maximum beam current of 180 mA. Zn metal foil was used to calibrate the beam energy by setting the first inflection point to 9569 eV. The EXAFS spectra for adsorption samples were collected at Zn K-edge in fluorescence mode using a Canberra 13 element ultra low energy germanium diode array detector. Multiple scans were collected to improve the signal to noise ratio. Data reduction was conducted using Athena interface to IFEFFIT software. The scans were aligned, merged and deglitched. Standard procedures were used to extract the EXAFS spectra (Fay et al., 1992).

The threshold energy (E_0) was determined from the maximum of the first derivative of μ(E) and was used to convert the energy axis to photoelectron wave vector units ($Å^{-1}$). The resulting data were weighted by k^3 to compensate for damping of the EXAFS spectrum at higher energies. The *k*-weighted χ(*k*) spectra were then Fourier transformed over the wave vector *k* range of 2-10$Å^{-1}$ using a Kaiser-bessel apodization window to produce radial structure functions (RSF) that isolate first and second shell components.

Ab initio phase shift and amplitude functions of Zn-O and Zn-Al, Zn-P, Zn-Zn, and Zn-Fe scattering paths were extracted using Zn-Al LDH, hopeite ($Zn_3(PO_4)_2 \cdot 4H_2O$), zincite (ZnO), and franklinite using FEFF 6.0 code. The peaks of interest were isolated and backtransformed in *k* space using a Kaiser-bessel window. Structural parameters (element identity, coordination number, and radial distance) were determined by a non linear least squares curve fitting approach using Artemis interface to IFEFFIT software. Single shell fits were conducted for the first and second peaks selected at R of 1.0-2.2 and 2.3-3.2 Å, respectively. The value of S_0^2 was set to 0.84 and determined by fixing the coordination number for Zn-O in aqueous Zn to 6 (Alcacio et al., 2001; Scheinost et al., 2002; Roberts et al., 2003).

5.3 Results and Discussion

5.3.1 Macroscopic Zn adsorption

Figures 5.1 and 5.2 show Zn adsorption to the mixed ferrihydrite-gibbsite and single gibbsite systems in the presence and absence of ligands, respectively. The effect of ligands on the adsorption of Zn differed among the mineral systems. While ligands enhanced Zn adsorption in the mixed system (with the exception of DFO-B), only HA and PO_4 enhanced Zn removal in the single mineral system (Figures 5.1 and 5.2). The differences are due to the presence of ferrihydrite in the mixed system, as heavy metals have higher affinity for iron oxides than for aluminum oxides (Violante et al., 2003). In addition, the surface area of ferrihydrite was much larger than that of gibbsite.

Comparing adsorption in the control, more Zn was adsorbed to the mixed than to the single mineral system at any given pH value (Figures 5.1a and 5.2a). In the mixed mineral system, Zn adsorption increased from 5 to 100% with increase in pH from 4.5 to 7.5 in the control (Figure 5.1a). The adsorption edge was sigmoid, typical of metals adsorbed to oxide mineral surfaces, and complete adsorption occurred within a narrow pH range (Angove et al., 1999).

In the single gibbsite system, minimal adsorption was observed at pH 4.5 and 5.5, and an abrupt increase in adsorption occurred in the narrow pH range of 6.5 to 7.5. The pH adsorption edge displayed in this study for the gibbsite system is similar to that reported by Roberts et al. (2003), who reported that negligible quantities of Zn were adsorbed below pH 5.5. They reported surface loadings at pH 6.5 and 7.5 to be 0.68 and 1.79 $\mu mol/m^2$, respectively.

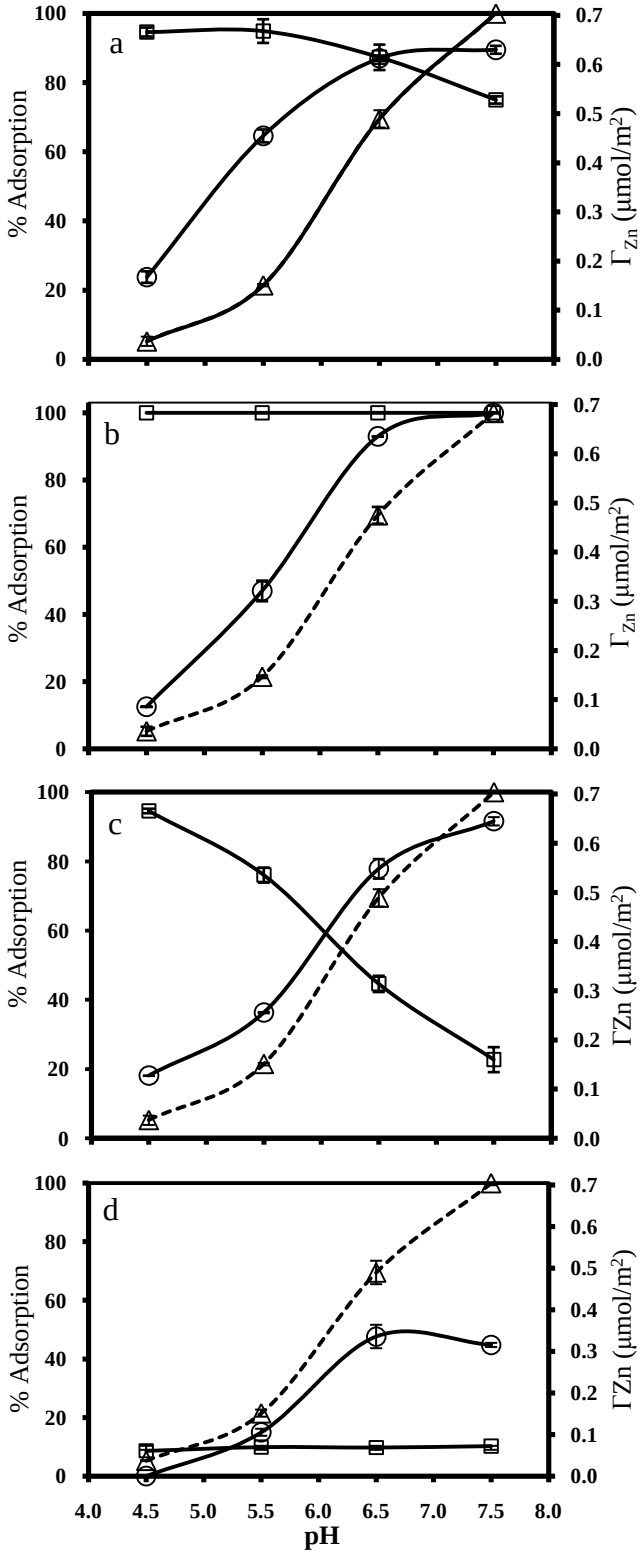

Figure 5.1 Zn adsorption in mixed mineral system (ferrihydrite-gibbsite) in the presence of citrate (a), PO_4 (b), HA (c), DFO-B (d) as a function of pH.(△) Zn adsorption in the control, (○) Zn adsorption in presence of ligand, (□) adsorption of ligand.

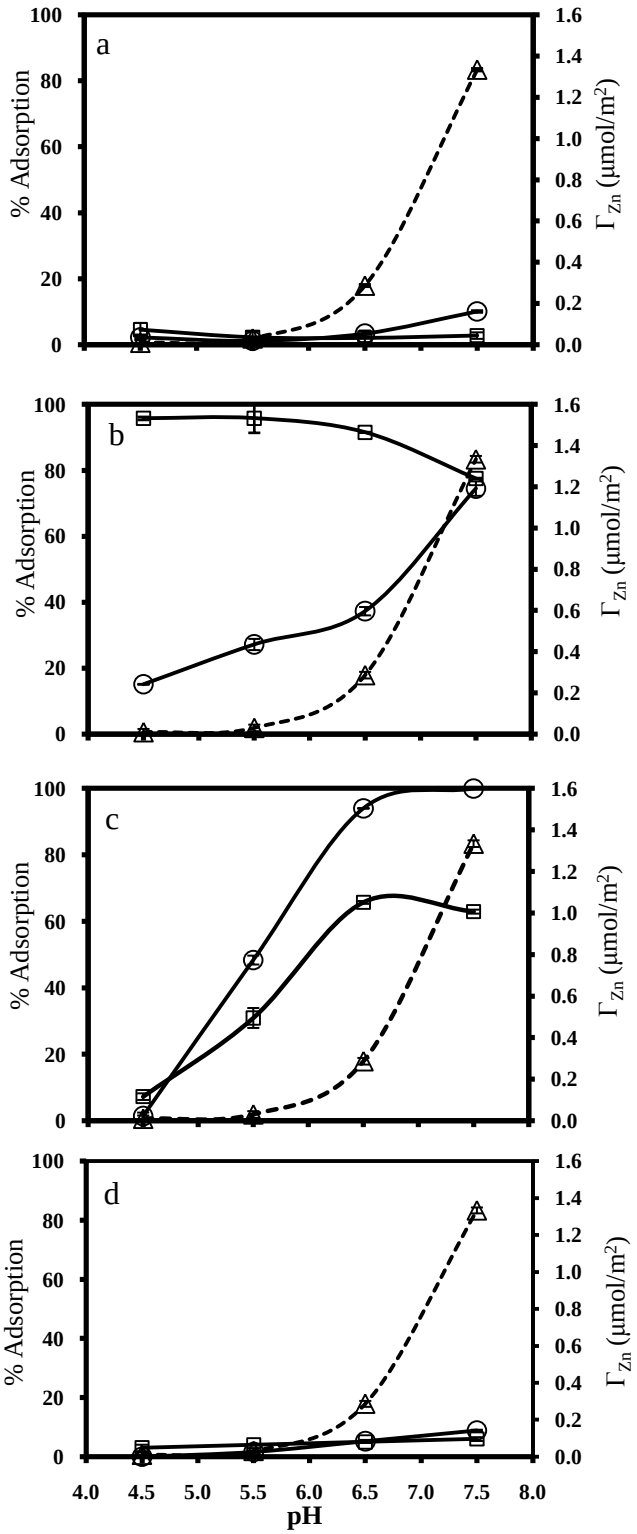

Figure 5.2 Zn adsorption in single mineral system (gibbsite) in the presence of citrate (a), PO_4 (b), HA (c), DFO-B (d) as a function of pH.(△) Zn adsorption in the control, (○) Zn adsorption in presence of ligand, (□) adsorption of ligand.

While citrate suppressed the adsorption of Zn in the single system, it enhanced it in the mixed (Figures 5.1a and 5.2a). The presence of citrate in the latter resulted in enhanced adsorption of Zn at pH below 7.5, where the largest increase of 43% was found at pH 5.5 (Figure 5.1a). Suppressed adsorption in the single system was likely due to competition between citrate and the surface mineral groups for Zn. The difference in citrate impact on Zn adsorption between the two mineral systems may be related to the amount of citrate that can adsorb to the mineral surface. Citrate enhances metal adsorption to oxide mineral surfaces as long as citrate itself is adsorbed to the surface. Once the surface sites are saturated with adsorbed citrate, excess solution citrate begins to compete with the surface for the metal, thus reducing metal adsorption (Boily and Fein, 1996). The adsorption of citrate was high in the mixed system (95 and 75% at pH 4.5 and 7.5, respectively) and negligible in the single mineral system. Citrate was found to enhance Cd adsorption to Al_2O_3 in the pH range from 3.5-7.2 (Boily and Fein, 1996), while it reduced Ni adsorption to gibbsite at neutral pH (Yamaguchi et al., 2002). Low molecular weight acid anions exhibit an increase in adsorption to variable mineral surfaces with decrease in pH below the pH_{pzc} (Geelhoed et al., 1998). Citrate adsorption in the mixed system exhibited a decrease of 20% within the pH range of investigation. Citrate and other organic acids adsorb strongly to hydroxylated surfaces at low pH, enhancing metal adsorption by either forming ternary complexes or by providing more negative surface charge.

Figures 5.1b and 5.2b show Zn adsorption in the mixed and single mineral systems in the presence of PO_4, respectively. While adsorption was enhanced in the mixed system, Zn removal from solution in the single system was a result of precipitate formation rather than enhanced adsorption (shown by EXAFS analysis). In the mixed system, the adsorption edge was shifted to lower pH in the presence of PO_4 where Zn adsorption was enhanced by 8% at pH 4.5 and by

25% at pH 5.5 and 6.5. In addition, PO_4 adsorption was complete throughout the pH range of investigation. Modeling the data using the DLM in Visual MINTEQ confirmed the complete adsorption of PO_4 in the pH range of investigation and absence of a PO_4 precipitate. The low pH dependency of PO_4 adsorption to iron oxide surfaces such as goethite has been reported previously (Venema et al., 1997; Gao and Mucci, 2001). Enhanced adsorption of metals such as Cd and Zn in the presence of PO_4 has been reported (Diaz-Barrientos et al., 1990; Venema et al., 1997; Wang and Xing, 2004).

Luengo et al. (2006) reported that at pH 4.5, bidentate protonated $(FeO)_2(OH)PO$ and bidentate non protonated $(FeO)_2PO_2$ complexes of PO_4 formed at the surface of goethite. At pH 7.5, the dominating surface species was $(FeO)_2PO_2$. Khare et al. (2007) confirmed that at pH 6.0, PO_4 adsorbed to ferrihydrite predominantly in the form of a bidentate binuclear complex. Arai and Sparks (2001) reported that at pH 7.5 nonprotonated bidentate binuclear complexes ($\equiv Fe_2PO_4$) and protonated complexes form at pH 4-6. Figures 5.1c and 5.2c show adsorption in the presence of HA. It can be seen that HA enhanced Zn adsorption in both systems at pH below 7.5. In the mixed system, there was an apparent shift in the adsorption edge to lower pH values and adsorption increased by 13, 15 and 8% with pH increase from 4.5 to 6.5, respectively. At pH 7.5, however, adsorption decreased by 9%. In the single mineral system, increases of 15 and 27% were recorded at pH 4.5, 5.5 and 6.5. As in the mixed mineral system, adsorption of Zn was reduced by 9% at pH 7.5 in the presence of HA. HA adsorption in the mineral systems was consistent with the anion exchange or electrostatic interaction mechanism in which adsorption decreased with pH increase. The presence of soluble HA at pH 7.5 likely resulted in competition between HA and the surface groups of minerals for Zn, hence reducing the quantities of Zn adsorbed at this pH. The pH dependence of HA adsorption to goethite coated sand and enhanced

Cd adsorption in HA presence was reported by Lai et al. (2002). In natural water systems, trace metal ions were reported to have higher affinity for the functional groups of humic substances attached to oxide surfaces than for the oxide surface sites (Davis and Leckie, 1978). Similar results were reported by Vermeer et al. (1999) who showed that metal ions had higher affinity for a mixture of HA and iron oxides than for oxides only. In the single mineral system, 67% of HA was adsorbed at pH 4.5 and increased to 92% at pH 5.5.

The presence of DFO-B in the mixed mineral system resulted in reduction of Zn adsorption, specifically at pH 7.5 where adsorption decreased by 55% (Figure 5.1d). The positively charged soluble H_2ZnDFO^+ complex dominates at pH ~7.0, resulting in suppressed Zn adsorption to ferrihydrite due to electrostatic repulsion with the positively charged surface (Kraemer et al., 1999; Neubauer et al., 2002). The presence of DFO-B in the single mineral system suppressed Zn adsorption at all pH levels where only 8% of Zn was adsorbed at pH 7.5. Siderophores promote the dissolution of iron oxides, which may also impact metal adsorption. However, results indicated that dissolution of Fe from ferrihydrite was 0.07μmol/m^2 regardless of pH.

5.3.2 EXAFS Analysis

5.3.2.1 First Shell Coordination

Figures 5.3 and 5.4 show the normalized k^3-weighted EXAFS spectra, the corresponding Fourier transformed Radial Structural Functions (uncorrected for phase shifts), and Fourier back transformed spectra for Zn adsorption to the mixed and single mineral systems at pH 7.5, respectively. The solid lines represent the raw spectra and dashed lines represent the best fits. Data analysis obtained from fitting the backtransformed χ spectra are shown in Tables 5.1 and 5.2. First shell data analysis of the mixed system indicates that Zn formed tetrahedral

coordination with first shell oxygen atoms in all of the adsorption samples as evident by the interatomic radial distances (R_{Zn-O}) and first shell coordination numbers (Table 5.1). Zn may form tetrahedral, octahedral, or a mixture of both coordination spheres with first shell oxygen atoms (Waychunas et al., 2002; Roberts et al., 2003). While most studies conducted on ferrihydrite have shown that Zn forms tetrahedral coordination with first shell oxygen atoms (Trivedi et al., 2001; Waychunas et al., 2002; Trivedi et al., 2004), octahedral coordination was reported by Trivedi et al. (2001) at pH 6-8. In their study, Zn was bond via outer sphere complexation and therefore maintained octahedral coordination. Nachtegaal and Sparks (2004) reported octahedral first shell coordination in Zn adsorbed to goethite and to a goethite-kaolinite system at pH 7.0 and where Zn had formed inner sphere complexes with the mineral surfaces.

Zn is reported to favor tetrahedral coordination with increase in pH where it exhibits a transition in first shell coordination from octahedral to tetrahedral. Bochatay and Persson (2000) reported that with increase in pH from neutral to high, Zn exhibited a transition from a mixture of coordination spheres to predominantly tetrahedral upon adsorption to manganite. Waychunas et al. (2002) indicated that this transition is favored as a result of increase in the oxygen bond valence sum to ~2.0 as opposed to ~1.83 for octahedral coordination.

In the single mineral system, octahederal coordination was evident in the citrate, HA and DFO-B samples. In aluminum oxides, formation of either coordination sphere has been reported. Roberts et al. (2003) reported a mixture of tetrahedral and octahedral coordination upon adsorption to high surface area gibbsite at surface loadings ranging from 0.31-2.89 $\mu mol/m^2$. In alumina powders, surface loading was found to impact first shell coordination, where Zn formed tetrahedral coordination at low sorption densities (Γ=0.2-1.1 $\mu mol/m^2$) and formed octahedral coordination at high densities due to hydrotalcite like precipitate formation (Trainor et al., 2000).

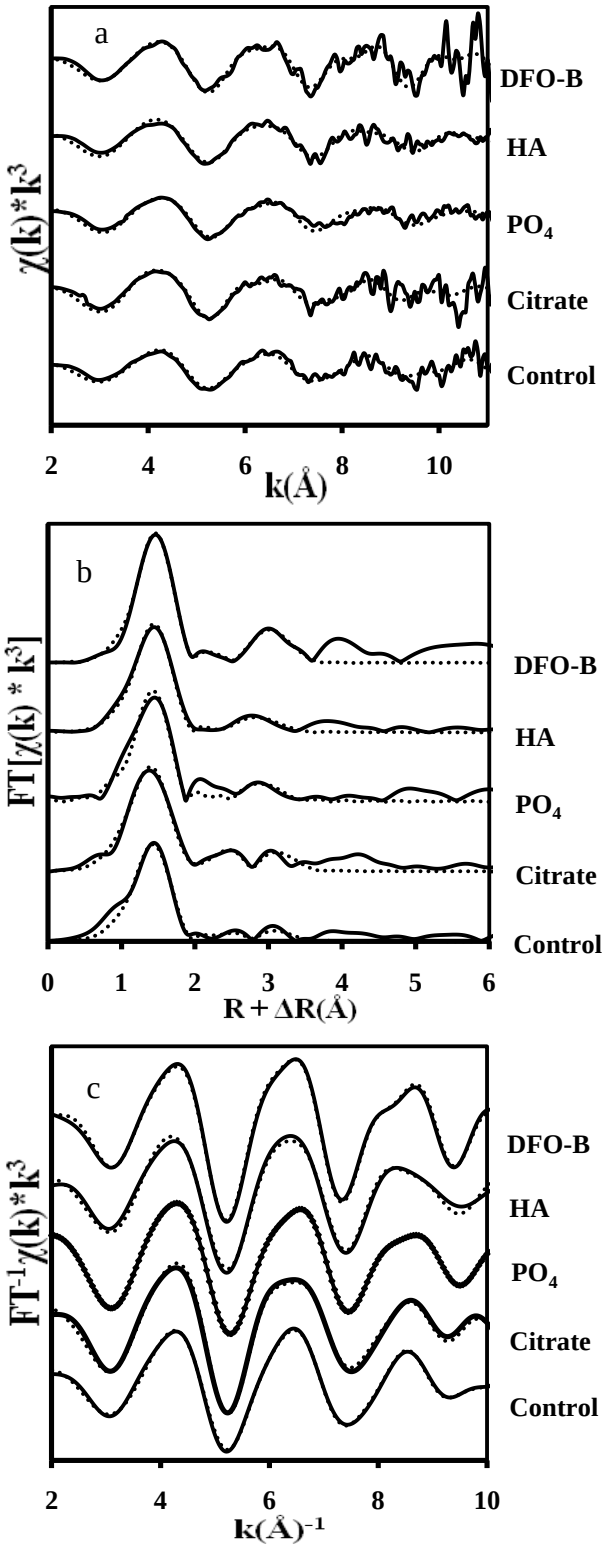

Figure 5.3 k^3-weighted $\chi(k)$ of Zn adsorbed to mixed mineral system (ferrihydrite-gibbsite) at pH 7.5 (a), their respective Fourier transforms (b), and inverse Fourier transforms (c). The solid lines represent the raw spectra and the dotted lines represent best fits.

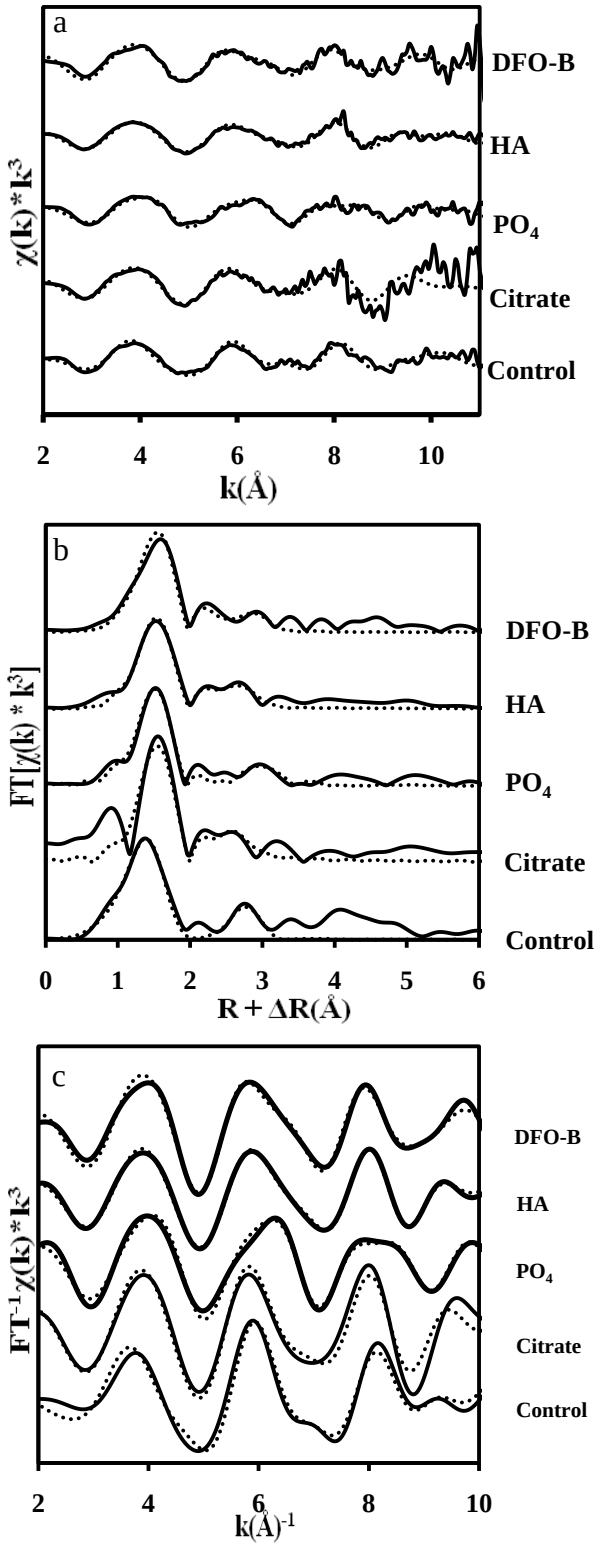

Figure 5.4 k^3-weighted $\chi(k)$ of Zn adsorbed to single mineral system (gibbsite) at pH 7.5 (a), their respective Fourier transforms (b), and inverse Fourier transforms (c). The solid lines represent the raw spectra and the dotted lines represent best fits.

The first shell fitting results displayed in Table 5.1 show low Debye Waller values for all sorption samples except in the presence of citrate which had a value of 0.011, indicating a first shell of high static or thermal disorder.

Table 5.1 Structural parameters for Zn sorbed in mixed ferrihydrite and gibbsite system at pH 7.5 in the presence and absence of ligands derived from EXAFS spectral data analysis

Ligand	Shell	N	R(Å)	σ^2(Å^2)
Control	Zn-O	3.77	1.91	0.006
	Zn-Al	0.92	3.18	0.009
	Zn-Fe/Zn	1.58	3.55	0.003
Citrate	Zn-O	4.89	1.91	0.011
	Zn-Al	0.73	2.99	0.001
	Zn-Fe/Zn	0.67	3.55	0.001
PO_4	Zn-O	4.03	1.91	0.007
	Zn-Fe/Zn	3.44	3.52	0.015
HA	Zn-O	4.47	1.92	0.007
	Zn-Fe/Zn	4.61	3.47	0.018
DFO-B	Zn-O	4.37	1.92	0.004
	Zn-C	2.30	2.90	0.003
	Zn-Fe/Zn	1.90	3.54	0.005

N = coordination number, R = radial distance (Å), σ^2 = Debye-Waller factor (Å^{-2}).The uncertainties in N are estimated to be 30%. Variations in R are estimated to be 0.03 for all shells.

5.3.2.2 Second Shell Coordination

The Radial Structural Functions (RSF) for the mixed mineral sorption samples displayed in Figure 5.3b show that a single higher shell was present between 2.8 and 3.0 Å(uncorrected for phase shift) in the case of HA, PO_4 and DFO-B. The control and citrate samples both exhibited two higher shells at 2.5 and 3.0Å in which the former was due to Al and the latter due to Fe or Zn backscattering.

5.3.2.3 Zn Adsorption Mechanisms to Ferrihydrite

Zn and Fe have similar phase shift and amplitude functions, which makes it is difficult to identify if the higher shell backscattering atom is Zn or Fe. Thus, distinguishing between Zn forming inner sphere complexes with ferrihydrite and formation of Zn polynuclear complexes is difficult using EXAFS analysis alone (Lee and Anderson, 2005; Ha et al., 2009). Since Zn hydroxide phases may form even under unsaturated conditions, the formation of Zn polymerization cannot be ruled out and backscattering due to Zn should be considered (Lee and Anderson, 2005; Bochatay and Persson, 2000).

Fitting results from Table 5.1 show that in the HA sample, the Zn-Fe/Zn radial distance was 3.47Å whereas it was ~3.55Å for the remaining samples. Since we have a tetrahedral first shell coordination, the Zn-Fe/Zn interatomic radial distance of 3.47Å is consistent with that of a Zn hydroxide phase (ε-$Zn(OH)_2$), where typical values range from 3.40-3.46Å (Bochatay and Persson, 2000; Lee and Anderson, 2005). However, since the formation of Zn polymers seems unlikely in the presence of HA, backscattering of the second shell may be attributed to Fe atoms rather than Zn. Waychunas et al. (2002) reported that a Zn-Fe distance of 3.45 Å was consistent with ZnO_4 tetrahedra sharing the apical oxygens of two adjacent FeO_6 octahedra in ferrihydrite (corner sharing bidentate).

The distances of 3.52 to 3.55Å in the remainder of samples is longer than that of Zn hydroxide phases such as γ-$Zn(OH)_2$ (typical values ranging from 3.30-3.36Å) and ε-$Zn(OH)_2$. Despite that the radial distance is also consistent with that of Zn-Zn in hydrozincite (Waychunas et al., 2002), we can rule out the formation of Zn octahedral phases such as hydrozincite since the Zn-O first shell is tetrahedral and as atmospheric CO_2 was excluded from the adsorption system. These distances are consistent with ZnO_4 forming corner sharing with FeO_6 of

ferrihydrite (O'Day et al., 1998). Trivedi et al. (2001) found that Zn formed inner sphere complexes with goethite and reported the occurrence of 2 Fe atoms at an interatomic radial distance of 3.51Å. It may be concluded that Zn polymerization was absent from any of the sorption samples and that higher shell backscattering was due to Fe atoms not Zn.

The absence of Zn precipitate formation or polymerization is possible despite reports that polymerization may occur at low surface loadings. Zn polymerization or precipitate phase formation was reported to occur at a low surface loading of 1.1 μmol/m^2 in manganite (Bochatay and Persson, 2000). The highest loading in our study for the mixed system was 0.70μmol/m^2. Nachtegaal and Sparks (2004) found that Zn formed inner sphere complexes with goethite rather than form a precipitate phase when the surface loading was 1.2μmol/m^2. Trainor et al. (2000) reported that with sorption densities up to 1.1μmol/m^2, Zn predominantly formed sorption complexes with alumina rather than form Zn polynuclear complexes.

5.3.2.4 Zn Adsorption Mechanisms to Gibbsite

As previously mentioned, inner sphere complexation with gibbsite in the mixed system was evident only in the control and citrate samples. The second shell in the control was best fit with 0.92Al atoms at an interatomic distance of 3.18 Å and with 0.73Al atoms at 2.99 Å in the case of citrate (Table 5.1). Since Zn was in tetrahedral coordination with first shell oxygen atoms, the Zn-Al radial distance of 3.18 Å is consistent with ZnO_4 tetrahedra forming corner sharing linkages with AlO_6 octahedra of gibbsite (Trainor et al. 2000). In addition, the Zn-Al distance of 2.99 Å and coordination number of 0.73 are consistent with ZnO_4 tetrahedra sharing edges with AlO_6 octahedra. For corner sharing complexes to give Zn-Al radial distances less than 3.0Å, the Zn-O-Al bond angle would have to be small, which is unlikely due to steric constraints (Trainor et al., 2000).

It can be concluded that in the mixed system, Zn formed corner sharing linkages in the control and edge sharing linkages in the citrate sample. Trainor et al. (2000) found that at low sorption densities (<1.1μmol/m^2), a second shell Al backscatterer was identified at radial distances ranging from 2.95 to 2.99Å and concluded the formation of edge sharing complexes with alumina surface groups. Roberts et al. (2003) reported that Zn-Al distance of 3.02Å was consistent with edge sharing adsorption geometry, with Zn being in either tetrahedral or octahedral first shell coordination.

In the single mineral system, a Zn-Al radial distance of 3.09Å was found for the control sample (Table 5.2). This distance may coincide with corner-sharing monodentate geometry where Zn-Al distances range from 3.07-3.75Å (Trainor et al., 2000). Zn has to undergo significant distortion to form edge sharing complexes at a Zn-Al radial distance of 3.09Å (Bochatay and Persson, 2000).

For the citrate and HA samples of the single system, the Zn-Al radial distances were ~2.99 Å (Table 5.2), similar to the Zn-Al distance of the citrate sample in the mixed system (Table 5.1). These values are consistent with ZnO_6 octahedra forming edge sharing linkages with AlO_6 of gibbsite. Roberts et al. (2003) reported that ZnO_6 octahedra formed edge sharing complexes with gibbsite evident by the Zn-Al radial distance of 3.02Å. The Zn-Al distance of 3.20 Å in the DFO-B sample (Table 5.2) is consistent with ZnO_6 octahedra forming corner sharing complexes with gibbsite. It can be concluded that in the single system, edge sharing complexes with gibbsite was the main uptake mechanism in the citrate and HA sorption samples. In the mixed system, edge sharing was evident only in the citrate sample. Corner sharing linkages in the single system were evident in the control and DFO-B sorption samples.

Table 5.2 Structural parameters for Zn sorbed on gibbsite at pH 7.5 in the presence and absence of ligands derived from EXAFS spectral data analysis

Ligand	Shell	N	R(Å)	σ^2(Å^2)
Control	Zn-O	4.79	1.94	0.011
	Zn-Al	1.07	3.09	0.003
Citrate	Zn-O	5.14	2.02	0.006
	Zn-C	3.64	2.78	0.001
	Zn-Al	4.42	2.98	0.02
PO4	Zn-O	3.22	1.98	0.006
	Zn-P	0.69	3.28	0.001
HA	Zn-O	5.02	2.01	0.007
	Zn-C	3.43	2.80	0.001
	Zn-Al	1.93	2.99	0.006
DFO-B	Zn-O	5.50	2.03	0.009
	Zn-C	3.37	2.72	0.002
	Zn-Al	1.21	3.20	0.003

N = coordination number, R = radial distance (Å), σ^2 = Debye-Waller factor (Å^{-2}).The uncertainties in N are estimated to be 30%. Variations in R are estimated to be 0.03 for all shells.

The coordination number for the citrate sample in the single system was 4.42 and the Debye -Waller factor value was 0.02 indicating large static or thermal disorder in the Al shell (Table 5.2). Since CN and σ^2 values are highly correlated, interpretation of their absolute value is suspect (O'Day et al., 1998).

The absence of Zn backscattering contribution to the second shell in the single mineral system (Table 5.2) indicates the absence of Zn polymerization or precipitate formation such as Zn-Al LDH. While studies have shown that Zn precipitate formation in aluminum oxides can occur at low surfaces loadings, other studies have indicated the absence of precipitate formation at surface loadings similar to our study (~1.6 μmol/m^2) and higher. Roberts et al. (2003) studied

Zn adsorption to gibbsite and reported the absence of Zn precipitate formation at neutral pH and surface loadings upto 2.89μmol/m^2. Zn backscattering contribution was detected in the high surface area gibbsite at surface loadings of 3.76 μmol/m^2. Trainor et al. (2000) similarly reported considerable Zn precipitate formation in alumina at surface loadings of 1.7 μmol/m^2 and higher.

5.3.3 Discussion

As indicated by the macroscopic adsorption data (Figure 5.1), Zn adsorption in the mixed system was enhanced in the presence of ligands with the exception of DFO-B. However, the mechanisms of Zn adsorption to ferrihydrite remained unaffected by the presence of ligands. In all of the mixed mineral adsorption samples, ZnO_4 tetrahedra formed corner sharing linkages with FeO_6 octahedra of ferrihydrite as evident by the Zn-Fe radial distances of 3.47 to 3.55 Å. Zn was adsorbed to gibbsite in the mixed system in the control and citrate samples, while no evidence of complexation was evident in the PO_4, HA or DFO-B samples (Table 5.1). It is possible that outer sphere complexes formed with gibbsite in these samples. However, EXAFS spectroscopy cannot detect outer sphere complexation in the presence of inner sphere complexes of the same element (Ha et al., 2009).

In the single mineral system, Zn adsorption to gibbsite was impacted by the presence of ligands, where HA was the only ligand that enhanced adsorption. Citrate and DFO-B suppressed adsorption by competing with the gibbsite surface groups for Zn, and PO_4 formed a precipitate with Zn (Figure 5.2). The effect was also reflected on the adsorption mechanisms of Zn to gibbsite. In the citrate and HA samples, ZnO_6 octahedra formed bidentate mononuclear complexes with AlO_6 octahedra of gibbsite as evident by the Zn-Al radial distances of ~2.99Å. In the control and DFO-B samples, corner sharing linkages with gibbsite were the main mechanisms of uptake.

The absence of Zn backscattering contribution to the higher shell indicate that Zn polymerization or precipitate formation was absent from these mineral systems (Tables 5.1 and 5.2). The formation of Zn-Al LDH upon adsorption to gibbsite in either mineral system can therefore be ruled out.

5.4 References

Alcacio, T.E., D. Hesterberg, J.W. Chou, J.D. Martin, S. Beauchemin, and D.E. Sayers. 2001. Molecular scale characteristics of Cu(II) bonding in goethite–humate complexes. Geochim. Cosmochim. Ac. 65(9): 1355–1366.

Angove, M.J., J.D. Wells, B.B. Johnson. 1999. The influence of temperature on the adsorption of cadmium(II) and cobalt(II) on goethite. J. Colloid Interface Sci. 211, 281–290.

Arai, Y., and D.L. Sparks. 2001. ATR–FTIR Spectroscopic Investigation on Phosphate Adsorption Mechanisms at the Ferrihydrite–Water Interface. J. Colloid Interf. Sci.241: 317–326.

Bochatay, L., and P. Persson. 2000. Metal ion coordination at the water-manganite (γ-MnOOH) interface II. An EXAFS study of zinc(II). J. Colloid Interface Sci. 229: 593-599.

Boily, J.F., and J.B. Fein. 1996. Experimental study of cadmium-citrate co-adsorption onto α-Al_2O_3. Geochim. Cosmochim. Ac. 60(16):2929-2938.

Bradl, H.B. 2004. Adsorption of heavy metal ions of soils and soils constituents. J. Colloid Interf. Sci. 277: 1–18.

Collins, C.R., K.V. Ragnarsdottir, and D.M. Sherman. 1999. Effect of inorganic and organic ligands on the mechanism of cadmium sorption to goethite. Geochim. Cosmochim. Ac. 63(19): 2989-3002.

Davis, J.A., and J.O. Leckie. 1978. Effect of adsorbed complexing ligands on trace metal uptake by hydrous oxides. Environ. Sci. Technol. 12(12): 1309-1315.

Diaz-Barrientos, E., L. Madrid, M.C. Contreras, and E. Morillo. 1990. Simultaneous adsorption of zinc and phosphate on synthetic lepidocrocite. Aust. J. Soil. Res. 28: 549-557.

Fay, M.L., A. Proctor, D.P. Hoffman, M. Houalla and D. Hercules. 1992. Determination of the Mo Surface Environment of Mo/TiO_2 Catalysts by EXAFS, XANES and PCA. Mikrochim. Acta. 109: 281 – 293.

Gao, Y. and A. Mucci. 2001. Acid base reactions, phosphate and arsenate complexation, and their competitive adsorption at the surface of goethite in 0.7M NaCl solution. Geochim. Cosmochim. Ac. 65 (14): 2361-2378.

Geelhoed, J.S., T. Hiemstra, and W.H. Vanriemsdijk. 1998. Competitive interaction between phosphate and citrate on goethite. Environ. Sci. Technol. 32: 2119-2123.

Ha, J., T.P. Trainor, F. Farges, and G.E. Brown Jr. 2009. Interaction of aqueous Zn(II) with hematite nanoparticles and microparticles. Part 1. EXAFS study of Zn(II) adsorption and precipitation. Langmuir 25(10): 5574-5585.

Khare, N., J.D. Martin, and D. Hesterberg. 2007. Phosphate bonding configuration on ferrihydrite based on molecular orbital calculations and XANES fingerprinting.Geochim. Cosmochim. Ac.71: 4405–4415.

Kraemer, S.M., S. Cheah, R. Zapf, J. Xu, K.N. Raymond, and G. Sposito. 1999. Effect of hydroxamate siderophores on Fe release and Pb(II) adsorption by goethite. Geochim. Cosmochim. Ac. 63(19-20): 3003-3008.

Lai C.H., C.Y. Chen, B.L.Wei and S.H. Yeh. 2002. Cadmium adsorption on goethite-coated sand in the presence of humic acid. Water Res. 36: 4943–4950.

Lee, S. and P.R. Anderson. 2005. EXAFS study of Zn sorption mechanisms on hydrous ferric oxide over extended reaction time. J. Colloid Interf. Sci. 286: 82-89.

Luengo, C., M. Brigante, J. Antelo, and M. Avena. 2006. Kinetics of phosphate adsorption on goethite: Comparing batch adsorption and ATR-IR measurements. J. Colloid Interf. Sci. 300: 511–518.

Nachtegaal, M., and D.L. Sparks. 2004. Effect of iron oxide coatings on zinc sorption mechanisms at the clay-mineral/water interface. J. Colloid Interf. Sci. 276: 13–23.

Neubauer, U., G. Furrer, and R. Schulin. 2002. Heavy metal sorption on soil minerals affected by the siderohpore desferrioxamine B: the role of Fe(III) (hydr)oxides and dissolved Fe(III). Eur. J. Soil Sci. 53: 44-55.

O'Day, P.A., S.A. Carroll, and G.A. Waychunas. 1998. Rock-water interactions controlling zinc, cadmium, and lead concentrations in surface waters and sediments, U.S. tri-state mining district. 1. Molecular identification using X-ray absorption spectroscopy. Environ. Sci. Technol. 32(7): 943-955.

Roberts, D. R., R. G.Ford and D. L. Sparks. 2003. Kinetics and mechanisms of Zn complexation on metal oxides using EXAFS spectroscopy. J. Colloid Interf. Sci. 263(2): 364-376.

Sarret, G., A. Manceau, J.L. Hazemann,A. Gomez,and M. Mench. 1997. EXAFS study of the nature of zinc complexation sites in humic substances as a function of Zn concentration. J. Phys. IV France 7: 799-802.

Scheinost, A.C., R. kretzschmar, and S. Pfister, and D.R. Roberts. 2002. Combining Selective Sequential Extractions, X-ray Absorption Spectroscopy, and Principal Component Analysis for Quantitative Zinc Speciation in Soil. Environ. Sci. Technol. 36: 5021-5028.

Scheckel, K.G., A.C. Scheinost, R.G. Ford, and D.L. Sparks. 2000. Stability of layered Ni hydroxide surface precipitates-a dissolution kinetics study. Geochim. Cosmochim. Ac. 64(16): 2727-2735.

Schlegel, M.L., A. Manceau, and L.Charlet. 1997. EXAFS study of Zn and ZnEDTA sorption at the goethite (α-FeOOH)/water interface.J. Phys IV Fr. 7C-3:823-824.

Schwertmann, U., Cornell, R.M., 2000. Iron Oxides in the Laboratory. Wiley-VCH, Weinheim.

Swift, R.S. 1996. Organic matter characterization (chap 35). pp. 1018-1020. In D.L. Sparks et al. (eds) Methods of soil analysis. Part 3. Chemical methods. Soil Sci. Soc. Am. Book Series: 5. Soil Sci. Soc. Am. Madison, WI.

Trainor, T.P., G.E. Brown, and G.A. Parks. 2000. Adsorption and Precipitation of Aqueous Zn(II) on Alumina Powders. J. Colloid Interf. Sci.231:359 –372.

Trivedi, P., L. Axe, and T.A. Tyson. 2001. An Analysis of Zinc Sorption to Amorphous versus Crystalline Iron Oxides Using XAS. J. Colloid Interf. Sci. 244: 230–238.

Venema, P., T. Hiemstra, and W.H. Van Riemsdijk. 1997. Interaction of Cadmium with Phosphate on Goethite. J. Colloid Interf. Sci. 192: 94–103.

Vermeer, A.W.P., J.K. McCulloch, W.H. Van Riemsdijk, and L.K. Koopal. 1999. Metal ion adsorption to complexes of humic acid and metal oxides: deviations from the additivity rule. Environ. Sci. Technol. 33: 3892-3897.

Violante, A., M.R. Ricciardella, and M. Pigna. 2003. Adsorption of heavy metals on mixed Fe–Al oxides in the absence or presence of organic ligands. Water Air Soil Poll. 145: 289–306.

Wang, K. and B. Xing. 2004. Mutual effects of cadmium and phosphate on their adsorption and desorption by goethite. Environ. Pollut. 127:13–20.

Waychunas, G.A., C.C. Fuller, and J.A. Davis. 2002. Surface complexation and precipitate geometry for aqueous Zn(II) sorption on ferrihydrite I: X-ray absorption extended fine structure spectroscopy analysis. Geochim. Cosmochim. Ac. 66(7): 1119-1137.

Xia, K., W. Bleam, and P.A. Helmke. 1997. Studies of the nature of binding sites of first row transition elements bound to aquatic and soil humic substances using X-ray absorption spectroscopy. Geochim. Cosmochim. Ac. 61(11): 2223-2235.

Xue, J., and P.M. Huang. 1995. Zinc adsorption--desorption on short-range ordered iron oxide as influenced by citric acid during its Formation. Geoderma 64:343-356.

Yamaguchi, N.U., A.C. Scheinost, and D.L. Sparks 2002. Influence of gibbsite surface area and citrate on Ni sorption mechanisms at pH 7.5. Clays Clay Miner. 50(6): 784-790.

CHAPTER 6

SURFACE COMPLEXATION OF ZINC ON MIXED KAOLINITE AND GOETHITE SYSTEM IN THE PRESENCE OF ORGANIC AND INORGANIC LIGANDS AS A FUNCTION OF pH

6.1 Introduction

Soils are important sinks for trace metals in the environment acting as filters protecting surface and groundwater from various contaminants. Understanding metal interaction with mineral surfaces in the soil is therefore essential to the understanding of metal fate and transport, bioavailability and ultimately toxicity. For example, outer-sphere trace metal complexes formed in the soil are weak and readily exchangeable, whereas inner sphere complexes are strong and may potentially sequester metals. The task of elucidating the adsorption mechanisms of Zn and other metals in soils is faced with challenges due to the heterogeneous complex nature of soil systems. Researchers have therefore used individual mineral systems to elucidate the adsorption mechanisms of Zn and other metals. X-Ray Absorption Fine Structure Spectroscopy (XAFS) has been a powerful tool in that regard as it allowed the probing of Zn adsorption at the molecular level.

Previous research has investigated the binding mechanisms of Zn to mineral surfaces as a function of reaction time, pH, ionic strength and surface loading. Surface loading was found to impact the adsorption mechanisms of Zn to ferrihydrite, where bidentate mononuclear complexes dominated at high surface loading and pH values above 5, whereas monodentate mononuclear complexes were dominant at lower surface loading and lower pH values (Dyer et al. 2003 and Trivedi et al. 2003). In alumina powders, inner sphere bidentate complexes dominated at low densities and hydrotalcite type precipitates formed at high sorption densities (Trainor et al. 2000). It was also found that Zn favored octahedral first shell coordination at low pH and

tetrahedral coordination at high pH upon adsorption to various minerals such as Fe/Al oxides and silica (Waychunas et al., 2002; Roberts et al., 2003).

Naturally occurring ligands in the environment released by plant roots and microorganisms play a significant role in heavy metal transport in soils. The ligands investigated in this study include phosphate (PO_4), citrate, humic acid (HA) and siderophore (DFO-B). Phosphorus is a major plant nutrient that is widely distributed in the soil and is also considered a non-point source pollutant resulting from animal fertilizers. It is of significant importance as a result of its relation to soil fertility, eutrophication and erosion control (Tejedor-Tejedor, 1990; Wang and Xing, 2002). Humic substances are widely distributed in soils, sediments and water bodies. They are high molecular weight compounds with low mobility in the soil, which give them the capacity to immobilize heavy metals (Arias et al., 2002). The most important surface functional groups in humic acid are the carboxylic, carbonyl, and phenolic groups (Bradl, 2004). On average, 50% of the total acidity is due to carboxylic groups. They have a greater tendency to ionize at low pH and are therefore most likely to be involved in the adsorption reactions (Xia et al., 1997; Lai et al., 2002).

Studies have shown that ligands may either hinder or promote metal adsorption to mineral surfaces depending on the affinity of metal-ligand complexes for adsorption (Violante et al., 2003; Buerge-Weirich et al., 2003). The effect of a ligand on Zn adsorption depends on the relative strength of interaction between the ligand, mineral surface and metal, as well as on the concentration of each of these species (Angove et al., 1999). Geelhoed et al. (1998) showed that citrate adsorption to goethite strongly increased with pH decrease below the PZC of 9.2. Buerge-Weirich et al. (2003) found that oxalate decreased Cu and Ni adsorption to goethite at high pH, but had no impact on Cd adsorption. Violante et al. (2003) found that Pb adsorption on mixed

Fe-Al oxides was influenced by the concentration and sequence of Pb and ligand addition. Few studies have investigated the adsorption mechanisms of Zn and other metals formed with mineral surfaces in the presence of ligands. One study investigated the binding mechanisms of Cd adsorbed to goethite in the presence of organic and inorganic ligands (Collins et al., 1999).

Low molecular weight ligands differ in terms of their impact on heavy metal adsorption to mineral surfaces depending on their ability to complex metals (formation constants with metals). Buerge-Weirich et al. (2003) found that oxalate decreased Cu and Ni adsorption to goethite at pH above 6.0 more than pyromelliate as a result of the former being a stronger complexant. Wu et al. (2003) showed that EDTA had a higher capacity to decrease Pb adsorption to goethite than citric acid as a result of the former being a stronger metal chelator than the latter. It was concluded that the stronger the chelator, the less Pb is adsorbed to goethite.

Violante et al. (2003) indicated that the critical concentration of a low molecular weight organic ligand to prevent the adsorption of heavy metals is dependent on the chelating ability of ligand for a metal, pH, and sorbent surface properties. They also found that the sequence of addition of metal and ligand impacts metal adsorption. When tartrate was added before Pb, more Pb was adsorbed to mixed Fe/Al oxides than when Pb was added before or alone. They hypothesized that the added anion increased the surface negative charge and hence promoted Pb adsorption.

The objectives of this study are to: 1) investigate the adsorption of Zn to a single goethite and a mixed goethite-kaolinite mineral system in the presence of citrate, PO_4, HA, and DFO-B as a function of pH, and to 2) elucidate the adsorption mechanisms of Zn to kaolinite and goethite in the mineral systems at pH 5.5 and 7.5 using X-Ray Absorption Fine Structure Spectroscopy (XAFS).

6.2 Materials and Methods

6.2.1 Preparation of Kaolinite

The kaolinite used in this study was the low defect Georgia kaolinite (KGa-1) purchased from the Clay Minerals Society. To ensure complete dispersion, kaolinite was prepared in 10^{-4}M $NaHCO_3$ with pH adjusted to 9.0 (Seibner-Freibach et al., 2004). The <2 μm fraction was then extracted by the sedimentation method according to Stokes law. Since KGa-1 contains impurities, it was purified by removing carbonates, iron oxides, and organic matter. Carbonate removal was conducted using the method of Jackson (1956) in which kaolinite was heated in sodium acetate (pH 5.0) at 95ºC for 30 minutes. Kaolinite was then washed via centrifugation with 1M NaCl solution. Iron removal was conducted using the citrate-bicarbonate-dithionite method described by Aguilera and Jackson (1953). Afterwards, kaolinite was washed 4 times via centrifugation with a solution of 0.025 M HCl and 0.5 M NaCl (Ammann, 2003).

Organic matter was removed by heating in 3% H_2O_2 at 50ºC for 1 hour, then heating at 70ºC to destroy remaining H_2O_2 (Schlegel et al., 1999). Kaolinite was then washed 5 times with 1M NaCl and washed again with deionized water to remove excess salt (Janssen et al., 1997; Nachtegaal and Sparks, 2003). Kaolinite was dialyzed against double deionized water until no Cl^- remained as tested by $AgNO_3$. Dialysis bags were pretreated by boiling in a 2% $NaHCO_3$ and 1 mM EDTA solution and washed with deionized water to remove contaminating minerals and polysaccharides (Morillo et al., 2006). The purified kaolinite was then freeze dried, ground and sieved prior to use. The 5 point N_2-BET surface area for kaolinite in this study was found to be 16.39 m^2/g. The reported point zero charge (PZC) and CEC for KGa-1b are 6.0 and 1.83 meq/100g (Křepelová, 2007).

6.2.2 Preparation of Goethite

Goethite was prepared using the method of Schwertmann and Cornell (2000) and under continuous flow of ultra pure N_2 gas. Poorly crystalline iron oxides were removed from the freshly produced goethite by treating with ammonium oxalate and ammonium acetate in the dark (Alcacio et al. 2001). Goethite was then washed with 1 M NaCl to remove oxalate and then several times with deionized water (Alcacio et al., 2001). The material was then placed in dialysis bags to remove excess electrolytes. Prior to that, dialysis bags were pretreated by boiling in a 2% $NaHCO_3$ and 1 mM EDTA solution and washed with deionized water to remove contaminating minerals and polysaccharides (Morillo et al., 2006). Goethite was then freeze dried, ground and sieved prior to use. XRD patterns indicated that the mineral synthesized was goethite. The 5 point N_2-BET surface area for kaolinite in this study was found to be 43.63 m^2/g.

6.2.3 Preparation of Ligands

Phosphate (PO_4), citrate, and desferrioxamine B (DFO-B) ligands were prepared from sodium dihydrogen phosphate, trisodium citrate dihydrate, and desferrioxamine mesylate (DFO-B) salts, respectively. HA was obtained from Sigma-Aldrich (H16752) and was purified by acid washing and subsequent removal of ash content according to the International Humic Substance Society method (Swift, 1996). Briefly, HA was acidified to pH 1.5, allowed to stand for 16 hours, settled by low speed centrifugation and then the supernatant was decanted. HA was resuspended under N_2 gas to pH 7.0 using 1 M NaOH and allowed to stand for 24 hours. The precipitation and subsequent redissolution was repeated four times. To remove the ash content from HA, the precipitate was suspended in 0.1 M HCl/0.3M HF and shaken overnight. The process was repeated once and then HA was dialyzed until free of Cl^- as tested using $AgNO_3$. The material was freeze dried and mixed well prior to use.

6.2.4 Sorption Experiment

Adsorption experiments were conducted in 50 ml centrifuge tubes under continuous purging of ultra pure N_2 gas. The experimental setup included 4 pH levels (4.5, 5.5, 6.5, and 7.5), five ligand treatments (citrate, phosphate, HA, DFO-B, and $NaNO_3$-control) and replicated twice. Both the goethite and kaolinite concentrations were 10gm/l. The metal:ligand ratio constituted a 1:1 molar ratio of 1.5mM. HA was prepared on the basis of total carbon content (determined using TOC analyzer), so that total carbon content was similar to that of citrate. The background electrolyte concentration of 0.01 M $NaNO_3$ dominated the ionic strength of the adsorption suspension.

The minerals in the single and mixed mineral systems were first allowed to hydrate for 24 hours in $NaNO_3$.The ligand solution of citrate, PO_4, HA or DFO-B was then added to their respective tubes and allowed to react with the goethite-kaolinite mixture for 10 minutes. Zn was then added dropwise from an acidified solution under constant stirring of suspension. The pH was adjusted to its respective value using 0.1 M of either HNO_3 or NaOH (pre-purged with N_2). The final volume was completed and the reaction time was 24 hours. The pH was continuously monitored (under N_2 purging) and adjusted so that values exhibited minimal fluctuations.

The solid was separated from the solution by centrifugation and the solution was filtered using 0.4 μM filters. Soluble concentrations of Zn, P, Si and Al were determined using ICP-AES (Spectro). Concentrations of dissolved organic carbon in the system determined were determined using TOC analyzer (Shimadzu). The amounts of Zn and ligand adsorbed were determined by the difference in initial and final concentrations in solution. The solid portion was stored as a paste at 4ºC until use for XAFS spectroscopy analysis.

6.2.5 EXAFS Data Collection and Analysis

EXAFS data were collected on the Ge (220) double-crystal monochromator beamline at the Center for Advanced Microstructures and Devices in Baton Rouge, Louisiana. The electron beam energy was 1.3 GeV with a maximum beam current of 180mA. Zn metal foil was used to calibrate the beam energy by setting the first inflection point to 9569eV. The EXAFS spectra for adsorption samples were collected at Zn K-edge in fluorescence mode using a Canberra 13 element ultra low energy germanium diode array detector. Multiple scans were collected to improve the signal to noise ratio.

Data reduction was conducted using Athena interface to IFEFFIT software. The scans were aligned, merged and deglitched. Standard procedures were used to extract the EXAFS spectra (Fay et al., 1992). The threshold energy (E_0) was determined from the maximum of the first derivative of $\mu(E)$ and was used to convert the energy axis to photoelectron wave vector units ($Å^{-1}$). The resulting data were weighted by k^3 to compensate for damping of the EXAFS spectrum at higher energies. The *k*-weighted $\chi(k)$ spectra were then Fourier transformed over the wave vector *k* range of 2-10$Å^{-1}$ using a Kaiser-bessel apodization window to produce radial structure functions (RSF) that isolate first and second shell components.

Ab initio phase shift and amplitude functions of Zn-O and Zn-Al, Zn-P, Zn-Zn, and Zn-Fe scattering paths were extracted using Zn-Al LDH, hopeite ($Zn_3(PO_4)_2 \cdot 4H_2O$), and zincite (ZnO), and franklinite using FEFF 6.0 code. The peaks of interest were isolated and backtransformed in *k* space using a Kaiser-bessel window. Structural parameters (element identity, coordination number, and radial distance) were determined by a non linear least squares curve fitting approach using Artemis interface to IFEFFIT software. Single shell fits were conducted for the first and second peaks selected at R of 1.0-2.2 and 2.3-3.2Å, respectively. The

value of S_0^2 was set to 0.84 and determined by fixing the coordination number for Zn-O in aqueous Zn to 6 (Alcacio et al., 2001; Scheinost et al., 2002; Roberts et al., 2003).

6.3 Results and Discussion

6.3.1 Macroscopic Zn Adsorption

Figures 6.1and 6.2 show Zn adsorption in the presence and absence of ligands in the single goethite and mixed goethite-kaolinite mineral systems, respectively. In the absence of ligands, Zn adsorption was ~15% at pH 4.5 in both the single goethite and mixed goethite-kaolinite mineral systems (Figures 6.1a and 6.2a). With increase in pH above 4.5, more Zn was adsorbed in the single mineral system than in the mixed. The largest difference in adsorption was at pH 6.5, where 27% more of Zn was adsorbed in the single than in the mixed mineral system. This may be due to the fact that the surface area and affinity of goethite for Zn adsorption is much higher than that of kaolinite.

Wu et al. (2003) found that the adsorption capacity for Pb at pH 6.0 was much higher in goethite than in kaolinite, being 11.04 mg/g in the former and 0.91 mg/g in the latter. Nachtegaal and Sparks (2004) on the other hand, found that Zn had higher affinity for the goethite coated kaolinite than for either the kaolinite or goethite alone, possibly due to the formation of extra sorption sites created by goethite sorption onto kaolinite. Our system is different from that of Nachtegaal and Sparks (2004) in the sense that both goethite and kaolinite existed as adsorbing minerals rather than as iron oxide coatings on the kaolinite surface. Differences in adsorption edges of the two mineral systems are evident, where it appears to be sigmoid in the goethite single mineral system despite the narrow pH range of this study. The mixed mineral system shows a different curvilinear adsorption edge, likely due to the presence of kaolinite in the system.

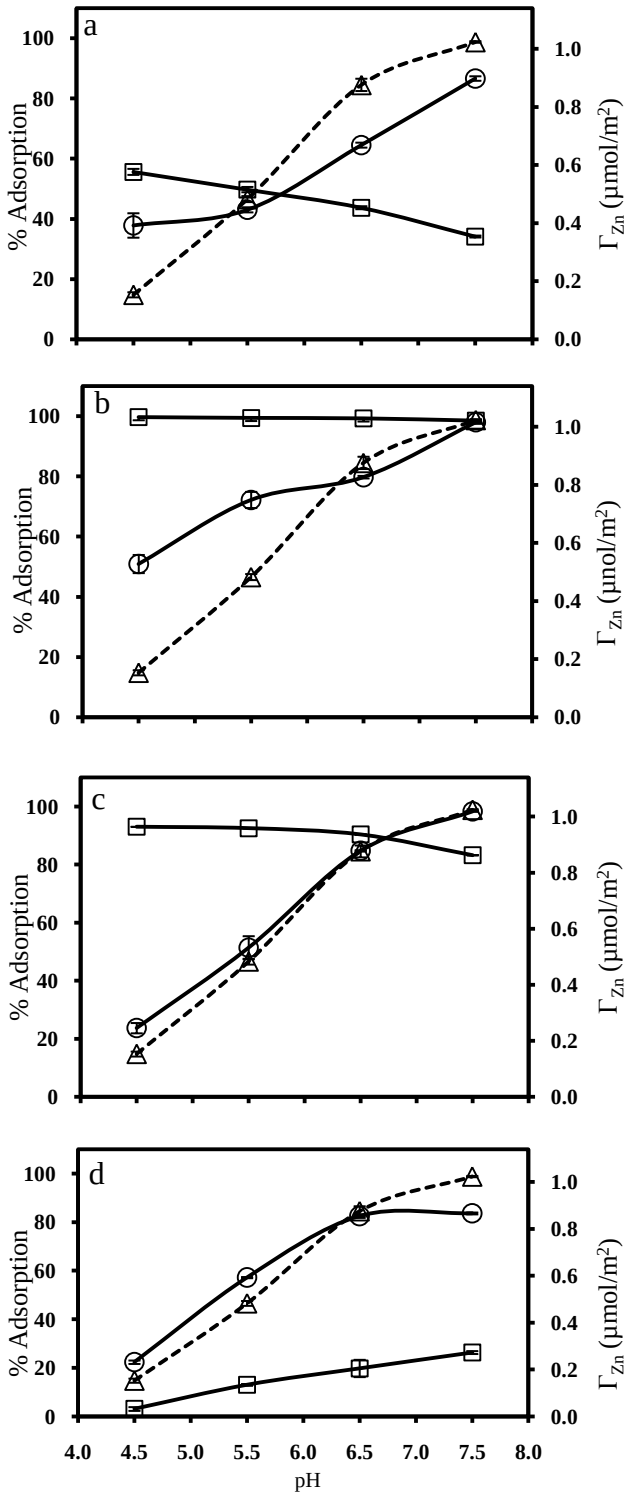

Figure 6.1 Zn adsorption in single mineral system (goethite) in the presence of citrate (a), PO_4 (b), HA (c), DFO-B (d) as a function of pH.(△) Zn adsorption in the control, (○) Zn adsorption in presence of ligand, (□) adsorption of ligand.

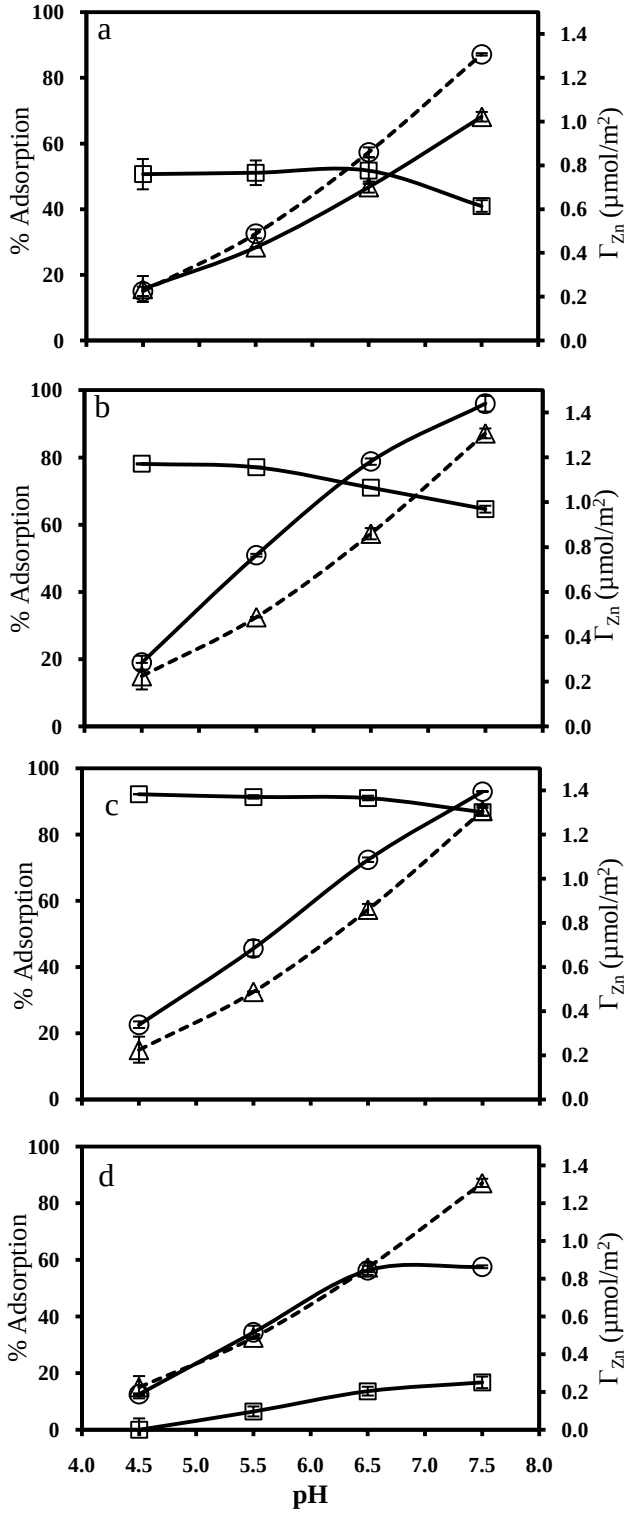

Figure 6.2 Zn adsorption in mixed mineral system (goethite and kaolinite) in the presence of citrate (a), PO_4 (b), HA (c), DFO-B (d) as a function of pH.(△) Zn adsorption in the control, (○) Zn adsorption in presence of ligand, (□) adsorption of ligand.

The typical adsorption edges of metals adsorbed to oxide mineral surfaces are sigmoid and complete adsorption occurs within a narrow pH range (Angove et al., 1999). For example, Spathariotis and Kallianou (2007) found that Zn adsorption to goethite and to a goethite-kaolinite mixed system was complete in the pH range from 3.7 – 6.0. They postulated that the mixed system had obtained an oxide adsorption behavior. In our study, although the adsorption of Zn in the mixed system was lower than that of goethite, it was higher than in the single kaolinite system (data not available), indicating that adsorption was intermediate between the two single systems.

Figures 6.1(a) and 6.2(a) show Zn adsorption in the presence of citrate in the single and mixed systems, respectively. It can be seen from the mixed system that Zn adsorption was reduced in the presence of citrate and that this reduction became more significant as pH increased (Figure 6.2a). In the single system, citrate reduced Zn adsorption at pH values higher than 5.5. At pH 4.5 however, Zn adsorption was higher in the presence of citrate by more than double (15% adsorption in the absence of citrate as compared to 38% in its presence). This may be due to the fact that at low pH, organic acids adsorb strongly to hydroxylated surfaces, which may enhance metal adsorption by either forming ternary complexes or by providing more negative surface charge.

Davis and Leckie (1978) indicated that the functional groups of an adsorbed ligand may serve as new adsorption sites for metals and that these new sites may be more reactive than the isolated oxide surface. Buerge-Weirich et al. (2003) found that Cd adsorption to goethite was enhanced at acidic pH in the presence of pyromellitate due to ternary complex formation. In the mixed goethite-kaolinite system, no difference in Zn adsorption was observed at pH 4.5 in the presence or absence of citrate despite that the same quantity of citrate was adsorbed in this

system as in the single mineral system. It seems that citrate adsorption in the mixed mineral system had not provided extra negative surface charge or formed ternary complexes, which would have enhanced Zn adsorption.

Citrate adsorption in the single system was consistent with anion adsorption where adsorption decreased with pH increase. The presence of considerable concentrations of citrate in solution indicates that the surface reaction sites in both systems were saturated with the anion, resulting in competition between soluble citrate and the mineral surface functional groups for Zn, which was more profound at higher pH. Similar results were found for Cd adsorption to goethite or kaolinite in the presence of organic acids (Liao, 2006). Wu et al. (2003) found that Pb adsorption onto goethite decreased with increasing concentrations of citric acid at pH of 6.0 and ionic strength of 0.02 M. However, it was found that with increase in pH and in the presence of 60 mg/l of citric acid, Pb adsorption was not impacted.

It is noticeable from both Figure s 6.1(a) and 6.2(a) that citrate adsorption was similar in both single and mixed mineral systems. Approximately 50% of citrate was adsorbed at pH 4.5 in both systems. Lackovic et al. (2003) however, reported that far more citric acid was adsorbed to goethite than to kaolinite across a pH range from 3 to 10. The gradual increase in citrate adsorption with pH decrease in the goethite system is a result of increase in surface positive charge below the PZC (8.1). Geelhoed et al. (1998) found that citrate adsorption to goethite decreased with pH increase upto PPZC, above which almost no citrate was adsorbed. Above the PPZC, both the citrate and goethite surface are negatively charged, whereas at pH values below PPZC, the surface of goethite becomes positively charged increasing citrate adsorption (Filius et al., 1997). Citrate is expected to reach an adsorption maximum with decreasing pH as it becomes protonated and its charge diminishes (Filius et al., 1997).

Citrate is adsorbed to the goethite surface by ligand exchange forming inner-sphere complexes, where the surface hydroxyl group is replaced with the adsorbed anion. Outer sphere complexes are assumed to be formed only with singly coordinated $FeOH_2$ groups (Cornell and Schindler, 1980; Filius et al., 1997; Geelhoed et al., 1998).

Low molecular weight ligands differ in terms of their impact on heavy metal adsorption to mineral surfaces depending on their ability to complex metals (formation constants with metals). Buerge-Weirich et al. (2003) found that oxalate decreased Cu and Ni adsorption to goethite at pH above 6.0 more than pyromelliate as a result of the former being a stronger complexant. Wu et al. (2003) showed that EDTA had a higher capacity to decrease Pb adsorption to goethite than citric acid as a result of the former being a stronger metal chelator than the latter. It was concluded that the stronger the chelator, the less Pb is adsorbed to goethite. Violante et al. (2003) indicated that the critical concentration of a low molecular weight organic ligand to prevent the adsorption of heavy metals is dependent on the chelating ability of ligand for a metal, pH, and sorbent surface properties. They also found that the sequence of addition of metal and ligand impacts metal adsorption. When tartrate was added before Pb, more Pb was adsorbed to mixed Fe/Al oxides than when Pb was added before or alone. They hypothesized that the added anion increased the surface negative charge and hence promoted Pb adsorption.

Figures 6.1(b) and 6.2(b) show Zn adsorption to the single goethite and mixed goethite-kaolinite mineral systems in the presence of PO_4, respectively. In the single mineral system, PO_4 enhanced Zn adsorption only at pH 4.5 and 5.5, while no differences were observed at higher values. In the mixed system, PO_4 enhanced Zn adsorption at all pH levels, but were highest at pH 5.5 and 6.5 where 18 and 21% increases were recorded, respectively.

Enhanced adsorption of metals in the presence of PO_4 has been reported by previous researchers. Venema et al. (1997) found that PO_4 had a positive impact on Cd adsorption to goethite in the pH range from 4 to 8. Diaz-Barrientos (1990) found that for a given P concentration, the amount of Zn adsorbed to lepidocrocite (crystalline iron oxyhydroxide) increased with pH increase.

Collins et al. (1999) reported enhanced adsorption of Cd onto goethite in the presence of PO_4 at pH 5.0. They suggested that enhancement was due to electrostatic interaction, where the adsorption of PO_4 reduced the overall positive charge of goethite. The PO_4 anion has an effect on Cd adsorption similar to the effect of OH^- anion, i.e. decreasing the electrostatic potential near the surface (Venema et al., 1997). Contrary to the findings of those studies, one report found reported that PO_4 pretreatment of hematite suppressed the adsorption of Cd and Cu. It was concluded that suppression was a result of competition between the metals and PO_4 for the ≡FeOH adsorption sites (Li et al., 2006).

Figures 6.1(b) and 6.2(b) show that PO_4 adsorption in both mineral systems exhibited minimal pH dependency. In addition, the goethite system exhibited stronger affinity for PO_4 than the mixed system. While almost complete adsorption of PO_4 at all pH levels was evident in the single goethite system, adsorption in the mixed system exhibited a slight decrease from 77% to 65% over the experimental pH range. The strong affinity of goethite for PO_4 has been reported by Gao and Mucci 2001, who found 57% of PO_4 to be adsorbed at pH 4.0. Venema et al. (1997) reported low pH dependency of PO_4 adsorption onto goethite with the experimental pH range of 3-10. Even at high ionic strength of 0.7M NaCl, Gao and Mucci (2001) found that pH had little effect on PO_4 adsorption at pH <6.5, above which pH dependency became evident. They indicated that the fraction of PO_4 adsorbed was not an intrinsic property of goethite, but a

function of the solid/solution ratio. At pH values higher than presented here, PO_4 adsorption is expected to decrease as a result of competition between the PO_4 and OH^- anions for adsorption sites (Chitrakar et al., 2006).

PO_4 anions are adsorbed to the mineral surface forming inner sphere or outer sphere complexes with the positively charged surface functional groups. Outer sphere and inner sphere complexation can be represented as follows, respectively (Mustafa et al., 2008):

$$\equiv Fe - OH + H_xPO_4^{-3+x} + H_2O \leftrightarrow \equiv Fe - OH_2^{+} \cdots H_xPO_4^{-3+x} + OH^-$$

$$\equiv Fe - OH + H_xPO_4^{-3+x} \leftrightarrow \equiv Fe - H_xPO_4^{-3+x} + OH^-$$

Figures 6.1(c) and 6.2(c) show Zn adsorption in the presence of HA in the single and mixed systems, respectively. It can be seen that Zn adsorption was not impacted by the presence of HA in the single system, whereas it slightly increased in the mixed system. In the latter, Zn adsorption increased by 8, 13, 15, and 6% at pH 4.5 to 7.5, respectively. These results deviated from the general consensus that HA enhances the adsorption of metals to oxide surfaces, especially at low pH. Lai et al. (2002) reported enhanced adsorption of Cd to goethite in the presence of HA over the pH range from 2-6. Arias et al. (2002) reported enhanced adsorption of Cd and Cu onto kaolinite in the presence of HA. However, studies have shown that the role of HA on metal adsorption may deviate from the general consensus. Zuyi et al. (2000) reported that fulvic acid did not impact the adsorption of Zn to Al_2O_3 at pH< 7. They concluded that the effect of humic substances on metal sorption was dependent on the nature of both the oxide and humic substance. Lai et al. (2002) reported that HA may bind directly to the iron oxide and block the metal adsorption sites, which may decrease metal adsorption to the mineral surface.

Despite that Zn adsorption was not substantially enhanced in our study, HA adsorption was high in both mineral systems and at all pH levels. HA adsorption was similar in both mineral

systems at all pH levels, where ~93% of HA was adsorbed at pH 4.5 and ~85% adsorbed at pH 7.5 (Figures 6.1c and 6.2c). HA adsorption to variable charged surfaces is expected to follow the anion exchange or electrostatic interaction mechanism, where the negatively charged HA is adsorbed to the positively charged mineral surface (Lai et al., 2002).

Figures 6.1(d) and 6.2(d) show Zn adsorption in the presence of DFO-B in the single and mixed mineral systems, respectively. In the mixed system, Zn adsorption was not impacted at pH 6.5 and below, whereas at pH 7.5 adsorption decreased by 30%. In the single system, Zn adsorption increased by ~10% at pH 4.5 and 5.5 and decreased by 15% at pH 7.5.

The Figure s also show that DFO-B adsorption slightly increased with pH in both mineral systems. These results are in agreement with Rosenberg and Maurice (2003) who reported that the adsorption of DFO-B on kaolinite was consistent with cation adsorption, where DFO-B adsorption increased above the pH_{PZC} of kaolinite. Within the pH range of this study, DFO-B adsorption increased from 0 to 17% and from 3 to 26% in the mixed and single systems, respectively. It seems that goethite had higher affinity for DFO-B than kaolinite. In a previous study, we found that DFO-B hindered metal adsorption to kaolinite at the same pH range (data not shown). Contrary to our findings, other researchers have indicated that kaolinite had higher affinity for DFO-B than goethite (Rosenberg and Maurice, 2003).

6.3.2 EXAFS Data Analysis

6.3.2.1 First Shell Coordination

Figures 6.3 and 6.4 show the normalized k^3 weighted EXAFS spectra (a), corresponding Fourier transforms (b) and Fourier back transformed spectra (c) for Zn adsorption to the mixed goethite-kaolinite system at pH 5.5 and 7.5, respectively. Table 6.1 shows the structural parameters derived from EXAFS data fitting for the mixed mineral system. As evident by the

Zn-O radial distance and first shell coordination number (N), Zn formed tetrahedral coordination with first shell oxygen atoms at both pH values and in all the sorption samples investigated. The Zn-O radial distance for compounds in which Zn forms tetrahedral coordination with oxygen ranges from 1.92 to 1.99ºA. Typical values for octahedral compounds range from 2.02 to 2.12 ºA (Robert et al., 2003).

Zn may form either tetrahedral or octahedral coordination with first shell oxygen atoms (Roberts et al., 2003). With increase in pH, studies have shown that Zn exhibits a first shell coordination transition from octahedral to tetrahedral upon adsorption to oxide mineral surfaces. Bochatay and Persson (2000) found that upon adsorption to manganite, Zn(II) switched coordinations at the surface from a mixture of tetrahedral and octahedral at neutral pH to predominantly tetrahedral at high pH. In addition, Roberts et al. (2003) reported that Zn adsorbed to silica exhibited a transition in first shell coordination from octahedral to tetrahedral with increase in pH. Our results show that a transition was not evident as tetrahedral coordination was dominant at both low and high pH levels. Nachtegaal and Sparks (2004) studied Zn adsorption to goethite and kaolinite and reported octahedral coordination at pH 5.0 and 7.0. Octahedral coordination was also dominant in the goethie-kaolinite mixture of their study. The differences in reported results may be due to differences in surface loading, which also plays a role in the form of first shell coordination spheres.

6.3.2.2 Second Shell Coordination

- **Control**

The RSFs for the control sample at pH 5.5 and 7.5 displayed in Figure s 6.3 (b) and 6.4 (b) show second and third shells at 2.6 and 3.1 Å (uncorrected for phase shift). Fitting results in Table 6.1 show that the binding mechanisms remained the same at both pH levels, as evident by

similarity in radial distances for the second and third shells at both pH levels. Fe and Zn have similar phase and amplitude functions which makes it difficult to determine if the second shell backscattering contribution comes from Fe or Zn (Waychunas et al., 2002; Lee and Anderson, 2005).

Assuming that the third shell backscattering was due to Zn atoms, the Zn-Zn/Fe interatomic distances would be consistent with tetrahedral Zn hydroxide phases such as γ-$Zn(OH)_2$ and ε-$Zn(OH)_2$, where reported values range from 3.30-3.36Å for the former and 3.40-3.46 Å for the latter (Bochatay and Persson, 2000; Lee and Anderson, 2005). Attributing the second shell to Zn backscattering is assuming that a large portion of Zn was polymerized or had precipitated, which seems unlikely specifically at pH 5.5. It is therefore more likely that the third shell resulted from Fe backscattering. The Zn-Fe radial distance of 3.39 and 3.44Å are consistent with ZnO_4 tetrahedra forming double corner sharing linkages with FeO_6 octahedra of goethite. Waychunas et al. (2002) reported a Zn-Fe distance of 3.45 Å for Zn forming corner sharing bidentate linkages with ferrihydrite. The Zn-Fe radial distance of 3.39Å for the pH 5.5 sample is smaller than typical values for corner sharing linkages.

Table 6.1 shows that the second shell was a result of Al backscattering and pH did not impact the Zn-Al radial distance, i.e adsorption mechanism. The Zn-Al radial distances of 2.98 and 3.0Å would imply ZnO_4 tetrahedra forming edge sharing complexes with kaolinite. Based on the Al-O distance of 1.93Å for the kaolinite structure (Vasconcelos et al., 2008) and Zn-O distance of 1.96 Å (this study), the edge sharing geometry would suggest a Zn-Al distance of 2.75Å assuming an Al-O-Zn angle of 90°. It is therefore unlikely that these linkages are corner sharing bidentate due to steric constraints (Trainor et al., 2000).

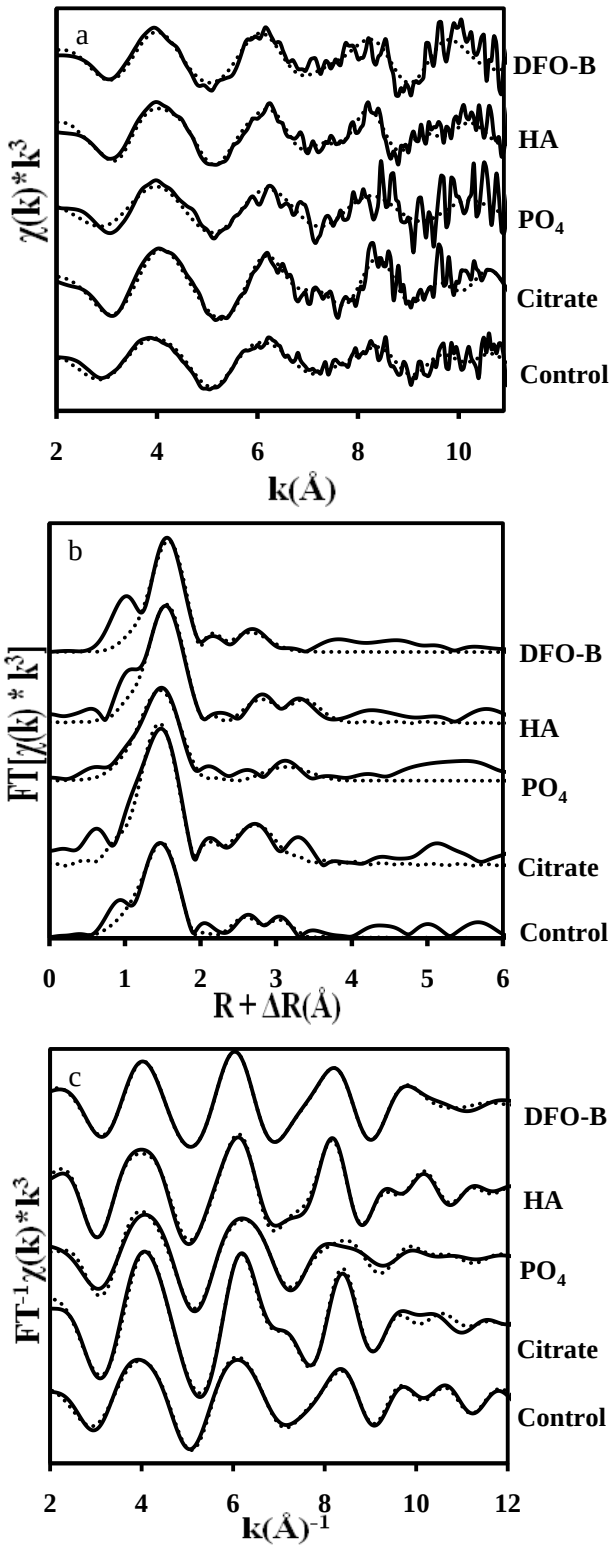

Figure 6.3 k^3-weighted $\chi(k)$ of Zn adsorbed to mixed mineral system (goethite-kaolinite) at pH 5.5 (a), their respective Fourier transforms (b), and inverse Fourier transforms (c). The solid lines represent the raw spectra and the dotted lines represent best fits.

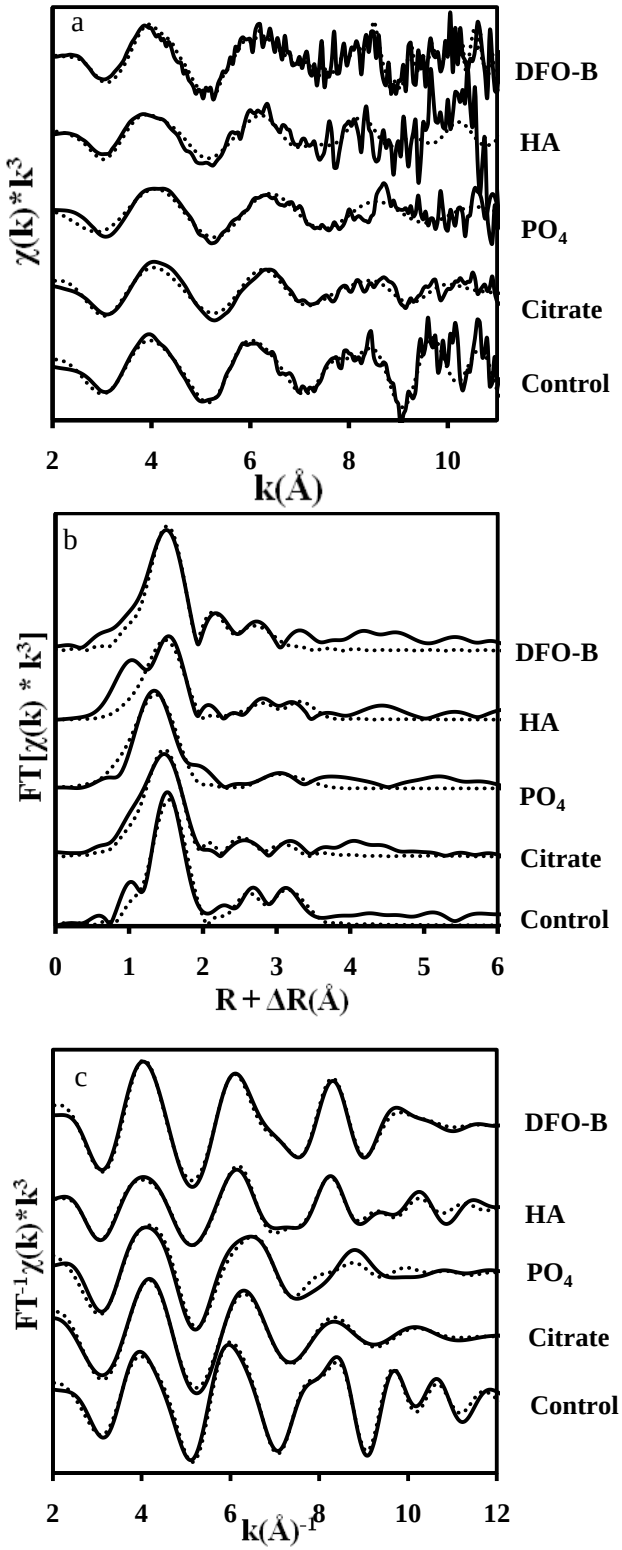

Figure 6.4 k^3-weighted $\chi(k)$ of Zn adsorbed to mixed mineral system (goethite-kaolinite) at pH 7.5 (a), their respective Fourier transforms (b), and inverse Fourier transforms (c). The solid lines represent the raw spectra and the dotted lines represent best fits.

Table 6.1 Structural parameters for Zn sorbed on goethite-kaolinite in the presence and absence of ligands derived from EXAFS spectral data analysis.

	pH 5.5				pH 7.5			
Ligand	Shell	N	R(Å)	σ^2(Å^2)	Shell	N	R(Å)	σ^2(Å^2)
Control	Zn-O	4.88	1.96	0.009	Zn-O	4.45	1.96	0.00
	Zn-Al	0.64	2.98	0.001	Zn-Al	1.06	3.00	0.001
	Zn-Fe/Zn	0.44	3.39	0.001	Zn-Fe/Zn	1.26	3.44	0.001
Citrate	Zn-O	4.90	1.93	0.008	Zn-O	4.17	1.96	0.008
	Zn-C	1.80	2.67	0.008	Zn-C	1.38	3.03	0.001
	Zn-Fe/Zn	0.80	3.08	0.001	Zn-Fe/Zn	1.92	3.43	0.020
PO_4	Zn-O	4.81	1.96	0.008	Zn-O	4.57	1.91	0.008
	Zn-Zn/Fe	1.51	3.64	0.007	Zn-Zn/Fe	2.18	3.61	0.011
HA	Zn-O	4.81	1.99	0.007	Zn-O	4.02	1.96	0.008
	Zn-Al	0.98	3.08	0.001	Zn-Al	1.08	3.10	0.005
	Zn-Fe\Zn	2.11	3.61	0.01	Zn-Fe	2.51	3.62	0.006
DFO-B	Zn-O	4.19	1.99	0.004	Zn-O	4.69	1.96	0.007
	Zn-C	1.62	2.69	0.003	Zn-C	2.85	2.72	0.003
	Zn-Fe/Zn	0.61	3.03	0.003	Zn-Fe/Zn	0.71	3.10	0.005

N = coordination number, R = radial distance (Å), σ^2 = Debye-Waller factor (Å^{-2}).The uncertainties in N are estimated to be 30%. Variations in R are estimated to be 0.03 for all shells.

It can be concluded from the fitting results that in the absence of ligands and at both pH levels, Zn formed inner sphere complexes with goethite and kaolinite surface functional groups. At both pH levels, Zn formed edge sharing linkages with kaolinite and corner sharing linkages with goethite. The formation of inner sphere complexes at low pH has been confirmed by other researchers.

Nachtegaal and Sparks (2004) studied Zn adsorption to goethite coated kaolinite and found that at pH 5.0, Zn formed inner sphere complexes with both kaolinite and goethite surface functional groups. Gräfe et al. (2007) on the other hand, found that Cd(II) formed outer sphere complexes with kaolinite at pH 6.0 and concluded that the Si tetrahedral sheet of kaolinite hindered Cd adsorption to the Al octahedral sheet. Inner sphere complexation with goethite can be explained by the fact that the pH range of this study is below the PZC of goethite (8.1), which means that both Zn ions and the goethite surface were positively charged. Zn adsorption

therefore would not occur as a result of electrostatic interaction, but as a result of non-columbic, specific interactions (Vermeer et al., 1999; Lai et al., 2002).

- **Citrate**

The RSF for the citrate sample at pH 5.5 shows two peaks at 2.8 and 3.2 Å (uncorrected for phase shift) (Figure 6.3 b). At pH 7.5, the second and third shells were located at 2.4 and 3.2 Å (uncorrected for phase shift), respectively (Figure 6.4 b). Fitting results in Table 6.1 show that Zn formed inner sphere complexes with goethite at both pH levels. The higher shells at pH 5.5 were fit with 1.8 C and 0.8 Fe/Zn atoms at interatomic distances of 2.67 and 3.08 Å, respectively. At pH 7.5 however, fitting results revealed 1.38 C and 1.92 Fe/Zn atoms at interatomic distances of 3.03 and 3.43 Å, respectively. In a previous study on kaolinite, we found that citrate suppressed the adsorption of Zn to kaolinite at pH > 5.5. Therefore, the absence of Al backscattering contribution in the results presented here coincides well with our previous results.

Various studies have shown that Zn forms outer sphere complexes with goethite in the presence of low molecular weight organic acids. Schlegel et al. (1997) found that the structure of ZnEDTA was preserved during adsorption to goethite, precluding a ligand exchange sorption mechanism, i.e. inner sphere complex formation. Collins et al. (1999) found outer sphere complexation of Zn citrate with the goethite surface and concluded that a Cd citrate precipitate had formed at pH 5.4. Ha et al. (2009) reported ternary A complex formation of Zn with hematite in the presence of oxalate, without ruling out the possibility of formation of Zn oxalate precipitates as EXAFS analysis is unable to distinguish between inner and outer sphere complexation in such cases. Similarly, although Zn formed inner sphere complexes with goethite in this study, the formation of Zn citrate precipitate is also possible, especially that the second shell was a result of C backscattering.

The Zn-Zn/Fe radial distance of 3.08 Å at pH 5.5 (Table 6.1) is consistent with ZnO_4 forming edge sharing bidentate linkages with goethite. Although the Zn-Zn/Fe radial distance of 3.43 Å at pH 7.5 (Table 6.2) is consistent with that of Zn-Zn in corner sharing ε-$Zn(OH)_2$ (reported values range from 3.40-3.46 Å), Zn polymerization and precipitate formation is unlikely to dominate in the presence of citrate, hence excluding Zn as a possible backscatterer. If we assume that backscattering was due to Fe rather than Zn atoms, the Zn-Fe distance of 3.43 Å is consistent with ZnO_4 forming corner-sharing bridging bidentate complex (Trainor et al., 2000).

- **Phosphate (PO_4)**

The RFSs for the PO_4 sample at pH 5.5 and 7.5 displayed in Figures 6.3 (b) and 6.4 (b) show a second shell at 3.1 Å (uncorrected for phase shift). Fitting results in Table 6.1 show that the second shell was best fit with Zn/Fe atoms at 3.64 and 3.61 Å for the pH 5.5 and 7.5 samples, respectively. These distances are consistent with ZnO_4 tetrahedra forming bidentate corner sharing complexes with FeO_6 octahedra of goethite. These results are consistent with those reported by Collins et al. (1999), where Cd formed a bidentate double corner sharing complexes with goethite in the presence of PO_4.

- **Humic Acid (HA)**

The RSFs for the HA sample at pH 5.5 and 7.5 displayed in Figures 6.3 (b) and 6.4 (b) show two peaks at 2.8 and ~3.3Å (uncorrected for phase shift). Fitting results in Table 6.1 show that the binding mechanisms remained the same at both pH levels, as evident by similarity in radial distances for the second and third shells at both pH levels. At both pH levels, the third shell was best fit with Fe/Zn atoms at interatomic distance of 3.6 Å, consistent with ZnO_4 tetrahdera forming corner sharing linkages with FeO_6 of goethite. Adsorption data in the

presence of HA indicated that the amount of Zn adsorbed in the mixed system was intermediate between that of the single kaolinite and goethite mineral systems. The Zn-Al radial distances of 3.08 and 3.10Å indicate edge sharing linkages with kaolinite. Assuming an Al-O distance of 1.93Å in kaolinite (Vasconcelos et al., 2008) and a Zn-O distance of 1.99, the Zn-O-Al bond angle would be ~106° implying an edge sharing linkage. Corner sharing linkage is not expected to produce such a small angle due to steric constraints.

- **Siderophore (DFO-B)**

The RSFs for the DFO-B sorption samples (Figures 6.3b and 6.4b) show second and third shell features at 2.2 and 2.7Å (uncorrected for phase shift). Fitting results in Table 6.1 show that the second and third shell backscattering atoms were C and Fe. The Zn-Fe radial distance of 3.03 for the sorption sample at pH 5.5 suggests edge sharing linkages with goethite. For corner sharing linkages to produce a small radial distance of 3.03 Å, the Al-O-Zn angle would have to be <105° giving rise to strong repulsion (Bochatay and Persson, 2000; Trainor et al., 2000). For the slightly longer radial distance of 3.10 Å (pH 7.5 sample), the Zn-O-Al angle would be <107°, also implying edge sharing linkage. Ha et al. (2009) reported that Zn-Fe radial distances of 3.10-3.12 Å were consistent with Zn forming edge sharing linkages with hematite. It can be concluded that in the presence of DFO-B, Zn formed inner sphere edge-sharing bidentate complexes with goethite at both pH 5.5 and 7.5.

6.4 References

Aguilera, N.H., and M.L. Jackson. 1953. Iron oxide removal from soils and clays. Soil Sci. Soc. Amer. Proc. 17: 359-364.

Alcacio, T.E., D. Hesterberg, J.W. Chou, J.D. Martin, S. Beauchemin, and D.E. Sayers. 2001. Molecular scale characteristics of Cu(II) bonding in goethite–humate complexes. Geochim. Cosmochim. Ac. 65(9): 1355–1366.

Ammann, L. 2003. Cation exchange and adsorption on clays and clay minerals. Ph.D. thesis. Christian-Albrechts-Universität, Kiel, Germany.

Angove, M.J., J.D. Wells, and B.B. Johnson. 1999. Adsorption of cadmium(II) onto goethite and kaolinite in the presence of benzene carboxylic acids. Colloid Surface A. 146: 243-251.

Arias, M., M.T. Barral and J.C. Mejuto. 2002. Enhancement of copper and cadmium adsorption on kaolin by the presence of humic acids. Chemosphere 48: 1081–1088.

Bochatay, L. and P. Persson. 2000. Metal ion coordination at the water-manganite (γ-MnOOH) interface II. An EXAFS study of zinc(II). J. Colloid Interf. Sci. 229: 593-599.

Bradl, H.B. 2004. Adsorption of heavy metal ions on soils and soils constituents. J. Colloid Interf. Sci. 277: 1- 18.

Buerge-Weirich, D., P. Behra, and L. Sigg. 2003. Adsorption of copper, nickel, and cadmium on goethite in the presence of organic ligands. Aquatic Geochemistry. 9(2): 65-85.

Chitrakar, R., S. Tezuka, A. Sonoda, K. Sakane, K. Ooi, and T. Hirotsu. 2006. Phosphate adsorption on synthetic goethite and akaganeite. J. Colloid Interf. Sci. 298: 602-608.

Collins, C.R., K.V. Ragnarsdottir, and D.M. Sherman. 1999. Effect of inorganic and organic ligands on the mechanism of cadmium sorption to goethite. Geochim. Cosmochim. Ac. 63(19): 2989-3002.

Cornell, R.M., and P.W. Schindler. 1980. Infrared study of the adsorption of hydroxycarboxylic acids on α-FeOOH and amorphous Fe(III) hydroxide. Colloid Polym. Sci. 258: 1171-1175.

Davis, J.A., and J.O. Leckie. 1978. Effect of adsorbed complexing ligands on trace metal uptake by hydrous oxides. Environ. Sci. Technol. 12(12): 1309-1315.

Diaz-Barrientos, E., L. Madrid, M.C. Contreras, and E. Morillo. 1990. Simultaneous adsorption of zinc and phosphate on synthetic lepidocrocite. Aust. J. Soil Res. 28: 549-557.

Dyer, J., and D. Sparks. 2003. Lead Sorption onto Ferrihydrite. 1. A Macroscopic and Spectroscopic Assessment. Environ. Sci. Technol. 37: 908-914.

Fay, M.L., A. Proctor, D.P. Hoffman, M. Houalla and D. Hercules. 1992. Determination of the Mo Surface Environment of Mo/TiO_2 Catalysts by EXAFS, XANES and PCA. Mikrochim. Acta. 109: 281 – 293.

Filius, J.D., T. Hiemstra, and W.H. van Riemsdijk. 1997. Adsorption of small weak organic acids on goethite: Modeling of mechanisms. J. Colloid Interf. Sci. 195: 368-380.

Gao, Y., and A. Mucci. 2001. Acid base reactions, phosphate and arsenate complexation, and their competitive adsorption at the surface of goethite in 0.7M NaCl solution. Geochim. Cosmochim. Ac. 65 (14): 2361-2378.

Geelhoed, J.S., T. Hiemstra, and W.H. Van Riemsdijk. 1998. Competitive interaction between phosphate and citrate on goethite. Environ. Sci. Technol. 32: 2119-2123.

Gräfe, M., B. Singh, and M. Balasubramanian. 2007. Surface speciation of Cd(II) and Pb(II) on kaolinite by XAFS spectroscopy. J. Colloid Interf. Sci. 315: 21–32.

Jackson, M.L. 1956. Soil chemical analysis, advanced course. In Soil Survey Laboratory Methods Manual. Soil Survey Investigation Report No.42, Version 4.0, November 2004. Washington, DC.

Janssen, R.P.T., M.G.M. Bruggenwert, and W.H. van Riemsdijk, 1997. Interactions between citrate and montmorillonite–Al hydroxide polymer systems. Eur. J. Soil Sci. 48: 463–472.

Ha, J., T.P. Trainor, F. Farges, and G.E. Brown Jr. 2009. Interaction of aqueous Zn(II) with hematite nanoparticles and microparticles. Part 1. EXAFS study of Zn(II) adsorption and precipitation. Langmuir 25(10): 5574-5585.

Křepelová, A. 2007. Influence of Humic Acid on the Sorption of Uranium(VI) and Americium(III) onto Kaolinite. Ph.D. thesis. Technischen Universität Dresden.

Lackovic, K., B.B. Johnson, M.J. Angove, and J.D. Wells. 2003. Modeling the adsorption of citric acid onto muloorina illite and related clay minerals. J. Colloid Interf. Sci. 267: 49-59.

Lai, C.H., C.Y. Chen, B.L. Wei, and S.H. Yeh. 2002. Cadmium adsorption on goethite-coated sand in the presence of humic acid. Water Res. **36**: 4943–4950.

Lee, S. and P.R. Anderson. 2005. EXAFS study of Zn sorption mechanisms on hydrous ferric oxide over extended reaction time. J. Colloid Interf. Sci. 286: 82-89.

Li, W., S. Zhang, W. Jiang, and X. Shan. 2006. Effect of phosphate on the adsorption of Cu and Cd on natural hematite. Chemosphere 63: 1235-1241.

Liao, M. 2006. Effects of organic acids on adsorption of cadmium onto kaolinite, goethite, and bayerite. Pedosphere. 16(2): 185-191.

Morillo, J.A., M. Aguilera, A. Ramos-Cormenzana, and M. Monteoliva-Sanchez. 2006. Production of a metal-binding exopolysaccharide by Paenibacillus jamilae using two-phase olive-mill waste as fermentation substrate. Current Microbiology. 53:189–193.

Mustafa, S., M.I. Zaman, R. Gul, and S. Khan. 2008. Effect of Ni^{+2} loading on the mechanism of phosphate anion sorption by iron hydroxide. Sep. Purif. Technol. 59: 108-114.

Nachtegaal, M., and D.L. Sparks. 2003. Nickel sequestration in a kaolinite-humic acid complex. Environ. Sci. Technol. 37:529-534.

Nachtegaal, M., and D.L. Sparks. 2004. Effect of iron oxide coatings on zinc sorption mechanisms at the clay-mineral/water interface. J. Colloid Interf. Sci. 276: 13–23.

Roberts, D.R., R.G. Ford, and D. L. Sparks. 2003. Kinetics and mechanisms of Zn complexation on metal oxides using EXAFS spectroscopy. J Colloid Interface Sci. 263(2): 364-376.

Rosenberg, D.R., and P.A. Maurice. 2003. Siderophore adsorption to and dissolution of kaolinite at pH 3 to 7 and 22ºC. Geochim. Cosmochim. Ac.67 (2): 223-229.

Scheinost, A.C., R. Kretzschmar, and S. Pfister, and D.R. Roberts. 2002. Combining Selective Sequential Extractions, X-ray Absorption Spectroscopy, and Principal Component Analysis for Quantitative Zinc Speciation in Soil. Environ. Sci. Technol. 36: 5021-5028.

Schlegel, M.L., A. Manceau, and L.Charlet. 1997. EXAFS study of Zn and ZnEDTA sorption at the goethite (α-FeOOH)/water interface.J. Phys IV Fr. 7C-3:823-824.

Schlegel, M.L. A. Manceau, D. Chateigner, and L. Charlet. 1999. Sorption of Metal Ions on Clay Minerals I. Polarized EXAFS Evidence for the Adsorption of Co on the Edges of Hectorite Particles. J. Colloid Interf. Sci. 215:140-158.

Seibner-Freibach, H.S., Y. Hadar, and Y. Chen. 2004. Interaction of Iron Chelating Agents with Clay Minerals. Soil Sci. Soc. Am. J. 68:470–480.

Spathariotis, E., and C. Kallianou. 2007. Adsorption of copper, zinc, and cadmium on goethite, aluminum-substituted goethite, and a system of kaolinite-goethite: surface complexation modeling. Commun. Soil Sci. Plan. 38: 611-635.

Swift, R.S. 1996. Organic matter characterization. Chapter 35. *In* D.L. Sparks (ed.) Methods of soil analysis. Part 3. SSSA Book Ser. 5. SSSA, Madison, WI.

Tejedor-Tejedor, M.I. and M.A. Anderson. 1990. Protonation of phosphate on the surface of goethite as studied by CIR-FTIR and electrophoretic mobility. Langmuir 6: 602-611.

Trainor, T.P., G.E. Brown, and G.A. Parks. 2000. Adsorption and precipitation of aqueous Zn(II) on alumina powders. J. Colloid Interf. Sci. 231: 359-373.

Trivedi, P., J.A. Dyer, and D.L. Sparks. 2003. Lead sorption onto ferrihydrite. 1. A macroscopic and spectroscopic assessment. Environ. Sci. Technol. 37: 908-914.

Vasconcelos, i.F., E.A. Haack, P.A. Maurice, B.A. Bunker. 2008. EXAFS analysis of cadmium(II) adsorption to kaolinite. Chem. Geol. 249:237-249.

Venema, P.,T. Hiemstra, and W.H. van Riemsdijk. 1997. Interaction of cadmium with phosphate on goethite. J. Colloid Interf. Sci. 192: 94-103.

Vermeer, A.W.P., J.K. McCulloch, W.H. Van Riemsdijk, and L.K. Koopal. 1999. Metal ion adsorption to complexes of humic acid and metal oxides: deviations from the additivity rule. Environ. Sci. Technol. 33: 3892-3897.

Violante, A., M.R. Ricciardella, and M. Pigna. 2003. Adsorption of heavy metals on mixed Fe–Al oxides in the absence or presence of organic ligands. Water Air Soil Poll. 145: 289–306.

Wang, K. and B. Xing. 2002. Adsorption and desorption of cadmium by goethite pretreated with phosphate. Chemosphere 48: 665-670.

Waychunas, G.A., C.C. Fuller, and J.A. Davis. 2002. Surface complexation and precipitate geometry for aqueous Zn(II) sorption on ferrihydrite I: X-ray absorption extended fine structure spectroscopy analysis. Geochim. Cosmochim. Ac. 66(7): 1119-1137.

Wua, Z., Z. Gu, X. Wang, L. Evans, and H. Guo. 2003. Effects of organic acids on adsorption of lead onto montmorillonite, goethite and humic acid. Environ. Pollut. 121: 469–475.

Xia, K., W. Bleam, and P.A. Helmke. 1997. Studies of the nature of Cu^{+2} and Pb^{+2} binding sites in soil humic substances using X-ray absorption spectroscopy. Geochim. Cosmochim. Ac. 61 (11): 2211-2221.

Zuyi, T., C. Taiwei, D. Jinzhou, D. XiongXin, and G. Yingjie. 2000. Effect of fulvic acids on sorption of U(VI), Zn, Yb, I and Se(IV) onto oxides of aluminum, iron and silicon. Appl. Geochem. 15: 133-139.

CHAPTER 7

XAFS SPECTROSCOPIC INVESTIGATION OF ZINC ADSORPTION TO MONTMORILLONITE

7.1 Introduction

Zinc (Zn) adsorption to clay minerals such as montmorillonite controls its availability and transport in the soil environment. Zn may adsorb to the permanently charged sites of montmorillonite by weak electrostatic interaction forming an outer sphere complex and to the edge sites forming an inner sphere complex (Kaya and Ören, 2005). The type of complex formed impacts the fate of Zn in the soil, as outer sphere complexes are weak and reversible and inner sphere complexes are strong and usually irreversible (Schlegel et al., 2001). In addition to formation of inner and outer sphere complexes, Zn may be sequestered into a precipitate phase such as a mixed Zn-Al layered double hydroxide (Zn-Al LDH) or Zn phyllosilicate phase (Ford and Sparks, 2000). These precipitate phases are known to occur in phyllosilicates and Al oxide minerals at neutral pH. Another type of layered Zn phase may form under acidic conditions when Zn enters the Al-hydroxy (Al-OH) interlayers of clay minerals (Scheinost et al. 2002; Voegelin et al. 2005). What all these phases share in common is the incorporation of Zn into octahedral sheets of layered minerals (Voegelin et al., 2005). Release of Al and Si from clay mineral weathering controls metal precipitate formation and transformation (Ford et al., 1999). Voegelin et al. (2005) indicated that the availability of Al and Si favor the formation of Zn-LDH and that their supply is controlled by the dissolution of primary and secondary minerals (Voegelin et al., 2005). Zn-Al LDH formation was reported in montmorillonite (Lee et al., 2004), kaolinite (Nachtegaal and Sparks, 2004), gibbsite (Roberts et al., 2003), and alumina (Trainor et al., 2000). Studies have confirmed the formation of Zn-Al LDH and Zn-phyllosilicate phases in contaminated soils (Voegelin et al., 2005).

Phosphate is ubiquitous in the soil environment and originating from natural weathering and anthropogenic activites such as mining, ore processing, and fertilization. It is of environmental concern as its release into surface waters results in eutrophication (Gao and Mucci, 2001). Phosphate adsorption to phyllosilicate clay minerals involves two steps; the first is an initial rapid stage complete within 24 hours and a slow step that continues for weeks. The former is significant under neutral to alkaline pH conditions, whereas the latter is significant under acidic conditions (Edzwald et al., 1976). Zn adsorption to iron oxide surfaces has been reported to increase in the presence of phosphate due to increase in negative charge of the inner Helmholtz plane (Diaz-Barrientos et al., 1990). Pretreatment of phyllosilicates with phosphate has been shown to enhance the adsorption of various heavy metals such as Cd and Pb.

X-Ray Absorption Fine Structure (XAFS) Spectroscopy is a valuable tool that allows probing of the local coordination environment of Zn. Although there are abundant studies that have investigated Zn adsorption to clay minerals at the molecular level using XAFS spectroscopy, the impact of phosphate on Zn adsorption has not been investigated at the molecular level. The objectives of this study are to elucidate the adsorption mechanisms of Zn to montmorillonite in the presence of levels of phosphate at pH 7.0, and to investigate the impact of reaction time on adsorption mechanisms.

7.2 Material and Methods

7.2.1 Preparation of Montmorillonite

Montmorillonite used in this study was the Na-rich Wyoming montmorillonite (Swy-2) obtained from the Clay Minerals Society (Moll, 2001). The <2 μm fraction was obtained by sedimentation according to Stokes law. To ensure that montmorillonite was void of impurities, a purification process was used to remove carbonates, iron oxides, and organic matter. Carbonate

removal was conducted using the method of Jackson (1956) in which Swy-2 was heated in sodium acetate (pH 5.0) at 95ºC for 30 minutes. Swy-2 was then washed with 1M NaCl three times to remove acetate. Iron removal was conducted using the citrate-bicarbonate-dithionite method described by Aguilera and Jackson (1953). Afterwards, Swy-2 was washed 4 times via centrifugation with a solution of 0.025 M HCl and 0.5 M NaCl (Ammann, 2003). Organic matter was removed by heating in 3% H_2O_2 at 50ºC for 1 hour, then heating at 70ºC to destroy remaining H_2O_2 (Schlegel et al., 1998). Swy-2 was then washed 5 times with 1 M NaCl and washed again with deionized water to remove excess salt (Janssen et al., 1997; Nachtegaal and Sparks, 2003). Swy-2 was dialyzed against double deionized water until no Cl^- remained as tested by $AgNO_3$. Dialysis bags were pretreated by boiling in a 2% $NaHCO_3$ and 1 mM EDTA solution and washed with deionized water to remove contaminating minerals and polysaccharides (Morillo et al., 2006). The purified kaolinite was then freeze dried, ground and sieved prior to use. The 5 point N_2-BET surface area for montmorillonite in this study was found to be 40 m^2/g. The reported pH at point zero charge (PZC) for Swy-2 ranges from 7.5 to 8.5 (Lee et al., 2004).

7.2.2 Zn Adsorption Experiment

Adsorption experiment was conducted in 250 ml centrifuge tubes under continuous purging of ultra pure N_2 gas. The experimental setup included four phosphate concentrations (0, 0.05, 0.2, and 0.5 mM), initial Zn concentration of 1.0 mM, Swy-2 concentration of 10g/l, background electrolyte of 0.1 M $NaNO_3$, pH 7.0, and two replications. Suspensions of Swy-2 were equilibrated for 24 hrs in background electrolyte under constant shaking. Then, necessary amounts of phosphate were added from a 5 mM NaH_2PO_4 stock solution to achieve initial phosphate concentrations of 0, 0.05, 0.2, and 0.5 mM. The suspensions were allowed to react for

1 hour under constant shaking. Then, necessary amounts of Zn were added in small increments of 100-µl from an acidified $Zn(NO_3)_2$ stock solution to each of the centrifuge tubes. The pH was adjusted to its value of 7.0 using 0.1 M of either HNO_3 or NaOH (pre-purged with N_2). The final volume was completed and the samples were placed on a shaker. Aliquots of 20 ml were then extracted from the centrifuge tubes after 4hrs and continued over a period of 6 months. The pH was continuously monitored (under N_2 purging) and adjusted so that values exhibited minimal fluctuations. The solid was separated from the solution by centrifugation and the solution was filtered using 0.4 µM filters. Soluble concentrations of Zn, P, Si and Al were determined using ICP-AES (Spectro). The amounts of Zn and phosphate adsorbed were determined by the difference in initial and final concentrations in solution. The solid portion was stored as a paste at 4ºC until use for XAFS spectroscopy analysis.

7.3 Results and Discussion

7.3.1 Effect of Phosphate on Zinc Adsorption

Figure 7.1a shows Zn adsorption to montmorillonite in the presence of various concentrations of phosphate as a function of time. It can be seen that the presence of phosphate at concentrations higher than 0.05 mM enhanced Zn adsorption to montmorillonite. In comparison with the control, the presence of 0.2 mM phosphate increased Zn adsorption by 7 and 23% after 4 hours and 6 months, respectively. The presence of 0.5 mM phosphate increased Zn adsorption by ~23% after 4 hours and 6 months adsorption. At each of the phosphate concentration levels, Zn adsorption increased with time, where increases of ~9% were observed with increase in reaction time upto 6 months for all samples. Continued adsorption of Zn to montmorillonite over long periods may be due to the replacement of Na^+ ions by Zn on the outer surface or interlayers

of montmorillonite (Kaya and Ören, 2005). Figure 7.1b shows phosphate adsorption to montmorillonite as a function of time.

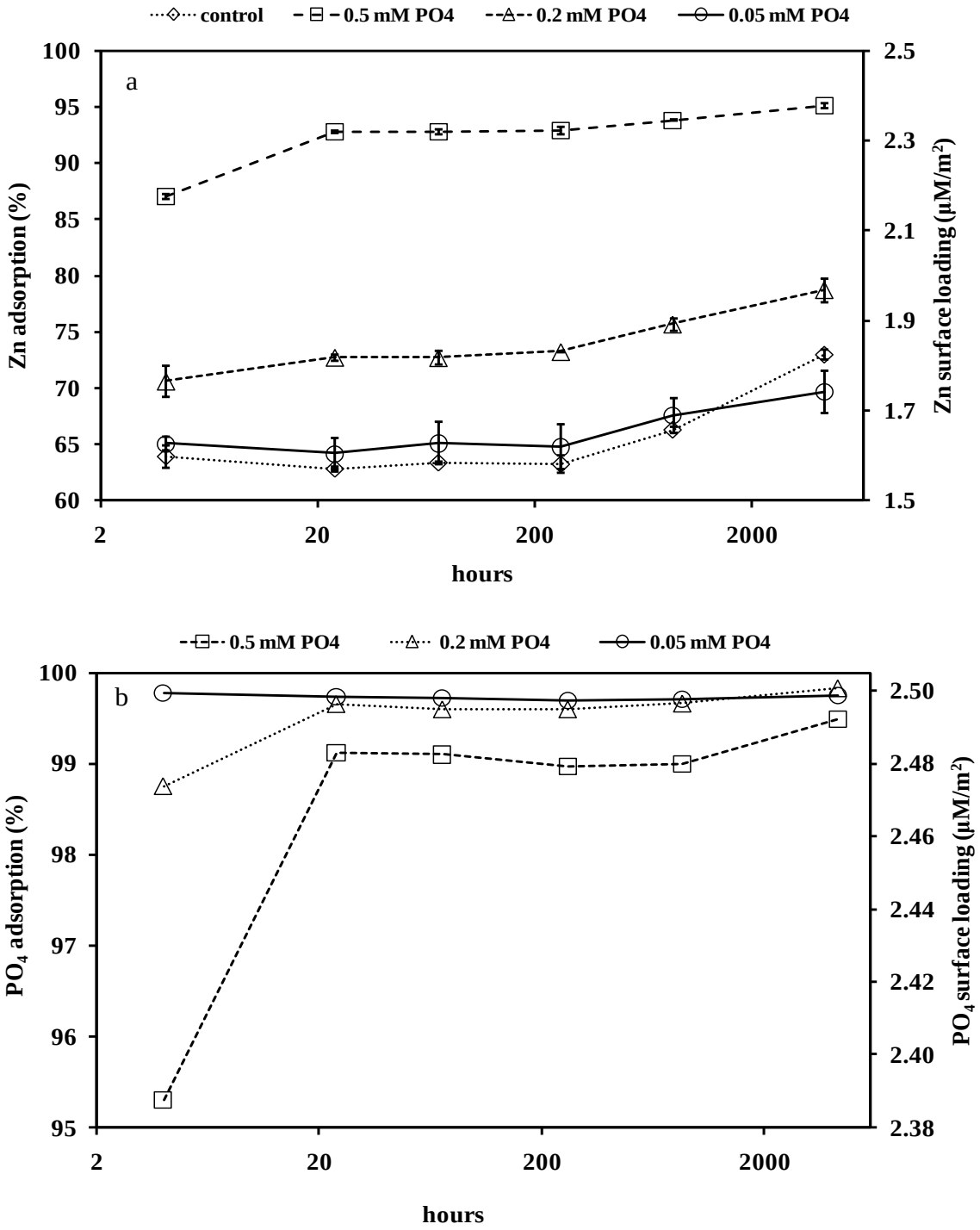

Figure 7.1 Zn adsorption to montmorillonite in the presence of PO_4 as a function of time (a), PO_4 adsorption to montmorillonite as a function of time (b).

It can be seen that more than 95% of phosphate was adsorbed to montmorillonite at all concentrations and at any given reaction time. Phosphate-treated kaolinite was found to enhance the adsorption of Pb and Cd to kaolinite (Adebowale et al., 2006). Increasing concentrations of phosphate on an iron oxide (lepidocrocite) strongly enhanced the adsorption of Zn to the mineral surface. It was concluded that indicated that the specific adsorption of phosphate causes increase in negative charge of the inner Helmholtz plane, having a positive effect of cation adsorption (Diaz-Barrientos et al., 1990). Phosphate was found to enhance Cd adsorption to goethite by reducing pH_{pzc} and surface potential (Wang and Xing, 2002).

7.3.2 X-Ray Absorption Fine Structure Spectroscopy

7.3.2.1 EXAFS Data Analysis of Zn Model Compounds

Figure 7.2 (a-c) shows Zn K-edge XANES spectra, k^3-weighted $\chi(k)$spectra and their respective Radial Structural Functions (RSF) for Zn model compounds. Data analysis obtained from fitting the backtransformed χ spectra are shown in table 7.1. Aqueous Zn is a compound in which Zn forms a single coordination shell with six oxygen atoms representing an outer sphere complex of octahedral coordination. The $\chi(k)$spectrum for this compound shows that the amplitude decreases monotonically with $k(Å)$, characteristic of outer sphere complexes (Nachtegaal and Sparks, 2004). The RSF shows outer sphere complexation as evident by the absence of a second coordination shell (Figure 7.2 c). The second Zn model compound chosen was Zn-Al Layered Double Hydroxide (Zn-Al LDH) which represents a precipitate phase that may form on the surface of phyllosilicate minerals. Zn here is incorporated in the octahedral sheets of layered minerals (Voegelin et al., 2005). Characteristic features of Zn-Al LDH include a shoulder at 9680 eV in its XANES spectrum, a split in $\chi(k)$ spectrum at ~8Å, and a second shell at 2.4Å in its RSF (figure 7.2 a-c).

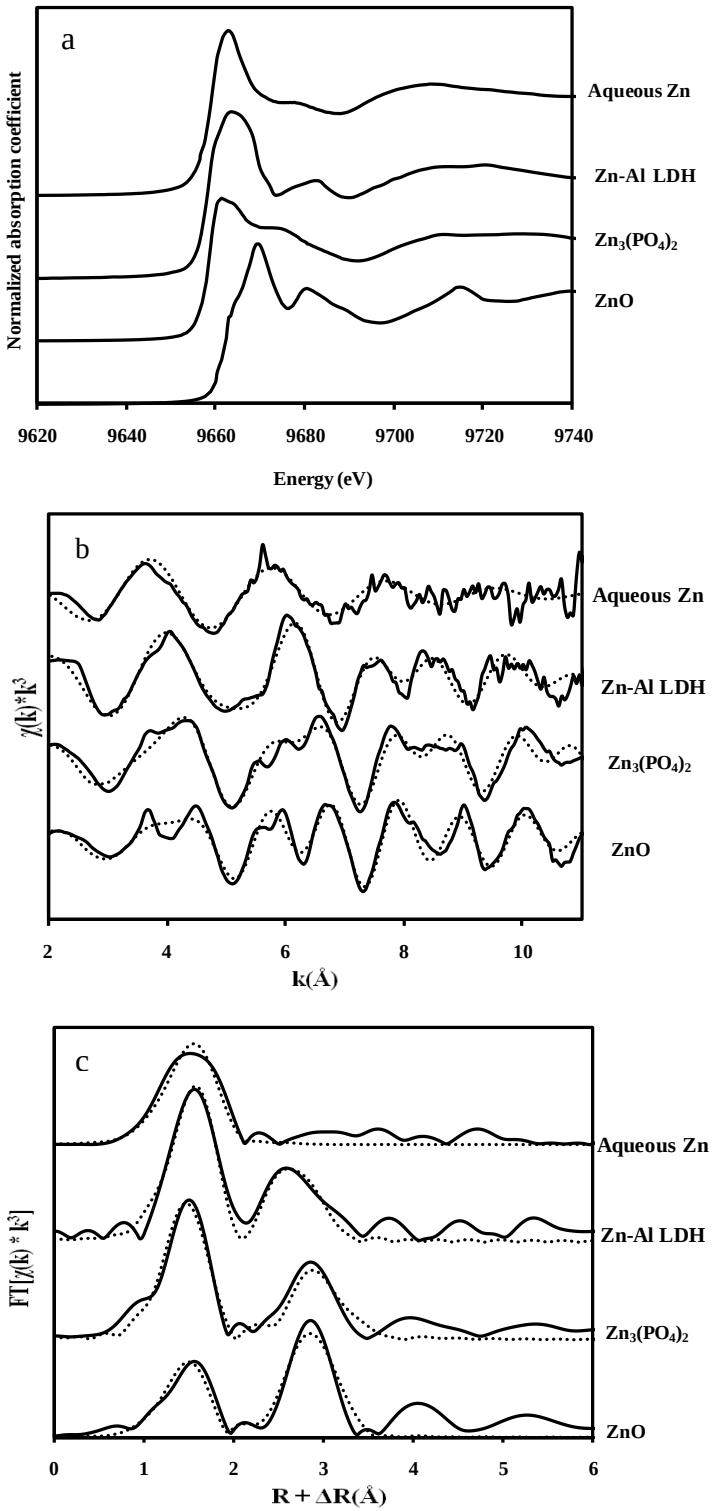

Figure 7.2 Zn K-edge XANES spectra (a), k^3-weighted $\chi(k)$spectra (b), and their respective Fourier transforms (c) for Zn model compounds. The solid lines represent the raw spectra and the dotted lines represent best fits.

$Zn_3(PO_4)_2$ was included in the model compounds to investigate the formation of Zn-PO_4 precipitates. Its characteristic XANES features include a small drop in absorption after the edge and a shoulder at 9672eV (Figure 7.2a).

Table 7.1 Structural parameters for Zn reference compounds derived from EXAFS spectral data analysis

Compound	Shell	N	R(Å)	σ^2(Å^2)
$Zn^{+2}_{(aq)}$	Zn-O	5.77	2.07	0.012
Zn-LDH	Zn-O	6.63	2.03	0.010
	Zn-Zn	4.63	3.06	0.012
	Zn-Al	2.18	3.05	0.012
$Zn_3(PO_4)_2$	Zn-O	4.09	1.96	0.006
	Zn-P	2.32	3.11	0.003
	Zn-Zn	4.96	3.26	0.008
ZnO	Zn-O	3.27	1.95	0.008
	Zn-Zn	12.41	3.23	0.012

7.3.2.2 EXAFS Data Analysis of Sorption Samples

Figure 7.3 shows the Zn-edge K-spectra, normalized k^3-weighted EXAFS spectra, and the corresponding Fourier transformed Radial Structural Functions (RSF) (uncorrected for phase shifts) for samples of Zn adsorption to montmorillonite in the presence of phosphate at pH 7.5. Data analysis obtained from fitting the backtransformed χ spectra are shown in Table 7.2. The Table shows that Zn adsorbed to Swy-2 forming outer sphere complexes in all sorption samples regardless of reaction time or phosphate levels. This is evident in the RSF for the sorption samples shown in Figure 7.3c where a single coordination shell is present. The only structural differences that were found among the samples were in the first neighbor coordination shell.

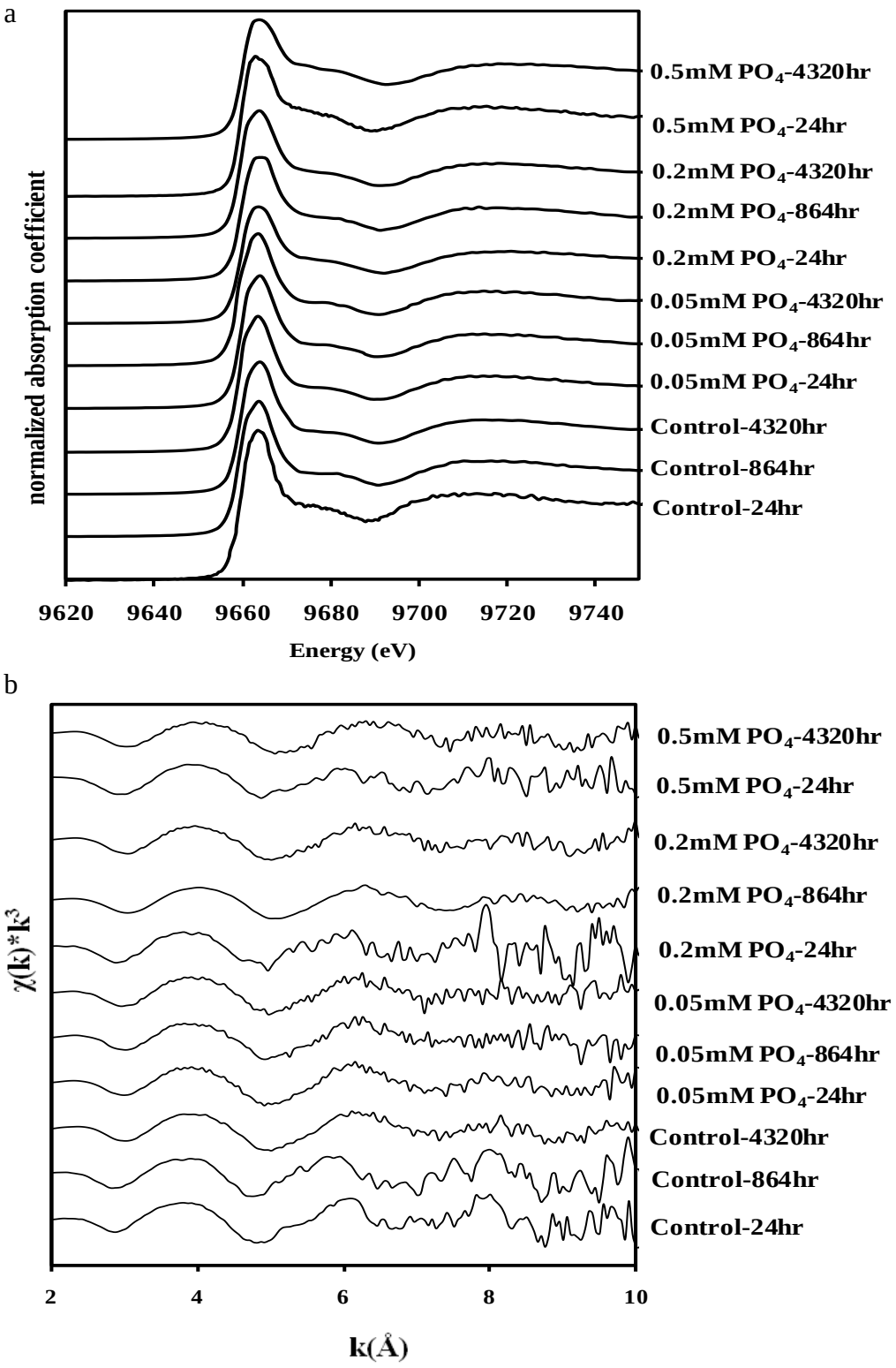

Figure 7.3 Zn K-edge XANES spectra (a),and k^3-weighted $\chi(k)$spectra (b) for Zn adsorption samples.

Figure 7.3 Con'd (c) Fourier transforms for Zn adsorption samples.

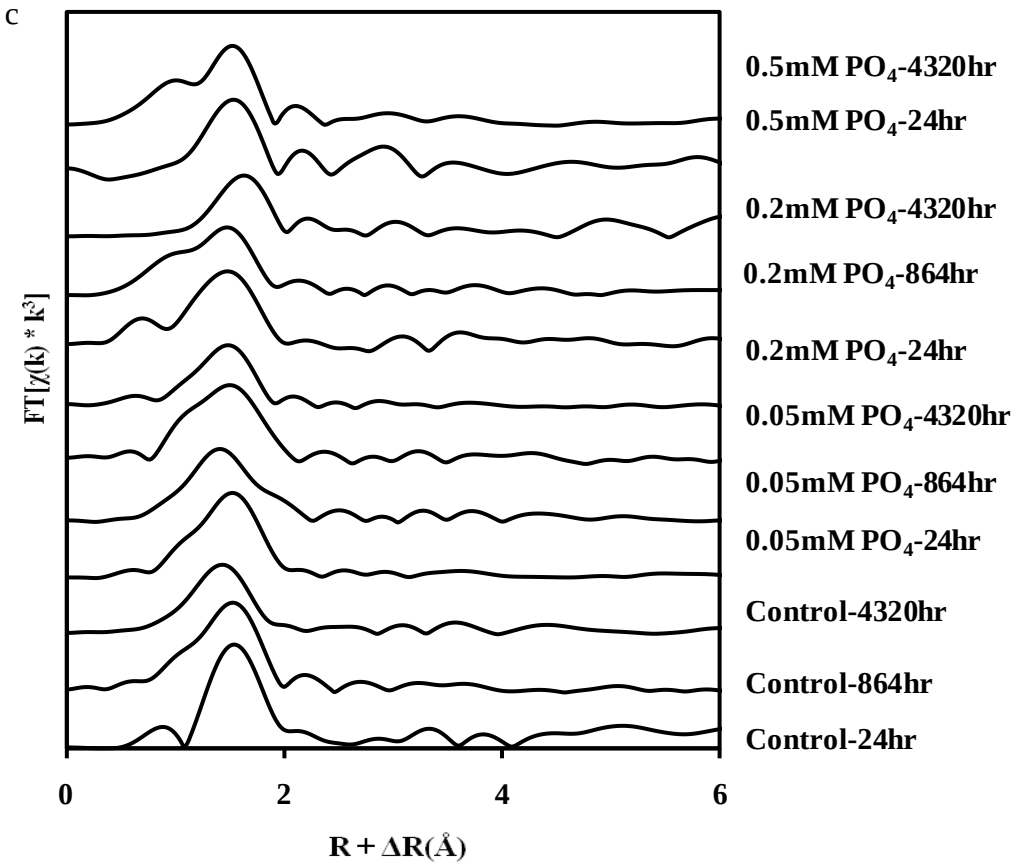

Zn may form tetrahedral or octahedral coordination with first shell oxygen atoms (Roberts et al., 2003). It can be seen from Table 7.2 that Zn formed octahedral coordination with first neighbor atoms in the absence of phosphate after 24 and 864 hours of adsorption as evident by the Zn-O radial distance of ~2.03 and coordination numbers 5.52 and 6.35, respectively. Characteristic Zn-O radial distances for tetrahedral and octahedral coordination range from 1.92 to 1.99Å and from 2.02 to 2.12Å, respectively (Roberts et al., 2003). For the same control sample after 4320 hours of adsorption, the radial distance slightly decreased to 1.99Å, which may hint to the formation of a mixture of octahedral and tetrahedral coordination spheres on the surface of montmorillonite.

Pan et al. (2004) reported that Zn was adsorbed to manganite in a mixture of tetrahedral and octahedral coordination at an average radial distance of 2.0Å. Formation of octahedral coordination with first shell oxygen atoms in the control is consistent with previous research on Zn adsorption to phyllosilicates. Zn forms octahedral coordination upon adsorption to montmorillonite (Lee et al., 2004), kaolinite (Nachtegaal and Sparks, 2004), pyrophyllite (Ford and Sparks, 2000), and hectorite (Schlegel et al., 2001). Tetrahedral coordination was reported to occur upon adsorption to oxide mineral surfaces such as ferrihydrite (Waychunas et al., 2002), goethite, and alumina powders (Trainor et al., 2000).

Table 7.2 Structural parameters for Zn adsorption to montmorillonite in the presence of PO_4 derived from EXAFS spectral data analysis

PO_4 concentration (mM)	Adsorption time (hours)	Zn - O		
		N	R(Å)	σ^2(Å^2)
0	24	5.52	2.02	0.004
0	864	6.35	2.03	0.004
0	4320	5.27	1.99	0.011
0.05	24	4.72	1.99	0.008
0.05	864	5.86	1.94	0.017
0.05	4320	5.49	1.99	0.015
0.20	24	4.64	1.93	0.008
0.20	864	4.90	1.97	0.013
0.20	4320	4.70	1.95	0.010
0.50	24	5.41	2.05	0.007
0.50	4320	3.77	1.96	0.007

N = coordination number, R = radial distance (Å), σ^2 = Debye-Waller factor (Å^{-2}). The uncertainties in N are estimated to be 30%. Variations in R are estimated to be 0.03 for all shells.

There are several scenarios that may occur under the experimental conditions of this study. In terms of adsorption, Zn may form inner or outer sphere complexes, or a combination of both. In case of inner sphere complexation, a Zn polynuclear complex or surface precipitate may

also form. In addition to adsorption and surface precipitation, Zn may be incorporated into the octahedral sheet of montmorillonite, forming a Zn-Al LDH. The absence of a second coordination shell in any of the samples rules out the formation of inner sphere, Zn polymerization, or LDH formation. The absence of diagnostic spectral features provides further evidence for the absence of these sorption mechanisms. For the Zn-Al LDH model compound shown in Figure 7.2, a peak is present at 9680eV in its XANES spectrum, a split in the oscillation of its χ spectrum at ~8Å^{-1}, and a second shell at 2.4Å (uncorrected for phase shift). For the sorption samples in Figure 7.3, the XANES spectra show a small peak at 9677eV that resembles that of aqueous Zn (Figure 7.2a). In addition, the χ spectra of sorption samples do not exhibit structural information that would hint to the formation of a LDH such as the split in oscillation at ~8Å^{-1}. Most importantly, the Fourier transforms for the sorption samples do not exhibit a second shell which would rule out Zn-Al LDH formation, inner sphere complexation, or Zn polymerization. In fact, the χ spectra for most of the sorption samples exhibit a drastic decrease in amplitude with *k*, similar to that of outer sphere aqueous Zn model compound.

The absence of inner sphere complexation may be supported by existing research. Lee et al. (2004) used similar experimental conditions as presented here and found that Zn formed polynuclear complexes upon adsorption to montmorillonite in the first 11 days of adsorption. After 20 days adsorption, a Zn phyllosilicate like phase has formed. What supports the results presented here is that inner sphere complexes were absent in their study for the first 11-20 days. Schlegel et al. (2001) reported that Zn was initially adsorbed as outer sphere complexes on the interlayer sites of hectorite and then migrated to the layer edges forming inner sphere complexes.

7.4 References

Adebowale, K.O., I.E. Unuabonah, and B.I. Olu-Owolabi. 2006. The effect of some operating variables on the adsorption of lead and cadmium ions on kaolinite clay. J. Hazard. Mater. B 134: 130–139.

Aguilera, N.H., and M.L. Jackson. 1953. Iron oxide removal from soils and clays. Soil Sci. Soc. Amer. Proc. 17: 359-364.

Ammann, L. 2003. Cation exchange and adsorption on clays and clay minerals. Ph.D. thesis. Christian-Albrechts-Universität, Kiel, Germany.

Diaz-Barrientos, E., L. Madrid, M.C. Contreras, and E. Morillo. 1990. Simultaneous adsorption of zinc and phosphate on synthetic lepidocrocite. Aust. J. Soil. Res. 28: 549-557.

Edzwald, J.K., D.C. Toensing, and M.C.Y Leung. 1976. Phosphate adsorption reactions with clay minerals. Environ. Sci. Technol. 10(5): 485-490.

Ford, R.G., A.C. Scheinost, K.G. Scheckel, and D.L. Sparks.1999.The link between clay mineral weathering and the stabilization of Ni surface precipitates. Environ. Sci. Technol. 33: 3140-3144.

Ford, R.G., and D.L. Sparks. 2000. The nature of Zn precipitates formed in the presence of pyrophyllite. Environ. Sci. Technol. 34:2479-2483.

Gao, Y., and A. Mucci. 2001. Acid base reactions, phosphate and arsenate complexation, and their competitive adsorption at the surface of goethite in 0.7M NaCl solution. Geochim. et Cosmochim. Ac. 65(14): 2361-2378.

Jackson, M.L. 1956. Soil chemical analysis, advanced course. In Soil Survey Laboratory Methods Manual. Soil Survey Investigation Report No.42, Version 4.0, November 2004. Washington, DC.

Janssen, R.P.T., M.G.M. Bruggenwert, and W.H. van Riemsdijk, 1997. Interactions between citrate and montmorillonite–Al hydroxide polymer systems. Eur. J. Soil Sci. 48: 463–472.

Kaya, A., and A.H. Ören. 2005. Adsorption of zinc from aqueous solutions to bentonite. J. Hazardous Materials B125. 183-189.

Lee, S., P.R. Anderson, G.B. Bunker, and C. Karanfil. 2004. EXAFS Study of Zn Sorption Mechanisms on Montmorillonite. Environ. Sci. Technol. 38: 5426-5432.

Moll, W.F. 2001. Baseline studies of the Clay Minerals Society source clays: geological origin. Clay Clay Miner. 49(5): 374-380.

Morillo, J.A., M. Aguilera, A. Ramos-Cormenzana, and M. Monteoliva-Sanchez. 2006. Production of a metal-binding exopolysaccharide by Paenibacillus jamilae using two-phase olive-mill waste as fermentation substrate. Current Microbiology. 53:189–193.

Nachtegaal, M., and D.L. Sparks. 2003. Nickel sequestration in a kaolinite-humic acid complex. Environ. Sci. Technol. 37:529-534.

Nachtegaal, M., and D.L. Sparks. 2004. Effect of iron oxide coatings on zinc sorption mechanisms at the clay-mineral/water interface. J. Colloid Interf. Sci. 276: 13–23.

Pan, G., Y. Qin, X. Li, T. Hu, Z. Wu and Y. Xie. 2004. EXAFS studies on adsorption-desorption reversibility at manganese oxides-water interfaces I. Irreversible adsorption of Zn onto manganite (γ-MnOOH). J. Colloid Interf. Sci. 271: 28-34.

Roberts, D.R., R.G. Ford and, D. L. Sparks. 2003. Kinetics and mechanisms of Zn complexation on metal oxides using EXAFS spectroscopy. J. Colloid Interf. Sci. 263(2): 364-376.

Scheinost, A.C., R. kretzschmar, and S. pfister, D.R. Roberts. 2002. Combining selective sequential extractions, X-ray absorption spectroscopy, and principal component analysis for quantitative zinc speciation in soil. Environ. Sci. Technol. 36: 5021-5028.

Schlegel, M.L. A. Manceau, D. Chateigner, and L. Charlet. 1998. Sorption of metal ions on clay minerals I. Polarized EXAFS evidence for the adsorption of Co on the edges of hectorite particles. J. Colloid Interf. Sci. 215:140-158.

Schlegel, M.L., A. Manceau, L. Charlet, and J.L. Hazemann. 2001. Adsorption mechanisms of Zn on hectorite as a function of time, pH, and ionic strength. American Journal of Science 301: 798–830.

Trainor, T.P., G.E. Brown, and G.A. Parks. 2000. Adsorption and precipitation of aqueous Zn(II) on alumina powders. J. Colloid Interf. Sci. 231: 359 –372.

Voegelin, A., S. Pfister, A. Scheinost, M.A. Marcus, and R. Kretzschmar. 2005. Changes in zinc speciation in field soil after contamination with zinc oxide. Environ. Sci. Technol. 39: 6616-6623.

Wang, K. and B. Xing. 2001. Adsorption and desorption of cadmium by goethite pretreated with phosphate. Chemosphere 48: 665–670.

Waychunas, G.A., C.C. Fuller, and J.A. Davis. 2002. Surface complexation and precipitate geometry for aqueous Zn(II) sorption on ferrihydrite I: X-ray absorption extended fine structure spectroscopy analysis. Geochim. Cosmochim. Ac. 66(7): 1119-1137.

CHAPTER 8

EFFECT OF ORGANIC MATTER OXIDATION ON THE FRACTIONATION OF COPPER, ARSENIC, ZINC, AND LEAD IN SEWAGE SLUDGE AND AMENDED SOILS

8.1 Introduction

Sewage sludge (SS) has been used as a soil fertilizer due to its high organic matter (OM) content, low C/N ratio, and richness in nutrients such as N and P (Adani and Tambone, 2005). In addition to fertility value for arable farming, application of SS to soils is an economically and environmentally sound alternative to landfill disposal and incineration (Stacey et al., 2001). One of the major concerns of continued land application of SS is increased trace metal concentration in soil and uptake by plants. Due to the presence of chemically active surfaces in SS such as OM, Fe/Mn oxides, and calcium carbonates, addition of SS to soil is not a simple addition of trace metals to soils. Metals added to soils as constituents of biosolids are generally less phytoavailable than the addition of metal salts alone to soils (Hettiarchchi et al., 2003).

The phases responsible for the hindering of metal availability in biosolid-amended soils remains, however, disputed (Li et al., 2001). While some studies have postulated that it is the organic fraction of biosolids that plays this role of reduced metal phytoavailability, other studies have indicated that the inorganic surfaces added to biosolids during SS processing are the responsible phases (Hettiarachchi et al., 2006; Li et al., 2001). This uncertainty has led to a controversy over the consequences of long term application of biosolids. If the organic fraction was the responsible phase for reduced metal bioavailability, then the long term application of biosolids would result in the release of heavy metals into the soil due to OM mineralization, also known as the “Time Bomb” (TB) hypothesis (Bergkvist et al., 2005; Hettiarachichi et al., 2006; Li et al., 2001; McBride, 1995, 2003). If on the other hand, it were the inorganic fractions of biosolids (amorphous Fe and Mn oxides, carbonates, phosphates) that were responsible for the

reduced availability of metals, then the long term application of biosolids would present no hazard, due to the high adsorptive capacity of these phases. This is known as the "Protection" (PT) hypothesis (Frost et al., 2000; McBride 1995, 2003). As a matter of fact, legislative standards for sludge use in the United States partly depend on this PT hypothesis (Bergkvist et al., 2005). To date, the long term fate of metals from biosolid application is still not understood (Bergkvist and Jarvis 2004; Bergkvist et al., 2005; Hettiarachchi et al., 2006; Li et al., 2001).

Various studies have investigated trace metal availability in SS as a result of OM degradation. In an aging study of biosolids, Stacey et al. (2001) found that SS decomposition did result in the release of Zn and Cd to plant available pools. In contrast, Hettiarachchi et al. (2006) used μ-XANES and μ-XRF to identify Fe and Mn oxides associated with metals before and after the removal of OM from SS, and showed that even if metals were associated with the organic fraction of SS, the degradation of OM should not lead to substantial increase in metal availability due to complexation with Fe and Mn oxides. In addition, Oliver et al. (2005) investigated Cu availability in soils amended with SS for 7 years and found that OM degradation with time did not result in significant increases in Cu availability. Both of these studies attributed the retention of metals to the binding by inorganic fractions, which seemed to refute the TB hypothesis. Antoniadis et al. (2007) found that incubating SS amended soils for approximately 1year resulted in reduced organic carbon (OC) by 31%, and this OC reduction changed metal adsorption behavior by lowering the distribution coefficient (Kd) of Cd and increasing it for Zn. In a different study, Bergkvist and Jarvis (2004) modeled organic carbon dynamics to predict scenarios under which the fate of Cd would behave as predicted by either the PT or TB hypothesis. They reported that either of the two scenarios was likely to occur depending on the ratio of sludge adsorption capacity to soil adsorption capacity, proportion of sludge adsorption

capacity contributed by inorganic fraction, and Cd sludge loading. On the other hand, complete removal of OC from SS reduced Cd adsorption in SS but not in SS amended soils, indicating the importance of both OC and Fe/Mn oxides in retaining Cd (Hettiarachchi et al., 2003). These studies suggest that the nature of heavy metal dynamics upon OM degradation could be controlled by many factors including specificity of a trace metal, SS, and soil properties.

Most previous studies, to date, had primarily used a single-step extraction to assess metal bioavailability in different soil amendments. In this study, we have focused on exploring the distribution of trace metals in different pools of bioavailability in SS and SS-amended soils at different stages of OM degradation using a sequential fractionation. Metals in environmental matrices such as soils can be fractioned into the exchangeable, carbonate-bound, Fe/Mn oxide-bound, organically bound, and residual fractions. The exchangeable fraction contains metals that are weakly adsorbed to mineral surfaces and that can be released by ion exchange processes (Banerjee 2003; Filgueiras et al. 2002). The carbonate fraction is a loosely bound phase that is susceptible to pH change (Kazi et al., 2005; Li et al., 2001). This fraction represents metals that would be released into the environment if conditions were to become acidic (Usero et al., 1998). The Fe/Mn oxide fraction contains heavy metals that are released when the matrix is subject to reducing conditions (Kazi et al., 2005). This fraction includes easily reducible fraction (Mn oxides), moderately reducible fraction (amorphous Fe oxides), and poorly reducible fraction (crystalline Fe oxides) (Filgueiras et al., 2002). The organic matter fraction includes metals that are released under oxidizing conditions. These metals are non-mobile, non-available, and are bound to stable high molecular weight substances (Kazi et al., 2005). Metallic pollutants associated with this fraction are assumed to remain in the soil for a long time, but may be released as soluble forms due to organic matter degradation (Filgueiras et al., 2002). The residual

fraction includes metals that are retained within the crystal lattices of minerals (Kazi et al., 2005). Metals in this fraction have the strongest association with minerals and are the most difficult to separate from sewage sludge or other matrices (Usero et al., 1998).

In this study, four metals commonly found in SS, but with different strength of complexing with SOM and existing forms were selected for this evaluation. The specific objectives of this study were to (i) evaluate the distribution of Cu, Zn, Pb and As in SS of different ages and to (ii) elucidate the impact of OM degradation in SS and in SS-amended soils on the distribution of Cu, Zn, Pb and As into the various chemical forms.

8.2 Materials and Methods

8.2.1 Sewage Sludge (SS) and Soil

Municipal SS used for this study was obtained from the Thibodaux wastewater treatment plant (WWTP) in Thibodaux, Louisiana. Within the WWTP are ponds that contain SS of various ages. Composite samples of three sludges were taken from ponds containing SS of 6 month (SS1), 5 year (SS2), and 10 years old (SS3). Two Louisiana surface soils, an acidic Crowley silt loam and a calcareous Norwood silt loam were also collected. Collected sewage sludge and soils were air dried, ground to pass through 2-mm sieve, and stored at 4°C and room temperature, respectively, prior to use. To characterize SS, extracts of SS/deionized water at a ratio of 1:10 [w/v] were prepared in 50 ml centrifuge tubes and shaken for 18 hrs. The suspensions were then centrifuged at 15,000 rpm for 10 minutes and the supernatants were filtered using 0.45-μm filter. The filtrates were determined for sludge pH, electrical conductivity (EC), and soluble metals using pH meter, EC meter, and inductively coupled plasma (ICP, Spectro), respectively (Usman et al., 2004; Vulkan et al., 2002). In addition, total elemental concentration in SS was determined by digesting samples with *aqua regia* (3:1 HCl and HNO_3 mixture) at room temperature for 16

hr, followed by ICP measurement (Pueyo et al., 2003). Total organic matter content was determined based on loss on ignition of samples at 550°C for 1hr (Soil Survey Staff, 1996). Soil cation exchange capacity (CEC) was determined using repeated saturations of 1 M NH_4OAc (Soil Survey Staff, 1996) and particle size distribution was determined using a pipette method (Gee and Bauder, 1986). In addition, clay mineralogy was characterized using X-ray diffraction. The selected physiochemical properties of SS and soils used in this study are presented in Table 8.1 and Table 8.2, respectively.

Table 8.1 Selected physical and chemical properties of the three sewage sludges (SS).

Parameter	SS1	SS2	SS3	Pollutant concentration limits (USEPA, 1993,part 503)
pH	5.4	5.4	5.9	
EC (dS m^{-1})	3.7	0.18	2.7	
Organic matter (g kg^{-1})	420	380	400	
Total elements (mg kg^{-1})				
Fe	39150	50667	40200	
Al	12525	17777	18730	
Mn	2800	9565	5683	
Ca	30490	10330	20150	
Mg	2107	1685	2508	
K	1330	1277	1970	
Na	365	245	293	
P	15670	26116	22518	
Cu	807	801	661	<1500
Zn	2614	2908	2718	<2800
Pb	107	219	177	<300
As	137	129	120	<41
Soluble elements (mg kg^{-1})				
Fe	3.1	3.7	3.6	
Al	1.5	2.9	2.2	
Mn	814	1.2	2.1	
Ca	5627	289	5313	
Mg	674	23	220	
K	135	35	149	
Na	203	69	119	
P	9.0	90	24	
Cu	1.3	3.5	0.9	
Zn	85	11	12	
Pb	<0.02	<0.02	<0.02	
As	<0.03	<0.03	<0.03	

Table 8.2 Selected physical and chemical properties of Norwood and Crowley soils.

	Crowley	Norwood
pH	5.4	7.6
Organic matter (g kg^{-1})	20.3	16.1
CEC (cmol kg^{-1})	10.4	10.7
Particle size distribution (g kg^{-1})		
Sand	110	60
Silt	640	700
Clay	250	240
Clay mineralogy (%)		
Kaolinite	30	17
Montmorillonite	45	38
Vermiculite	20	---
Illite	5	38
Chlorite	---	7

8.2.2 Incubation Experiment

Incubation of SS was conducted at 25 ± 0.2 °C for 3 and 6 months to assess the effect of OM oxidation through incubation on the behavior of trace metals. In doing so, samples of 10 g of each SS were placed in 125ml Erlenmeyer flasks, watered to field capacity, and placed in an incubator in a completely randomized arrangement. During the incubation, the flasks containing SS were periodically weighed and rewetted to maintain constant moisture content, and were left open to maintain oxic conditions. The incubation experiment was replicated three times. After incubation, SS in the flasks were oven dried at 40°C, extracted with deionized H_2O (1:1 solid to H_2O ratio), and analyzed for pH and EC in sludge extracts as previously described. The rate of OM decomposition was calculated using the loss on ignition method. In addition, the fractionation of different metals was determined using a selective sequential extraction (SSE) procedure described below.

8.2.3 Chemical Oxidation Experiment

Direct chemical oxidation using diluted hydrogen peroxide (H_2O_2) was also carried out to assess the effect of OM degradation on trace metal distribution in SS. SS-amended soils were generated by mixing each of the three SSs thoroughly with Norwood or Crowley soils at a 1:1 ratio (air dry weight basis). Ten grams of each SS and SS-amended soil were weighed in 250 ml Erlenmeyer flasks and watered to field capacity. The flasks containing SS and SS-amended soils were heated to 70°C on a hot plate and 0.1 ml of 30% hydrogen peroxide were added (H_2O_2 diluted to approximately 5% at field capacity). The mixtures were allowed to react under constant stirring until frothing ceased. The flasks were then removed from the hot plate and left in the open air. The addition of hydrogen peroxide was repeated every other day until OM loss reached 30% and 70%, respectively as determined by loss on ignition. After completion of oxidation, SS and SS-amended soils were oven dried at 40°C, ground, and mixed before use for sequential extractions. Oxidation experiment was replicated twice.

8.2.4 Sequential Extractions

Samples of 1 g of each SS and SS-amended soil were weighed, placed in 50 ml centrifuge tubes and sequentially extracted based on a modified SSE scheme of Tessier et al. (1979). This SSE scheme fractionates trace metals sequentially into exchangeable (F1), carbonate bound (F2), Fe/Mn oxide bound (F3), organically bound (F4), and residual (F5) form. In doing so, following reagents were sequentially added for F1, F2, and F3 extractions, respectively and shaken for the time specified as follows: 1 M $MgCl_2$ for 1 hr (Tessier et al., 1979), 1 M NaOAc (pH 5.0) for 5 hr (LaForce and Fendorf, 2000; Tessier et al., 1979), 0.4 M $NH_2OH{\cdot}HCl$ (pH 1.5) for 6 hr (McLaren and Clucas, 2001). For the organically bound fraction (F4), 30% H_2O_2 was used to remove OM and 3.2 M NH_4OAc was used to extract heavy metals

(Tessier et al., 1979). The remaining fraction was digested using *Aqua regia* to determine the residual fraction (F5) (Pueyo et al., 2003). After each extraction, the suspensions were centrifuged at 15,000 rpm for 10 min and filtered using a 0.45-μm filter. The quantity of entrapped solution from a previous extraction was calculated by weighing each centrifuge tube before and after addition of extractant, and corrected for the calculation of metal contents in SS and SS-amended soils. All sequential extractions were replicated twice.

8.2.5 Statistical Analysis

Analysis of variance (ANOVA) statistical analysis was performed using SPSS 17 (SPSS, Inc., Chicago, Illinois) and comparison of means was undertaken using a Bonferroni test to determine any significant differences at $p \leq 0.05$.

8.3 Results and Discussion

8.3.1 Characterization of Sewage Sludge

Three SS materials exhibited similar pH ranging from 5.4-5.9, indicating slightly acidic conditions (Table 8.1). The OM content ranged from 38 to 42%, with the fresher 6-month SS1 slightly higher than the more aged aged 5-year SS2 and 10-year SS3. The overall remaining mineral matter content was, therefore, 58-62%, indicating the presence of considerable inorganic fractions in these SS sources (Alonso et al., 2005). The EC of SS1 was also higher than the more aged SS2 and SS3, with the reflection of higher concentration of the most soluble cationic macroelements in SS1 than the SS2 and SS3 (Table 8.1). Among the concerned trace metals, Zn was the only one found in large concentration in the water extract, with the highest being in SS1 (85 mg/kg). Total elemental analysis indicated that these SS materials were dominated with Fe, Al, Ca, and Mn followed by Mg, K, and Na. The same trend of total metals was also reported by Fuentes et al. (2004). The high levels of total Fe, Al, and Ca, and Mn indicated the presence of

major inorganic surfaces of Fe/Al/Mn oxides and calcium carbonates (Alonso et al., 2005). In addition, total P ranged from 1.6% to 2.6% in these SS samples, also similar to those reported by others (Alonso et al., 2005). The results could suggest the presence of reactive phosphates (Traina and LaPerche, 1999). The fresher SS1 had higher total Ca, whereas more aged SS2 and SS3 contained more total Al and Mn. On the other hand, SS2 contained the highest total Fe among the three SS materials (Table 8.1). These results likely suggested the dominance of different inorganic surfaces in these SS sources. For the trace metals of the interest, Zn exhibited the highest total content followed by Cu, Pb and As, consistent with the occurrence of these trace metal abundance in SSs reported by others (Wong et al., 2001). The total concentration of Cu and Pb in all samples was lower than the pollutant concentration limits for land application of SS recommended by the USEPA (USEPA, 1993). The total concentration of Zn was close to or higher than pollutant limits and As was higher than pollutant limits for all samples. Overall, the composition and general properties of these SSs were consistent with those reported in the literature (Alonso et al., 2005; Fuentes et al., 2004; Hettiarchchi et al., 2006; Wong et al., 2001).

8.3.2 Fractionation of Cu, Zn, Pb, and As in Sewage Sludge

The distribution of Cu, Zn, Pb and As forms in the three SS materials is presented in Table 8.3. A major fraction of total Cu (47-75%), Pb (51-62%), and As (67-75%) in the SSs was associated with OM followed by either Fe/Mn oxide bound or residual fractions, depending on specific SS and metal, and then by much smaller fractions of carbonate-bound and exchangeable. More Pb was in the residual fraction than Cu and As, whereas the latter two were found more in the carbonate-bound fraction than Pb (Table 8.3). Previous research showed that Cu and Pb were primarily in the OM and residual fractions (Fuentes et al., 2004; Planquart et al., 1999; Wong et al., 2001). The mobility of Cu and Pb in SS was also found to be very low, unlike Zn and Ni

(Ščančar et al., 2000). On the other hand, most previous studies showed that As was mainly associated with the residual, Fe/Mn oxide or carbonate fractions (Gomez et al., 2000; Sarkar et al., 2007), although some did report a considerable amount to be associated with OM (Baig et al., 2009). The dominance of As association with OM in this study could suggest the presence of organic As such as monomethylarsonaic acid (MMAA) and dimethylarsinic acid (DMAA) in these SS materials. MMAA and DMAA have been shown to be able to be retained by various constituents in SS (Carbonell-Barrachina et al., 1999).

Table 8.3 Distribution of total Cu, As, Zn, and Pb in sewage sludge (SS) samples. The numbers in parentheses indicate percentage for each fraction as calculated based on the total of sum

	Sewage sludge		
Metal form	SS1	SS2	SS3
Cu (mg kg^{-1})			
Exchangeable	25.0 (2.3%)	10.0 (1.1%)	7.4 (0.9%)
Carbonate bound	39.1 (3.6%)	67.6 (7.3%)	39.6 (4.7%)
Fe/Mn oxide bound	73.0 (6.8%)	340.4 (36.8%)	135.3 (16.0%)
Organically bound	808.0 (75.3%)	434.7 (47.0%)	564.3 (66.4%)
Residual	128.3 (12.0%)	73.2 (8.0%)	103.3 (12.2%)
Zn (mg kg^{-1})			
Exchangeable	494.4 (14.4%)	367 (9.4%)	100 (2.7%)
Carbonate bound	615.4 (17.9%)	599.0 (15.2%)	661.5 (17.8%)
Fe/Mn oxide bound	1949.4 (56.8%)	2475 (63.0%)	2399.5 (64.6%)
Organically bound	262.1 (7.6%)	409 (10.4%)	468.4 (12.6%)
Residual	109.3 (3.2%)	80.4 (2.05%)	87.9 (2.4%)
Pb (mg kg^{-1})			
Exchangeable	3.9 (2.7%)	7.3 (2.8%)	3.1 (1.5%)
Carbonate bound	1.1 (0.8%)	0.3 (0.1%)	1.1 (0.5%)
Fe/Mn oxide bound	30.1 (21.4%)	43.4 (17.0%)	26.9 (12.7%)
Organically bound	72.1 (51.4%)	158.6 (61.3%)	130.7 (61.6%)
Residual	33.3 (23.7%)	48.5 (18.8%)	56.2 (23.8%)
As (mg kg^{-1})			
Exchangeable	0.5 (0.3%)	1.2 (0.9%)	1.4 (1.1%)
Carbonate bound	1.6 (1.1%)	12.6 (8.9%)	1.3 (1.0%)
Fe/Mn oxide bound	18.5 (12.0%)	19.2 (13.5%)	15.6 (11.5%)
Organically bound	113.1 (72.8%)	95.5 (67.0%)	101.5 (75.2%)
Residual	21.7 (13.9%)	13.9 (9.8%)	15.2 (11.2%)

The majority of Zn (57-65%) in the three SSs was associated with Fe/Mn oxides and only a small fraction of total Zn (7-12%) was bound with OM (Table 8.3), reflecting general weak complexation of Zn with OM as compared with Cu, Pb and As (McBride, 1994).

The higher Zn fraction of Fe/Mn oxides bound was consistent with those reported by Dudka and Chlopecka (1990) and Pérez-Cid et al. (1999), although others also showed that Zn was not associated with any dominant chemical phase (Fuentes et al., 2004; Wong et al., 2001). Besides Fe/Mn oxide bound fractions, Zn also had relatively large fractions in carbonate bound (15-18%) as compared to Cu, Pb and As, suggesting strong inorganic role in retaining Zn in SS. However, these three SS exhibited the smallest residual fraction of Zn as compared to Cu, Pb, and As which was different from that reported by Pérez-Cid et al. (1999) who also showed a relatively large portion of Zn in the residual fraction. Nonetheless, while a small fraction of total Cu (≤2.3%), As (≤1.1%), and Pb (≤2.8%) was found in the exchangeable form, a considerable amount of Zn was found to be in the exchangeable form with 494 mg kg^{-1} (14%) in SS1, 367 mg kg^{-1} (9%) in SS2, and 100 mg kg^{-1} (3%) in SS3, respectively (Table 8.3). This result was consistent with those of others (Alonso et al., 2006; Ščančar et al., 2000a; Wong et al., 2006). Since metals within the exchangeable fraction could be easily solubilized and become readily available (Narwal and Singh, 1998), these results would indicate high probability of Zn uptake by plants upon application of these SS.

8.3.3 Organic Matter Oxidation of Sewage Sludge

The oxidation of OM in the three SS materials was first conducted through 6 month incubation at moisture content of field capacity. The incubation resulted in a relatively small OM oxidation of approximately 4% in the three SSs and had no statistically significant impact on the distribution of total Cu, As, Zn, and Pb among the different fractions (data not shown). The

major portion of Cu, As, and Pb in all three SSs remained bound with OM following incubation, whereas the majority of Zn remained bound with Fe/Mn oxides. The fact that the exchangeable fractions of these metals remained unaffected by incubation with 4% loss in OM suggested that a larger portion of OM degrdation could be required to cause any significant change in different pools of these metals.

On the other hand, the lack of change in exchangeable Zn as well as exchangeable Cd fraction was also reported by Stacey et al. (2001) in a 100-day incubation of lagoon sludge. The same study, however, showed a significant increase in exchangeable Zn and Cd, respectively, in a filtered sludge. While it did not determine the total OM change as in our study, they did show a significant change in hot-water extractable C after 100 day incubation (Stacy et al., 2001). It was likely that different extent of OM oxidation for different types of sludge sources would be required to lead to a significant change in available pools of metals.

The effects of direct chemical oxidation of OM on the relative distributions of Cu, Zn, Pb, and As in SS and SS-amended soils are presented in Figure 8.1 to Figure 8.4, respectively. Each metal behaved differently as a result of OM oxidation. Oxidation of OM resulted in a significant decrease of organically bound Cu (F4), the dominant pool, allowing its redistribution to other fractions (Figure 8.1).

Among the three sewage sludge sources, SS1 exhibited the largest decrease in organically bound Cu (75% to 7%) following oxidation treatment at 70% as compared to SS2 (47% to 10%) and SS3 (66% to10%) respectively, suggesting that the fresher sludge likely releases Cu into other pools upon OM oxidation. The OM oxidation also significantly reduced the residual Cu (F5) especially at 70% OM reduction. On the other hand, OM oxidation significantly increased Fe/Mn oxide bound Cu (F3) as well as carbonate bound Cu (F2) in all three SS materials at 70%

OM oxidation. This increase appeared to be more in older SS (SS2 and SS3) as compared to the fresher SS (SS1) (Figure 8.1). The latter, however, had the largest increase in exchangeable Cu (F1) at 30% OM oxidation as compared to the former. The OM oxidation at 70% did not result in a further increase in exchangeable Cu but a decreased exchangeable Cu in two out of the three SS materials. The fact that at 70% OM oxidation, Cu was primarily associated with Fe/Mn oxides of SS materials followed by carbonates strongly suggested that these inorganic constituents could play a significant role in binding Cu as OM is degraded, even though these fractions had different stability implication with respect to soil condition change (Kazi et al., 2005). Nonetheless, our result did suggest the potential release of large portion of exchangeable Cu at initial oxidation of OM especially if a fresher SS had been applied.

It is interesting to note that OM oxidation in SS-amended acidic Crowley and calcareous Norwood soils did not change the general trend of effect on various Cu pools as observed in SS alone (Figure 8.1). The major increases, following OM oxidation, were also Fe/Mn oxide-bound Cu followed by carbonate bound Cu in soils amended with all three SS although the magnitude of increase varied slightly more in the SS-amended Norwood than in the SS-amended Crowley. In addition, the increase in exchangeable Cu occurred primarily at 30% of OM oxidation following the reduction in organically bound Cu. These results could suggest that the SS property likely play a more dominant role in controlling the speciation of Cu than the SS-receiving soils.

The OM oxidation had a quite different effect on the relative distribution of Zn in SS (Figure 8.2). It also resulted in a reduction of organically bound Zn especially at 70% of OM oxidation. Unlike Cu, since a small fraction of total Zn was generally associated with OM in all SS samples, such a loss in organically bound Zn was relatively small with respect to total Zn.

However, the OM oxidation generally decreased the Fe/Mn oxide bound Zn, the dominant fraction, as well as carbonate bound Zn fraction. The oxidation process had little effect on residual Zn pool in two SSs but did also decrease this fraction in one SS. The major effect of these losses in different pools of Zn, as a result of OM oxidation, was the major increase in exchangeable Zn in all three SS sources but especially with the SS1 (from 14% to 67%) as compared to SS2 (9% to 35%) and SS3 (3% to 35%) at 70% of OM oxidation. The results clearly demonstrated that the OM oxidation likely increase the exchangeable pool of Zn.

These results were also validated in SS-amended Crowley and Norwood soils as the OM oxidation led to similar increase in the exchangeable Zn fraction (Figure 8.2). One exception was that there was a modest increase in exchangeable Zn, which corresponded to an increase, rather than decrease or unchange, in both organically bound and residual Zn at 70% OM oxidation in the SS2-amended Crowley soil. The latter could be due to the combined effect of the relatively higher OM content in Crowley and the higher Zn content in SS2 (Tables 8.1 and 8.2).

The OM degradation also had a different effect on relative distribution of Pb. Like Cu, Pb was primarily present in SS as organically bound fraction. However unlike Cu, the OM oxidation at 70% significantly increased the organically bound Pb fraction in SS1, the fresher SS (Figure 8.3).

It had no significant effect on the organically bound Pb in more aged SS2 and SS3 sources although the fractions also increased numerically. The OM reduction at 30% and 70% o slightly increased Fe/Mn oxide bound Pb in two of the three SS. On the other hand, the corresponding decreased fraction upon OM oxidation was residual Pb in SS. The latter was consistent with the observation of reduction in residual Pb fraction upon losing OM during the composting of SS (Nomeda et al., 2008). There was no significant increase in both exchangeable

Pb and carbonate bound Pb (Figure 8.3), suggesting that Pb is likely remained as less mobile as compared to Zn and Cu upon OM oxidation. The OM oxidation in SS-amended Crowley and Norwood soils did not change the major trend of Pb fractionation as observed with SS alone.

It is interesting to note that Pb remained primarily in organically bound fraction even at 70% OM oxidation, whereas Cu had a significant reduction in its organically bound fraction (Figure 8.1 and Figure 8.3). This phenomenon suggested that Cu and Pb, although both primarily bound to OM, could interact differently with organic constituents in SS. Based on μ-XRF imaging and regression analysis of metals before and after OM removal, showed that Cu likely binds to OM that is binding to Fe oxides, whereas Pb could bind between OM and Fe oxides in SS (Hettiarchchi et al., 2006). In our study, we did not completely remove OM from SS but we speculate that this different binding arrangement between Cu and Pb could result in differential redistribution of the two metals as a result of OM reduction upon oxidation. The slight increase in organically bound Pb was also found in SS after composting for 28 days with a modest removal of OM at 4% (Nomeda et al., 2008).

In the case of As, 30% OM oxidation significantly reduced organically bound fraction in all three SSs with a corresponding increase in Fe/Mn oxide bound fraction (Figure 8.4), suggesting a strong role of Fe/Mn oxides in binding As. The latter could be attributed to the strong sorption of As by Fe oxides (Sarkar et al., 2007). The OM oxidation at 70% did not further decrease organically bound As. The oxidation did decrease the residual As fraction in the fresher SS1, suggesting the easiness of mobilizing residual As upon OM oxidation. Overall like Pb, the majority of As also remained in the organically bound fraction after OM oxidation especially for more aged SS sources, SS2 and SS3. Arsenic has been shown to exist in the chemical states of both As (III) and AS (V) in SS, depending on source and municipal treatment

(Fujiwara et al., 2007; Nagoshi et al., 2005). The major species in SS include arsenite, arsenate, MMAA, and DMAA (Carbonell-Barrachina et al., 1999). Due to the fact that As exist as an anion, the binding between As and OM would likely be formed through cation bridging mechanism although direct formation of As-OM complexes has also be suggested (Wang and Mulligan, 2006). The dominance of organically bound As even at 70% OM oxidation (Figure 8.4) could suggest strong presence of organic As species such as DMAA and MMAA, which were retained by various constituents in SS (Carbonell-Barrachina et al., 1999). There was no significant increase in exchangeable As and carbonate bound As upon OM oxidation. Like, Cu, Zn and Pb, there was little change in the relative distribution of As among the various fractions in these SS-amended Crowley and Norwood soils as compared to SS alone (Figure 8.4).

Recent studies showed that the potential release of trace metals into the environment following OM degradation likely depended on the composition of SS (Fujiwara et al., 2007; Stacey et al., 2001). Hettiarchchi et al. (2006) also suggested that trace metal mobility would not be enhanced as a result of OM degradation due to the presence of Fe/Mn oxides in SS. We report here however, that besides the composition, the metal release could also very much depend on the property of a specific metal of concern. A large portion of total Cu was released into the exchangeable form after OM degradation even when the oxide and carbonate bound Cu fractions increased, suggesting that the role of Fe/Mn oxides in binding Cu may be limited.

Zn also exhibited large increases in the exchangeable fraction as a result of OM degradation, despite that a small fraction of Zn in these SS was associated with OM to begin with. On the other hand, exchangeable Pb and As fractions were minute prior to and following OM degradation, suggesting limited effect on bioavailability of these two metals. The Fe/Mn oxides played a significant role in binding As with an increasing capacity and without a

corresponding increase in exchangeable As following OM degradation. The latter could suggest that OM degradation does not increase the soluble fraction of As and therefore does not abide by the "Time Bomb" hypothesis. Also interestingly, Pb, like As, was largely associated with the OM fraction in all SS samples. Yet, OM degradation did not have a significant impact on the Pb-bound organic fraction in the more aged SS2 and SS3. The Fe/Mn oxide fraction of Pb showed the least change following OM degradation, suggesting that Fe/Mn oxides likely played a minor role in binding Pb. However we did not evaluate this effect under the condition of a complete removal of OM.

It should be pointed that OM oxidation decreased fractions of Zn bound to carbonates and Fe/Mn oxides. It was possible that inorganic surfaces such as carbonates and oxides were affected by the hydrogen peroxide treatment, which might have altered the portions of Zn bound to these phases. Previous report suggested that hydrogen peroxide may cause the dissolution of carbonates, phosphates and oxide phases (Hettiarchchi et al., 2003).

However, the fact that Cu fractions binding to carbonates and Fe/Mn oxides as well as As fraction binding to Fe/Mn oxides increased in the same oxidation process (Figure 8.1 and Figure 8.4), suggesting that this effect could be minor, since these metals have stronger binding than Zn to these surfaces (McBride, 1994). A more plausible explanation for the decreased Zn fraction bound to Fe/Mn oxides upon OM oxidation was likely due to the competitive effect of Cu. The Cu was shown to have strong binding to Fe oxide surfaces which can displace Zn (Violante et al., 2003), as large portion of Cu was released and become available upon OM oxidation.

It was also interesting that amending SS with soil did not change the fractionation of Cu, Zn, Pb, or As in our study. Bergkvist et al. (2005) reported that mixing SS with soil may result in

long term increases or decreases in Cd solubility and sorption, depending on the affinity of Cd itself for the sludge or for soil. Our results could suggest that the affinity of these metals for SS constituents was higher than for soil. However, the latter may require further evaluation in a system with slow but long term oxidation of SS OM.

8.3.4 Conclusion

The results demonstrated that Cu, Zn , Pb, and As in SS were distributed differently among the various chemical forms. The majority of Cu, Pb and As were associated with the OM fraction, whereas the majority of Zn was bound to the Fe/Mn oxide fraction in all three SSs. Incubation of SS for 6 months at 25°C did not result in substantial degradation of OM content (≤ 4%) and any significant change in the distribution of Zn and Cu into different fractions. Direct chemical degradation of OM using diluted H_2O_2 resulted in a significant decrease of organically bound Cu and increase in exchangeable, carbonate bound and oxide bound Cu fractions. Although carbonates and oxides played a role in adsorbing Cu following degradation, the significant increase in exchangeable fraction indicated that the potential release of metals into the environment is possible.

OM degradation also significantly increased the exchangeable Zn fraction and decreased fractions in which Zn was bound to oxides or carbonates. The degradation of OM did not increase exchangeable As or Pb, where the Fe/Mn oxide fraction was likely to play a role in binding these metals. Overall the property of SS had the more dominant role in controlling the fractionation of the trace metals than that of soil. The impact of OM degradation on the relative distribution of Cu, Zn, Pb, and As and therefore their bioavailability vary among the elements.

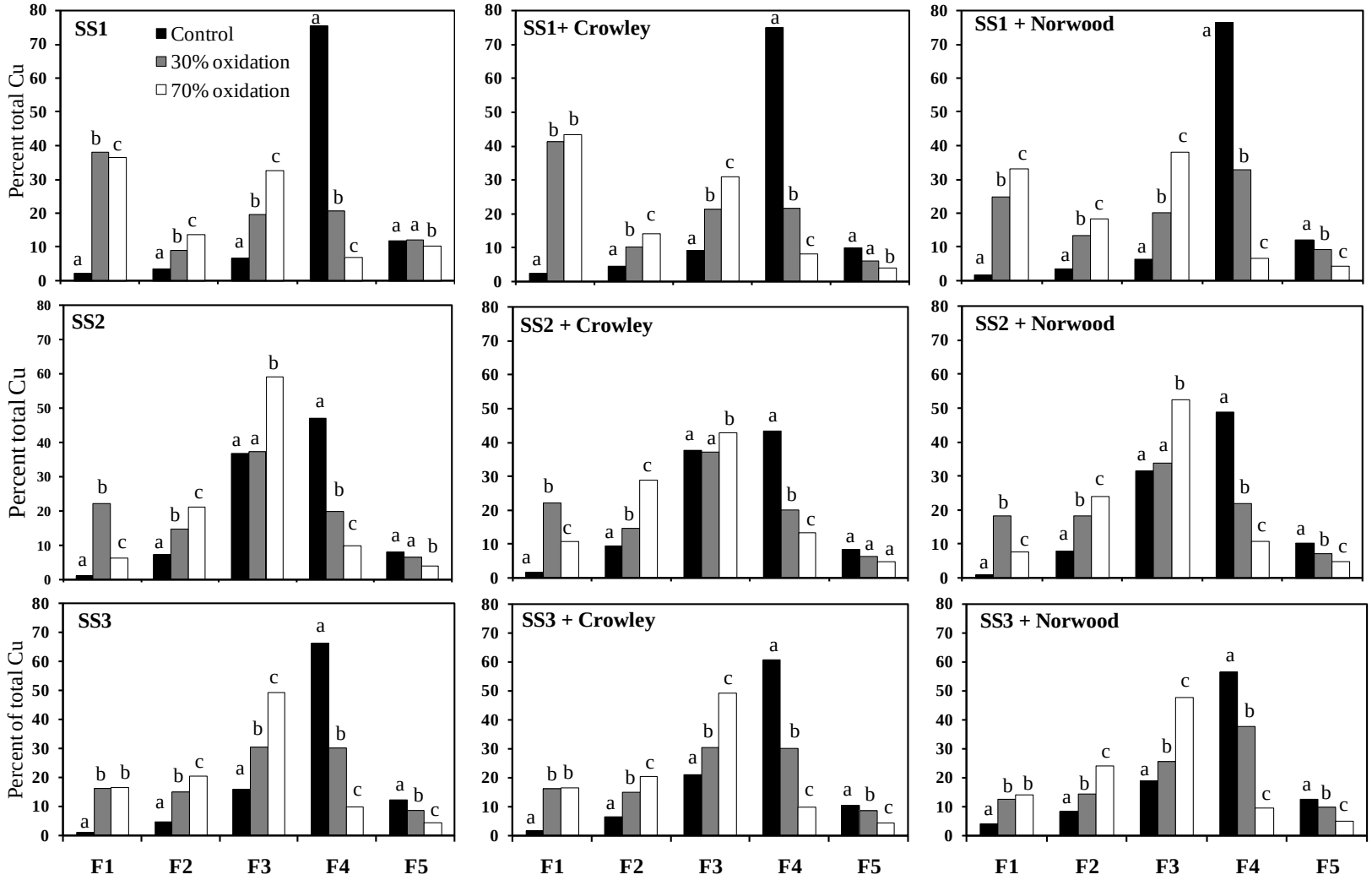

Figure 8.1 Relative distribution of Cu in three SS and SS-amended soils as affected by chemical oxidation. F1(exchangeable), F2 (carbonate bound), F3 (Fe/Mn oxide bound), F4 (organically bound), F5(residual). Similar letters on top of histograms for each fraction indicate that mean values are not significantly different at $p \leq 0.05$ according to Bonferroni's test.

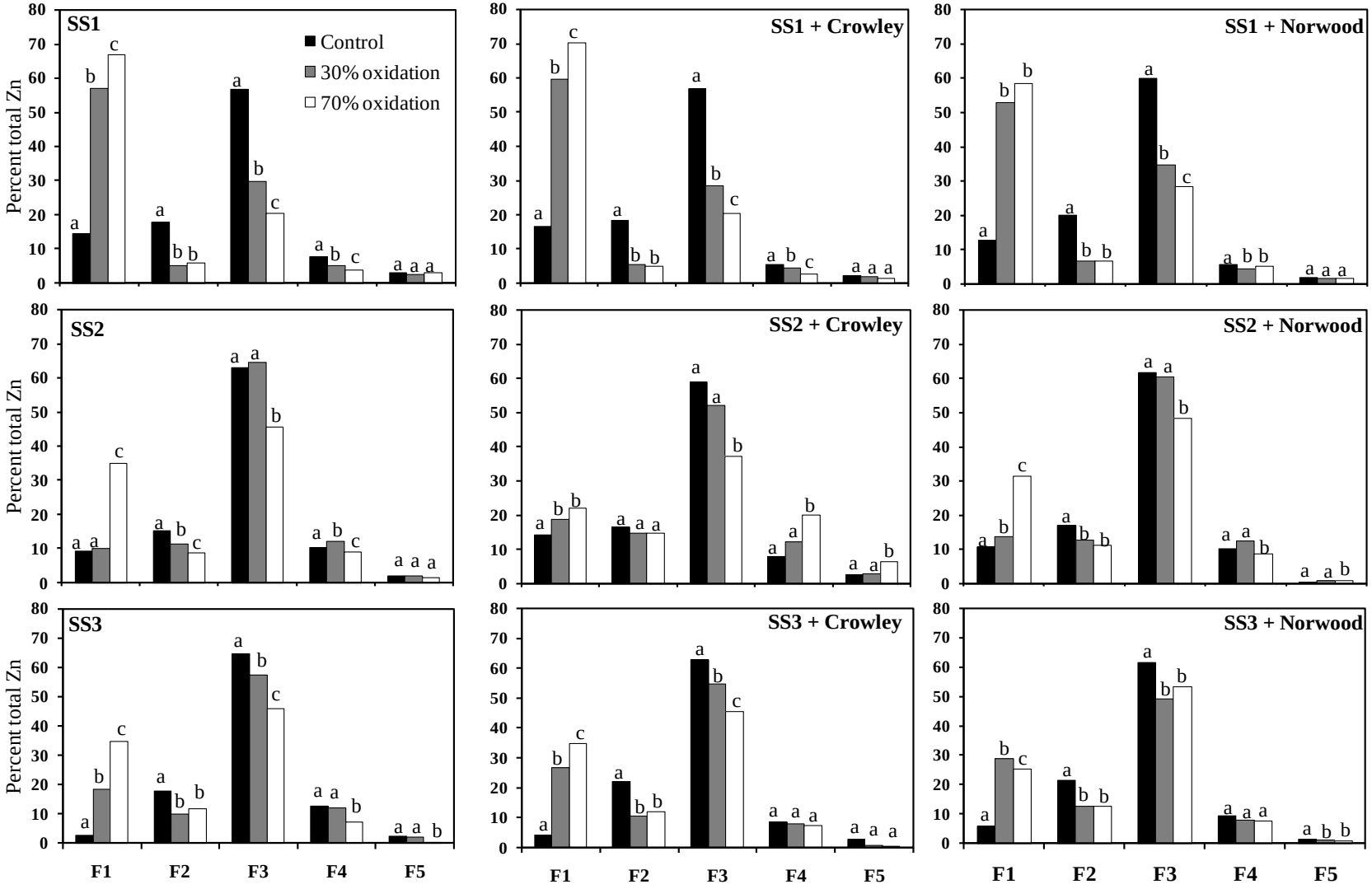

Figure 8.2**.** Relative distribution of Zn in three SS and SS-amended soils as affected by chemical oxidation. F1(exchangeable), F2 (carbonate bound), F3 (Fe/Mn oxide bound), F4 (organically bound), F5(residual). Similar letters on top of histograms for each fraction indicate that mean values are not significantly different at $p \leq 0.05$ according to Bonferroni's test.

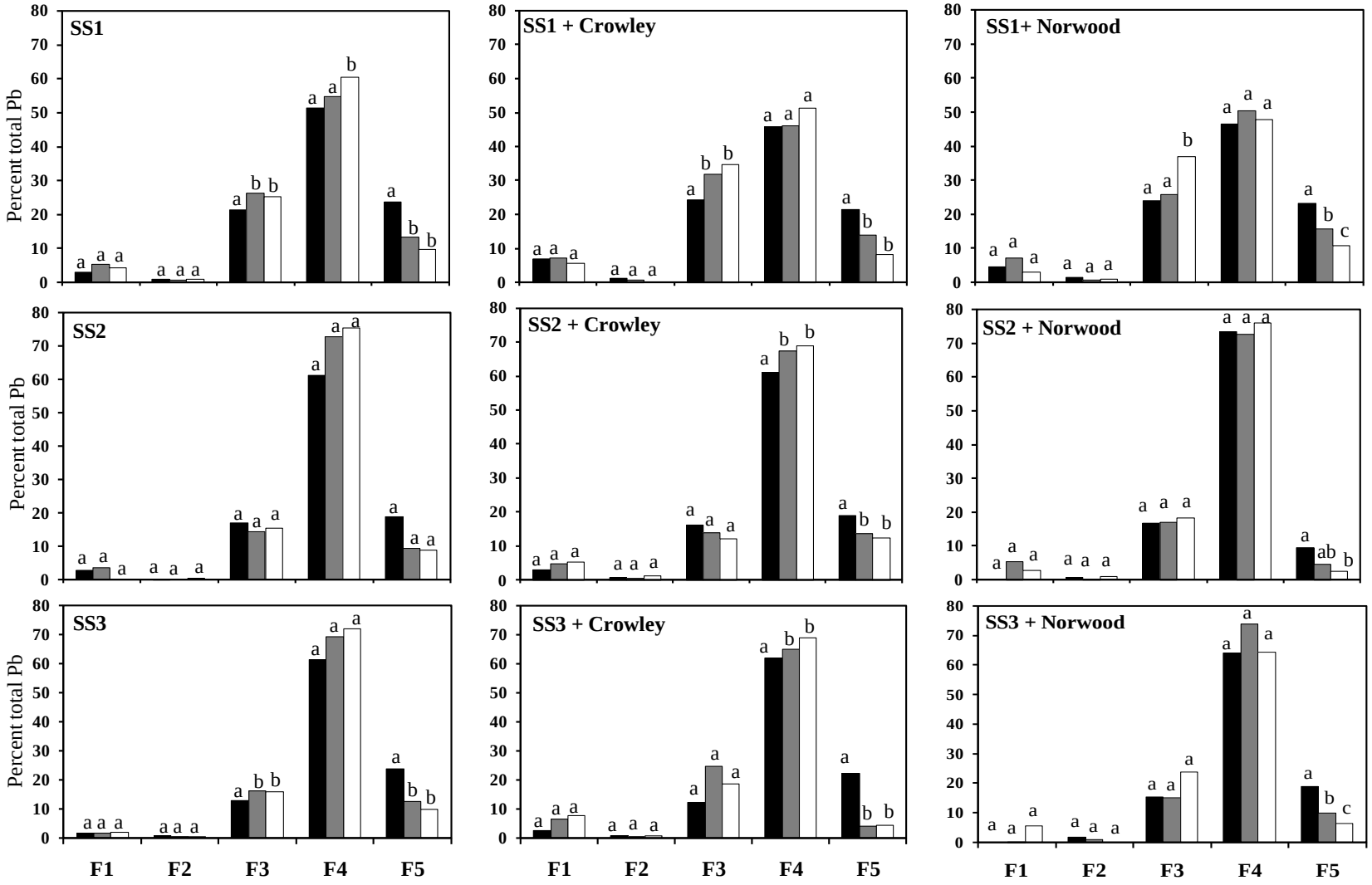

Figure 8.3 Relative distribution of Pb in three SS and SS-amended soils as affected by chemical oxidation. F1(exchangeable), F2 (carbonate bound), F3 (Fe/Mn oxide bound), F4 (organically bound), F5(residual). Similar letters on top of histograms for each fraction indicate that mean values are not significantly different at $p \leq 0.05$ according to Bonferroni's test.

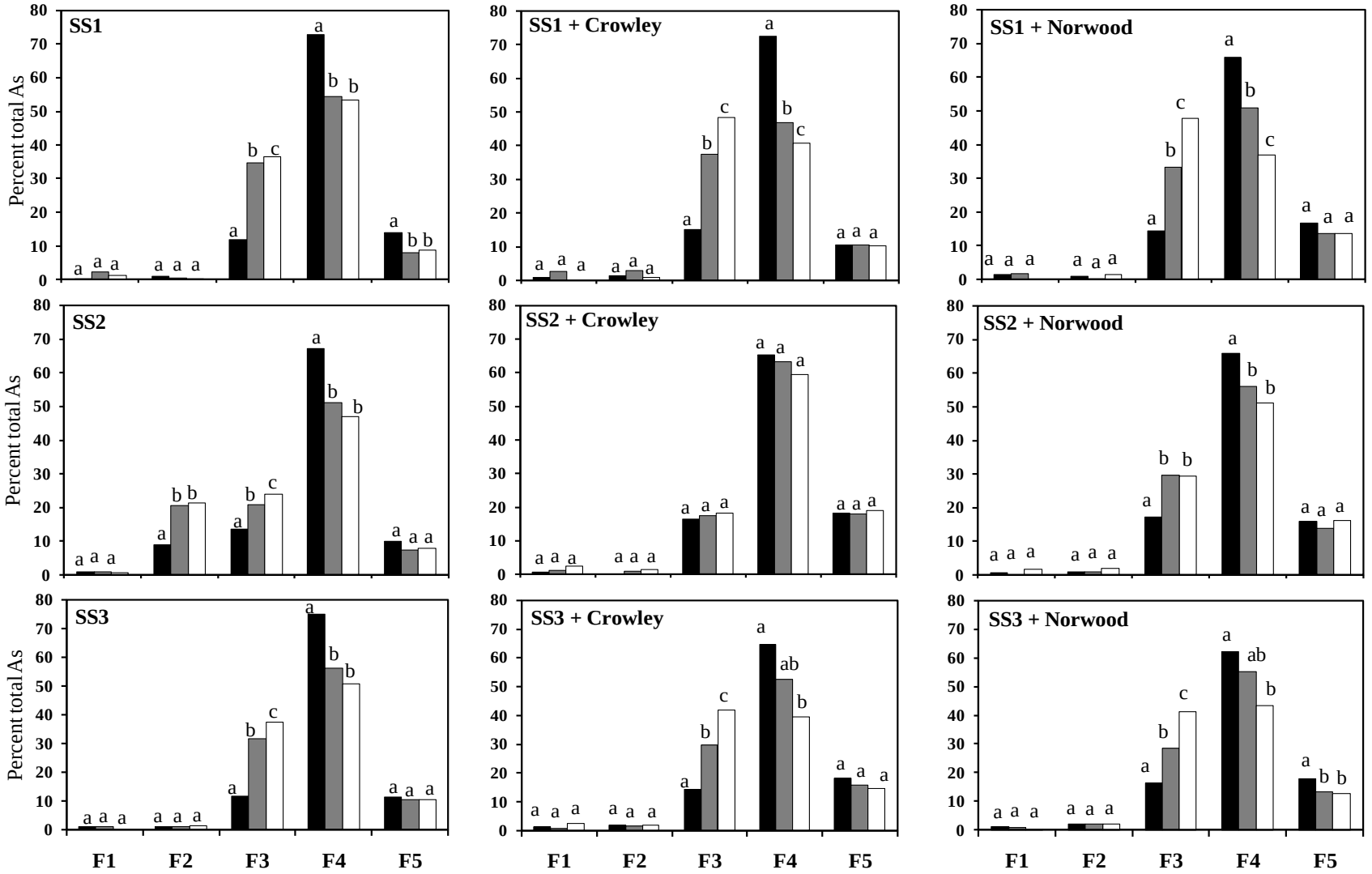

Figure 8.4 Relative distribution of As in three SS and SS-amended soils as affected by chemical oxidation. F1(exchangeable), F2 (carbonate bound), F3 (Fe/Mn oxide bound), F4 (organically bound), F5(residual). Similar letters on top of histograms for each fraction indicate that mean values are not significantly different at $p \leq 0.05$ according to Bonferroni's test.

8.4 References

Adani, F., Tambone, F., 2005. Long-term effect of sewage sludge application on soil humic acids. Chemosphere. 60, 1214–1221.

Alonso, E., Villar, P., Santos, A., Aparicio, I., 2006. Fractionation of heavy metals in sludge from anaerobic waste water stabilization ponds in southern Spain. Waste Manage. 26, 1270-1276.

Antoniadis, V., Tsadilas, C.D., Ashworth, D.J., 2007. Monometal and competitive adsorption of heavy metals by sewage sludge-amended soil. Chemosphere. 68, 489–494.

Baig, J.A., Kazi, T.G., Arain, M.B., Shah, A.Q., Sarfraz, R.A., Afridi, H.I., Kandhro, G.A., Jamali, M.K., Sumaira Khan. M.K., 2009. Arsenic fractionation in sediments of different origins using BCR sequential and single extraction methods. J. Hazard. Mater. 167, 745-751.

Banerjee, A.D.K., 2003. Heavy metal levels and solid phase speciation in street dusts of Delhi, India. Environ. Pollut. 123, 95–105.

Bergkvist, P., Jarvis, N., 2004. Modeling organic carbon dynamics and cadmium fate in long-term sludge-amended soil. J. Environ. Qual. 33, 181–191.

Bergkvist, P., Berggren, D. Jarvis, N., 2005. Cadmium solubility and sorption in a long-term sludge-amended arable Soil. J. Environ. Qual. 34,1530–1538.

Carbonell-Barrachina, A.A., Jugsujinda, A., Burlo, F., DeLaune, R.D., Patrick, Jr. W.H., 1999. Arsenic chemistry in municipal sewage sludge as affected by redox potential and pH. Water Res. 34, 216-224.

Dudka, S., Chlopecka, A., 1990. Effect of solid-phase speciation on metal mobility and phytoavailability in sludge-amended soil. Water, Air, Soil Pollut. 51, 153-160.

Filgueiras , A.V., Lavilla, I., Bendicho, C., 2002. Chemical sequential extraction for metal partitioning in environmental solid samples. J. Environ. Monit. 4, 823 –857.

Frost, H.L., Ketchum, L.H., 2000. Trace metal concentration in durum wheat from application of sewage sludge and commercial fertilizer. Adv. Environ. Res. 4, 347-355.

Fujiwara, S., Kawano, T., Nagoshi, M., 2007. Analysis of chemical states of heavy metals in environmental samples using XAFS. JFE Technical Report. 9, 37-42.

Fuentes, A., Lloréns, M., Sáez, J., Soler, A., Aguilar, M. I., Ortuño, J.F., Meseguer, V.F., 2004. Simple and sequential extractions of heavy metals from different sewage sludges. Chemosphere 54(8), 1039-1047.

Gee, G.W., Bauder, J.W., 1986. Particle-size analysis. p. 383–412. *In* A. Klute (ed.) Methods of soil analysis. Part 1. 2nd ed. Agron. Monogr. 9. ASA and SSSA, Madison, WI.

Hettiarachchi, G.M., Ryan, J.A., Chaney, R.L., LaFleur, C.M., 2003. Sorption and desorption of cadmium by different fractions of biosolids-amended soils. J. Environ. Qual. 32,1684–1693.

Hettiarachchi, G.M., Scheckel, K.G., Ryan, J.A., Sutton, S.R., Newville, M., 2006. μ-XANES and μ-XRF investigations of metal binding mechanisms in biosolids. J. Environ. Qual. 35, 342–351.

Kazi, T.G., Jamali, M.K., Kazi, G.H., Arain, M.B., Afridi, H.I., Siddiqui, A., 2005. Evaluating the mobility of toxic metals in untreated industrial wastewater sludge using a BCR sequential extraction procedure and a leaching test, Anal. Bioanal. Chem. 383, 297–304.

LaForce, M.J., Fendorf, S., 2000. Solid-phase iron characterization during common selective sequential extractions. Soil Sci. Soc. Am. J. 64, 1608–1615.

Li, Z., Ryan, J.A., Chen, J.L., Al-Abed, S.R., 2001. Adsorption of cadmium on biosolids-amended soils. J. Environ. Qual. 30, 903–911.

Li, X.D., Shen, Z.G., Wai, O.W.H., Li, Y.S., 2001. Chemical forms of Pb, Zn and Cu in the sediment profiles of the Pearl River Estuary. Mar. Pollut. Bull. 42, 215–223.

McBride, M.B., 1994. Environmental chemistry of soils. Oxford University Press, Oxford.

McBride, M.B., 1995. Toxic metal accumulation from agricultural use of sludge: Are USEPA regulations protective? J. Environ. Qual. 24, 5–18.

McBride, M.B., 2003. Toxic metals in sewage sludge-amended soils: Has promotion of beneficial use discounted the risks? Adv. Environ. Res. 8, 5–19.

McLaren, R.G., Clucas, L.M., 2001. Fractionation of Copper, Nickel, and Zinc in Metal-Spiked Sewage Sludge. J. Environ. Qual. 30,1968–1975.

Nagoshi, M., Kawano, T., Fujiwara, S., Miura, T., Udagawa, S., Nakahara, K., Takaoka, M., Uruga, T., 2005. Chemical states of trace heavy metals in sewage sludge by XAFS spectroscopy. Physica Scipta.115, 946-948.

Narwal, R.P., Singh, B.R., 1998. Effect of organic materials on partitioning, extractability and plant uptake of metals in an alum shale soil. Water, Air, Soil Pollut. 103, 405-421.

Nomeda, S., Valdas, P., Chen, S., Lin, J., 2008. Variations of metal distribution in sewage sludge composting. Waste Manage. 28,1637-1644.

Oliver, I.W., Hass, A., Merrington, G., Fine, P., McLaughlin, M.J., 2005. Copper availability in seven Israeli soils incubated with and without biosolids. J. Environ. Qual. 34, 508-513.

Pérez-Cid, B., Lavilla, I., Bendicho, C., 1999. Application of microwave extraction for partitioning of heavy metals in sewage sludge. Analytica Chimica Acta. 378, 201-210.

Planquart, P., Bonin, G., Prone, A., Massiani, C., 1999. Distribution, movement and plant availability of trace metals in soils amended with sewage sludge composts: application to low metal loadings. Sci. Total Environ. 241,161-179.

Pueyo, M., Sastre, J., Hernández, E., Vidal, M., López-Sánchez, J.F., Rauret, G., 2003. Prediction of Trace Element Mobility in Contaminated Soils by Sequential Extraction. J. Environ. Qual. 32, 2054–2066.

Sarkar, D., Makris, K.C., Parra-Noonan, M.T., Datta, R., 2007. Effect of soil properties on arsenic fractionation and bioaccessibility in cattle and sheep dipping vat sites. Environ. Int. 33, 164-169.

Ščančar, J. R., Milačič, M., Stražar,Burica. 2000. Total metal concentrations and partitioning of Cd, Fe, Ni and Zn in sewage sludge. Sci. Total Environ. 250, 9-19.

Soil Survey Staff. 1996. Soil survey laboratory methods manual. Soil Survey Investigations Rep. 42, Version 3.0. USDA-NRCS, Lincoln, NE.

Stacey, S., Merrington, G., McLaughlin, M.J. 2001. The effect of aging biosolids on the availability of cadmium and zinc in soil. Europ. J. Soil Sci. 52, 313-321.

Tessier, A., P.G.C. Campbell, and M. Bisson. 1979. Sequential extraction procedure for the speciation of particulate trace metals. Anal. Chem. 51: 844-851.

Traina, S.J., Laperche, V., 1999. Contaminant bioavailability in soils, sediments, and aquatic environments. Proc. Natl. Acad. Sci. USA 96:3365–3371.

US Environmental Protection Agency. 1993. Standards for the use or disposal of sewage sludge. Fed Regist 58, 9248– 415.

Usman, A.R. Y., Kuzyakov, Stahr, K., 2004. Dynamics of organic C mineralization and the mobile fraction of heavy metals in a calcareous soil incubated with organic wastes. Water, Air, Soil Pollut. 158(1),1573-2932.

Usero, J., Gamero, M., Morillo, J., Gracia, I., 1998. Comparison study of three sequential extraction procedures formetals inmarine sediments. Environ. Int. 24,487–496.

Violante, A., Ricciardella, M.R., Pigna, M., 2003. Adsorption of heavy metals on mixed Fe–Al oxides in the absence or presence of organic ligands. Water, Air, Soil Pollut. 145, 289–306.

Vulkan, R., Mingelgrin, U., Ben-Asher, J., Frenkel, H., 2002. Copper and zinc Speciation in the solution of a soil–sludge mixture. J. Environ. Qual. 31,193–203.

Wang, S., Mulligan, C.N., 2006. Effect of natural organic matter on arsenic release from soil and sediments into ground water. Environ. GeoChem Health 28,197-214.

Wong, J.W.C., Li, K., Fang, M., Su, D.C., 2001.Toxicity evaluation of sewage sludges in Hong Kong. Environ. Int. 27, 373–380.

CHAPTER 9

CONCLUSION

Adsorption of zinc (Zn) to mineral surfaces controls its bioavailability and fate in the soil environment. The amounts of Zn adsorbed to mineral surfaces and the mechanisms of Zn adsorption were impacted by pH and by the presence of citrate, humic acid (HA), desferrioxamine-B (DFO-B), and phosphate (PO_4). In the ferrihydrite mineral system, Zn adsorption was enhanced in the presence of citrate and PO_4, whereas decreased in the presence of DFO-B. In the presence of HA, Zn adsorption increased below pH 6.0 and decreased above that pH. Results from X-Ray Absorption Fine Structure Spectroscopy (XAFS) showed that Zn formed both edge and corner-sharing linkages with ferrihydrite at pH 7.5 in the control, citrate, and PO_4 sorption samples whereas formed only corner-sharing linkages in the presence of HA and DFO-B. The study suggests that in the control and presence ligands that enhanced Zn adsorption (citrate and PO_4), Zn forms strong linkages with high affinity edge sites of ferrihydrite. In the presence of ligands that reduced Zn adsorption at pH 7.5 (HA and DFO-B), Zn forms weaker, low affinity linkages with ferrihydrite. From an environmental perspective, Zn is more likely to be desorbed from the ferrihydrite surface in the presence HA and DFO-B.

In the kaolinite mineral system, Zn adsorption was enhanced in the presence of HA, whereas decreased in the presence of citrate and DFO-B. In the presence of PO_4, Zn removal from solution was enhanced due to the formation of Zn-PO_4 precipitate. XAFS spectral analysis showed that at pH 5.5, Zn formed inner sphere edge-sharing linkages with the aluminol surface groups of kaolinite in the control and in presence of citrate, HA, and DFO-B. With increase in pH to 7.5, the same sorption geometry was exhibited for the HA and DFO-B samples, whereas it changed for the control and citrate samples. In the control, Zn was incorporated into a Zn-Al LDH precipitate, whereas formed outer sphere complexes in the presence of citrate. This study

suggests that at low pH, Zn may form inner sphere complexes with kaolinite that are not impacted by the presence of ligands. Additionally, the formation of Zn-Al layered double hydroxide (LDH) at high pH is likely to be suppressed in the presence of ligands.

Results from the mixed ferrihydrite-gibbsite mineral system showed that Zn adsorption was enhanced in the presence of citrate, HA, and PO_4, whereas decreased in the presence of DFO-B. EXAFS spectral analysis indicated that Zn formed corner-sharing linkages with ferrihydirte at pH 7.5 in the control and in the presence of all ligands under investigation. In the mixed system, edge-sharing with gibbsite was evident only in the citrate sample. Corner sharing linkages in the single system were evident in the control and DFO-B sorption samples. The results of this study suggest that in the mixed mineral system, Zn forms low affinity corner-sharing linkages with ferrihydrite, unlike in the single mineral ferrihydirte system.

The final section of this study investigated the fate of heavy metals in sewage sludge following the oxidation of organic matter (OM). Long-term use of sewage sludge for land application has caused concern over the potential release of trace metals into the environment following the degradation of OM. Selective sequential exraction showed that the majority of Cu, As, and Pb were bound to OM, whereas the majority of Zn was bound with the Fe/Mn oxides. Degradation of OM resulted in small decrease in organically bound Zn, but resulted in significant increase in the exchangeable fractions in sewage sludge. In addition, oxide and carbonate bound Zn fractions decreased following degradation of OM. Exchangeable fractions of As and Pb were minute prior to and following degradation indicating that the release of these elements into the environment is unlikely following the loss of OM. The distribution of Cu, As, Zn, and Pb in sewage sludge-amended soils was similar to that of sewage sludge, indicating that the properties of sewage sludge played a dominant role in controlling metal distribution

following organic matter degradation. Degradation likely increased the mobility and bioavailability of Zn and Cu, whereas it had less impact on Pb and As.

VITA

Hashem Stietiya was born in June, 1974, in Amman, Jordan, to the family of Samir Stietiya and Lotfiya Attili. He graduated from the Jordan University of Science and Technology in 1997, Irbed, Jordan, with a Bachelor of Science in Agriculture. He obtained his Master of Science in Agricultural Resources and Environment from the University of Jordan in 2000. He worked as Deputy Project Manager for an environmental consultants company in Doha, Qatar, from 2002 to 2005. He got married to Hiba Bawadi in 2005 and has two children, Zeena and Samir. He began his doctoral program at the School of Plant, Environmental, and Soil Sciences, Louisiana State University in 2006.